IntechOpen

Energy Efficiency Improvements in Smart Grid Components

Edited by Moustafa M. Eissa

ENERGY EFFICIENCY IMPROVEMENTS IN SMART GRID COMPONENTS

Edited by **Moustafa M. Eissa**

Energy Efficiency Improvements in Smart Grid Components
http://dx.doi.org/10.5772/58493
Edited by Moustafa M. Eissa

Contributors

Tao Zhu, Chunhua Zheng, Guoqing Xu, Jianing Liang, Kun Xu, Yanhui Zhang, Rune E Gustavsson, Leif Marcusson, Abdellah Chehri, Luís Fernando Caparroz Duarte, Rodrigo Bacurau, Elnatan Ferreira, Rabah Benabid, Mohamed Boudour, Moustafa Eissa, Mahboubeh Dolatyari, Ali Rostami, Ghasem Rostami, Pegah Amini, Kenneth Eloghene Okedu, Roland Uhunmwangho, Lucian Mihet-Popa, Voicu Groza, Jiahe Chen, Lassaad Sbita, Miriam Benedetti, Vittorio Cesarotti, Vito Introna

Notice

First published in Croatia, 2015 by INTECH d.o.o.
eBook (PDF) Published by IN TECH d.o.o.
Place and year of publication of eBook (PDF): Rijeka, 2019.
IntechOpen is the global imprint of IN TECH d.o.o.
Printed in Croatia

Legal deposit, Croatia: National and University Library in Zagreb

Additional hard and PDF copies can be obtained from orders@intechopen.com

Energy Efficiency Improvements in Smart Grid Components
Edited by Moustafa M. Eissa

p. cm.

ISBN 978-953-51-2038-4

eBook (PDF) ISBN 978-953-51-4225-6

Meet the editor

M M Eissa is a Professor at Helwan University. He authored more than 100 papers. He is an editor for three books and three chapters. In 1999, he was invited to be a Visiting Research Fellow at Calgary University - Canada. From 2008 till 2010 he was a chair Prof. for "DSM and Energy Efficiency" project funded from Saudi Electricity Company. From 2010 to 2014 he was the PI for "smart grid" project funded from NTRA. Dr. Eissa research interests are digital relaying, application of WAM to power systems, PMU applications, smart grid, smart meters, wireless application on power system, demand side management, energy efficiency, etc. He also owns five prizes; ETRERA 2020 Prize in the category Smart Grids (2014) – Europ, Ministry of Higher Education – Research Excellence Prize- 2012, University - Excellence Prize, 2005, University - Encouragement Prize- 2011, State – Encouragement prize in the advanced technology science from Academy of Scientific Research and Technology (Egypt), 2002.

Contents

Preface

The recent trends including increased demand needs and advancements in grid components and management technologies are causing the electric utility and regulators how the grid is managed. The utility is starting to employ smart grids that use information and communication technologies, advanced sensors, and renewable resources to make electric power systems more reliable and efficient. These components and technologies will help enable higher levels of renewable energy and additional energy efficiency. Smart Grids are in focus of several international R&D past and present efforts. Smart grid systems can be part of world strategy to meet environmental and energy policy goals. There are many components to be considered such as renewable portfolio standards and energy efficiency programs. The driving forces behind the efforts on Smart Grids include (Demands of increased energy efficiency to meet the world goals, Demands of integrating new energy sources such as DER and DER in a massive way into generation and transmission of future energy systems, Establishment of a de-regulated customer oriented energy market, including new types of energy based service markets). The transition from today's mostly hierarchical power grids towards tomorrow´s Smart Grids poses several challenges to be properly addressed and harnessed.

The book contains four sections; Section-1 Energy Efficiency Improvements in Smart Grid Components - Monitoring, Management and Measures, Section-2 Energy Efficiency Improvements in Smart Grid Components - Intelligent Control System, Section-3 Energy Efficiency Improvements in Smart Grid Components - Optimization in Electrical Power System, Section-4 Energy Efficiency Improvements in Smart Grid Components - Recent Developments. Many authors with academic and industrial expertise in the field of the energy efficiency development that contributed to this book which will increase the knowledge and information in this topic for engineering, academics and students.

Section-1 Energy *Efficiency Improvements in Smart Grid Components - Monitoring, Management and Measures* - This section describes Wide Area Monitoring Systems in smart grid with management and measures techniques. Wide Area Monitoring System (WAMS) based on Frequency Disturbance Recorders (FDRs) as a family of the PMUs deployed on Power grid for mapping and visualization of all system parameters will be described. A compilation of several studies regarding systems that are able to report detailed information about the power consumption of a residence, discrediting the consumption of each appliance and providing information the households can rely on to change their behavior towards energy efficiency will be discussed. Both Traditional Load Monitoring systems and Non-Invasive Load Monitoring systems were cited as techniques able to provide this kind of information. The "smart home" concept is used to explain how domestic tasks can be atomized and new information technology is used to improve the management of the home. This chapter explores the feasibility of using interactive automated techniques for energy management in

homes powered by renewable technologies. A new conceptual scheme to organize and classify Energy Efficiency measures is defined, leading from the definition of Energy Cost per Product Unit and further breaking it up in order to identify and define all possible areas of intervention, providing for each of them a brief overview of possible measures and opportunities and a specific literature review.

Section-2 *Energy Efficiency Improvements in Smart Grid Components - Intelligent Control System* - This section presents different intelligent control system for energy efficiency in smart grid components. The development and implementation of simulation models for Distributed Energy Resources (DER) components in a distribution network, with focus on control strategies using active loads and energy storage systems for PV penetration will be given. The study will show the variability and the interaction between feeders, including Electric Vehicles (EV) and Vanadium Redox Battery (VRB), PV system and actively controlled devices. Many different types of voltage controllers have also been developed. This section will also presents a comparative study of different intelligent controllers; fuzzy logic controller, artificial neural networks and neuro-Fuzzy controller for maximum power tracking in various irradiation. This chapter will emphasize the best performance of some control system for speed witch, a good an increasing of step response and decrease of error. The developed work will concern the modeling of the PV pumping system components. In this section, the energy-related issues for EVs will be discussed in detail. The primary aim of this section is to give a clear and systematic understanding of the energy processing and control for EVs and to introduce some latest energy saving and optimal control technologies and present the key results regarding this area.

Section-3 *Energy Efficiency Improvements in Smart Grid Components - Optimization in Electrical Power System* - This section deals with optimization techniques in electrical power system. The hybrid optimization model for electrical renewable (HOMER) software is an optimization model, which can evaluate a range of equipment options over varying constraints and sensitivities to optimize power systems. The flexibility in the use of HOMER makes it useful in the evaluation of design issues in the planning and early decision-making phase of power projects. This section presents the use of HOME software in the analysis of a power system comprising a wind turbine, solar, photovoltaic, AC generator, converter, primary load and battery system. The Increasing in Energy Efficiency by Reducing Losses and Promoting Value Propositions in AC power systems is also given in the section. Reducing losses relates to the physical processes of generating, transmission and distribution of electric power will be discussed. Addressing the challenges of balancing are a very complex physical system in real time while meeting customers' expectations on energy and energy related reliable services is the core of the emerging Smart grid. In order to give perspectives on those societal challenges some technological as well as business and societal backgrounds will be illustrated by many suggested solutions with some implemented examples. Various optimization problems and solution such as heuristic methods namely: Improved Ant Colony Optimization (IACO) and Improved Biogeography-Based Optimization (IBBO) able to manage the combinatory and constrained optimization problems will be proposed. The impact study of the fault resistance and the series compensation degree values on the overcurrent and distance relays performances is carried out. The proposed IACO and IBBO show a high efficiency to solve such complex optimization problem, and ensure a good coordination of distance and overcurrent relays that improve the electrical protection system efficiency.

Section-4 *Energy Efficiency Improvements in Smart Grid Components - Recent Developments* - Many recent technologies development in the field of energy saving are appeared recently. Upon reviewing of the recent technology developments on the silicon material, cell device architecture and manufacturing processing for the silicon based solar cell, this section raises the prospective trends of solar industry driven by the global market demands. Light-emitting diodes (LEDs) are light sources that were developed in the last few decades. The basic function of an LED is to generate light following the injection of an electrical current into the semiconductor material. Quantum dot based LED is one types of light emitting diodes which we will investigate and analyze in this section As an emerging technology for environmental protection, there have been extensive researches on using non-thermal plasma (NTP) over the past 20 years. The major advantages of NTP technology include the moderate operation conditions (normal temperature and atmospheric pressure), moderate capital cost, compact system, easy operations and short residence times, Etc., compared to the conventional technologies) will be discussed.

Prof. M. M. Eissa
Faculty of Engineering at Helwan-Helwan University
Egypt

Section 1

Energy Efficiency Improvements in Smart Grid Components - Monitoring, Management and Measures

Chapter 1

Egyptian Wide Area Monitoring System (EWAMS) Based on Smart Grid System Solution

M.M. Eissa, Mahmoud M. Elmesalawy, Ahmed Soliman, Ahmed A. Shetaya and Mahmoud Shaban

Additional information is available at the end of the chapter

http://dx.doi.org/10.5772/60051

1. Introduction

Wide-area measurement systems (WAMS) in smart grid can be defined as a system that captures measurements in the power grid over a wide area and across traditional control boundaries, and then uses those measurements to improve grid stability and events through wide-area situational awareness and advanced analysis.Authors have achieved Wide Area Monitoring System (WAMS) based on Frequency Disturbance Recorders (FDRs) as a family of the PMUs deployed on Egyptian Power grid for mapping and visualization of all system parameters. The FDRs are deployed on live 220kV/500kV Egyptian grid system in cooperation with the Egyptian Electricity Transmission Company (EETC). The project is funded from the National Telecommunication Regulatory Authority (NTRA). The Egyptian Wide Area Monitoring System (EWAMS) achieved at the Helwan University can gather information from many FDR units geographically dispersed throughout the boundary of the Egyptian power grid and data manipulated at a data center contains many servers at Helwan University. The Synchrophasor system with wide deployment of using (FDRs) phasor measurement units and high-speed communications to deliver and collect synchronized high-speed grid operating data, along with analytics and other advanced on-line applications will improve real-time situational awareness and decision support tools to enhance system stability. The EWMS is a good environment for many applications that can help the EETC to enhance the Egyptian Grid. This manual Guide explains the remote access for the EWAMS established at Faculty of Engineering through the EETC. The access will be for displaying the FDRs' parameters with different configuration through web service.

The growing global population is driving an even greater increase in the demand for electricity. Added to this, governments around the world are focusing on reducing carbon dioxide (CO2) emissions by increasing the utilization of renewable energy sources in the power chain. Today, existing grids are under pressure to deliver the growing demand for power, as well as provide a stable and sustainable supply of electricity. These complex challenges are driving the evolution of smart grid technologies. The greatest future challenge is the integration with the renewable energy resources and controlling of it to reflect the best impact on the massive energy production [1].

Optimal use of ageing assets strategy is as much determined by economic factors as it is by technical issues. Factors such as obsolescence need to be considered when determining future needs. Increasingly companies are turning to risk based assessments to provide a holistic approach. Any Asset Strategy should be implemented and supported by a range of policies covering process safety, maintenance and inspection, renewal, and competence. The smart power transmission networks are conceptually built on the existing electric transmission infrastructure. However, the emergence of new technologies (e.g new materials, electronics, sensing, communication, computing, and signal processing) can help improve the power utilization, power quality, and system security and reliability, thus drive the development of a new framework architecture for transmission networks [2]. The traditional power grid is unidirectional in nature. Electricity is often generated at a few central power plants by electromechanical generators, primarily driven by the force of flowing water or heat engines fueled by chemical combustion or nuclear power. In order to take advantage of the economies of scale, the generating plants are usually quite large and located away from heavily populated areas. The generated electric power is stepped up to a higher voltage for transmission on the transmission grid. The transmission grid moves the power over long distances to substations. Upon arrival at a substation, the power will be stepped down from the transmission level voltage to a distribution level voltage. As the power exits the substation, it enters the distribution grid. Finally, upon arrival at the service location, the power is stepped down again from the distribution voltage to the required service voltage(s) [3]. Fig. 1 shows an example of the traditional power grid [4].

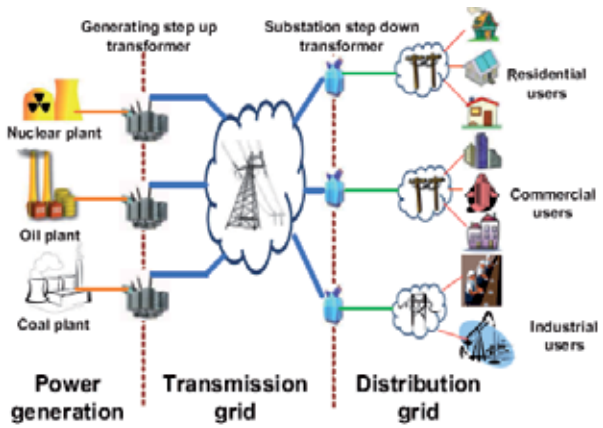

Figure 1. Traditional power grid [4].

http://dx.doi.org/10.5772/60051

The future grids can be regarded as an electric system that uses information, two-way, cyber-secure communication technologies, and computational intelligence in an integrated fashion across electricity generation, transmission, substations, distribution and consumption to achieve a system that is clean, safe, secure, reliable, resilient, efficient, and sustainable. This description covers the entire spectrum of the energy system from the generation to the end points of consumption of the electricity [5]-[6]. Fig. 2 shows a typical configuration for the future grid.

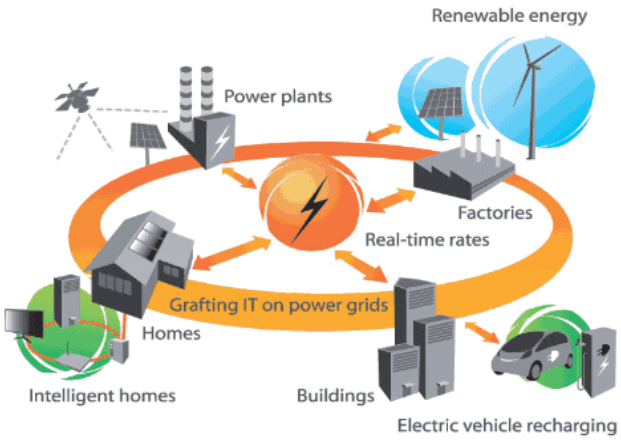

Figure 2. Future power grid [7].

The following Table 1 shows a comparison between the traditional and future power grid from different point of view.

Traditional power grid	Future power grid
Electromechanically	Digital
One way power flow	Multi-way power flow
One way communications	Multi-way communications
Few sensors	A lot of IED sensors
Low power quality	High power quality
Limited power flow control	Full power flow control (FACTS)
Manual monitoring	Self-wide area monitoring
Manual restoration	Self-Healing
Failures and blackouts	Adaptive and Islanding
Few consumer choice	Demand side management
No interconnected Renewable resources	Accept Renewable resources

Table 1. Comparison between Traditional and future power grid

2. EWAMS architecture

Egyptian Wide Area Monitoring System (EWAMS) is a 3G based wide area sensor network consisting of a special type of high precision family of the phasor measurement units (PMUs) and a central data management and processing system. EWAMS is a smart grid system designed to collect real-time synchronized frequency, voltage, and phase angle measurements at the transmission level 220kV/500kV of the power grid.

The structure of the EWAMS can be classified into five levels. The first level represents the placements of power stations on the power grid in which the sensors are installed. The second level contains the GPS enabled sensors that provide frequency, voltage magnitude, and voltage angle measurements. The third level is the communication infrastructure that provides the integrated wide area communication media for data measurements transmission. The fourth level is the remote data management and processing center that provides data gathering, storage, web service, post-disturbance analysis and other information management functions. The last level is the secure remote access connection for different EETC sectors and other remote clients. The following Figure shows the EWAMS architecture deployed for the Egyptian power grid. In order to discuss the unique characteristics of the EWAMS, the main building blocks of the EWAMS are discussed in more details in the following subsections.

The TCP and IP headers have numerous fields that are used to support the intended TCP and IP functionality as shown in Figure 6(a). In the proposed wide area measurement system, IP is used for delivering the different measurements collected by FDRs distributed over a wide area to the correct Data Concentrator Server (DCS) located at DMS while TCP is used to provide a reliable communication channels between FDR devices and the DCS.

The TCP connection between each FDR and the DCS is established through a three-way handshake process, ensuring that both FDR and DCS have an unambiguous understanding of the sequence number space. The operation of the connection is as follows:

a. The FDR sends the DCS an initial sequence number to the predefined destination port, using a SYN packet.

b. The DCS responds with an ACK of the initial sequence number and the initial sequence number of the FDR in a response SYN packet.

c. The FDR responds with an ACK of this DCS sequence number.

d. The connection is opened.

The operation of this algorithm is shown in following Figure. The performance implication of this protocol exchange is that it takes one and a half round-trip times (RTTs) for each FDR and DCS to synchronize state before any data can be sent. After the connection has been established, the TCP protocol manages the reliable exchange of data between FDRs and DCS. The existing UMTS mobile communication infrastructure is used to provide Internet access connection for FDRs. High speed packet access (HSPA) USB modems connected to 3G routers are used to provide the Internet access connection. Client server model is used to provide the communi-

http://dx.doi.org/10.5772/60051

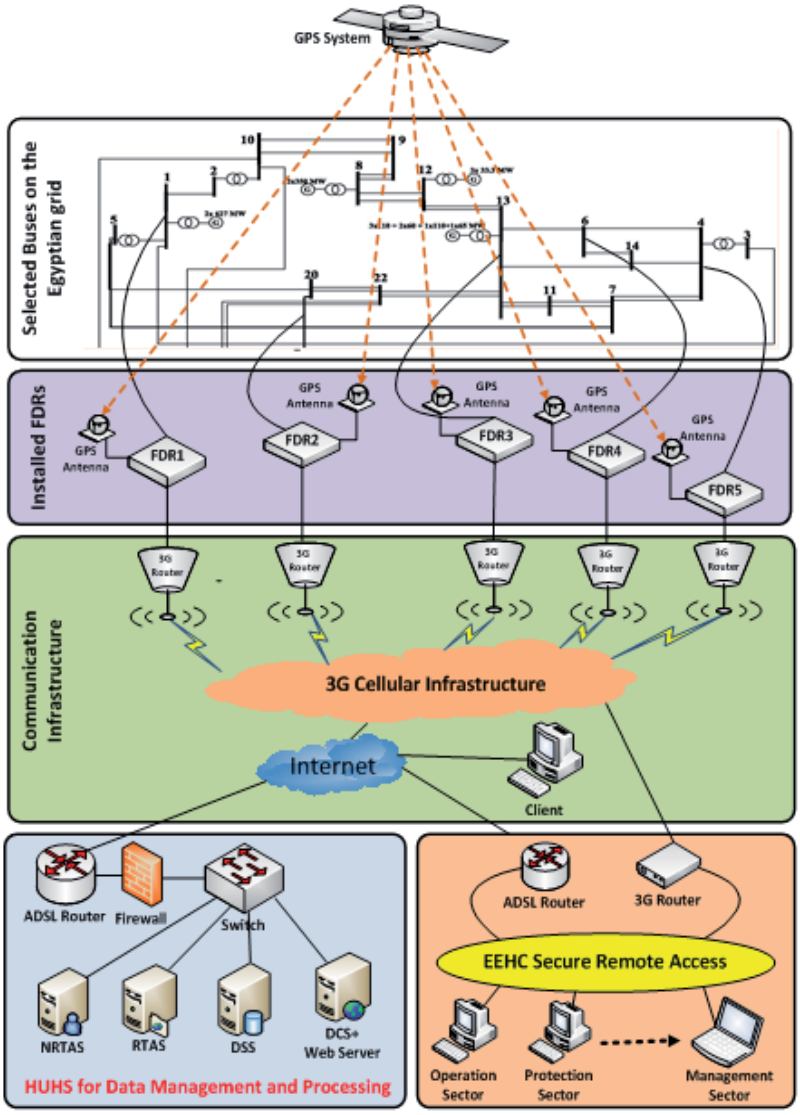

Sheme 1. EWAMS Architecture.

cation between FDRs devices and DCS server. Each FDR device is act as a client and requesting to make a connection with the DCS server. The measurements data is transmitted from FDRs devices to the DCS server using a standard network protocols, Transmission Control Protocol (TCP)/Internet Protocol (IP).

a. EWAMS Sensors (FDRs)

In EWAMS, the FDR is especially designed and implemented to have two power inputs. The first one is the single phase voltage (57.73VAC) which is taken from the 220/500 kV voltage

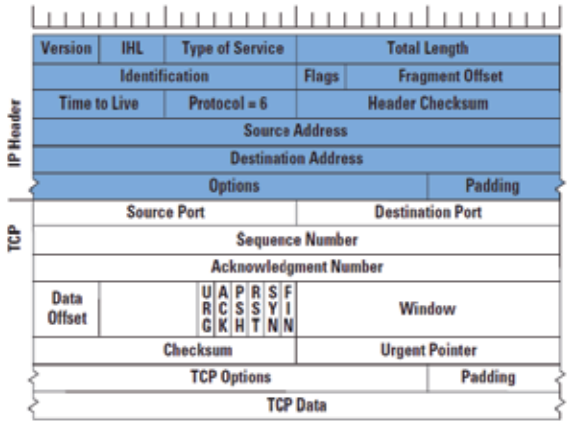

Sheme 2. The TCP/IP Datagram.

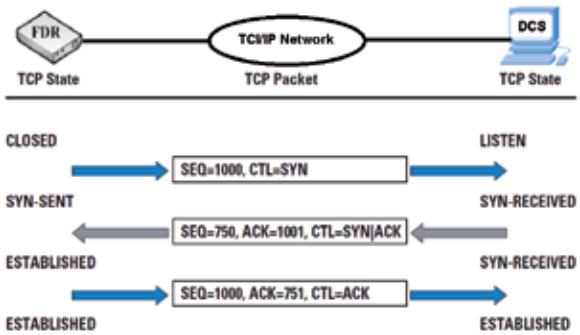

Sheme 3. TCP Connection establishment between FDR and DCS.

transformer output in each power station and is used for estimating the three required parameters (frequency, voltage magnitude, and voltage angle). The other input is 220 VAC from power outlet which is used to supply the FDR device with the required power for its electronic circuit operation.

b. Communication Infrastructure for EWAMS

In EWAMS, FDR devices are distributed over a wide area, covering various locations within the boundary of the power system. The FDR devices are then connected to the remote data center through communication network. Public telecommunication infrastructure (Internet) will be used to provide the communication channels between FDRs and the data concentrator server (DCS) in the data center. The Data Concentrator Server (DCS) located at the Egyptian Wide Area Monitoring System "EWAMS" hosted at Helwan University. Transmission Control Protocol/Internet Protocol (TCP/IP) is used in building the system. The TCP connection between each FDR and the DSC is established through a three-way handshake process, ensuring that both FDR and DSC have an unambiguous understanding of the sequence

http://dx.doi.org/10.5772/60051

number space. The FDR sends the DSC an initial sequence number to the predefined destination port, using a SYN packet. The FDRs transmits their measurements over the Internet to the DCS using the standard Internet Protocol suite TCP/IP. Since, the Internet Protocol doesn't guarantee any quality of service which it provides best effort delivery for data packets. The missed data at the DCS is expected as a result of a number of factors including packet drop due to network congestion, buffer overflow at the FDR or DCS, and corrupted packets rejected in-transit or faulty networking hardware.

3. Helwan University Host Servers (HUHS)

The HUHS is data management and processing center operated by several dedicated servers. The logic behind decomposing the HUHS to several numbers of servers is to distribute the computation power which had the advantage of increasing the systems redundancy and reliability. The HUHS consists of four servers connected together through local area Network (LAN). HUHS can divided in terms of functionality to four servers, the data concentrator server (DCS), the real-time application server (RTAS), the Non-Real-time application server (NRTAS), the web server, and the data storage server (DSS). The main functions of each server are described below.

4. EWAMS capabilities

EWAMS includes many applications in real time mode. The system includes real time situational awareness in different mode for displaying different parameters. The EWAMS system includes also many vital applications. The different software EWAMS capabilities are summarized in four main applications, see Figure 3.

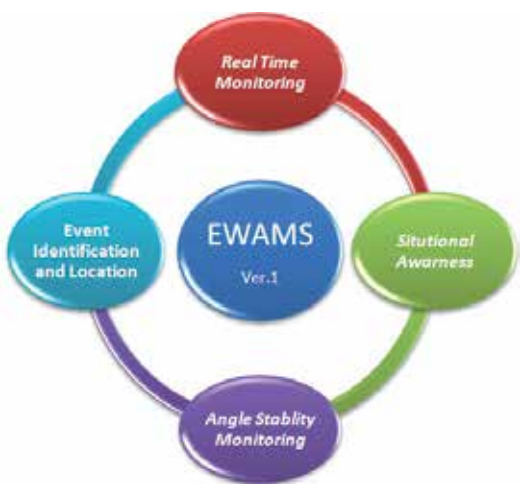

Figure 3. The four different applications in the EWAMS.

a. Real Time Monitoring

In this application, the system introduces the features of the real time monitoring. In this step, the EWAMS system displays many measurements as trends. All measurements are synchronized at same time using GPS timing system.

b. Real Time Situational Awareness

In this application, the system introduces the features of the real time situational awareness. The situational awareness application will display many measurements in color mapping way on the Single Line Diagram of the Egyptian power grid that help the operator in taking decisions in real time in case of situational awareness issued from one screen.

c. Real Time Stability Monitoring

The most effect way to predict the grid operating state is "the real time angle stability monitoring". In this application, the angles of the monitored buses reflect the state of the areas of the angles on the Egyptian grid to indicate any alerts during the angle divergence. This application will give the operator complete image about the state of the system to take fast actions.

d. Event Identification

The EWAMS system has the ability to detect events and define its type either generator tripping or load shedding. It also estimates the mismatch power amount that rejected from the grid and defines the area of the event. The measurements during this event could be visualized at any time and date for current event or any another historical events. This study partially completed and under construction now for remote access.

e. Historical Data

One feature of the EWAMS system is the possibility to access at any time and date for getting historical data. This data facility introduces transient analysis for any historical events on the grid, planning for future work on the grid through parameters monitoring, forecasting analysis, etc. This features as a remote access is under the construction but it is available on the EWAMS.

4.1. Main Features of the Real time monitoring and situational awareness

- The frequency mapping will define the islanded areas and how it effects on the rest of the grid.
- The angle mapping will define the oscillated areas and also shows the weakness area on the grid.
- The voltage mapping will define the most loaded area to help in load shedding selection criteria.

http://dx.doi.org/10.5772/60051

4.2. Procedures Steps for EWAMS Accessing

This part explains in more details an explanation for the operator about the possibility of EWAMS access.

In the welcome page the user will first go to the main menu through the following page

1. Open your internet browser using Internet Explorer, Chrome or Firefox...etc.
2. Enter the main webpage has following Internet Link in the browser
3. Write the Username and Password in space fields.
4. Press Login Button and then the program webpage is displayed

Figure 4 shows the main menu.

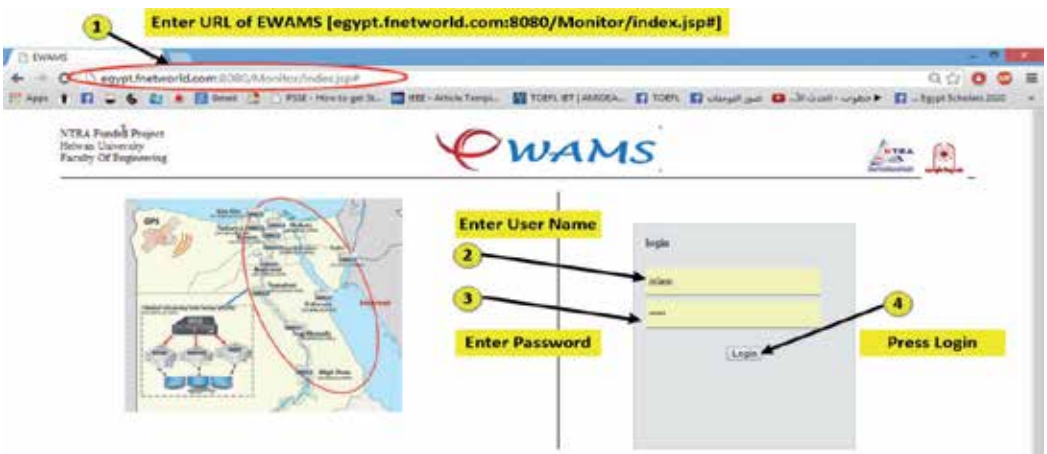

Figure 4. Main menu.

a. Accessing the "MAIN MENU" of the EWAMS

After logging in, the system will go to the monitoring menu. Figure 5 shows the EWAMS software system. As shown in the figure the menu contains:

Vertical Menu that contains:

- **Trends**
- **Maps**
- **SLD**
- **Applications**

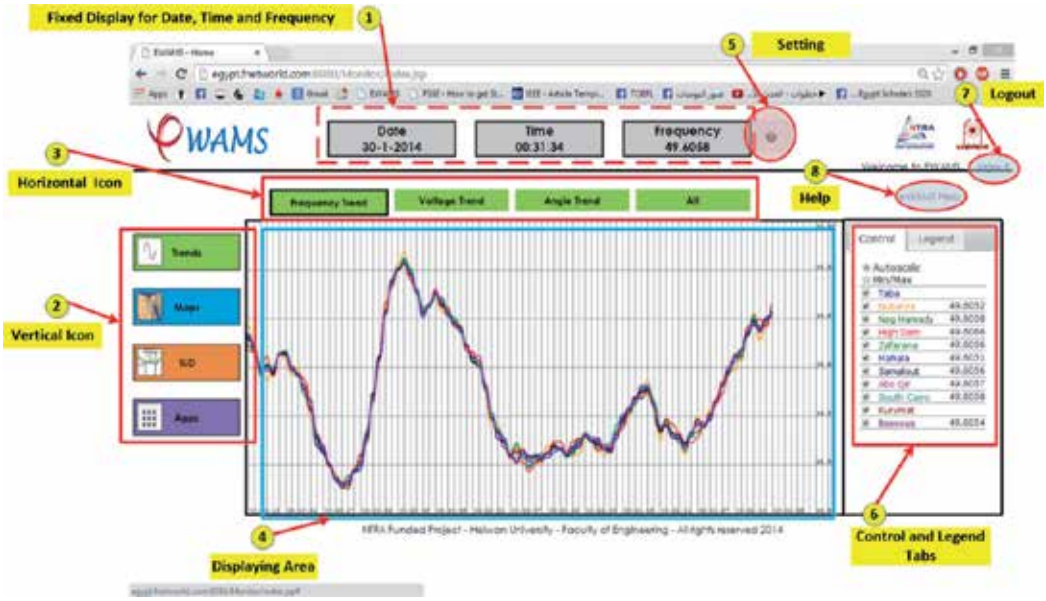

Figure 5. The main menu of the EWAMS system.

Trends: are used for displaying the frequency, voltage, phase angles and all trends of the system in trends mode.

Maps: are used to display the mapping of the system parameters on the Egyptian map in MAP MODE

SLD: is used to display the system parameters on a single line diagram of the Egyptian grid

Applications: are used for displaying the "real time stability monitoring".

Figure 5 shows the horizontal menu. This menu appears based on the vertical menu.

Figure 5 shows also the three displaying menu for the Date, Time and Frequency of the HIGH dam that taken as the reference for the system.

In Figure 5, the right hand side of the main menu there are two tabs; "control" and "legend". The control tab displays a list of the FDR stations, and the corresponding frequency readings. There is the option to select the FDR stations and their readings. Also, there is a tab with "legend" that displays the color bar ranges of the frequency or angle. This tab will appear only in the "SLD" and "MAPs" on the vertical menu. Figure 5 shows also the "setting icon" that uses for selecting the reference frequency for displaying it on the vertical icons. It also used for determine the max and min frequency thresholds.

b. Accessing "TRENDS"

This part will deal with "real time monitoring". Figure 6 shows the EWAMS system, when the operator wants to access the "Trends", he just clicks on the "Trends" icon". After clicking, a

http://dx.doi.org/10.5772/60051

horizontal menu will be appeared that displays four icons "Frequency Trends", "Voltage Trends", "Angle Trends", and "All". Every icon will display the trends of the parameters located. Figure 6 shows also the frequency trends that will come from "Frequency Trends" icon in the horizontal mode.

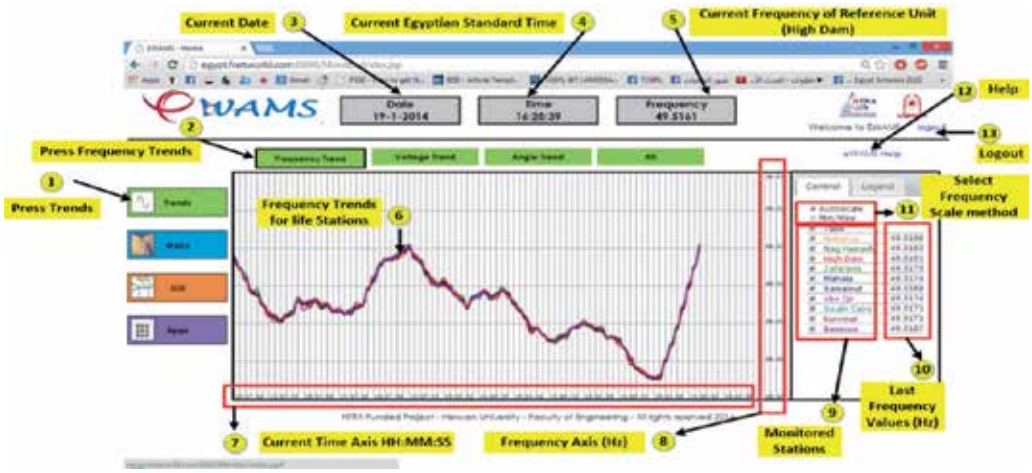

Figure 6. Accessing trends through EWAMS.

Figure 7 shows the voltage trends, which will come after clicking the "Voltage Trend" in the horizontal menu. Figure 8 shows the angle trends that come from the clicking on the "Voltage Trends" in the horizontal menu. Figure 9 shows the all trends that come by pressing on "all" tab.

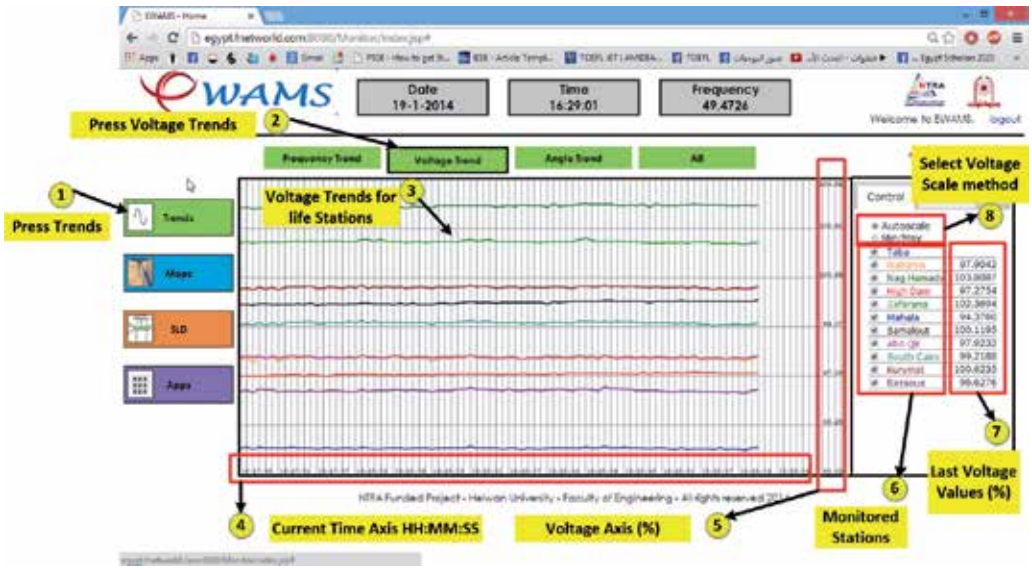

Figure 7. The voltage trends.

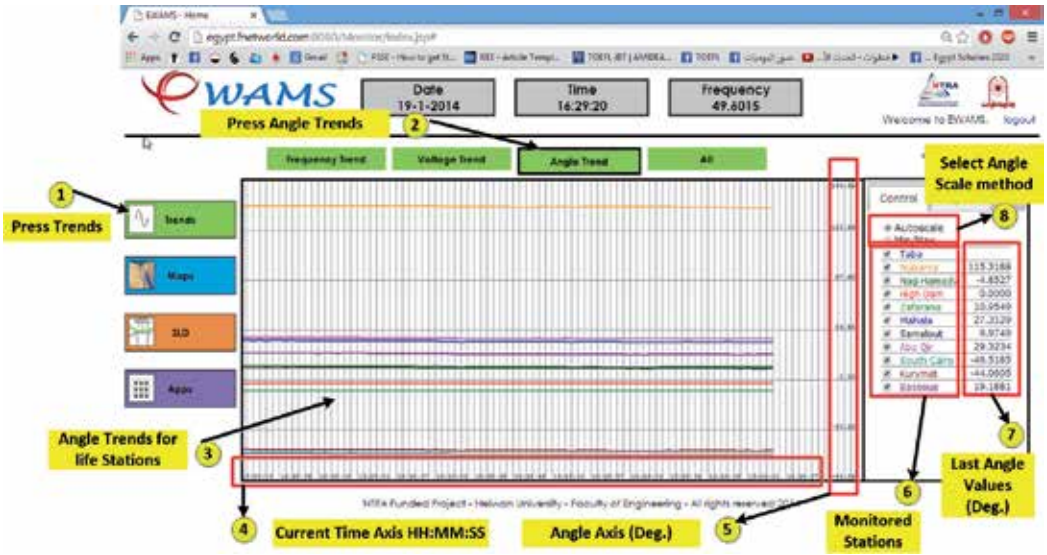

Figure 8. The voltage trends.

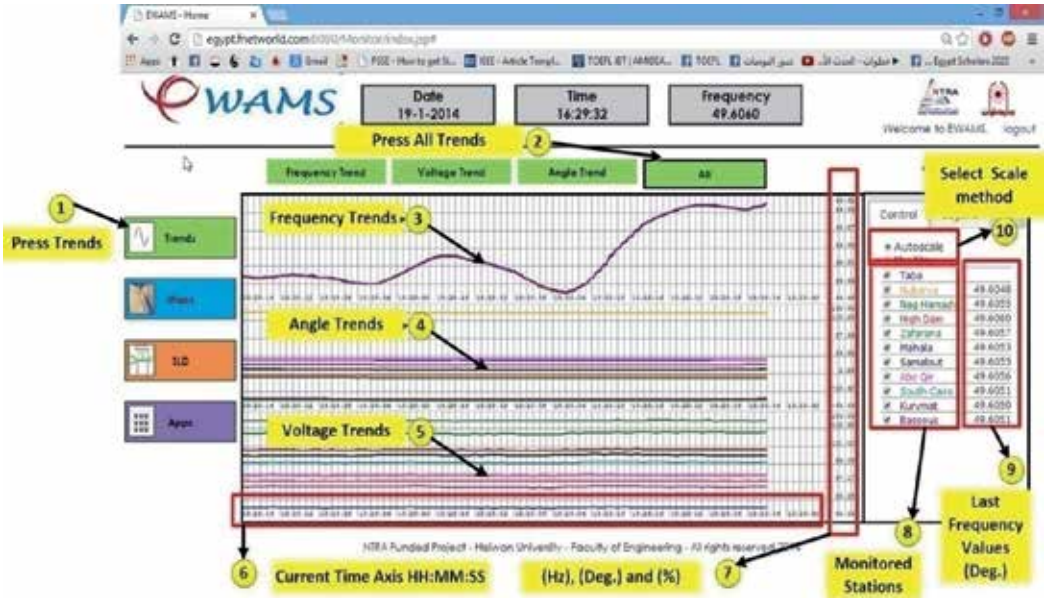

Figure 9. All trends.

Figure 8 shows the right hand list of the control icon. In this list all FDR with their values will be appeared. There is the option to select the displayed FDR stations.

http://dx.doi.org/10.5772/60051

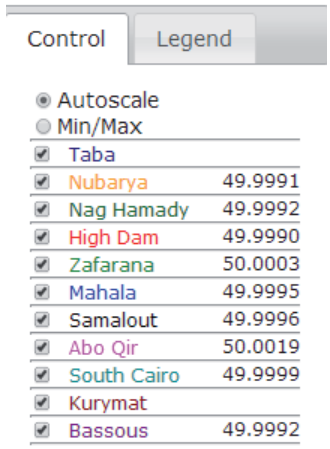

Figure 10. Control legend.

c. Accessing "MAPS"

This part will deal with "Real Time Awareness". In this tab the frequency, angle and voltage will be displayed on a Map. To access this application the user must follow these steps:

To display Situational awareness by frequency, press "Maps" Tab, then press "Frequency Map" Tab given on the horizontal bar. Figure 13 shows the "Maps" and "Frequency map" for the frequency displaying. And so on for the "Voltage Map" and "Angle Map". On the right hand side a color code for the frequency readings that corresponding FDRs.

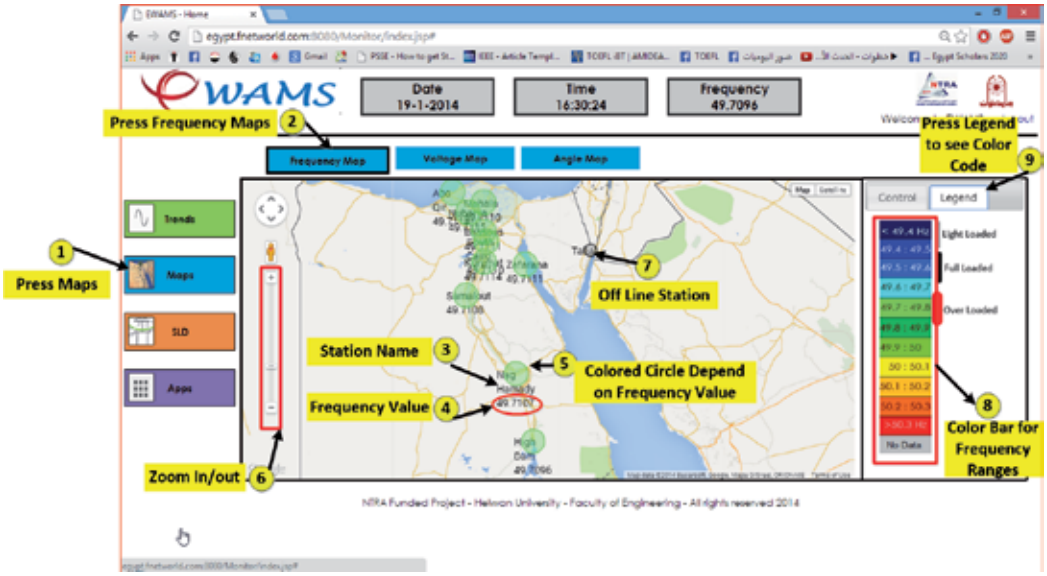

Figure 11. MAPS menu for the frequency displaying.

The FDR data can be used to enhance grid reliability for both real-time operations and offline planning applications [11]-[14], as listed below; the benefits of achieving such system will assist in:

- Wide-area situational awareness
- Real-time operations applications
- Frequency stability monitoring and trending
- Power oscillation monitoring
- Voltage monitoring and trending
- Alarming and setting system operating limits, event detection and avoidance
- Resource integration
- State estimation
- Dynamic line ratings and congestion management
- Outage restoration
- Operations planning

5. Conclusion

Wide Area Monitoring System on real 220kV/500kV Egyptian grid is achieved in cooperation with the Egyptian Electricity Holding Company in installing the devices. The EWAMS concerns the pioneers in the field of the smart grid wide area monitoring system. This system is a part of Smart grid system through transmission levels. On-line monitoring for different parameters is achieved. Many of new applications such as EWAMS Mapping and Visualization, Real time event detection and identification, Angle stability monitoring are applied based on remote access at the EETC. The system can satisfy many of the features for the Egyptian grid as Improved power system operation, Better use of existing equipment, Increased power transmission capacity, Lowered risks of power system instabilities, Improved power system planning, Less outage power and time, capability of integration renewable recourses, analysis and investigating many post-events.

Acknowledgements

The authors gratefully acknowledge funding and support from **National Telecom Regulatory Authority (NTRA)**, Egypt (http://www.ntra.gov.eg) to implement the network architecture proposed in this work. Also, I would like to thank Egyptian Electricity Transmission Company

(EETC) for help in implementing the FDRs devices on real system. More details about the project progress can be followed on (www.helwan-ntra.com).

Special thanks for Prof. Yilu Liu (UT/ORNL Governor's Chair Professor_ University of Tennessee), USA and Prof. Hossam Gaber (University of Ontario Institute of Technology, UOIT), Canada

Author details

M.M. Eissa[1*], Mahmoud M. Elmesalawy[2], Ahmed Soliman[2], Ahmed A. Shetaya[1] and Mahmoud Shaban[1]

*Address all correspondence to: mmmeissa@hotmail.com

1 Department of Electrical Engineering, Faculty of Engineering - Helwan University, Cairo, Egypt

2 Department of Electronics, Communications, and Computer Engineering, Faculty of Engineering - Helwan University, Cairo, Egypt

This work is related to the Faculty of Engineering at Helwan, Helwan University and Funded from the NTRA (National Telecom Regulatory Authority). It is outcome from the project titled by “Smart Grid Frequency Monitoring Network Architecture and Applications”. PI of the Project, Prof. Moustafa Mohammed Eissa (01003562971) – email: mmmeissa@hotmail.com

References

[1] PSGuarde, Improved Power System Performance through Wide Area Monitoring, Protection and Control, ABB, 2004.

[2] A. Bose. Smart transmission grid applications and their supporting infrastructure. IEEE Transcations on Smart Grid, 1(1):11–19, 2010.

[3] H. Farhangi., The path of the smart grid. IEEE Power and Energy Magazine, 8(1):18–28, 2010.

[4] Fang, Xi; Misra, Satyajayant; Xue, Guoliang; Yang, Dejun, "Smart Grid — The New and Improved Power Grid: A Survey," Communications Surveys & Tutorials, IEEE, vol.14, no.4, pp.944,980, Fourth Quarter 2012.

[5] Office of electricity delivery and energy reliability “Smart grid”, Internet: http://www.oe.energy.gov/ smartgrid.htm, Accessed: August 2009.

[6] Saint B, " Rural distribution system planning using Smart Grid Technologies", IEEE Rural Electric Power Conference, REPC '09, Page(s):B3 - B3-8, April 2009.

[7] Miroslav M. Begovic," Smart Grid R&D Perspectives from the US" 3rd IEEE PES ISGT Europe, Berlin, Germany, October 14 -17, 2012.

[8] M.D. Hadley; J.B. McBride; T.W. Edgar; L.R. O'Neil; J.D. Johnson, "Securing Wide Area Measurement Systems", U.S. Department of Energy, Office of Electricity Delivery and Energy Reliability, june 2006.

[9] Jian Zuo, "The Frequency Monitor Network (FNET) Design and Situation Awareness Algorithm Development", Doctor of Philosophy, Blacksburg, Virginia U.S.A, March 2008.

[10] Lang Chen; Markham, P.N.; Yilu Liu, "Wide-area dynamic model validation using FNET measurements," Innovative Smart Grid Technologies (ISGT), 2012 IEEE PES, vol., no., pp.1,7, 16-20 Jan. 2012.

[11] M.M. Eissa, Yilu Liu, Mahmoud M. Elmesalawy, and Hossam Gabbar, "Wide Area Synchronized Frequency Measurement System with Secure Communication infrastructure for 500kV/220kV Egyptian Grid", IEEE International Conference on Smart Grid Engineering (SGE'12)-27-29 August, 2012-UOIT, Oshawa, Canada.

[12] M.M. Eissa, Mahmoud M. Elmesalawy, Ahmed A. Shetaya, Ahmed H. Soliman, "Monitoring and Novel Applications of 220kV/500kV Egyptian Grid Parameters Using family of PMU based WAMS " 3rd international workshop for sustainable energy for all "transforming commitments to action", 22-24 February 2014, Christ university, Kengeri, India.

[13] Elmesalawy, M.M.; Eissa, M.M., "New Forensic ENF Reference Database for Media Recording Authentication Based on Harmony Search Technique Using GIS and Wide Area Frequency Measurements," Information Forensics and Security, IEEE Transactions on, vol.9, no.4, pp.633,644, April 2014.

[14] Moxley, R., Zweigle, G., Al-Mahrouq, A.: 'Wide-area measurements to improve generator and system modeling'. Innovative Smart Grid Technologies—Middle East (ISGT Middle East), 2011 IEEE PES Conf., 17–20 December 2011, pp. 1–7.

[15] M.M. Eissa, Wael M. Fayek, Marwa M.A. Hadhoud, Mahmoud M. Elmesalawy, Ahmed A. Shetaya "Frequency/voltage wide-area measurements over transmission control protocol/internet protocol communication network for generator trip identification concerning missed data", IET Generation, Transmission & Distribution, 2014, vol. 8, no.2, pp. 290 – 300.

[16] http://www.3gpp.org/technologies/keywords acronyms/99-hspa.

[17] M.M. Eissa, Yilu Liu, Mahmoud M. Elmesalawy, and HossamGabbar, "Wide Area Synchronized Frequency Measurement System with Secure Communication infra-

http://dx.doi.org/10.5772/60051

structure for 500kV/220kV Egyptian Grid", IEEE International Conference on Smart Grid Engineering (SGE'12)-27-29 August, 2012-UOIT, Oshawa, Canada.

[18] M.M. Eissa, Mahmoud M. Elmesalawy, Ahmed A. Shetaya, "Smart Grid Frequency System on 220kV/500kV Egyptian Grid – Architecture and application" IAC 2014 International Conference on Industry Academia Collaboration, 3-5 March Fairmont Heliopolis Cairo-Egypt.

Chapter 2

Focus on Energy Efficiency Through Power Consumption Disaggregation

Rodrigo M. Bacurau, Luís F. C. Duarte and
Elnatan C. Ferreira

Additional information is available at the end of the chapter

http://dx.doi.org/10.5772/59311

1. Introduction

According to the American Council for an Energy-Efficient Economy – ACEEE, the worldwide energy consumption increases around 1% per year [1]. This is a worrying fact, since 80-90% of this energy is generated from non-renewable resources [2].

Utilities and government agencies all around the world have been implementing energy efficiency programs over the last thirty years (most significantly in the last decade) in a way to minimize depletion of resources and mitigate environmental impact.

According to [1] the cost of promoting energy efficient programs is about one third of the cost to generate the same amount of energy saved by these programs. Besides the environmental benefits, these programs also culminate in economic profits such as reducing the cost of energy generation, resulting benefits both for utilities and their customers.

An assortment of information technologies, that includes smart meters, is quickly becoming part of these programs [3]. Although those devices do not improve energy efficiency on their own, they are responsible for providing information on ways the household can reduce energy waste and improve energy savings in energy efficiency programs.

It has been shown that the effectiveness of an energy efficiency program depends strongly on the feedback that the consumers receive about their energy use. A good knowledge of where the energy is going is fundamental for the customers to decide how it is possible to reduce energy waste and to maximize energy savings. This fact was confirmed by a research conducted during 15 years (1995-2010) in several countries by ACEEE. The result indicates that the more detailed is the information that the users receive about their energy consumption,

the more significant the savings are. A better understanding of where (which device) and when (which period of the day) the energy is being used leads both to reduction of energy consumption and shift the energy consumption from peak periods to off-peak periods [4].

Recent studies have been shown that the most significant savings are achieved by providing to the households real-time information of how much energy each appliance is consuming. That can lead them to reach savings up to 19.5%, with average of 3.8% [1].

Over the last 30 years, researches all around the world has been developing systems, methodologies and algorithms to disaggregate the total energy consumption in order to assist the people on how to increase energy efficiency.

In recent years, several companies have created smart metering solutions that allow discrimination of power consumption and nowadays companies such as myEragy Energy Monitoring, Opower Home Energy Report, Open Energy Monitor, People Power, Smart Energy Groups, ThingSpeak, among others are offering services of smart metering.

(a) (b)

Figure 1. (a) myEragy Energy Monitoring and (b) Open Energy Monitor

These services allow the user to track their residential energy consumption, generate consumption reports and receive information on how they can save energy, but, as for now, despite the wealth of information offered by these services, none informs the individual amount of power consumed by every single appliance in a residence.

Detailed energy consumption information is not only important for customers but for energy service companies (ESCOs) as well. It can be used to resourcefully manage the supply-demand chain and accurately forecast the needs of investments in distribution systems.

Despite the variety of techniques and technologies used, the energy consumption monitoring systems can be divided in two main groups: Plug Level or Decentralized Load Monitoring Systems and Non-Intrusive Load Monitoring (NILM) Systems.

This chapter presents the major concepts of power consumption disaggregation techniques, given special attention to Non-Intrusive Load Monitoring Systems and the concept of Load Signature.

http://dx.doi.org/10.5772/59311

2. Plug level load monitoring

Plug Level Load Monitoring Systems, Decentralized Load Monitoring Systems, Intrusive Load Monitoring Systems or even Traditional Load Monitoring Systems are the names given to systems in which the power consumption of an appliance is individually measured by a smart meter that connects the appliance to the power outlet. The Plug Level Load Monitoring terminology was chosen to designate this section since the term itself properly illustrates the whole concept.

In this approach, each meter is able to monitor only one appliance at a time; thus, the use on every single appliance in a building turns to be extremely costly to install and maintain, although it is able to precisely provide the power consumption of each monitored load.

It is possibly the simplest way to gather information of the power consumption of an appliance on its own. Yet, this approach can still be a good option in cases where the information regarding the power consumption of a building doesn't need to be exceptionally detailed and/or when focusing on the power consumption of only a few targeted loads aggregates enough information for the household.

There are many power meters for plug level load monitoring available in the market. Even though the majority of these meters only present the power consumption of the monitored appliance on a LCD display, models like "Watts up? Pro" [5] can record the power consumption over time and then send the data to a computer via USB, while other models like "Watts up?.Net" [6] allow the recorded data to be reached via wired Internet. There are also models that send the data wirelessly to a central device that shows the information on a LCD display, like the "Kill A Watt CO2 Wireless" [7], and even make the information available to a computer wirelessly connected via Wi-Fi, like the "Ecobee Smart Plug" [8].

(a) (b) (c) (d)

Figure 2. (a) Watts up? Pro, (b) Watts up?.Net, (c) Kill A Watt CO2 Wireless and (d) Ecobee Smart Plug.

Researches in this field show that different types of Wireless Sensors Network (WSN) can be used to improve plug level load monitoring. It facilitates the data retrieve process, saves time and eliminates reading errors. The most used wireless communication protocol in this area is the ZigBee /IEEE 802.15.4, followed by Wi-Fi/IEEE 802.11; notwithstanding, hybrid networks can also be found in the literature as presented by [9] in which the use of ZigBee along with Power Line Communications (PLC) is shown.

In the end of the process, regardless of the communication method adopted to retrieve the information from the sensors, a computer application is used to process the data and report it to the user.

3. Non-intrusive load monitoring

Non-Intrusive Load Monitoring (NILM) is a term widely spread in the literature to address systems that are able to quantify the energy consumption of more than one appliance by measuring the power consumption at the utility service entrance or at the circuit box. It is also known as Non-Intrusive Appliance Load Monitoring (NALM / NIALM). The terminology comes from the fact that no access to the individual components is necessary for installing sensors or making measurements [10]. Since the technique uses only one power meter at the entrance or just a few power meters after the circuit breaks it is also called Centralized Load Monitoring and Building Level/Circuit Level Load Monitoring.

This approach is in general cheaper and easier to install and maintain than the intrusive ones [11-14]. However, NILM systems are, for now, unable to identify the power consumption of loads that exhibit non-discrete changes in the power and larger oscillations in the steady state, as some fluorescent lamps, refrigerators, AC variable speed drivers and other non-linear loads [15].

NILM systems perform the power consumption disaggregation based on the concept of load signature. Load signature consists in a set of characteristics regarding its electrical consumption behavior that are unique for each load. Almost all electrical parameters derived from voltage and current waveforms can be considered load signatures. Active power, reactive power, apparent power, power factor, rms voltage, rms current are the most commonly used parameters adopted to distinguish the loads. These parameters can be represented in the time domain, in the frequency domain, or even mathematically in terms of wavelets and, eigenvalues or singular value decomposition (SVD). Since every load has got a distinct electrical characteristic, by measuring and comparing these parameters, the system is able to recognize the loads in the circuit.

Regardless of the method used to represent the signatures, the recognition algorithm can operate considering the transient characteristics (the period of time in which the load is turned on or off), the steady state characteristics, or a combination of both.

The first NILM system was proposed in the 80's by MIT researchers [10]. Although the simplicity of the proposal compared to recent works, it is quite useful for exemplifying the use

http://dx.doi.org/10.5772/59311

of load signatures in load identification. In the developed technique, the operating schedules of individual loads were determined by identifying the instants where the power consumption changed from one steady state to another. These steady-state changes, known as events, correspond to the load either being turning on or off, and can be characterized by the magnitude and sign of active and reactive power values. In this approach, only the steady state brings the useful information and therefore the transients are eliminated in the analysis. A database of the operating schedules of each load must be obtained prior to the load identification. Figure 3 shows the power consumption curves of a refrigerator and a microwave oven, where two distinct signatures are overlapped. Knowing the frequency of each on and/off event and the magnitude of the power steps it is possible to identify when the refrigerator and the microwave oven are on in each instant and consequently determine the total energy consumption of each one.

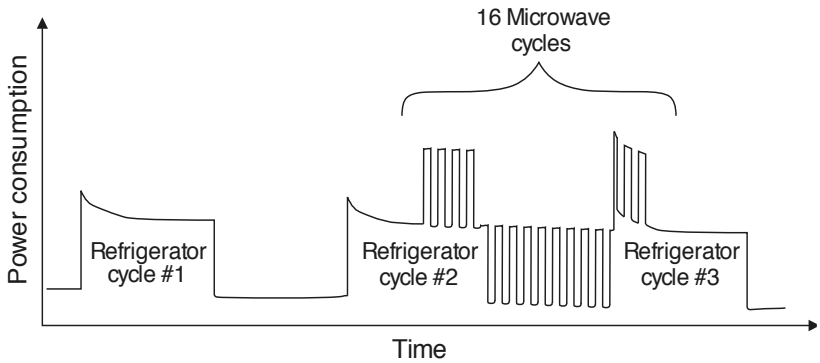

Figure 3. Characteristic signatures of a refrigerator and a microwave measured on the same circuit [16].

This method does not allow load identification in several cases: (i) when there are loads that overlap ambiguously in the ΔP-ΔQ plane, (ii) when two or more loads are switched on/off simultaneously, (iii) when the load is switched on/off faster than the power meters can capture the steady-state, and (iv) when a new appliance, not referenced in the database, is used [17].

In the 90's researchers introduced transient event detection to non-intrusive load monitoring. The MIT PhD thesis defended in 1993 [11] proposed a prototype of a multiscale event detector for residential NILM implemented in a digital signal processor. This system uses transient characteristics in the real and reactive power signature space to differentiate the loads. The paper in [18] presents a NILM for commercial buildings based on steady-state and transient load-detection algorithms. The developed prototype is able to differentiate appliances with near-simultaneous start-ups and similar power levels. Other techniques for load disaggregation based on transient were later proposed in [15, 19-21].

Researchers presented in 2000 the first approach for load identification using the harmonic content [15]. In this paper, they proposed a NILM system for three-phase environment that uses the first eight odd harmonics of the current signal of the loads both in transient and steady-state. Other proposes of systems that use harmonic features are presented in [14, 19, 22-25].

According to [17], harmonic analysis is very useful to distinguish loads that ambiguously overlap in the ΔP-ΔQ plane, suitable for non-linear loads identification.

In 2010 researchers presented a NILM system installed in the electrical panel after the circuit breakers that makes use of one power meter per electric circuit [26]. This method minimizes the number of loads the power meter has got to discriminate, facilitating the process of load recognition. This system also makes uses Bayesian network in order to take in account the user behavior in the recognition process. Another NILM system based on measurement at circuit level was proposed in [27]. The hardware of this system is composed basically of energy meter ICs that are responsible to acquire the electrical information from the circuits and a microcontroller used to send the collected data to the clouds. Embedded firmware running in the microcontroller performs the load identification and presents the amount of energy consumed by each appliance in web pages.

4. Electrical parameters used to define load signatures in NILM systems

Many papers presenting novel NILM systems [14, 19] and load identification algorithms [23, 28-32] have been published. However, none presents a detailed study about which electrical parameters derived from voltage and current curves are adequate for load identification.

The researchers diverge regarding which parameters are the best for load disaggregation. Most use the active power and current for defining load signatures, some use reactive power [13, 14, 22, 23, 29] other use power factor [27] and harmonic components in the current signal [14, 15, 19, 22-25, 30].

The choice of which electrical parameters are used to define load signature is a critical factor in the performance of NILM systems. The use of just a few parameters can reduce the accuracy on the load identification, particularly for complex loads such as computers, refrigerators, etc. On the other hand, the use of numerous parameters requires more complex algorithms and therefore more computational power. Since most of the NILM systems are designed as embedded systems with low power microcontrollers/DSP, the computational complexity to calculate the electrical parameters is a limiting factor for the development of these systems.

An electrical parameter suitable for defining load signatures has two basic characteristics: it presents quite different values for different appliances and gives repeated values for the same device at same operational condition. Preferably, these parameters should be obtained by simple operations requiring few computational resources to be calculated.

The analysis in the frequency domain for residential loads identification has been shown promising. However, there is no consensus regarding which harmonics are the best for this purpose. In [15] and [23] the authors used the first eight odd harmonics, in [18] the sixteen first even and odd harmonics were used, whereas in [14] only the 2^{nd} and 3^{rd} harmonics were taken in account. Considering the relatively high computational cost of the algorithms used to calculate the Discrete Fourier Transform (FFT, Goertzel, etc.), the calculation of many harmonic

http://dx.doi.org/10.5772/59311

components in real-time may become impractical. Moreover, the use of too few harmonic components can hinder the load identification process.

Recent studies conducted by the Department of Semiconductors, Instruments and Photonics of the School of Electrical and Computer Engineering, at the University of Campinas, indicate the active power, reactive power, power factor, rms voltage, rms current and the odd harmonics of the current signal are good parameters to be used in NILM systems. These studies also concluded that the most useful information in the frequency domain for load identification is in the first five odd harmonics of the current signal [33].

5. Smart meters for NILM systems

The NILM systems are composed of two basic components: the measuring module (smart meter) and the load discrimination algorithm. The data acquired by the smart meters is sent to the discrimination algorithm that performs the energy breakdown based on the principle of load signature.

The smart meter is a critical part of the NILM systems since an accurate measurement of the electrical parameters needed for NILM systems is essential for their performance [30].

A number of equipment can be used for measuring the electrical parameters used in NILM systems. In [21] the author used an oscilloscope to sample the voltage and current curves and post process them using a Matlab script. In [31] commercial electronic power meters were used to obtain the active power. In [23], a harmonic analyzer was used for acquiring the harmonic components of the current signal. In [5], a three-phase power quality recorder was used to measure the harmonic components of the current signal. An oscilloscope and a Data Acquisition Module (DAQ) was used in [19] to obtain the frequency spectrum of the current signal. In [27] the author used an energy meter IC to measure the active and apparent power in a circuit. In [14] the authors built a smart meter using a microcontroller capable of calculating the real and reactive powers, and 2^{nd} and 3^{rd} harmonics of the current signal.

Each of these approaches presents advantages and disadvantages. Electronic power meters are easy to install, however can measure only the active power. Power quality recorders, harmonic analyzers, oscilloscopes and DAQs can measure a large number of electrical parameters; but have high cost and big physical dimensions, making them suitable only for lab experiments. Energy metering ICs present low cost and small size, however, they are not flexible regarding the electrical parameters which can be measured [34].

Many energy metering ICs (for example, the ADE7763 from Analog Devices and the CS5463 from Cirrus Logic) are capable of measuring voltage, current, active, reactive and apparent power and power factor. Some more complex ICs, such as the ADE7880 from Analog Devices, are also capable of computing harmonics in the voltage and current [35]. Yet, these circuits can only provide the magnitude of the harmonics giving no information about the phase whatsoever. Since harmonics are complex numbers, both magnitude and phase information are needed by breakdown algorithms [34].

Smart meters based on microcontrollers are, in general, cheaper, smaller, and fully customizable, allowing the designers to decide which electrical parameters will be measured. Moreover, unlike energy metering ICs, microcontrollers can be programed to measure harmonics magnitude and phase among other desired parameters to be taken as load signatures.

6. Proposal of a microcontroller based smart meters module for NILM systems

Recently, the Department of Semiconductors, Instruments and Photonics of the School of Electrical and Computer Engineering, at the University of Campinas developed a prototype of a smart meter module for NILM systems to be used in a pilot energy efficiency program [33].

This smart meter module was developed using a low cost ultra-low power microcontroller. It is capable of measuring: active power, power factor, rms voltage and current and the first five odd harmonics of the current signal, presenting the harmonics in terms of magnitude and phase. All the measured parameters can be retrieved via SPI interface.

Shown in Figure 4, the developed module has 36 mm wide by 38 mm high. It was designed to measure the electrical parameters of home appliances at circuit level. Thus, the system needs one module for each monitored circuit. This module can be used for monitoring single-phase and two-phase circuits.

Figure 4. Prototype of the smart meter module [33].

The module on its own does not have power source neither voltage signal conditioning elements. It was designed to be very minimalistic, sharing the conditioned voltage signal and power source from a concentration module with other smart meter modules in parallel.

The concentration module can obtain the voltage signals of up to three mains phases. These signals are isolated and conditioned by transformers with 110/220 V_{RMS} nominal input and 8 V_{RMS} output, ensuring galvanic isolation to the measuring circuit. The transformer outputs are

http://dx.doi.org/10.5772/59311

attenuated by resistive divider composed of a 24 kΩ and 1 kΩ resistors, resulting in 320 mV_{RMS} (452.5 mV peak) nominal output voltage. Using effective 16-bit A/D converters, with full scale of ± 600 mV, it is possible to measure voltages up to 145 V_{RMS} with resolution of 4.42 mV_{RMS} or voltages up to 290 V_{RMS} with resolution of 8.85 mV_{RMS}.

Two 4x1 multiplexers in the smart meter modules are used to select the voltage to be sampled, enabling the smart meter to measure six different voltage combinations: "Phase A to Neutral", "Phase B to Neutral", "Phase C to Neutral", "Phase A to Phase B", "Phase B to Phase C" and "Phase A to Phase C". This feature allows the modules to be suitable for single-phase and two-phase circuits.

The current signal comes from a current transformer (CT) that should be installed around the hot wire after the circuit breaker. Every smart meter module is connected to an individual CT with input/output rate of 50:0.106 A, 1% accuracy and 50 A_{RMS}. A 5.6 Ω resistor is used as border resistor to match this CT. With 16-bit A/D converter operating at ± 600 mV of full scale it is possible to measure currents up to 50 A_{RMS} with 1.53 mA_{RMS} resolution.

Figure 5 presents a block diagram showing an example of how the smart meter module receives the voltage and current signals. In this example the smart meter module is monitoring the circuit #2, with the CT installed just after the circuit breaker and with the multiplexers configured to get the voltage from phase C to neutral.

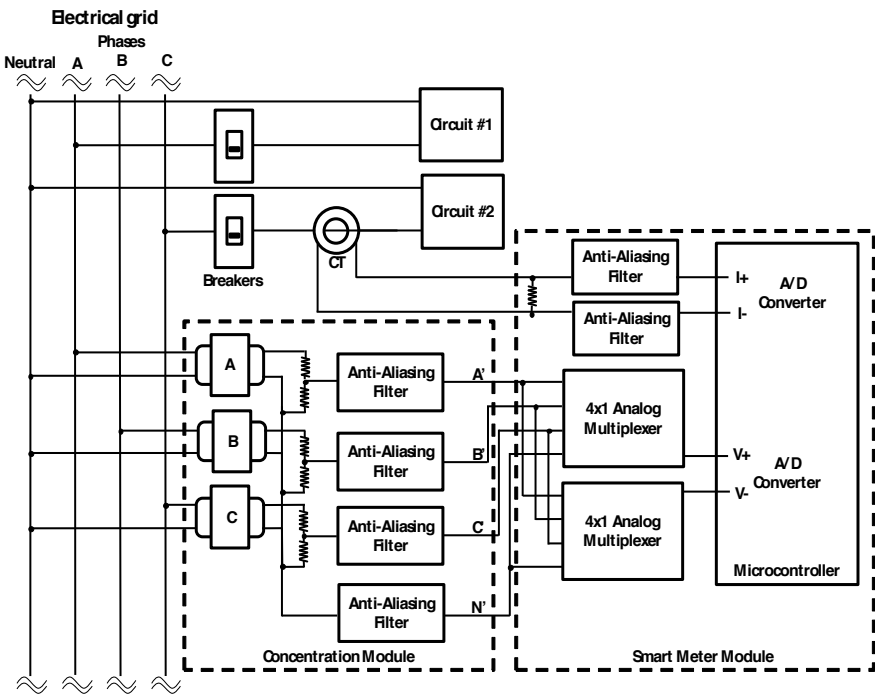

Figure 5. Block diagram of concentration module and the smart meter module sensing circuit #2.

The Texas Instruments MSP430AFE253 microcontroller was chosen as processor unit for the smart meter module. This low cost and ultra-low power consumption microcontroller is very suitable for single-phase power meters. It contains a 16-bit RISC processing unit running up to 12 MHz, 16 KB flash memory, 512 B SRAM memory, UART and SPI communication interfaces, 16-bit hardware multiplier, 16-bits TIMERS, 11 digital input/output pins and three independent 24-bit sigma-delta A/D converters that can operate in synchronized mode [36]. Moreover, they have 1.2 V internal reference voltage with 50 ppm/°C maximum variation. All these features make this microcontroller a great choice to implement a smart meter.

In this project, two A/D converters were used for simultaneously sampling the voltage and current signals. The simultaneous sampling is necessary to calculate the active power and power factor. These converters are configured to operate with 16-bit resolution, differential bipolar inputs, with ± 600 mV of full scale and unity gain.

According to [37], the A/D converters must operate with sampling rate multiple of the power grid frequency to minimize errors in the calculation of active power. With that in mind, the developed smart meter has the A/D converters operating with a sampling rate of 3.84 kS/s (64 * 60Hz). This sampling rate makes it possible to measure harmonic components up to 31st order, in accordance with the Nyquist theorem. The use of higher sampling rates results in greater accuracy in the electrical quantities calculated, especially if nonlinear loads (that have significant values of components of higher order harmonics) are plugged in the circuit.

The sigma-delta A/D converters used for sampling voltage and current signals were configured to operate with oversampling rate of 512. Thus, to read data at a rate of 3.84 kS/s the A/D operates at an effective rate of 1.96608 MS/s.

The use of sigma-delta A/D converters with high oversampling rate allows the use of low-order passive anti-aliasing filters. The anti-aliasing filters implemented are RC low-pass filters with cutoff frequency of-3 dB at 15.9 kHz. Each of them is composed of a 1 kΩ resistor and a 10 nF capacitor. In the bandwidth of interest, from 60 to 1.86 kHz (frequency of the 31st harmonic), the maximum attenuation is-0.06 dB (0.7%). Using a sampling rate of 1.96608 MS/s, these filters are able to attenuate signals at frequencies causing aliasing (1.964220 MHz above) in at least-37.78 dB (98.7%).

Figure 6 shows the power meter firmware flowchart. This program is divided in two parts: Initialization and Infinite Loop. Procedures presented in Initialization stage are executed only once, after the system is turned on, and only run again if the microcontroller restarts. Procedures described in Infinite Loop are periodically executed (until the microcontroller is off). The electrical parameters are calculated at this stage.

The first routines executed after microcontroller initialization are the ones that perform hardware configuration. These routines disable the watchdog and sets up the clocks, the A/D converters, SPI communication and digital I/O. The main microcontroller clock (Master Clock-MCLK) used by the processing unit is configured to use the signal generated internally by the microcontroller DCO (Digitally Controlled Oscillator). The DCO is configured to operate at 16 MHz. A 3.93216 MHz crystal oscillator generates the clock signal used by the A/D converters.

The voltage and current gains are retrieved from the flash memory (embedded into the microcontroller) after hardware configuration. These calibration variables are stored in non-

http://dx.doi.org/10.5772/59311

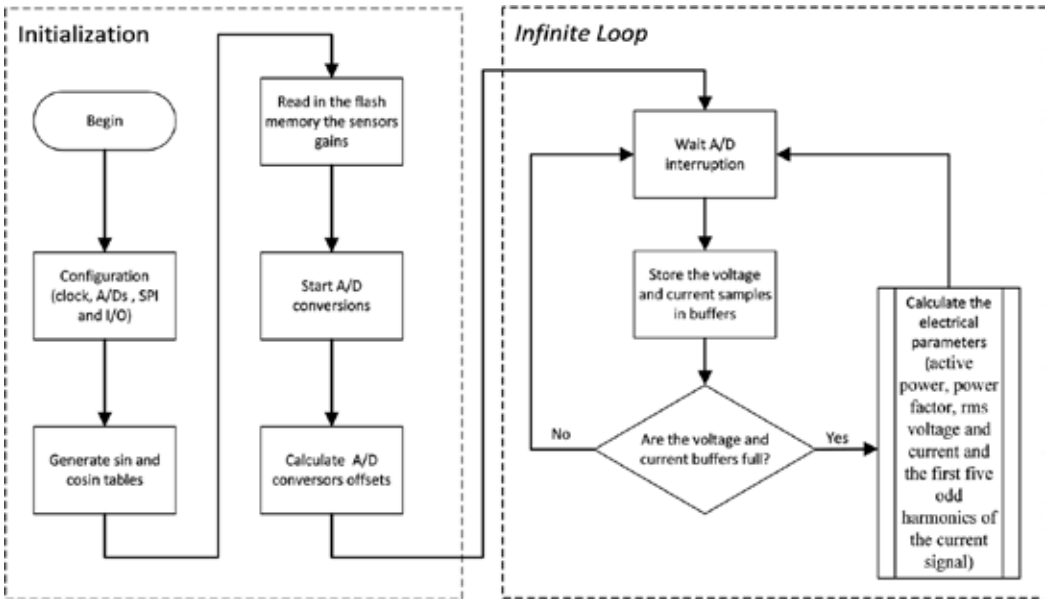

Figure 6. Smart meter firmware flowchart.

volatile memory in order to allow the modules to hold the calibration parameters even if it is turned off.

Following gain calibration, the A/D converters are started and calibrated for offset compensation. The A/D converters present in the MSP430AFE253 microcontroller have offset up to 0.2% [36] that can be almost completely eliminated by calibration.

After Initialization stage, the system goes into the Infinite Loop where the voltage and current samples are processed. Before being processed, the samples are stored in buffers (one for voltage and another for current samples). When the buffers are full (number of samples is equivalent to one power cycle) it is started the routine to calculate the electrical parameters. In the presented implementation, the A/D converters operate at 3.84 kS/s, so in 60 Hz grids, one power cycle corresponds to 64 samples.

As presented before, the electrical parameters calculated are: active power, power factor, rms voltage, rms current, and the magnitude and phase of the first five odd harmonics of the current signal.

The rms voltage is calculated using the following equation:

$$V_{RMS} = \frac{G_v}{N}\sqrt{\sum_{n=1}^{N} v[n]^2} \quad (1)$$

where V_{RMS} is the rms voltage, G_v is the voltage gain, n is the sample index, $v[n]$ is the n^{th} voltage sample and N the number samples. An analogous equation is used to calculate the rms current.

Equation 2 is used to calculate the active power.

$$P = \frac{G_i * G_v}{N} \sum_{n=1}^{N} (i[n] * v[n]) \quad (2)$$

In this equation, P is the active power value and G_i and G_v are, respectively, the current and voltage gains.

The apparent power is calculated from the rms values of voltage and current using Equation 3:

$$S = V_{RMS} * I_{RMS} \quad (3)$$

The power factor corresponds to the ratio of active power by the apparent power, as shown in Equation 4:

$$PF = \frac{P}{S} \quad (4)$$

The effective value of the harmonic components of the current signal is calculated using a formula based on the classical equation of the Discrete Fourier Transform, presented in Equation 5:

$$|I[k]_{RMS}| = \frac{\sqrt{Re\{I[k]\}^2 + Im\{I[k]\}^2}}{N} * G_i * \sqrt{2} \quad (5)$$

The phase is calculated using Equation 6:

$$\angle I[k] = arctan\left(\frac{Im\{I[k]\}}{Re\{I[k]\}}\right) \quad (6)$$

where k is the index of the harmonic component, $|I[k]_{RMS}|$ is the rms value of the module of the k^{th} harmonic, $\angle I[k]$ is the phase of the k^{th} harmonic and Re{I[k]} and Im{I[k]} are, respectively, the real and imaginary parts of the k^{th} harmonic component. Equations 7 and 8 present the formulas used to calculate Re{I[k]} and Im{I[k]}.

$$Re\{I[k]\} = \sum_{n=1}^{N} i[n] * cos\left(\frac{2\pi kn}{N}\right) \quad (7)$$

$$Im\{I[k]\} = \sum_{n=1}^{N} i[n] * sin\left(\frac{2\pi kn}{N}\right) \quad (8)$$

Observe that all equations, except 3 and 4, have a summation term. Observe also that the calculation of the electrical parameters can be separated in two steps: (i) calculation of the summation terms and (ii) calculation of the electrical parameters from the accumulators. Figure 7 presents the flowchart of the algorithm used to calculate the electrical parameters. This algorithm is the core of the smart meter firmware.

http://dx.doi.org/10.5772/59311

After the hardware configuration the A/D converters are started and the program runs in an infinite loop. This loop runs periodically in the frequency of A/D converter. When an A/D conversion is complete, an interruption is generated and the voltage and current samples are processed.

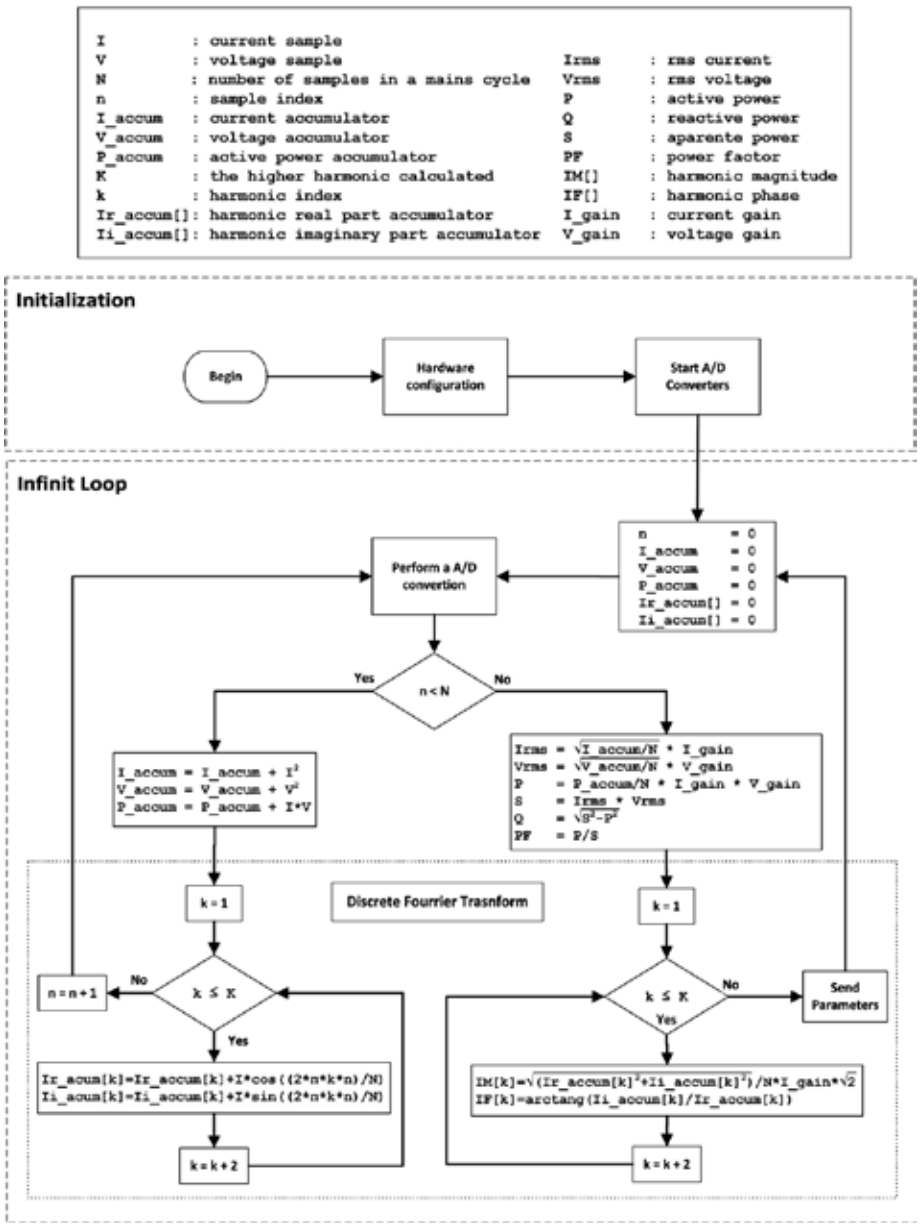

Figure 7. Smart meter core algorithm.

The parameters are calculated in two phases: first, the voltage and current samples are processed and stored in accumulators. Then, when an entire power line cycle is sampled, the electrical parameters are calculated from the accumulators. The left side of the flowchart corresponds to the summation processing, and the right side of the flowchart shows calculation of the parameters values.

In the microcontroller implementation, the left side of the algorithm is performed between two consecutives A/D conversions. The code that implements this algorithm runs in the A/D conversion interrupt routine and has the biggest priority in the program. The electrical parameters calculation (right side of the flowchart) runs in background and is preempted when an A/D conversion occurs.

7. Commercial NILM solutions

In recent years, several companies have created smart metering solutions that allow discrimination of consumption per appliance by measurement at a single point. We can cite as examples, the American: Bidgely (former MyEnerSave), LoadIQ, PlotWatt, Verdigris and Verlitics (former Emme); the British: Navetas and Onzo; the French: Fludia and Wattseeker; the Irish: Powersavvy and Wattics (former Veutility) and the German Yetu.

The American company Bidgely, founded in 2011 with the name MyEnerSave, has received until July 2013 eight million dollars funding through the venture capital company Khosla Ventures. Other companies that developed energy consumption breakdown technologies, such as PlotWatts, also received substantial investments through venture funding. The emergence of a large number of start-ups focusing on residential energy consumption monitoring systems and the massive investment in these companies clearly indicate the degree of interest in this area.

The system developed by Bidgely allows real time monitoring (at intervals from one second to one minute) of energy consumption in device level [38]. By using disaggregation algorithms based on the concept of load signature, this system is capable of measuring energy consumption of some residential appliances, identify energy-inefficient appliances and, when applicable, suggest behavioral changes that culminate in power savings. The disaggregation algorithm uses only the active power as input information. The active power is periodically obtained through a monitor module connected to the conventional power meter. The Bidgely monitor module is not compatible with all power meters used in USA. Another limitation of this system is the fact of it is not able to disaggregate the consumption of all devices present in a home. Only the following loads can be identified: refrigerator, heater, air conditioner, clothes dryer, heater and pool pump. The consumption of the other loads is classified as devices that are always connected, or others.

The solution proposed by the company PlotWatt is very similar to the one created by Bidgely, requiring the installation of a monitoring module along with conventional power meter. The following loads can be monitored: water heating, light, refrigerator, heater and air conditioning, water and light, electric vehicle charging, "always on" and others [39].

http://dx.doi.org/10.5772/59311

The French company Flundia, as well as the American PlotWatt and Bidgely, use monitoring modules connected to the conventional power meter through optical interface to obtain the instantaneous power consumption. Figure 8 presents the monitoring module Flundiometer; it is comprised of optical interface (white piece installed in front of the power meter) and data recorder (black box over the power meter).

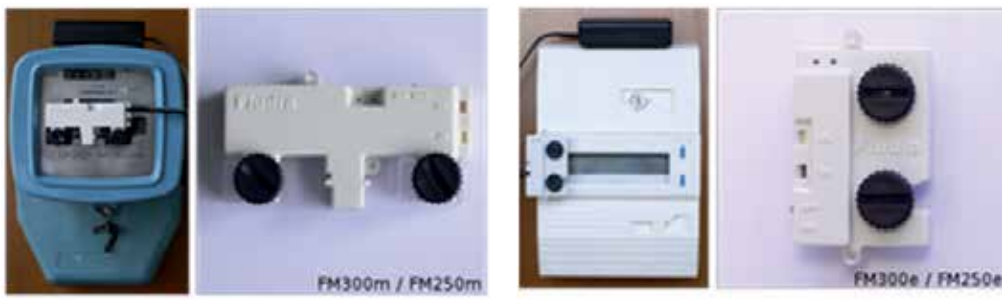

(a) (b)

Figure 8. Flundiometer: (a) monitoring module for electromechanical power meters (b) monitoring module for electronic power meters [40].

Flundia offers two different versions of optical interfaces, one for electromechanical and another for electronic power meters. This system has the advantage of allowing quick and easy installation, but is not compatible with all power meters [40]. Unlike the solutions proposed by Bidgely and PlotWatt the Flundiometer has no remote communication and therefore does not allow real-time monitoring. The data loggers have a USB interface for system configuration and also to retrieve the stored information. The loads disaggregation algorithm developed by Fludia, the Beluso, is able to distinguish the consumption of the following loads: lighting, refrigerator, washing machine, stand-by equipment, water heaters and other machines.

The system Enable.EI developed by the LoadIQ allows real-time energy consumption monitoring using the non-intrusive smart meter EI.Monitor, available in two versions: two-phase and three-phase. The three-phase EI.Monitor, shown in Figure 9, is able to measure rms voltage and current, active and apparent powers, power factor and phase unbalance [41]. This meter is provided with three communication interfaces: Ethernet RJ-45, WI-Fi and GSM.

The company Verlitics developed a smart meter module able to monitor each electrical circuit present in the house individually [42]. This module is provided of 4G/LTE communication.

As can be noticed, the commercial solutions of NILM systems, mostly just make use of active power for load discrimination. So far, there is no record of commercial solutions using harmonic information, or transient analysis to identify loads, despite the potential of these approaches.

Figure 9. Smart meter EI.Monitor [41].

8. Conclusions

This chapter presented a compilation of several studies regarding systems that are able to report detailed information about the power consumption of a residence, discretizing the consumption of each appliance and providing information the households can rely on to change their behavior towards energy efficiency. Both Traditional Load Monitoring systems and Non-Invasive Load Monitoring systems were cited as techniques able to provide this kind of information.

The literature has shown that Traditional Load Monitoring systems are complex to deploy and maintain and tends to be prohibiting expensive as the number of monitored appliances increases, although they can provide very precise information. It has also shown that Non-Invasive Load Monitoring systems are cheaper and much easier to deploy and maintain, even though, for the time being, they are not able to discriminate all the appliances in a residence. Despite of that, commercial solutions of both techniques have been emerging in the market and the current major players are hereby mentioned.

As a key part, the chapter presented the major concepts of power consumption disaggregation techniques, given special attention to Non-Intrusive Load Monitoring Systems and the concept of Load Signature. It presented the technologies adopted by energy meters in NILM systems and also detailed a proposal of a microcontroller based smart meter for NILM systems, developed by researchers at the University of Campinas.

Acknowledgements

This research was partially supported by CAPES.

http://dx.doi.org/10.5772/59311

Author details

Rodrigo M. Bacurau, Luís F. C. Duarte* and Elnatan C. Ferreira

*Address all correspondence to: lfduarte@demic.fee.unicamp.br

Department of Semiconductors, Instruments and Photonics, School of Electrical and Computer Engineering, University of Campinas, Campinas, Brazil

References

[1] York D. et al. Next Generation Programs Reach for High Energy Savings. Washington D.C.: ACEEE; 2013.

[2] Solomon, S. et al. Climate Change 2007: The physical science basis. Cambridge: Cambridge University Press; 2007.

[3] York D. et al. Frontiers of Energy Efficiency: Next Generation Programs Reach for High Energy Savings. Washington D.C.: ACEEE; 2013.

[4] Herhardt-Martinez K., Donnelly K. A., Laitner J. A. Advanced Metering Initiatives and Residential Feedback Programs : A Meta-Review for Household Electricity-Saving Opportunities. Washington D.C.: ACEEE; 2010.

[5] Watts Up? https://www.wattsupmeters.com/secure/products.php?pn=0&wai=200&more=4 (accessed 17 September 2014).

[6] Watts Up? https://www.wattsupmeters.com/secure/products.php?pn=0&wai=0&more=2 (accessed 17 September 2014).

[7] P3 International. http://www.p3international.com/products/p4250.html (accessed 17 September 2014).

[8] Ecobee. http://www.ecobee.com/solutions/accessories (accessed 17 September 2014).

[9] Duarte L. F. C. et al. Characterization and breakdown of the electricity bill using custom smart meters: A tool for energy-efficiency programs. International Journal of Circuits, Systems and Signal Processing 2011; v. 5 p. 116–123.

[10] Hart G. W. Nonintrusive appliance load monitoring. Proceedings of the IEEE 1992; v. 80, n. 12, p. 1870-1891.

[11] Leeb S. B. A conjoint pattern recognition approach to nonintrusive load monitoring. PhD. thesis. Department of Electrical Engineering and Computer Science – MIT; 1993.

[12] Chang H. H. Load identification of non-intrusive load-monitoring system in smart home. Wseas Transactions on Systems 2010; v. 9, p. 498-510.

[13] Chang H. C. et al. A New Measurement Method for Power Signaturesof Nonintrusive Demand Monitoring and Load Identification. IEEE Transactions on Industry Applications 2012; v. 48, p. 764-771.

[14] Huang S.-J. et al. Classification of Home Appliance Electricity Consumption Using Power Signature and Harmonic Features. In: IEEE PEDS, Singapore, p. 596-599; 2011.

[15] Cole A., Albick, A. Nonintrusive identification of electrical loads in a three-phase environment based on harmonic content. In: Instrumentation and Measurement Technology Conference, 2000-IMTC 2000: Proceedings of the 17th IEEE, Baltimore, v. 1, p. 24 – 29; 2000.

[16] Duarte L. F. C., Ferreira E. C., Dias J. A. S. Measurement Techniques for Energy Efficiency Programs. In: EISSA, M. Energy Efficiency-The Innovative Ways for Smart Energy, the Future Towards Modern Utilities. 1. ed. InTech, v. 1, p. 193-208; 2012.

[17] Najmeddine H. State of art on load monitoring methods. In IEEE Second International Conference on Power and Energy-PECon, pp. 1256-1258; 2008.

[18] Norford L. K., Leeb S. B. Non-intrusive electrical load monitoring in commercial buildings based on steady-state and transient load-detection algorithm. Energy and Buildings 1996; v. 24, n. 1, p. 51 – 64.

[19] Patel S. N. et al. At the Flick of a Switch: Detecting and Classifying Unique Electrical Events on the Residential Power Line. In: Proceeding UbiComp '07 Proceedings of the 9th international conference on Ubiquitous computing, p. 271-288; 2007.

[20] Robertson D. C. et al. Wavelets and electromagnetic power system transients. Power Delivery, IEEE Transactions, v. 11, n. 2, p. 1050-1058, Apr 1996. ISSN 0885-8977.

[21] Chang H.-H. Non-Intrusive Demand Monitoring and Load Identification for Energy Management Systems Based on Transient Feature Analyses. Energies 2012; v. 5, p. 4569-4589.

[22] Liang J. et al. Load Signature Study—Part I: Basic Concept,Structure, and Methodology. IEEE Transactions on Power Delivery 2010; v. 25.

[23] Srinivasan D., Ng W. S., Liew A. C. Neural-network-based signature recognition for harmonic source identification. IEEE Transactions on Power Delivery 2006; v. 21, n. 1, p. 398-405.

[24] Lee K. D. et al. Estimation of variable-speed-drive power consumption from harmonic content. IEEE Transactions on Energy Conversion 2005; v. 20, n. 3, p. 566-574.

[25] Shaw S. R., Laughman C. R. A Kalman-Filter spectral envelope preprocessor. IEEE Transactions on Instrumentation and Measurement 2007; v. 56, n. 5, p. 2010-2017.

http://dx.doi.org/10.5772/59311

[26] Lin G. et al. Applying Power Meters for Appliance Recognition on the Electric Panel. In: Proceedings of the 5th IEEE Conference on Industrial Electronics and Applications-ICIEA, Taichung, 15-17 June 2010, pp. 2254-2259; 2010.

[27] Moro J. Z. et al. A Home Appliance Recognition System Using the Approach of Measuring Power Consumption and Power Factor on the Electrical Panel, Based on Energy Meter ICs. Circuits and Systems 2013, v. 4 n. 3, pp. 245-251; 2013.

[28] Farinaccio L., Zmeureanu, R. Using a pattern recognition approach to disaggregate the total electricity consumption in a house into the major end-uses. Energy and Buildings 1999; v. 30, n. 3, p. 245–259.

[29] Rahimi S., Chan A. D. C., Goubran R. A. Usage Monitoring of Electrical Devices in a Smart Home. In: 33rd Annual International Conference of the IEEE EMBS, Boston; 2011.

[30] Bouhouras A. S. et al. Load signatures improvement through the determination of a spectral distribution coefficient for load identification. In: European Energy Market-EEM, Florence, p. 1-6; 2012.

[31] Baranski M., Voss J. Genetic algorithm for pattern detection in NIALM systems. In: Systems, Man and Cybernetics, 2004 IEEE International Conference, v. 4, p. 3462 – 3468; 2014.

[32] Marceau M. L., Zmeureanu R. Nonintrusive load disaggregation computer program to estimate the energy consumption of major end users in residential buildings. Energy Conversion Manage 2000; v. 41, p. 1389-1403.

[33] Bacurau R. M. A smart meter for energy consumption breakdown using power signatures. Master's thesis. University of Campinas. 2014.

[34] Bacurau R. M. et. al. Techniques for Efficient Implementation of Firmware in Microcontroller's Based Energy Consumption Breakdown Smart Meters. VIVECHAN International Journal of Research 2014; v.5.

[35] Analog Devices. Polyphase Multifunction Energy Metering IC with Harmonic Monitoring. ADE7880 Data Sheet; 2011.

[36] Texas Instruments. MSP430AFE2x3, MSP430AFE2x2, MSP430AFE2x1: Mixed signal microcontroller; 2011.

[37] Clark F. J. J., Stockton J. R. Principles and theory of wattmeters operating on the basis of regularly spaced sample pairs. Journal of Physics E: Scientific Instruments 1982; v. 15, p. 645-652, 1982.

[38] Bidgely. www.bidgely.com (accessed 3 January 2014).

[39] Plotwatt. www.plotwatt.com (accessed 3 January 2014).

[40] Fludia Smart Energy Components. www.fludia.com (accessed 3 January 2014).

[41] LoadIQ. www.loadiq.com (accessed 3 January 2014).

[42] Vertilics. www.verlitics.com (accessed 3 January 2014).

Chapter 3

Improving Energy Efficiency in Manufacturing Systems — Literature Review and Analysis of the Impact on the Energy Network of Consolidated Practices and Upcoming Opportunities

Miriam Benedetti, Vittorio Cesarotti and Vito Introna

Additional information is available at the end of the chapter

http://dx.doi.org/10.5772/59820

1. Introduction

Global energy context has become more and more complex in the last decades: raising prices of depleting fossil fuels, together with economic crisis and new international environmental and energy policies, are forcing companies (and manufacturing industry in particular, which is responsible for 90% of industry energy consumptions, in turn making up the 51% of global energy usage, as listed on EIA, the Energy International Agency, website, last accessed on the 5th of October 2014) to cut energy wastes and inefficiencies, and to control their consumptions.

Besides the existing analysis of the above mentioned regulatory and economic concerns, Energy Efficiency criticality for manufacturing systems has recently been investigated and proved also by the analysis of its connection with Productivity Efficiency [1-4], which resulted to be strong and mutual, and of the numerous non-energy benefits achieved while performing energy efficiency measures [5], such as the improvement of corporate image and the environmental impact reduction.

Over most recent years, Energy Efficiency has therefore become a critical factor for industrial plants' competitiveness, and is now definitely considered as a key driver to economic development and sustainability.

But, despite it all, it is often still difficult for many companies to understand its effectiveness, in good part because of the difficulties met in focusing its technical and economic benefits, as Laitner [6] highlights:

> "Energy Efficiency has been an invisible resource. Unlike a new power plant or a new oil well, we do not see energy efficiency at work. (...) energy efficiency may be thought of as the cost-effective investments in the energy we do not use either to produce a certain amount of goods and services within the economy."

As a matter of fact, Energy Efficiency still represents a challenging goal for most companies. As above mentioned, numerous problems are yet to overcome in quantifying its benefits and evaluating the cost-effectiveness of related investments, and most of all the huge variety, complexity and changeability of fields, technologies and methodologies involved in its improvement in production systems are responsible for the slowing down of their resolution and of the spread of Energy Efficiency measures and culture.

In fact, in order to individuate and prioritize suitable improvement interventions and Energy Efficiency opportunities, and to design and customize the Energy Management System or the Monitoring and Control System according to a particular company's needs, a deep and complete knowledge of many different subjects and disciplines (ranging from physics and thermodynamics to economy and project management) is needed, besides a good ability and practical sensibility to direct one's efforts in the right way.

Considering that Energy Efficiency isn't obviously the core business of manufacturing industry, such effort might sometimes be very laborious, and in recent years many companies have decided to demand Energy Management activities to specialized external companies, the so-called Energy Service Companies (ESCos). ESCos generally own the know-how required to individuate Energy Efficiency measures and are also able to fund Energy Efficiency investments (see [7] for a specific literature review); what they usually do not own is a deep understanding of the company's dynamics, situations and needs, as well as the capability to draw a long-term development path towards the achievement of a diffused Energy Efficiency culture within the company, which shall be consistent with the company's vision and policies and is essential in order to consolidate and continuously upgrade improvements in such sector. It is then crucial for companies to have at least a general consciousness of all intervention areas and of all possible improvements, both managerial (and/or behavioural) and technological, that could be pursued and achieved, in order to be able to lead their own way towards their sustainable development, and also to capitalize ESCOs' assistance and services.

In order to overcome part of these difficulties, and in particular to make it easier for companies to address their efforts and catch best efficiency opportunities, a logical and systemic approach is necessary: it would help not to overlook any possible area of improvement, to easily classify and understand those areas, but also to identify the most suitable and cost-effective, and eventually to prioritize them.

In the light of this, some studies have already been conducted in order to find out methods and tools to assess the current level of maturity of a company in the Energy Management field [8], and to help individuating a possible development path. However, although they point out some possible development scenarios, they do not provide a complete and organic categorization of all possible areas of intervention, so as to make it easier for practitioners to address their efforts into the right way.

http://dx.doi.org/10.5772/59820

In this chapter, a new conceptual scheme to organize and classify Energy Efficiency measures is defined, leading from the definition of Energy Cost per Product Unit and further breaking it up in order to identify and define all possible areas of intervention, providing for each of them a brief overview of possible measures and opportunities and a specific literature review. All scientific papers, books and technical papers considered for the literature review of each area (chosen on the basis of a wide literature research and on authors' on-field experience) are recalled and systematized in Table 1, so that the reader is guided through their examination and rapidly addressed to their consultation.

In addition, a qualitative evaluation of the impact of some possible Energy Efficiency measures from each area on the energy network is given, in order to give both practitioners and researchers a first input to further focus on this additional feasibility evaluation criteria for Energy Efficiency measures, which enables to evaluate them on a national or international level rather than considering the benefits or concerns belonging to a single company.

			Reference number
Specific Cost of Energy	Supplier and tariff choice	Amount of total energy consumption	28, 29, 30, 31
		Peak Demand	20, 23
		Demand Response and dynamic price systems	32, 33, 34, 35, 36, 37, 38, 39, 40, 41, 42, 43, 44
		Power Factor correction	45, 46, 47, 48, 49, 50
	Compliance to contractual purchasing conditions		22, 51, 52, 53
	Onsite energy production		54, 55, 56, 57, 58, 59, 60, 61, 62, 63, 64, 65, 66, 67, 68, 69, 70, 71, 72, 73, 74, 75, 76, 77
Specific Energy Consumption	Energy transformation, distribution and use (Design phase)	Technologies selection	22, 25, 78, 79, 80, 81, 82
		Modulation technique selection	22, 83, 84, 85, 86, 87
		Dimensioning	22
	Energy transformation, distribution and use (Operations and Maintenance phase)	Human behaviours	51, 53, 88, 89, 90, 91, 92
		Best practices	93, 94, 95, 96, 97, 98
		Monitoring and Control	22, 25, 45, 53, 99, 100, 101, 102, 103, 104, 105

Table 1. Summary of the specific literature review for each intervention area.

2. General scheme for the literature review

Energy Efficiency in industrial sector has often been interpreted and studied as Specific Energy Consumption of processes, machines and factories [9-13], referring to its thermodynamic meaning and stressing the concept of 'using less energy to provide the same amount of services or useful output' [14], as well as its connection to environmental and ecological issues (and in particular to carbon dioxide emissions [15-19]). Similar approaches have however the blemish of neglecting a critical aspect, which is probably the most important to companies (whose fundamental objective is to improve their business), which is the reduction of energy costs.

Energy costs are in fact obviously tightly connected to energy consumption, but it would be a significant conceptual error to ignore energy market flows, tariffs and options, and therefore the variability of the Specific Cost of Energy, while trying to minimize them.

From a business point of view, it might therefore be much more useful and complete to define a physical-economic index, and to evaluate Energy Efficiency through its evolution in time; the index here proposed is the Energy Cost per Product Unit (Cost of Energy and Production Volume ratio, the inverse ratio of Energy Productivity), i.e. the energy cost paid for the single product unit, that can be calculated as the product of Specific Cost of Energy (the cost of the single consumption unit, Cost of Energy and Energy Consumption ratio) and Specific Energy Consumption (the energy consumption for the single product unit, Energy Consumption and Production Volume ratio), as represented by the following formula, where Cost of Energy is expressed in Euros, Production Volume in units and Energy Consumption in kWh.

$$\frac{Cost\ of\ Energy}{Production\ Volume} = \frac{Cost\ of\ Energy}{Energy\ Consumption} \; x \; \frac{Energy\ Consumption}{Production\ Volume} \tag{1}$$

The reduction of energy costs can therefore be achieved by minimizing Specific Cost of Energy, Specific Energy Consumption or both, depending on companies' policies and existing opportunities.

Leading from the definition of this physical-economic index, it is possible to define a conceptual scheme to categorize Energy Efficiency measures in manufacturing systems. In fact, all possible intervention areas can be classified according to which one of the two main factors (Specific Cost of Energy or Specific Energy Consumption) they do affect, as Energy Efficiency measures are generally aimed at reducing one of them. Specific Cost of Energy and Specific Energy Consumption can then be respectively affected by interventions performed in three different areas, which are:

- *Supplier and tariff choice*, the choice of the most suitable energy purchasing contract, according to the company's own consumption and to the considered market;
- *Compliance to contractual purchasing conditions*, all of the actions aimed at being compliant to the chosen energy purchasing contract's clauses and provisions (and to avoid incurring into fees and sanctions), and

http://dx.doi.org/10.5772/59820

- *Onsite energy production*, i.e. the production of the needed energy onsite, reducing or eliminating the quantity of energy purchased, for the first one, and:
- *Energy transformation*, the process of changing a form of energy into a more usable one, to be held in the most efficient way, avoiding all possible losses;
- *Energy distribution*, the process of delivering energy to the place where it is needed, to be held in the most efficient way, avoiding all possible losses, and
- *Energy use*, the final use of energy that shall be effective and efficient, for the second one.

By acting to improve one of these areas (for example applying existing best practices of the particular sector), the company can reduce energy costs and increase Energy Efficiency.

In particular, four different improvement areas concur to the "Supplier and tariff choice" factor, i.e.:

- *Amount of total energy consumption*, the actual amount of energy used, that has to be accurately considered in order to take advantage of economies of scale;
- *Peak demand*, the maximum power employed at a time, that shall be compliant to the contractual conditions;
- *Demand response and dynamic price systems*, all of possible actions aimed at beng able to modify the plant's demand profile in order to improve the system's reliability and to take advantage of special tariffs and purchasing conditions, and
- *Power factor correction*, the process aimed at reducing the amount of reactive power and increasing the amount of the active power employed.

The measures and opportunities connected to the three intervention areas affecting the Specific Energy Consumption have different implications according to the life phase of the plant they are applied to (*Design phase* or *Operations and Maintenance phase*). During the Design phase, Energy Efficiency is influenced by:

- *Technologies selection*, the choice of the Best Available Technology from an Energy Efficiency point of view;
- *Modulation technique selection*, the choice of the best method or technology to follow production needs without reducing Energy Efficiency, and
- *Dimensioning*, the choice of the most appropriate system's dimension,

while during the Operations and Maintenance phase is influenced by:

- *Human behaviours*, i.e. actions taken by people on the basis of their education and information about Energy Efficiency issues;
- *Best practices*, lists of existing best methods and techniques to operate a system in the most efficient way, and
- *Monitoring and control*, all of the actions aimed at keeping the system under control once it has started to operate.

All possible Energy Efficiency measures can be framed into these categories. In the next paragraphs, all of these categories and sub-categories will be introduced and defined, a brief overview of some possible Energy Efficiency interventions will be given and a specific literature review (summarized in Table 1) will be presented for each intervention area.

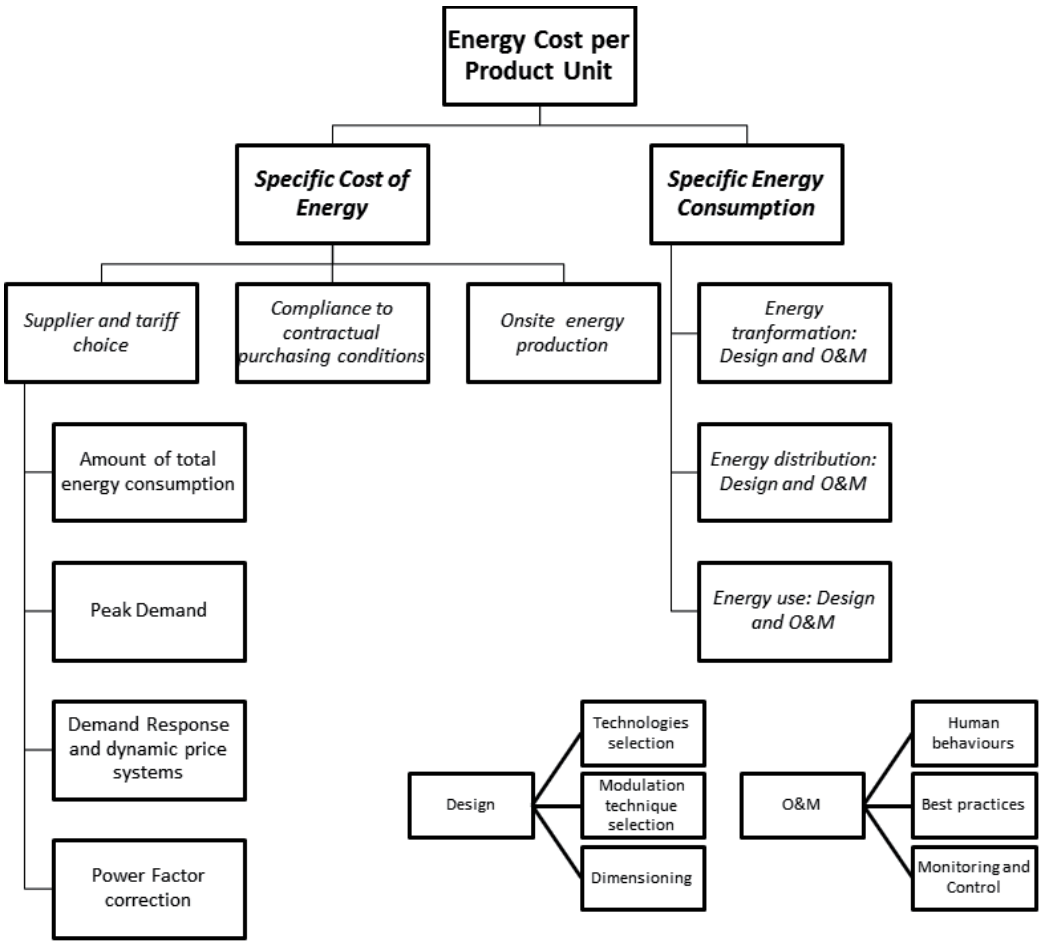

Figure 1. Conceptual scheme for Energy Efficiency measures' and intervention areas' categorization.

3. Specific cost of energy

Specific Cost of Energy [€/kWh], as aforementioned, is the payment due for the consumption of the single kWh (here expressed in Euros); its value and variability are often concerned and tackled by companies of remarkable dimensions (furthermore positively affected by scale effects), whilst medium and small sized companies are often not sufficiently aware of the problem, have little bargaining power, or have not got the possibility to take any measure.

http://dx.doi.org/10.5772/59820

Specific Cost of Energy directly depends on the capability to ensure energy supply at the lowest possible price, and therefore:

- On the capability to choose the most suitable supplier and tariff;
- On the capability to be compliant to contractual purchasing conditions;
- On the capability to produce the energy needed onsite.

To achieve these capabilities, having a complete knowledge of the present state of consumption, the historical consumption and the responsiveness of the system to changes (planned or unpredicted) is essential [20].

The importance of Specific Costs of Energy reduction is also due to the fact that it is achievable through immediate and cost-effective measures, that might generate huge savings in a very short period, and can therefore create an initial asset to finance further and more expensive improvements [21].

3.1. Supplier and tariff choice

The complexity of the supplier and tariff choice, here particularly referred to electricity, highly depends on the Country where the industrial site is located, as energy markets can be rather different from one Nation to another, as much as electricity bills' components (which are also inclusive of taxes and duties); anyway, as most of industrialized countries have nowadays adopted deregulated and liberalized markets (although important parts of the sector, like transmission and distribution, are usually still natural monopolies) [22], there is normally at least one element of the bill which is not subject to central government's regulation, but open to competition [23]. That situation leads to a huge complexity and quantity of options, but also to a wider range of savings opportunities and to customer services enhancement.

In order to take the right decision, several skills and tools are needed, which often require time consuming activities and transversal capabilities to be achieved: a deep knowledge of consumption logics and dynamics, a reliable forecasting system (based on predictive simulation models and tools), a complete comprehension of market rules and a continuous information process about available tariffs and options, as well as the capability to perform a comparative analysis.

In any case, a simulative approach might be implemented to characterize and forecast energy consumption, aiming at evaluating and comparing electricity rates by analysing the influence of all possible drivers on the electricity cost. Different methodologies have been proposed to allow industries developing their own strategies for the contracts' renewal. Some of them, like the one developed by Cesarotti, Di Silvio and Introna [24], focus on the use of statistical tools (like regression analysis and control charts) to characterize electricity consumption in the industrial process, forecast the energy demand basing on energy drivers and consumption characterization, and to analyze tariffs in detail, also performing a sensitivity analysis of energy price variability, that, for some of them, can also be coupled to the analysis of the cost of petroleum (and/or of other fossil fuels), by the introduction of a specific index (savings opportunities coming from that kind of price calculation can be consistent, but need users to

deeply understand the mechanisms used to generate the index, to analyse various forecasts of the index variability and to accept a very high risk [25]).

An alternative methodology has also been provided [25-27], based on budgeting techniques and on the development of a set of first and second level metrics and indicators to identify effects of external factors' variations (including energy price fluctuation) on energy consumption and cost.

Factors mainly affecting electricity cost for an industrial plant, which can discriminate various tariffs and suppliers' offers, are:

- Amount of total energy consumption;
- Peak demand;
- Demand Response and dynamic price systems;
- Power Factor correction.

3.1.1. Amount of total energy consumption

Purchasing a large amount of energy is the way to take the best advantage of economies of scale (the higher the amount of total energy purchased, the lower the cost of the single kWh), but difficulties may arise for both big and small companies, because of the fragmentation of production processes into different sites or because of moderate production volumes. Savings opportunities in that field might be found in concluding a unique contract for all scattered production sites or, referring to medium and small companies, in gathering in a consortium with other companies which have similar or compatible demand curves, loads' distribution and needs; that latter solution follows the 'industrial symbiosis' logic, which is the engagement of traditionally separate industries in a collective approach to business and environmental management [28-31], a managerial practice that has already given appreciable results in containing costs of other sources supply, like row materials and water.

Unfortunately, the practical implementation of these actions is often frustrated by big companies' purchasing policies, and by the unawareness of this problem of medium and small companies.

3.1.2. Peak demand

Electricity bills often include an additional fixed cost which depends on the maximum power employed (average values in a small time interval, usually of some minutes, are considered), and is introduced by many suppliers as a cost signal, an incentive for companies to control and reduce their capacity requirements, helping suppliers themselves to easily manage supply-demand balance. Thus, correctly forecasting energy consumption and load profile, principally basing on observation of historical data and statistical analysis, is essential to avoid penalties and surcharges [20]. By monitoring load profile and comparing actual peak load values to contractual one, it might be possible to highlight energy savings opportunities, summarized in the following table [23].

Peak Load	Saving Opportunity
Always exceeded	Negotiate a higher value of peak load to avoid penalties
Occasionally exceeded	Adapt operational practices and scheduling to contractual requirements
Always under the contractual value	Negotiate a lower value of peak load to achieve significant savings

Table 2. Savings opportunities in peak load value determination and monitoring.

3.1.3. Demand response and dynamic price systems

To enhance system's efficiency, cost signals (as aforementioned) are often send to end-users by suppliers, in order to steer their demand, flattening it as much as possible [32], and therefore improving system's reliability (as demonstrated by Samadi, Javidi and Ghazizadeh [33], who calculated the variations in the amount of Expected Energy Not Supplied after the implementation of different Demand Response programs through a Monte Carlo simulation); such strategy ends up in high electricity cost variability and/or in incentives assignment, principally depending on time of use, production and consumption scheduling, and capability to select a range of loads to be switched off if necessary.

Profitability of that solution for both suppliers and end-users has been studied and proved: Sezgen, Goldman and Krishnarao [34] used option-pricing methodology, a stochastic simulative approach which, by the means of Monte Carlo simulation (a tool that had already been exploited by Bhanot [35], having similar purposes) and of key financial components like forward curves of energy prices, price volatility, correlation between prices and interest rates, was capable to reproduce and forecast the stabilizing effect of Demand Response programs on electricity wholesale market; Faria and Vale [36] implemented a non-linear Demand Response simulator to calculate retailer's benefits when price variability is applied to single consumers or groups of similar consumers; finally, Torriti [37] and Gaiser and Stroeve [38] respectively highlighted the impact of variable tariffs on electricity demand and on end-users bills, considering residential customers.

Demand Response has been defined by U.S. Federal Energy Regulatory Commission (2012) as:

> "changes in electric use by demand-side resources from their normal consumption patterns in response to changes in the price of electricity, or to incentive payments designed to induce lower electricity use at times of high wholesale market prices or when system reliability is jeopardized."

End-users can generally response to price variations by implementing three kinds of actions: reduce the amount of electricity used during high pricing periods (incurring in reduction of quantity or quality of outputs, and therefore accepting deriving risks), shifting part of electricity usage from high pricing to low pricing periods (rescheduling some production activities) or partially satisfying demand during peak periods by the means of onsite generators (this very last action will be discussed in next chapters) [32]. The decision to implement

one or more of these actions and therefore to catch resulting saving opportunities has got to be supported by both the use of forecasting and simulating approaches (like the financial instruments based simulation proposed by Oren [39] to forecast electricity price behave, assuming it to be close to a Brownian motion process, or the mathematical model relying on Non Linear Integer Programming framework, developed by Fernandez, Li and Sun [40] to optimize buffer inventory management policies and determine corresponding load management actions to be taken without affecting production and quality), and of systemic managerial approaches (like the one conceived by Bush [41], following seven steps, from evaluating rate schedules and incentives to analysing operations plan, to identifying and quantifying interruptible loads, the one described by Wang and Li [42], who proposed a methodology to solve production system modelling and scheduling problems while optimizing energy efficiency and minimizing electricity related costs, or the model proposed for medium and small users by Bello et al. [43]). Catching opportunities in that field requires companies to have a high maturity level in energy efficiency implemetation, as a robust consumption plan and control system is needed.

Demand Response Programs are divided into two categories: Incentive Based Programs and Price Based Programs. The first one includes all those programs involving incentives assignment to end-users who manage to interrupt and/or curtail part of their load when required by the supplier, in order to ensure reliability and react to emergencies; these incentives can be 'Classic' (a fixed, periodic incentive to compensate users for their willingness to interrupt or curtail their load) or 'Market-based' (an incentive assigned in proportion to user's performance in interrupting or curtailing loads) [44]. The second one includes programs which propose fluctuating rates, following the real time cost of electricity, such as TOU (Time Of Use) program, in which different cost of energy coincide with different time of the day [42].

Principal Demand Response Programs are summarized in Figure 2.

3.1.4. Power factor correction

Control and correction of the network's Power Factor are almost common practice in manufacturing systems: they are implemented to both avoid incurring in penalties and fines established by suppliers and to improve energy efficiency of distribution system within the industrial plant (reducing Joule losses) [45].

Different methods for measuring and controlling Power Factor values have been developed, depending on the load's characteristic and on the quality of the transmission [46], and various methodologies have been proposed to optimize capacitors' number and allocation for industrial users, by the means of a wide range of simulative algorithms [47]. Those methodologies have been studied at an extremely high level of detail, including Life Cycle Cost Assessments, to justify the installation of a certain number of capacitors, evaluating the possibility to use these devices to face lines' disturbs or mitigate harmonics [48], and therefore to take more advantages from their usage, as well as accounting of external factors variations, such as air temperature, affecting their efficiency.

http://dx.doi.org/10.5772/59820

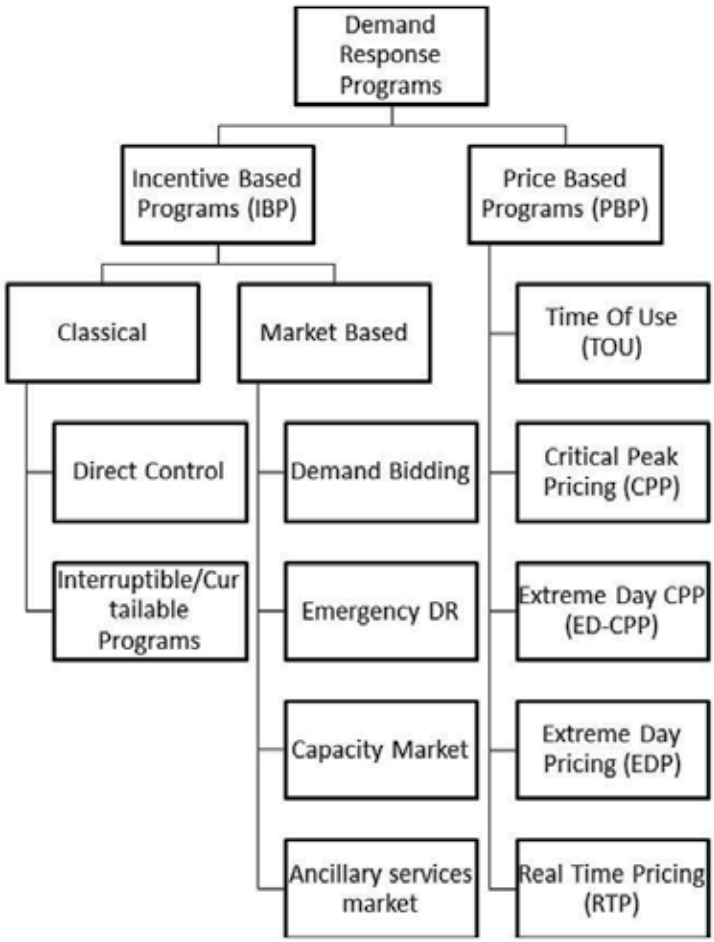

Figure 2. Classification of Demand Response programs [32].

Researches recently focused on Power Factor control through automatic system, and in particular by the means of artificial neural networks, a technology which eases variable loads control and provides more accurate and faster compensation compared to capacitor groups [49, 50].

3.2. Compliance to contractual purchasing conditions

Once all conditions illustrated in previous paragraphs have been contemplated and decisions have been taken according to companies' policy and existent saving opportunities, an anything but trivial source of Specific Cost of Energy variability is the capability of users to be compliant to contractual agreements.

On the one hand, in large firms, that capability strongly depends on various functions' commitment to energy saving and on their attitude in understanding process dynamics and

issues; in fact, the finance or purchasing department is often responsible for buying energy, but not for managing it, so it is essential to increase peoples' awareness of the implication of their choices on global costs and on energy management and consumption.

On the other hand, small and medium enterprises often lack in know-how and skills to efficaciously manage compliance to contractual agreements, and therefore have to strengthen their employees' understandings and abilities by the means of training, awareness and motivation programs [22, 51-53].

3.3. Onsite energy production

A drastic solution to abate energy costs (that also affects primary energy consumption) is to autonomously provide to its generation onsite, a decision that requires high initial investments and advanced managerial capability to correctly run the system, but can definitely be cost-effective, and also returns additional benefits, like enhancement of supply quality and security and support provision to Demand Response management.

This solution has recently widespread, thanks to the proliferation of new renewable energy production technologies, whose diffusion has been fostered by public funding, and also to Smart Grids' development, that has introduced the possibility to input extra energy production into the networks, being remunerated (the general impact of Smart Grids on Energy Efficiency will be discussed in the following paragraphs).

A wide range of technologies is available for energy onsite production; the selection of the most suitable technology strongly depends on the location, the existence of feed-in tariffs and the possibility to use available waste products as fuel, or to recover part of the energy that is unloaded and dispersed by different processes [54-56]. Several guides and methodologies have been developed and published to help companies evaluating different solutions and taking the right decision through the implementation of both simulation tools and feasibility studies, mainly focusing on hydroelectric and wind turbines and micro-turbines [57], solar photovoltaic [58], geothermal energy, biomasses, anaerobic digestion and fuel cells for electricity generation and solar thermal, biomasses [59] and heat pumps for thermal energy generation [60].

Anyway, in most industrial plants, electricity and heat production from renewable sources is not adequate to system's demand, because of the variability of its capacity according to different weather condition and to the limited power concentration. Therefore, the most implemented energy generation technologies in industrial plants are combined heat and power (cogeneration) and trigeneration systems, being available for production in various scales and particularly fitting those manufacturing systems using heat and steam in production process besides in spaces heating systems.

Cogeneration, the simultaneous generation of usable heat and power (mainly electrical, but also mechanical depending on the proper site's needs) within a single process [61], allows companies to reduce the total amount of primary energy needed to supply the whole plant; to achieve those systems' maximum efficiency, they have to be operated as much as possible near their nominal conditions, which means keeping the ratio between electricity and heat pro-

http://dx.doi.org/10.5772/59820

duced almost constant. To achieve this goal, exceeding electricity production can be sold to the network, while exceeding heat can be used in cooling systems, like heat pumps or absorption units (trigeneration systems), especially in summer, when heating needs are lower.

Convenience of cogeneration and trigeneration systems has been studied and proved by many authors, through surveys, case studies analysis and feasibility studies [62-68], and also simulative approaches [69-70].

Methods and systems to optimize their sizing and operation planning have been developed, generally based on non-linear simulations to minimize costs and/or to maximize efficiency, according to heat and electricity demand variability [71-75].

Other multi-energy systems are also currently being studied, basing on the same concept as cogeneration, i.e. improve energy efficiency by making different energy vectors (electricity, heat, cooling, fuels, and so on) interact at various levels, from both operational and planning point of view [76].

A viable alternative, particularly interesting for small and medium enterprises, who may find it difficult and onerous to manage and maintain generation systems, and to assume related risks, is to commission onsite energy production to third companies (Energy Service Companies), stipulating an agreement to share final savings [77].

4. Specific energy consumption

Specific Energy Consumption [kWh/unit] is the energy consumption for the single product unit; its minimization involves an actual energy efficiency improvement besides an economic benefit, and is linked to technical, managerial, thermodynamic and physical issues. Its optimization not only affects the final user, but also has environmental consequences, making primary sources exploitation become more sustainable.

It directly depends on the capability to maximize energy efficiency of manufacturing systems, and therefore to optimize energy transformation (minimizing the Energy Consumption and Energy Vector Produced ratio), distribution (minimizing Energy Vector Produced and Energy Vector Delivered ratio) and utilization (minimizing Energy Vector Delivered and Production Volume ratio) within the plant, i.e. to carefully design, operate and maintain utilities, distribution lines and production systems.

$$\frac{Energy\ Consumption}{Production\ Volume} = \frac{Energy\ Consumption}{Energy\ Vector\ Produced} \; x \; \frac{Energy\ Vector\ Produced}{Energy\ Vector\ Delivered} \; x \; \frac{Energy\ Vector\ Delivered}{Production\ Volume} \tag{2}$$

Utilities and distribution lines in particular have often a high influence on Specific Energy Consumption, as most part of energy losses and wastes are located in transformation and distribution phases, but also offer the largest number of energy saving opportunities, as they can be easily modified without affecting production or expose product quality to any risk.

Energy-oriented optimization of Design and Operations and Maintenance of utilities, distribution lines and production systems will be concurrently discussed below, as basic principles and methods can be assimilated.

4.1. Design

In order to minimize energy losses and wastes, Design phase requires considerable attention in selecting technologies to be adopted, choosing the most suitable modulation technique and correctly dimensioning systems; it both determines system's maximum energy efficiency and the possibility to keep it at its highest levels as long as possible.

4.1.1. Technologies selection

In order to maximize energy efficiency of a system, a cost-intensive opportunity, requiring high investments but also tremendously reducing operating costs, is to select and adopt Best Available Technologies (BATs), whose huge potential has been assessed by Saygin et al. [78] and Letschert et al. [79].

The adoption of some of those BATs is regulated by national and international policies (Joint Research Centre of European Commission periodically releases BATs lists for many industrial sector), while studies aimed at developing methodologies to identify BATs according to Countries' geo-economics are undergoing [80].

Different approaches to best technologies selection have been developed. Most environmentally suitable methodologies seem to be those based on Life Cycle Assessment [81, 22, 25], comparing different kinds of equipment on their whole-life cost, considering purchasing, maintaining, energy and release; less common, more simulative and analytics approaches rely on Multi-Criteria Decision Analysis or Analitic Network Process [82].

4.1.2. Modulation technique selection

Choosing the most suitable modulation technique for different machineries and systems means keeping energy efficiency as high as possible, as long as possible, by matching variable demand and production.

The more variable the demand (of vectors considering utilities, of product considering production systems), the more efficient shall be the modulation system, and therefore a preliminary assessment of demand variability is required when approaching this issue [22].

Considering as an example electrical motors-driven devices, if the demand is almost constant, a simple on/off modulation shall be sufficient, while if it regularly floats a stand-by system would be necessary, or a more efficient Variable Speed Drive [83-85], whose convenience can be assessed by the means of simple financial methodologies [86], or by the means of simulated environments [87]. This latter solution is required especially when a complex and multiple-machineries system is analysed, and an automatic control system is therefore needed.

http://dx.doi.org/10.5772/59820

4.1.3. Dimensioning

Besides choosing the best technology to implement, particular care must be given in selecting the optimal size for the designed systems, as oversizing might lead to technical difficulties and inefficiencies when modulation is required, while opting for modular and/or decentralized systems, made up of a number of small units working in parallel, might contrast advantages derivable from economies of scale [22].

4.2. Operations and maintenance

A huge number of cost-effective opportunities to enhance energy efficiency can be caught while planning and optimizing systems' Operations and Maintenance, acting on human behaviours, implementing best practices and monitoring and control techniques.

4.2.1. Human behaviours

Fostering employees' and staff's awareness of energy efficiency importance and their consequent correct behaviours, like switching devices off when not needed, correctly regulating set points, or point out malfunctioning, is an actually cost-effective energy efficiency opportunity, which is also often mandatory to enable all other improvements, and can bring high savings.

Lots of different activities have been realized to achieve that particular issue, from publishing an internal energy policy to planning periodic trainings, competitions and recognition [51, 53, 88] and to influencing people's behaviours by the means of awareness campaigns and social influence, even if, particularly in medium and small enterprises, they are still hardly put into practice, because commonly underestimated [89-92].

4.2.2. Best practices

Operation and Maintenance and energy efficiency measures have a mutual positive influence: the optimal management of a system is as significant as the efficiency of its components to energy saving purposes [93, 94], and energy consumption control can foster maintenance and operations planning and practices [95]. A number of different best operating and maintaining practices [96] have been identified and collected (principally through clustering, benchmarking tools and databases [97]), as well as methodologies to select the ones to be applied by determining energy savings potentials in various fields [98], and are also published per industrial sector or specific system by national and international research organisms (i.e. ENEA, IEA, U.S. DOE, Carbon Trust, Energy Star ecc.).

Most common and cost-effective best practices are related to optimal set points determination, operating procedures optimization, preventive maintenance planning and machineries optimal scheduling [95].

4.2.3. Monitoring and control

Many difficulties are certainty met by most companies in correctly implementing a Monitoring and Targeting system, that allows to continuously measure, control and forecast consumptions

as well as improvements actions' benefits (giving the possibility to immediately correct negative trends) [99-101], both analysed in relation to previously identified baselines and also influencing external factors, known as energy drivers [22, 25, 53, 102].

Those systems, besides bringing Energy Efficiency improvements, are also useful to identify Operation and Maintenance improvement measures for both utilities and production machineries, and to evaluate those already implemented, by the means of Energy Efficiency evaluation criteria.

Barriers in achieving a complete knowledge and understanding of consumption trends are partly due to the plethora of metrical instruments (listed and described by Beretta et al. [25] and Petrecca [45]) and information technology systems to buy, implement, operate, manage and maintain, and to the resulting amount of data to analyse.

Widespread of Energy Management Systems in recent years has fostered metering systems diffusion, as well as protocols and procedures guiding users to implement Monitoring and Targeting systems.

Metering and sub-metering methods, as well as metering schedules and strategies have been discussed by Carbon Trust's Metering practical guide [103]; Monitoring and Targeting systems and techniques have been instead illustrated in the International Performance Measurement and Verification Protocol by Efficiency Valuation Organization (2012), focusing on the identification of consumption variation's causes and energy drivers, and on savings evaluation, through the application of statistical tools and methods, in Carbon Trust's Monitoring and Targeting practical guide [104] and also by Morvay and Gvozdenac [22], discussing in detail applications of statistical methods to forecast and control consumptions (whose influence on energy efficiency is described by Cesarotti, Deli Orazi and Introna [105]).

5. Qualitative evaluation of the impact of Energy Efficiency measures on the energy network

The industrial energy demand is progressively undergoing a deep change process and, not considering the physiological fluctuation due to the production volumes' contraction, its reduction is partly guided by national and international strategies and partly imposed by the firms' need to abate energy costs, its impact being inevitably strong on the global primary energy and resources consumption.

The defined and presented Energy Efficiency intervention areas and measures will now be qualitatively evaluated according to the effect they have on the energy network, meant as the combination of energy production, distribution and utilisation systems interacting on a national or international level. In fact, by acting to reduce the Specific Cost of Energy and/or the Specific Energy Consumption, the company affects not only its own Energy Cost per Product Unit, but also the general balance and functioning of the whole energy network. The energy network has therefore to be able to counterbalance energy demand fluctuations that can be given by the implementation of Energy Efficiency measures (the analysis of all the

http://dx.doi.org/10.5772/59820

possible causes of energy demand fluctuations and the review of the methodologies and technologies currently used for this counterbalancing are demanded to more specific texts, here attending only to the evaluation of the impact on the network of the Energy Efficiency measures belonging to the previously examined intervention areas).

The effects that Energy Efficiency measures can have on energy demand, and therefore on the energy network management, can be grouped into three main categories:

- *Variation of the required amount of energy*, after the implementation of an Energy Efficiency measure the amount of energy required by the manufacturing system is reduced;
- *Variation of the energy demand profile*, after the implementation of an Energy Efficiency measure the manufacturing system requires energy at different times, i.e. at different hours of the day or in different periods of the year;
- *Partial or total isolation from the network*, after the implementation of an Energy Efficiency measure the manufacturing system does no more require energy from the network (or it can just occasionally require it).

As they have obviously different implications on the general balance of the network and usually require the adoption of very different strategies to be counterbalanced, their evaluation can be useful to deeply analyse the consequences of the implementation of an Energy Efficiency measure, to prioritize Energy Efficiency measures on a higher level (according to national and international policies and regulations) and eventually to study their influence on the global industrial energy demand.

Table 3 shows the qualitative evaluation of the impact of Energy Efficiency measures on the energy network, obtained by associating each intervention area defined in the previous paragraphs to the category or categories of the possible effects the Energy Efficiency measures of that particular area might have on the energy network.

In particular, from the analysis of Table 3 it is possible to observe that, referring to the "Supplier and tariff choice" area, the "amount of total energy consumption", the "peak demand management" and the "demand response and dynamic price systems" areas all insist mainly upon the variation of the demand profile (generally by shifting or shaving demand's peaks and by varying the production scheduling), while the "power factor correction" area abates the total amount of energy needed by both reducing the reactive power exchanged with the network and reducing Joule losses within the plant.

The onsite energy production can both isolate the plant from the network (considering cogeneration and trigeneration systems) and change the energy demand profile (considering renewable sources, such as photovoltaic, that produce energy in a determined range of hours per day).

Eventually, referring to the Specific Energy Consumption Reduction, all of the possible intervention areas affect both the amount of energy required and the energy demand profile (as they have all influences on the capability of the system to modulate and vary its demand according to the production fluctuations) but the Best Available Technologies Selection, that mainly affect the amount of energy required.

			Effects on the energy network		
			Variation of the required amount of energy	Variation of the energy demand profile	Partial or total isolation from the network
Specific Cost of Energy	Supplier and tariff choice	Amount of total energy consumption		X	
		Peak Demand		X	
		Demand Response and dynamic price systems		X	
		Power Factor correction	X		
	Compliance to contractual purchasing conditions		X	X	
	Onsite energy production			X	X
Specific Energy Consumption	Energy transformation, distribution and use (Design phase)	Technologies selection	X		
		Modulation technique selection	X	X	
		Dimensioning	X	X	
	Energy transformation, distribution and use (Operations and Maintenance phase)	Human behaviours	X	X	
		Best practices	X	X	
		Monitoring and Control	X	X	

Table 3. Qualitative evaluation of the impact of Energy Efficiency measures on the energy network.

5.1. Smart grids implementation

A brief but specific dissertation is here reserved to Smart Grids, whose development and diffusion over the last years have enabled and eased most of the previously illustrated Energy Efficiency opportunities (while the spread of Energy Efficiency culture all over the world has vice versa fostered Smart Grids' development), also allowing companies to manage and control their impact on the energy network (qualitatively discussed in the previous paragraph).

A Smart Grid is an electricity grid that allows the massive integration of unpredictable and intermittent renewable sources, and distributes power highly efficiently. It is an electricity network that uses distributed energy resources and advanced communication and control

http://dx.doi.org/10.5772/59820

technologies to deliver electricity more cost-effectively, with lower greenhouse intensity and with active involvement of the customers [106]. Smart Grids generally employ digital technologies and Information and Communication Technology (ICT) in order to improve reliability, security and efficiency of an electric system, coupling components that are typical of electricity grids (wires, substations, transformers, switches, etc.) and "smart" components, such as sensors (power meters, voltage sensors, fault detectors, etc.) and two-way digital communication technologies, which are able to continuously monitor the state of the network and of all the connected devices and therefore allow the real-time optimization of their functioning [107].

In other words, Smart Grids (or parts of them) are at the basis of most of the previously introduced Energy Efficiency measures, allowing companies to understand their own energy behaviour and needs, and therefore helping them making the best energy contract choice, verifying their compliance to contractual conditions, managing the integration of their onsite production to the energy distribution network, monitoring and controlling consumption and also verifying the effectiveness of the implemented Energy Efficiency measures.

It is a matter of fact that Smart Grids are currently used to correctly and effectively implement Demand Response Programs [108] and to take the best out of renewable sources, making it possible to overcome the problem of their intermittent and unreliable production. In addition, it is possible to state that they are essential to control and possibly mitigate (by promptly responding to the fluctuation of the monitored parameters) the variation of the amount of energy required and of the energy demand profile due to the implementation of Energy Efficiency measures, therefore gaining a relevant role in their feasibility evaluation.

Their role in implementing Energy Efficiency measure is about to be always more critical due to their continuous development and to their diffusion also at a medium and small scale and to the spread of the new Microgrids [107].

6. Conclusions

In the present chapter, authors have defined a conceptual scheme to organize and classify Energy Efficiency measures into different intervention areas in order to make it easier for practitioners to individuate and prioritize suitable improvement interventions and for researcher to frame their work in order to make it more accessible for industries.

While reviewing the specific literature of each intervention area, an evident gap between practical implementation and theoretical research evidently came out, also confirmed by authors' direct experiences and contacts with companies operating in the Italian context.

Considering that most researches in the field of Energy Efficiency of manufacturing systems are relatively recent and therefore not yet well known and widespread, companies are generally still far from being smart and efficient from that point of view, often applying quick fixes and improving isolated measures for Energy Efficiency enhancement rather than implementing a systemic and comprehensive approach, that would help catching all existent

opportunities and to whose development conceptual schemes like the one here presented can contribute.

Small and Medium Enterprises' situation is even more critical compared to big firms' one; main barriers to energy efficiency development are economic, information and behavioural, causing methods, tools and technologies discussed in previous paragraphs not or difficultly being implemented, as already highlighted for some of them, and also causing energy efficiency to be considered a marginal issue, scarcely correlated to systems' productivity and cost saving [109,110].

The present work and the approach to Energy Efficiency in manufacturing systems here proposed can therefore be considered as a starting point and a concrete contribution to the spread of the Energy Efficiency culture.

Eventually, a qualitative evaluation of the Energy Efficiency measures on the energy network has been proposed, in order to help evaluating benefits and consequences of the implementation of Energy Efficiency measure on a wider scale.

Author details

Miriam Benedetti[1*], Vittorio Cesarotti[2] and Vito Introna[2]

*Address all correspondence to: miriam.benedetti@uniroma2.it

1 Department of Industrial Engineering, "Tor Vergata" University of Rome, Rome, Italy

2 Department of Enterprise Engineering, "Tor Vergata" University of Rome, Rome, Italy

References

[1] Worrell E, Laitner JA, Ruth M, Finman H. Productivity benefits of industrial energy efficiency measures. Energy 2003;28 1081-1098.

[2] Boyd, GA, Pang, JX. Estimating the linkage between energy efficiency and productivity. Energy Policy 2000;28 289-296.

[3] Cesarotti V, Introna V, Scerrato G, Rotunno R. An empirical approach to investigate the relationship between Overall Equipment Effectiveness and Energy consumptions: an application in the manufacturing field. Proceedings of the XVIII Summer School Francesco Turco, Senigaglia (Italy), September 2013.

[4] Benedetti M, Cesarotti V, Introna V. Using simulation to study the influence of Overall Equipment Effectiveness on energy consumption of a single production machine.

http://dx.doi.org/10.5772/59820

Paper presented at the XIX Summer School Francesco Turco, Senigallia (Italy), September 2014.

[5] Pye M, McKane A. Making a stronger case for industrial energy efficiency by quantifying non-energy benefits. Resources, Conservation and Recycling 2000;28 171-183.

[6] Laitner JA. An overview of the energy efficiency potential. Environmental Innovation and Societal Transitions 2013;9 38-42.

[7] Benedetti M, Cesarotti V, Holgado M, Introna V, Macchi M. A framework for energy services within Product Service Systems classification. Paper presented at the XIX Summer School Francesco Turco, Senigallia (Italy), September 2014.

[8] Introna V, Cesarotti V, Benedetti M, Biagiotti S, Rotunno R. Energy management maturity model: an organizational tool to foster the continuous reduction of energy consumption in companies. International Journal of Cleaner Production, in press, DOI: 10.1016/j.jclepro.2014.07.001.

[9] Fysikopoulos A, Papacharalampopoulos A, Pastras G, Stavropoulos P, Chryssolouris G. Energy Efficiency of Manufacturing Processes: A Critical Review. Paper presented at the Forty Sixth CIRP Conference on Manufacturing Systems, Procedia *CIRP* 2013;7 628-633.

[10] Evans JA, Foster AM, Huet JM, Reinholdt L, Fikiin K, Zilio C, Houska M, Landfeld A, Bond C, Scheurs M, VanSambeeck TWM. Specific energy consumption values for various refrigerated food cold stores. Energy and Buildings 2014;74 141-151.

[11] Tangthieng C. Effect of tube diameter on the specific energy consumption of the ice making process. Applied Thermal Engineering 2011;31 701–707.

[12] Hosten C, Fidan B. An industrial comparative study of cement clinker grinding systems regarding the specific energy consumption and cement properties. Powder Technology 2012;221 183–188.

[13] Sharma GP, Prasad S. Specific energy consumption in microwave drying of garlic cloves. Energy 2006;31 1921–1926.

[14] Patterson MG. What is energy efficiency? Concepts, indicators and methodological issues. Energy Policy *1996*;5 (24) 377-390.

[15] Shao C, Guan Y, Wan Z, Chu C, Ju M. Performance analysis of CO2 emissions and energy efficiency of metal industries in China. Journal of Environmental Management 2014;134 30–38.

[16] Moya JA, Pardo N. The potential for improvements in energy efficiency and CO2 emissions in the EU27 iron and steel industry under different payback periods. Journal of Cleaner Production 2013;52 71–83.

[17] Choi Y, Zhang N, Zhou P. Efficiency and abatement costs of energy-related CO2 emissions in China: A slacks-based efficiency measure. Applied Energy 2012;98 198–208.

[18] Hasanbeigi A, Price L, Lin E. Emerging energy-efficiency and CO2 emission-reduction technologies for cement and concrete production: A technical review. Renewable and Sustainable Energy Reviews 2012;16 6220–6238.

[19] Morrow III WR, Hasanbeigi A, Sathaye J, Xu T. Assessment of energy efficiency improvement and CO2 emission reduction potentials in India's cement and iron & steel industries. Journal of Cleaner Production 2014;65 131-141.

[20] Duflou JR, Sutherland JW, Dornfeld D, Hermann C, Jeswiet J, Kara S, Hauschild M, Kellens K. Towards energy and resource efficient manufacturing: A processes and systems approach. CIRP Annals – Manufacturing Technology 2012;61 587-609.

[21] Carbon Trust. Focus on energy. A practical introduction to reducing energy bills. Action Energy second edition. Accessed 5 December 2013. http://www.east-ayrshire.gov.uk/Resources/PDF/E/EnergyAdvice-FocusonEnergy.pdf

[22] Morvay ZK, Gvozdenac DD. Applied Industrial Energy and Environmental Management. Chichester, UK: Jhon Wiley and Sons; 2008.

[23] Carbon Trust. Purchasing Power. Helping manufacturing companies in Northern Ireland buy and use electricity efficiently. Accessed 5 December 2013. http://www.manufacturingni.org/documents/J7655_Purchasing_power_NIM_report_INTERACTIVE.pdf

[24] Cesarotti V, Di Silvio B, Introna V. Evaluation of electricity rates through characterization and forecasting of energy consumption: A case study of an Italian industrial eligible customer. International Journal of energy sector management 2007;1(4) 390-412.

[25] Beretta F, De Carlo F, Introna V, Saccardi D. Progettare e gestire l'efficienza energetica [Designing and managing energy efficiency]. Milan: McGraw-Hill; 2012.

[26] Cesarotti V, Di Silvio B, Introna V. Energy budgeting and control: a new approach for an industrial plant. *International* Journal of energy sector management 2009;3(2) 131-156.

[27] Cesarotti V, Ciminelli V, Di Silvio B, Fedele T, Introna V. Energy budgeting and control for industrial plant through consumption analysis and monitoring. Paper presented at the 7th IASTED International Conference on Power and Energy Systems (EuroPES 2007), Palma de Maiorca, 29-31 August 2007 Proceedings 389-394.

[28] Chertow MR. Industrial Symbiosis, Literature and Taxonomy. Annual Review of Energy and the Environment 2000;25 313-337.

[29] Chertow MR. Uncovering Industrial Symbiosis. Journal of Industrial Ecology *2007;*11(1) 11-30.

[30] Chertow MR, Lombardi DR. Quantifying Economic and Environmental Benefits of Co-Located Firms." Environmental Science and Technology 2005;39(17) 6535-6541.

[31] Martin M, Svensson N, Eklund M. Who gets the benefits? An approach for assessing the environmental performance of industrial symbiosis. Journal of Cleaner Production, 2013 http://dx.doi.org/10.1016/j.jclepro.2013.06.024.

[32] Albadi MH, El-Saadany EF. A summary of demand response in electricity markets. Electric Power Systems Research 2008;78 1989-1996.

[33] Samadi M, Javidi MH, Ghazizadeh MS. The effect of Time-Based Demand Response Program on LDC and Reliability of Power System. Paper presented at the 21st Iranian Conference on Electrical Engineering (ICEE), 14-16 May 2013.

[34] Sezgen O, Goldman CA, Krishnarao P. Option value of electricity demand response. Energy 2007;32 108-119.

[35] Bhanot K. Value of an option to purchase electric power-the case of uncertain consumption. Energy Economics 2002;24 121-137.

[36] Faria P, Vale Z. Demand response in electrical energy supply: An optimal real time pricing approach. Energy 2011;36 5374-5384.

[37] Torriti J. Price-based demand side management: Assessing the impacts of time-of-use tariffs on residential electricity demand and peak shifting in Northern Italy. Energy 2012;44 576-583.

[38] Gaiser K, Stroeve P. The impact of scheduling appliances and rate structure on bill savings for net-zero energy communities: Application to West Village. Applied Energy 2014;113 1586-1595.

[39] Oren SS. Integrating real and financial options in demand-side electricity contracts. Decision Support Systems 2001;30 279-288.

[40] Fernandez M, Li L, Sun Z. 'Just-for-Peak' buffer inventory for peak electricity demand reduction of manufacturing systems. International Journal of Production Economics 2013;146 178-184.

[41] Bush V. Effective load management planning-a case study. Energy Engineering 2002;99(3).

[42] Wang Y, Li L. Time-of-use based electricity demand response for sustainable manufacturing systems. Energy 2013;63 233-244.

[43] Bello M, Fera M, Iannone R, Miranda S, Riemma S, Sarno D. A model for the estimation of the economic potential of a demand response system for the electric load

management. Proceedings of the XVII Summer School "Francesco Turco" Padua University, 2012.

[44] Aalami HA, Moghaddam MP, Yousefi GR. Demand response modeling considering Interruptible/Curtailable load and capacity market programs. Applied Energy 2010;87 243-250.

[45] Petrecca G. Industrial Energy Management: Principles and Applications, Norwell: Kluwer Academic Publishers; 2000.

[46] Prasanna Kumar,CS, Sabberwal SP, Mukharji AK. Power factor measurement and correction techniques. Electric Power Systems Research 1995;32 141-143.

[47] Mekhamer SF, El-Hawary ME, Mansour MM, Moustafa MA, Soliman SA. State of the art in optimal capacitor allocation for reactive power compensation in distribution feeders. Paper presented at the IEE large engineering systems conference on power engineering, *LESCOPE* 2002;02 61-75.

[48] Ortega JMM, Payan MB, Mitchell CI. Power factor correction and harmonic mitigation in industry. IEEE industry applications conference 2000;5 3127-3134.

[49] Sagiroglu S, Colak I, Bayindir R. Power factor correction technique based on artificial neural networks. Energy Conversion and Management 2006;47 3204-3215.

[50] Han Y, Khan MM, Yao G, Zhou L, Chen C. A novel harmonic-free power factor corrector based on T-type APF with adaptive linear neural network (ADALINE) control. Simulation Modelling Practice and Theory 2008;16 1215–1238.

[51] Austrian Energy Agency. Step by step guidance for the implementation of energy management. Wien: Österreichische Energieagentur; 2007.

[52] Carbon Trust. Energy Management. A comprehensive guide to controlling energy use. Accessed 5 December 2013. http://www.carbontrust.com/media/13187/ctg054_energy_management.pdf

[53] Energy Star. Guidelines for Energy Management. Accessed 29 January 2014. http://www.energystar.gov/buildings/sites/default/uploads/tools/Guidelines%20for%20Energy%20Management%206_2013.pdf?e4de-25bd.

[54] Carbon Trust. Renewable energy sources. Opportunities for business. Accessed 5 December 2013. http://www.carbontrust.com/media/7379/ctv010_-_renewable_energy_sources.pdf

[55] Viklund SB, Johansson MT. Technologies for utilization of industrial excess heat: Potentials for energy recovery and CO2 emission reduction. Energy Conversion and Management 2014;77 369-379.

[56] Fernandez I, Renedo CJ, Perez SF, Ortiz A, Mañana M. A review: Energy recovery in batch processes. Renewable and Sustainable Energy Review 2012;16 2260-2277.

[57] Carbon Trust. Small scale wind energy. Policy insights and practical guide. Accessed 5 December 2013. http://www.carbontrust.com/media/77248/ctc738_small-scale_wind_energy.pdf

[58] Carbon Trust. A place in the sun. Lessons learned from low carbon buildings with photovoltaic electricity generation. Accessed 5 December 2013. http://www.carbontrust.com/media/81357/ctg038-a-place-in-the-sun-photovoltaic-electricity-generation.pdf

[59] Carbon Trust. Biomass heating. A practical guide for potential users. Accessed 5 December 2013. http://www.forestry.gov.uk/pdf/eng-yh-carbontrust-biomass-09.pdf/$FILE/eng-yh-carbontrust-biomass-09.pdf

[60] Carbon Trust. Making sense of renewable energy technologies. Opportunities for business. Accessed 5 December 2013. http://www.carbontrust.com/media/63632/ctg011-renewable-energy-technologies.pdf

[61] Carbon Trust. Introducing combined heat and power. A new generation of energy and carbon savings. Accessed 5 December 2013. http://www.carbontrust.com/media/19529/ctv044_introducing_combined_heat_and_power.pdf

[62] Hepbasli A, Ozalp N. Co-generation studies in Turkey: an application of a ceramic factory in Izmir, Turkey. Applied Thermal Engineering 2002;22 679-691.

[63] Aras H. Condition and development of the cogeneration facilities based on autoproduction investment model in Turkey. Renewable and Sustainable Energy Reviews 2003;7 553-559.

[64] Emho L. District Energy Efficiency Improvement with Trigeneration: Basic Considerations and Case Studies. Energy Engineering 2003;100(2) 68-80.

[65] Hernandez-Santoyo J, Sanchez-Cifuentes A. Trigeneration: an alternative for energy savings. Applied Energy 2003;76 219-227.

[66] Temir G, Bilged D. Thermoeconomic analysis of a trigeneration system. Applied Thermal Engineering 2004;24 2689-2699.

[67] Ziher D, Poredos A. Economics of a trigeneration system in a hospital. Applied Thermal Engineering 2006;26 680–687.

[68] Sala A, Flores I, Sala JM, Millan JA, Gomez I, Lopez LM. Cogeneration technology for the metal-processing sector. Applied Energy 2008;85 516-527.

[69] Frangopoulos CA, Lygeros AI, Markou CT, Kaloritis P. Thermoeconomic operation optimization of the Hellenic Aspropyrgos refinery combined-cycle cogeneration system. Applied Thermal Engineering 1996;16 949-958.

[70] Arcuri P, Florio G., Fragiacomo P. A mixed integer programming model for optimal design of trigeneration in a hospital complex. Energy 2007;32 1430-1447.

[71] Gamou S, Yokoyama R, Ito K. Optimal unit sizing of cogeneration systems in consideration of uncertain energy demands as continuous random variables. Energy Conversion and Management 2002;43 1349–1361.

[72] Beihong Z, Weiding L. An optimal sizing method for cogeneration plants. Energy and Buildings 2006;38 189–195.

[73] Voorspools KR, D'haeseleer WD. Reinventing hot water? Towards optimal sizing and management of cogeneration: A case study for Belgium. Applied Thermal Engineering 2006;26 1972–1981.

[74] Salgado F, Pedrero P. Short-term operation planning on cogeneration systems: A survey. Electric Power Systems Research 2008;78 835–848.

[75] Matelli JA, Bazzo E, daSilva JC. An expert system prototype for designing natural gas cogeneration plants. Expert Systems with Applications 2009;36 8375–8384.

[76] Mancarella P. MES (multi-energy systems): An overview of concepts and evaluation models. Energy 2014;65 1–17.

[77] Sorrell S. The economics of energy service contracts. Energy Policy 2007;35 507-521.

[78] Saygin D, Patel MK, Worrell E, Tam C, Gielen DJ. Potential of best practice technology to improve energy efficiency in the global chemical and petrochemical sector. Energy 2011;36 5779-5790.

[79] Letschert V, Desroches L, Ke J, McNeil M. Energy efficiency e How far can we raise the bar? Revealing the potential of best available technologies. Energy 2013;59 72-82.

[80] Schollenberger H, Treitz M, Geldermann J. Adapting the European approach of Best Available Techniques: case studies from Chile and China. Journal of Cleaner Production 2008;16 1856–1864.

[81] Ibañez-Forés V, Bovea MD, Azapagic A. Assessing the sustainability of Best Available Techniques (BAT): methodology and application in the ceramic tiles industry. Journal of Cleaner Production 2013;51 162-176.

[82] Giner-Santonja G, Aragonés-Beltrán P, Niclós-Ferragut J. The application of the analytic network process to the assessment of best available techniques. Journal of Cleaner Production 2012;25 86-95.

[83] Du Plessis GE, Liebenberg L, Mathews EH. The use of variable speed drives for cost-effective energy savings in South African mine cooling systems. Applied Energy 2013;111 16–27.

[84] Tolvanen J. Saving energy with variable speed drives. World Pump June 2008 32-33.

[85] Abdelaziz EA, Saidur R, Mekhilef S. A review on energy saving strategies in industrial sector. Renewable and Sustainable Energy Reviews 2011;15 150–168.

[86] Thirugnanasambandam M, Hasanuzzaman M, Saidur R, Ali MB, Rajakarunakaran S, Devaraj D, Rahim NA. Analysis of electrical motors load factors and energy savings in an Indian cement industry. Energy 2011;36 4307-4314.

[87] Viholainen J, Vakkilainen E, Tolvanen J. VSD-control in simulated systems. World Pumps May 2009 40-48.

[88] Carbon Trust. Creating an awareness campaign. Accessed 29 January 2014. http://www.carbontrust.com/media/13089/ctg056_creating_an_awareness_campaign.pdf.

[89] Sweeney JC, Kresling J, Webb D, Soutar GN, Mazzarol T. Energy saving behaviours: Development of a practice-based model. Energy Policy 2013;61 371-381.

[90] Jain RK, Gulbinas R, Taylor JE, Culligan PJ. Can social influence drive energy savings? Detecting the impact of social influence on the energy consumption behavior of networked users exposed to normative eco-feedback. Energy and Buildings 2013;66 119–127.

[91] Chiang T, Mevlevioglu G, Natarajan S, Padget J, Walker I. Inducing [sub]conscious energy behaviour through visually displayed energy information: A case study in university accommodation. Energy and Buildings 2014;70 507–515.

[92] Spence A, Leygue C, Bedwell B, O'Malley C. Engaging with energy reduction: Does a climate change frame have the potential for achieving broader sustainable behaviour? Journal of Environmental Psychology 2014;38 17–28.

[93] Andreassi L, Ciminelli MV, Feola M, Ubertini S. Innovative method for energy management: Modelling and optimal operation of energy systems. Energy and Buildings 2009;41 436-444.

[94] Piper JE. Operations and Maintenance Manual for Energy Management, Sharpe Professional; 1999.

[95] U.S. Department of Energy. Operations & Maintenance Best Practices. A Guide to Achieving Operational Efficiency. Accessed 29 January 2014. http://www1.eere.energy.gov/femp/pdfs/omguide_complete.pdf.

[96] Trianni A, Cagno E, De Donatis A. A framework to characterize energy efficiency measures. Applied Energy 2014;118 207–220.

[97] Dai X, Kuosmanen T. Best-practice benchmarking using clustering methods: Application to energy regulation. *Omega* 2014;42 179-188.

[98] Dörr M, Wharens S, Bauernhans T. Methodology for energy efficiency on process level. Forty Sixth CIRP Conference on Manufacturing Systems, Procedia CIRP 2013;7 652 – 657.

[99] Cesarotti V, Di Silvio B, Introna V. Plant energy consumption reduction through monitoring and control system based on quality management concepts and tools. Paper presented at the 8th International Conference on The Modern Information Tech-

nology in the Innovation process of the Industrial Enterprises (MITIP 2006), 11-12 Septempber 2006, Proceedings 445-450.

[100] Cesarotti V, Di Silvio B, Introna V, Barile F. Energy monitoring and control for condition-based maintenance: case study of industrial cooling system. Paper presented at the 9th International Conference on The Modern Information Technology in the Innovation process of the Industrial Enterprises (MITIP 2007), Florence, 6-7 September 2007, Proceedings 327-332.

[101] Cesarotti V, Di Silvio B, Introna V. Improvement of maintenance practices through the introduction of energy consumption control system. Paper presented at the 11th International Conference on The Modern Information Technology in the Innovation process of the Industrial Enterprises (MITIP 2009), Bergamo, October 2009, Proceedings.

[102] Andreassi L, Ciminelli MV, Di Silvio B, Introna V, Ubertini S. Systematic approach to Energy Saving: an integrated methodology for industrial plant. International Journal of Energy Sector Management 2009; 3(2) 131-156.

[103] Carbon Trust. Metering. Introducing the techniques and technology for energy data management. Accessed 5 December 2013. https://www.carbontrust.com/media/31679/ctv027_metering_technology_overview.pdf

[104] Carbon Trust. Monitoring and targeting. Techniques to help organisations control and manage their energy use. Accessed 5 December 2013. http://www.carbontrust.com/media/31683/ctg008_monitoring_and_targeting.pdf

[105] Cesarotti V, Deli Orazi S, Introna V. Improve Energy Efficiency in manufactoring plants through consumption forecasting and real time control: case study from Pharmaceutical Sector. Paper presented at the International Conference on Advances in Production Management Systems (APMS 2010), Cernobbio, Como (Italy); 2010.

[106] Davoli F, Repetto M, Tornelli C, Proserpio G, Cucchietti F. Boosting energy efficiency through Smart Grids, ITU; 2012, http://www.itu.int/dms_pub/itu-t/oth/4B/01/T4B010000050001PDFE.pdf

[107] Clastres C. Smart grids: another step towards competition, energy security and climate change objectives. Energy Policy 2011;39 5399-5408.

[108] Mohsenian-Rad AH, Wong VWS, Jatskevich J, Schober R, Leon-Garcia A. Autonomous Demand-Side Management Based on Game-Theoretic Energy Consumption Scheduling for the Future Smart Grid. IEEE Transactions on Smart Grid 2010;1(3) 320-331.

[109] Trianni A, Cagno E, Worrell E, Pugliese G. Empirical investigation of energy efficiency barriers in Italian manufacturing SMEs. Energy 2013;49 444-458.

[110] Trianni A, Cagno E. Dealing with barriers to energy efficiency and SMEs: Some empirical evidences. Energy 2012;37 494-504.

Section 2

Energy Efficiency Improvements in Smart Grid Components - Intelligent Control System

Chapter 4

Energy Efficiency Improvements in a Distribution Network based on Local Voltage Control using Energy Storage Systems and Active Loads

Lucian Mihet-Popa and Voicu Groza

Additional information is available at the end of the chapter

http://dx.doi.org/10.5772/59308

1. Introduction

The European Union target for 2020, regarding CO_2decrease in the electricity sector,is of 20 %. This will assume animportant increase in PV installation all over Europe producing a few Giga Watts of additional capacity [1-4].

Today, the problem of energy efficiency becomes a very important issue. That means the entire industry is turning towards clean, renewable energy with different actively controlled loads, including Electric Vehicles (EV) and smart sensors. Increased distributed generation in the existing power systemsis becoming significant. In the near future it will be based on DER components including energy storage systems andon smart-grids [2, 5-12].

The battery package solutions are an interesting and useful option for storing surplus energy from the network (e.g. resulting from solar and wind intermittency) for a later use. It may also act as a peak shaving unit and thereby contribute to a stronger grid. Vanadium redox flow batteries have many advantages over other storage technologies, including storage efficiency, low maintenance costs and a long life cycle [13-17].

In order to study various aspects of Battery Storage Systems (BSS) accurate battery dynamic models are required [13-26].

Control strategies for battery energy storage systems have become a critical design issue. The challenge is to smooth the intermittent power output of RES, and to keep the rated voltage of the distribution substation within the standard limits [3, 9-12,19-24].

This paper focuses on simulation models, validated by measurements using experimental facility of an active and distributed power systems laboratory, with storage systems connected together with PV Systems and a Flex-House with controllable loads at a distribution network. Three types of local voltage control of the bus-bar to which the BSS was connected are also described, implemented and tested successfully.

This paper is structures as follows: in Section II, the distributed power system laboratory architecture is introduced; The Section III presents the simulation models of DER components used in this paper while the Section IV is devoted to implementation, simulation and testing of control strategies for DER components in a distribution network. Section V concluded this paper.

2. Distributed energy network architecture

The laboratory usedfor testing and to validate the simulation models in this research it is asmart grid with distributed control and with a high share of renewable systems.

The experimental facility of the lab contains a Wind/PV/Diesel Hybrid Mini-Grid with local storage and a novel control infrastructure. It includes two wind turbines (10 kW and 11 kW), three PV-plants (7.2 kW and 2 x 10 kW), a diesel gen-set (48 kW/60 kVA), an intelligent office building-Flex House with controllable loads (10 kW), a number of loads (75 kW, 3*36 kW), a Vanadium Redox Battery-VRB of 15 kW/120 kWh and three containers, each with an EV Li-ion battery pack of 50 Ah/16 kWh and 75 Ah/27 kWh, respectively and a bi-directional power converter of 90 kW.

The facility is spread across three sites located several hundred meters apart, as can be seen in Figure 1a).

At each of the sites there is a switchboard that let the already mentioned components to be connected to two bus bars. The components are all connected in one distributed control and measurement system that enables very flexible setup with respect to the experimental configuration [25-28], as it is shown in Figure 1b).

The acquisition of data and the control system (hardware and software) is capable for the supervision and control of the research platform with a high penetration of renewable energy systems. The software program, responsible for monitoring and supervision, is written in Java and is able to handle the data acquisition, and to control the outputs variable of the components. The sensors outputs are connected to a signal conditioning system, which in turn is connected to the data acquisition (DAQ) board based on SCADA System.

Certainof the active loads can be controlled by the centralized controller which is able to receive the data and the events from wireless switches and smart sensors. In control room, a small touch-screen graphical user interface can be used to change the controller policy (Figure 1c). The building controller can obtain information on the status of the power network, and based

http://dx.doi.org/10.5772/59308

on that will adapt its control strategy accordingly. The control system is based on a closed loop controller, in which the active policies, measurement data and user settings can be communicated back to the grid.

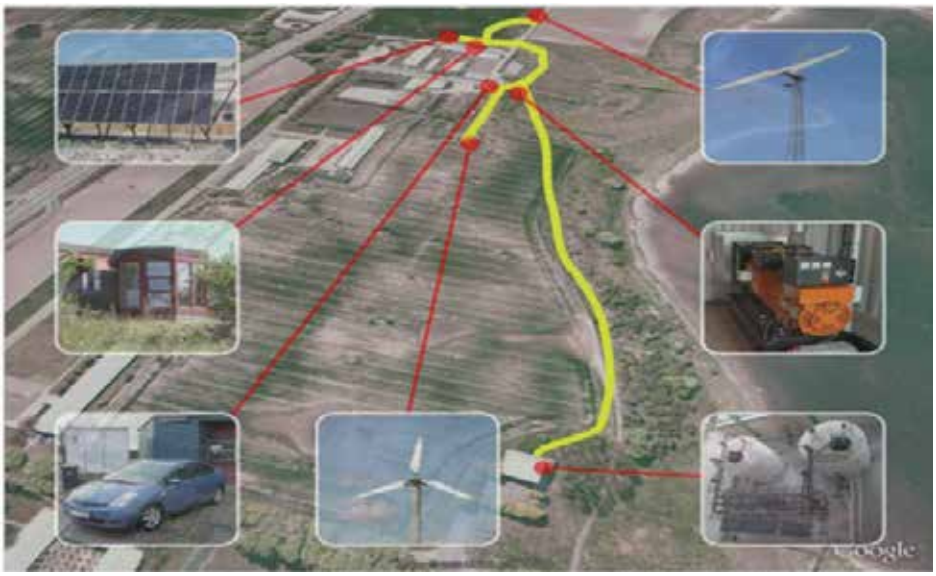

a)

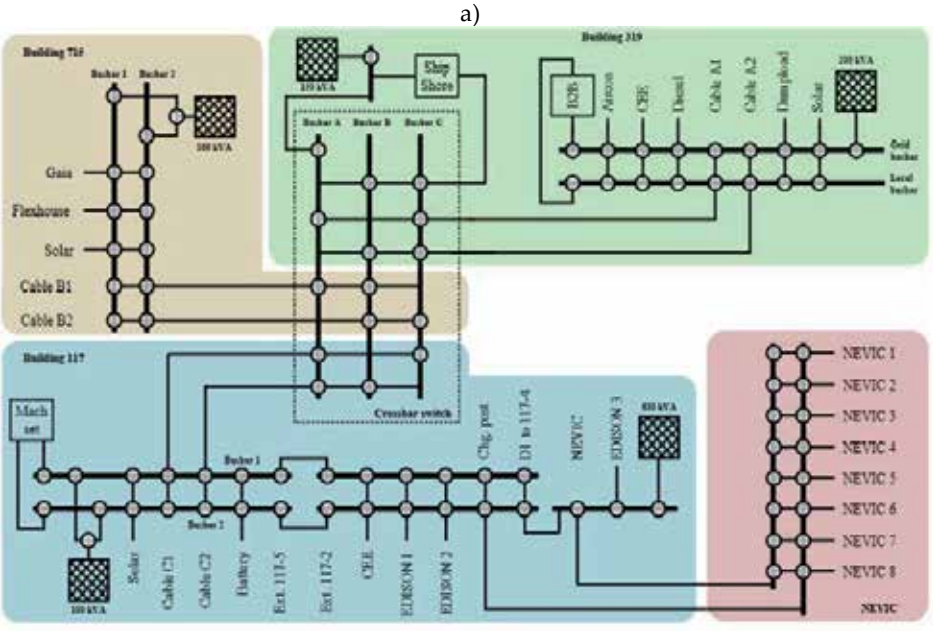

b)

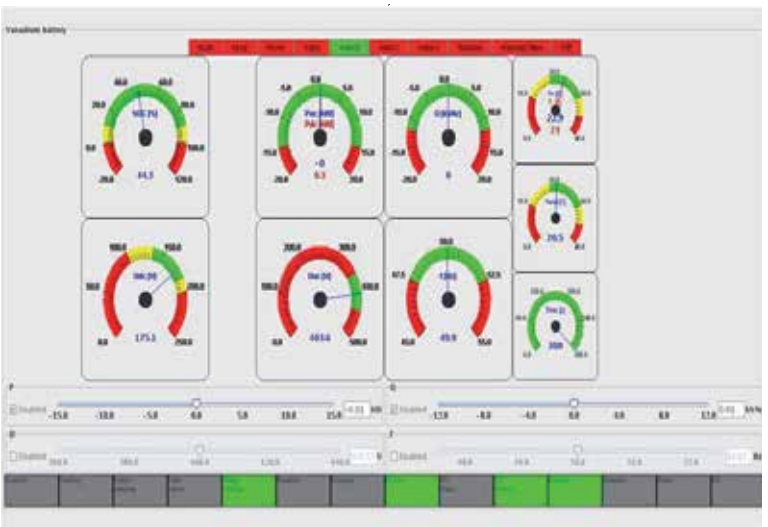

c)

Figure 1. a) The distributed power system laboratory with real components, b) details about the Micro-Grid architecture of the lab and c) GUI generated by SCADA for control system.

All units of the distribution network – generators, loads, storage systems, and the switchgear – are automated and remote-controllable.

Each unit is locally monitored and controlled by a specialized controller node.

The node is able to connect together an industrial PC, data storage, measurements and I/O interfaces into a portable and compact container with the backup power and the Ethernet switch inside.

The flexible control system was used for testing the components and the control strategies implemented, for the validation of the simulation models.

3. Distributed energy resources components modeling

3.1. PV panel and system modeling and validation

The model of the PV system contains the PV panel's model and the model of the inverter. It has as inputs the irradiation, the ambient temperature and the wind speed, which are converted into cell temperature and irradiation to be used as inputs for the model of the panels (Figure 2a), and as output the AC power from the inverter [25-28].The block *Measurements*, in Figure 1a), contains the inputs of the simulation model (irradiation, temperature and wind speed), which are used by the *Data processing* block as inputs to convert them into cell temperature and irradiation to be used further by *PV Panel* blocks, as inputs together with the number of cells in series (ns), the number of panels in series (nps) and with the number of strings in parallel (nsp).

http://dx.doi.org/10.5772/59308

The simulation model takes into account the variation of the parameters (open-circuit voltage-V_{OC} and short-circuit current-I_{SC}) with respect to temperature-T_{cell} and irradiation-G_{cell} and also the tilt angle and orientation of the panels.

The PV inverter is characterized by a power dependent efficiency where the input power of the model is the maximum DC power produced by the panels.

The dynamic model of the PV System (PV panels and PV inverter) has been built with standard block components from the library and also using the dynamic simulation language (DSL), in Power Factory, to implement the equations and to define the states and the parameters of the model.

The model of the panels is based on a single diode equivalent electrical circuit, described by an exponential equation [25-28], as can also be seen in Figure 2 b).

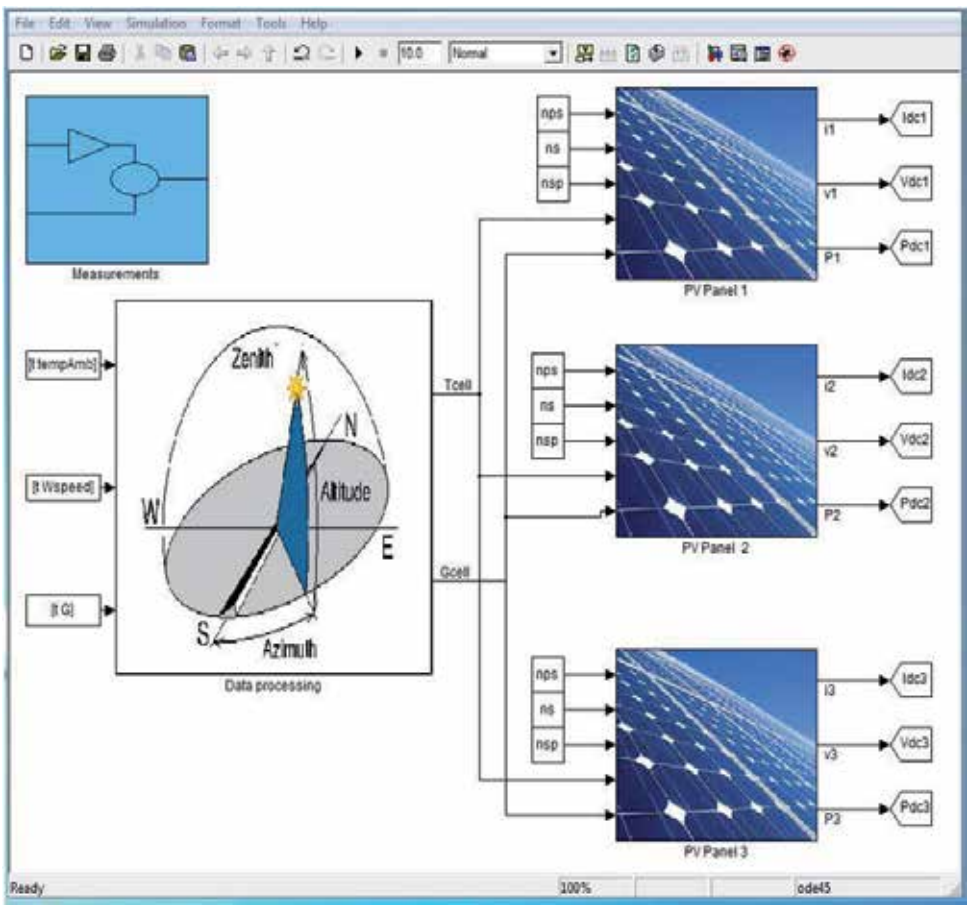

a)

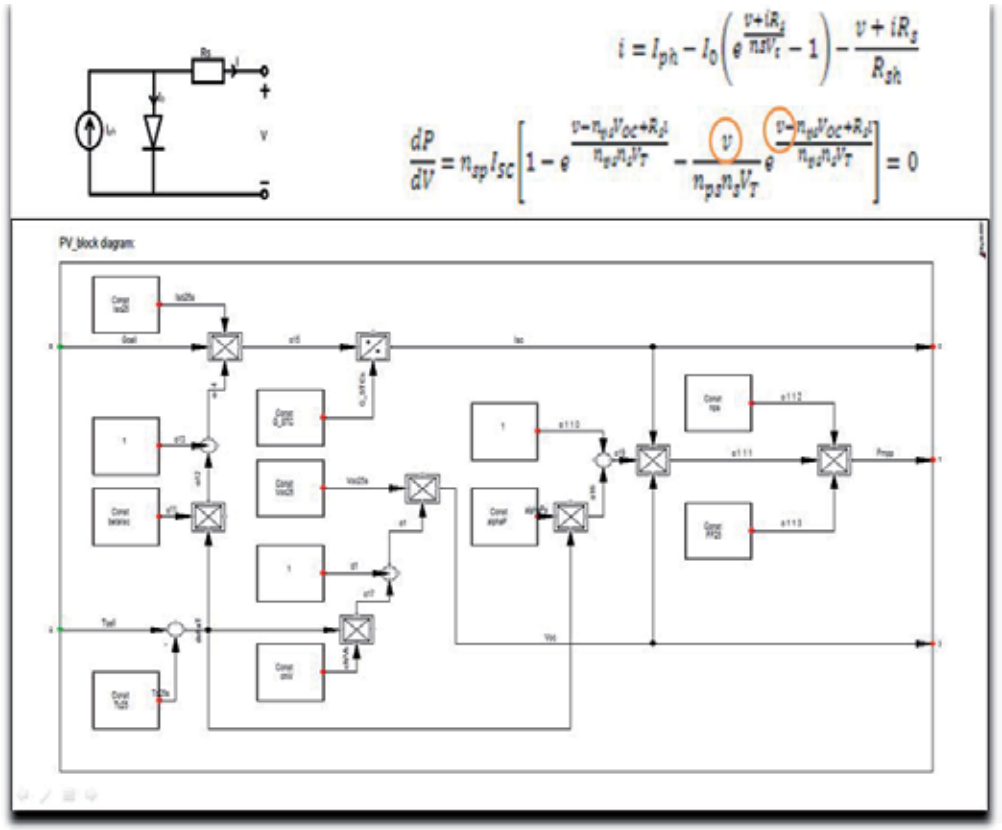

b)

Figure 2. Details about the single diode electrical circuit and the exponential equations of the PV model (on the top) and its implementation using standard block components.

The simulation model was validated using experiments carried out using experimental facility of a research and development lab with real components [25-28], as was shown in Figure 1.

A block diagram with the PV model implementation steps (Figure 3a) and with a comparison between simulation and measurements (Figure 3b) is shown in Figure 3.

To validate the simulation model of the PV components and PV systemsand to show the significance of considering the atmospheric conditions, such as irradiation, temperature and wind speed, and also the orientation of the panels and its tilt angle, the simulations were compared with experimental results (Figure 3b) carried out using the experimental facilities of the distributed power system laboratory-SYSLAB, shown in Figure 1.

The SCADA system facility disposes of two types of available measured data: ambient parameters (took from a weather station as can be seen in Fig. 3a) and electrical parameters (taken from the DAQ board of the PV inverter).

http://dx.doi.org/10.5772/59308

The ambient data are the wind speed, the ambient temperature and the horizontal solar irradiance. The data read from the weather station is measured in different conditions as the PV array: the irradiance is measured on a horizontal plane and the station is positioned further and higher than the PV array. The electric data represent the DC current, voltage and power on each of the three PV input strings, measured directly by the PV inverter.

The electric measurements have a time period of 1 seconds and the environment measurements have a sampling time of 10 seconds; thus the system changes states each 10 seconds, and only once in this 10 seconds interval the model takes the current value from the previous state.

In Figure3b) is shown a comparison between measured and simulated output power, voltage and current (P_{DC}, I_{DC}, V_{DC}) for a time series of 1 day. Considering the tilt angle and panels' orientation, the influence of solar irradiance and wind speed on the cell temperature the measurements and simulations are almost identically, as can be seen in Figure 3b).

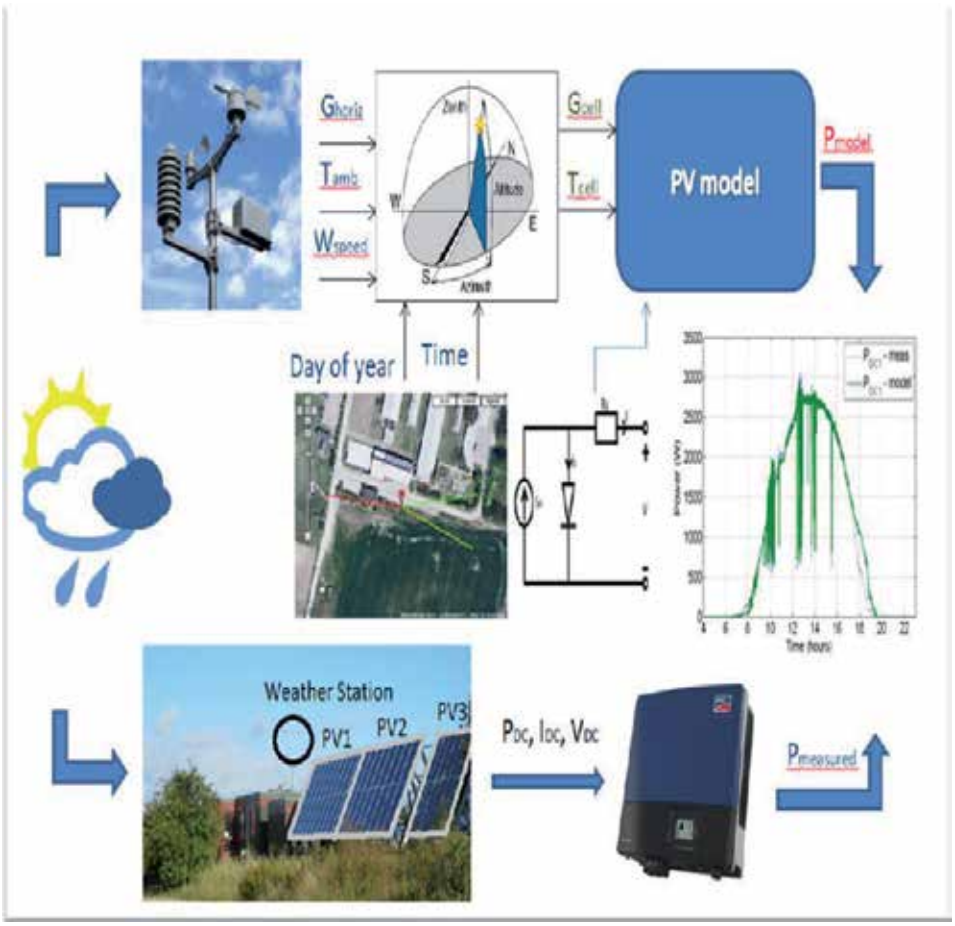

a)

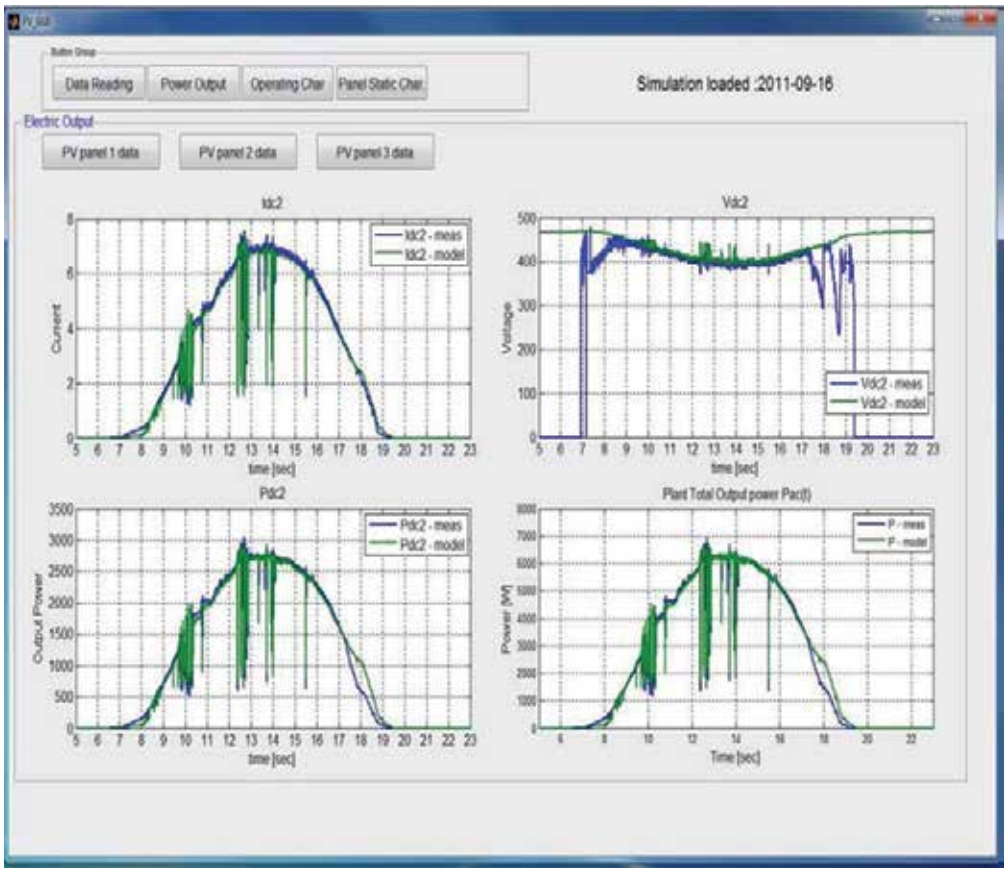

b)

Figure 3. a) A block diagram with details about the steps of PV simulation model implementation and b) comparison between simulations and measurements DC current, voltage and power for a PV panel and the output power of the inverter (Pac) as a function of time for 24h.

3.2. Actively controlled loads

The simulation model of the intelligent office building, called Flex-House, is based on the equivalent electro-thermal model of the building (Figure 4) using a stochastic discrete-time linear state-space model (1), combining with physical knowledge regarding heat transfer inside the house, together with statistical methods to estimate model parameters [28-29].

The office building is heated by 10 electrical heaters of 1 kW each, which can be used as active controllable loads in the distribution system.

The model for the building is formulated as one room lumped-RC-model in accordance with the commonly used thermal-electrical analogy:

http://dx.doi.org/10.5772/59308

$$\begin{cases} C_i \cdot \dfrac{dT_i}{dt} = \dfrac{1}{R_{ia}} \cdot (T_a - T_i) + \dfrac{1}{R_{im}} \cdot (T_m - T_i) + \dfrac{1}{R_{ih}} \cdot (T_h - T_i) + A_w \cdot G \\ C_m \cdot \dfrac{dT_m}{dt} = \dfrac{1}{R_{im}} \cdot (T_i - T_m) \\ C_h \cdot \dfrac{dT_h}{dt} = \dfrac{1}{R_{ih}} \cdot (T_i - T_h) + P_h \end{cases} \quad (1)$$

Where Ci is the heat capacity of the house, R_{ia} represents the thermal resistance from the indoor to the ambient, A_w is the effective window area of the house with heating influence. The state space variables are: T_i – inside temperature, T_m – second inside temperature which defines an internal medium and T_h – temperature in the electrical heater.

Figure 4 a) shows the heat flow diagram for the building (upper) and the equivalent RC-circuit, as well.

The implementation of the simulation model (Figure 4b) is based on (1) and is divided into four separate parts, a thermal model of the building (*FH_ThermalSlot* block), a controller model (*FH_Controller* block), a module to read input data (*FH_Input Measurement* block) and a load connected to a power system (*FH_LoadSlot* block). The input values are measured ambient temperature and solar radiation.From the right the blocks are: input data reader, thermal model of the building, the building temperature controller and the power system load model.

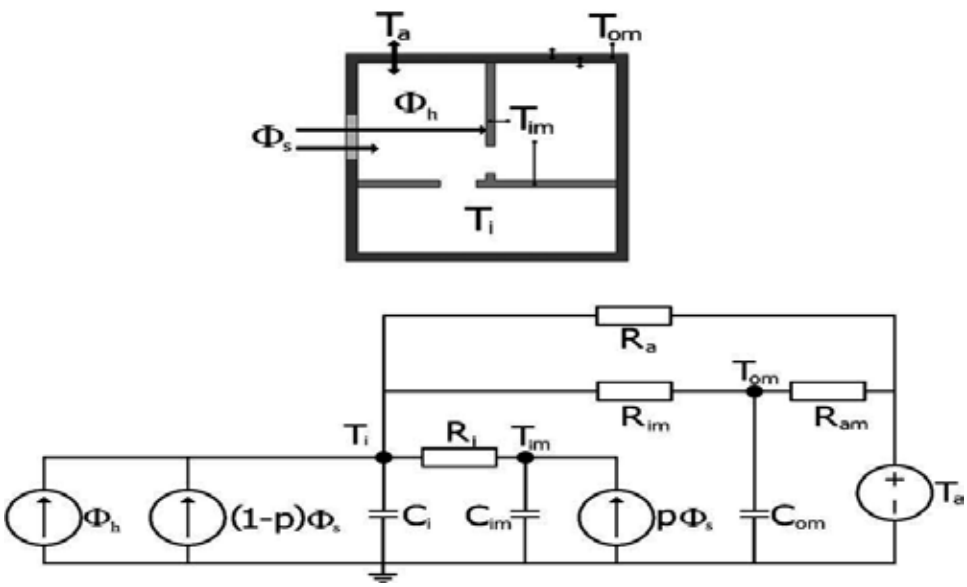

a)

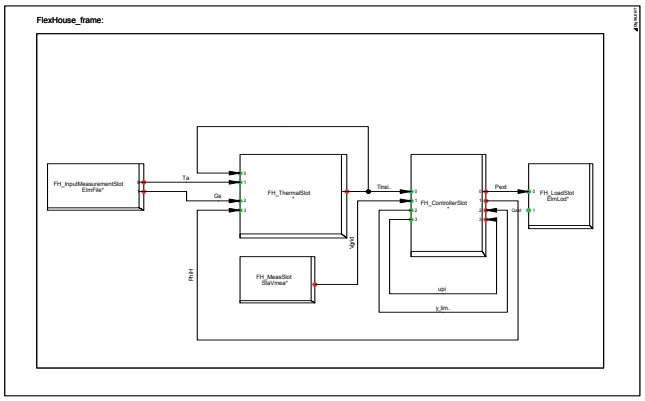

b)

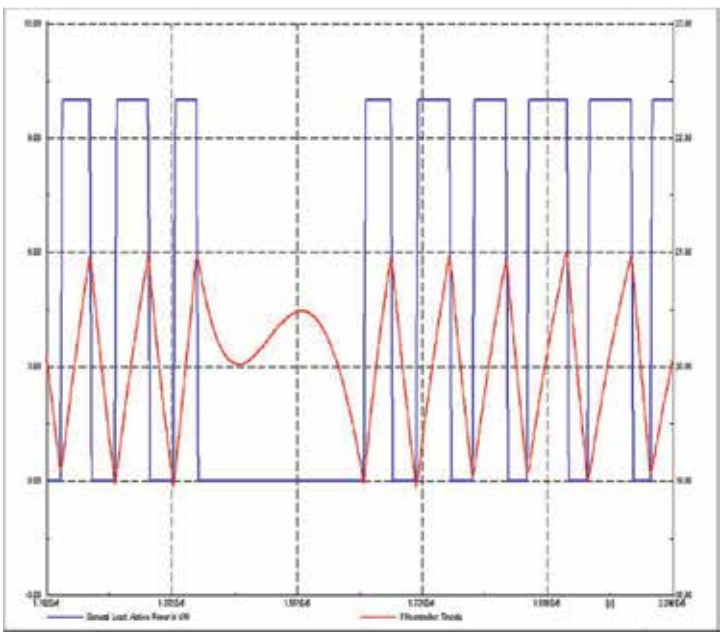

c)

Figure 4. a) Flex House office building heat-flow diagram (upper) and its equivalent single room RC-circuit diagram, b) implementation of the building model with actively controlled loads and c) simulation results of the temperature inside the building (T_{inside})and the power consumption of the heaters (Active Power) for one day.

Figure 4c) has shown a simulation of the temperature inside the building and the power consumption of the heaters, for one day, using measured temperature and solar radiation from SYSLAB via SCADA system, as inputs of the simulation model.

http://dx.doi.org/10.5772/59308

3.3. Battery energy storage components and systems modeling

We have used in this study, as battery energy storage components, 2 types of devices: a Li-ion battery of 26 kWh/75 Ah designed for EV applications and a Vanadium Redox Battery (VRB) package of 15 kW/190 kWh, for storing excess energy from the grid and to use it in order to control the grid voltage and frequency.

3.3.1. EV battery modeling and simulation

An equivalent circuit modeling with one or two RC block model is the common approach for lithium-cell batteries [14-17]. A single RC block model is adequate for many problems of industrial relevance and has also been used in this paper in combination with a runtime-based electrical battery model (Figure 5).

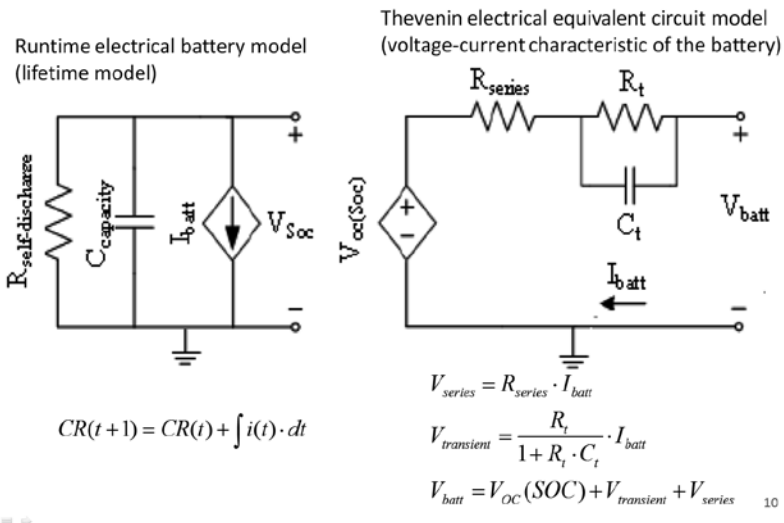

Figure 5. The electrical equivalent circuit model of the EV battery and its equations.

The runtime electrical battery model (on the left in Figure 5) represents the battery lifetime and contains a self-discharge resistor ($R_{self\text{-}discharge}$), a condenser ($C_{capacity}$) and a current-controlled source (I_{batt}). $R_{self\text{-}discharge}$ is used to characterize the self-discharge energy loss when batteries are stored for a long time and depends on SOC and temperature. $C_{capacity}$ represents the whole charge stored in the battery (SOC) and can be express like in Figure 5 [14].

Where Cn represents the nominal capacity of the battery and f_1(cycle) and f_2(T) are cycle number and temperature dependent correction factors.

On the right side in Figure 5 it is represented the Thevenin electrical circuit model which represents the voltage-current characteristic of the battery. The model contains a series resistor (Rs) and a RC parallel network (Rt, Ct) to predict the transient response of the battery. Each parameter of the Thevenin circuit is a function of SOC, current and temperature and was

implemented in MATLAB/Simulink and DIgSILENT Power Factory using two-dimensional look-up tables based on the measurements shows in Figure 6a).

The series resistance voltage droop (Vs) and the equivalent voltage transient response (Vt) are combined with the open-circuit voltage (VOC) to obtain the battery terminal voltage (V_{batt}), as it is described by the equations on the right side of the Figure 5.

The model of the battery pack was implemented based on the equations presented in Figure 5 and the measurements presented in [30] as shown in Figure 6. The model provides the SOC, power of the battery and the battery voltage as a function of SOC, current and temperature.

Each parameter of the Thevenin circuit is a function of SOC, current and temperature and was implemented using two-dimensional look-up tables based on the measurements at different SOC, current levels and temperatures using pulse current discharging/charging test.

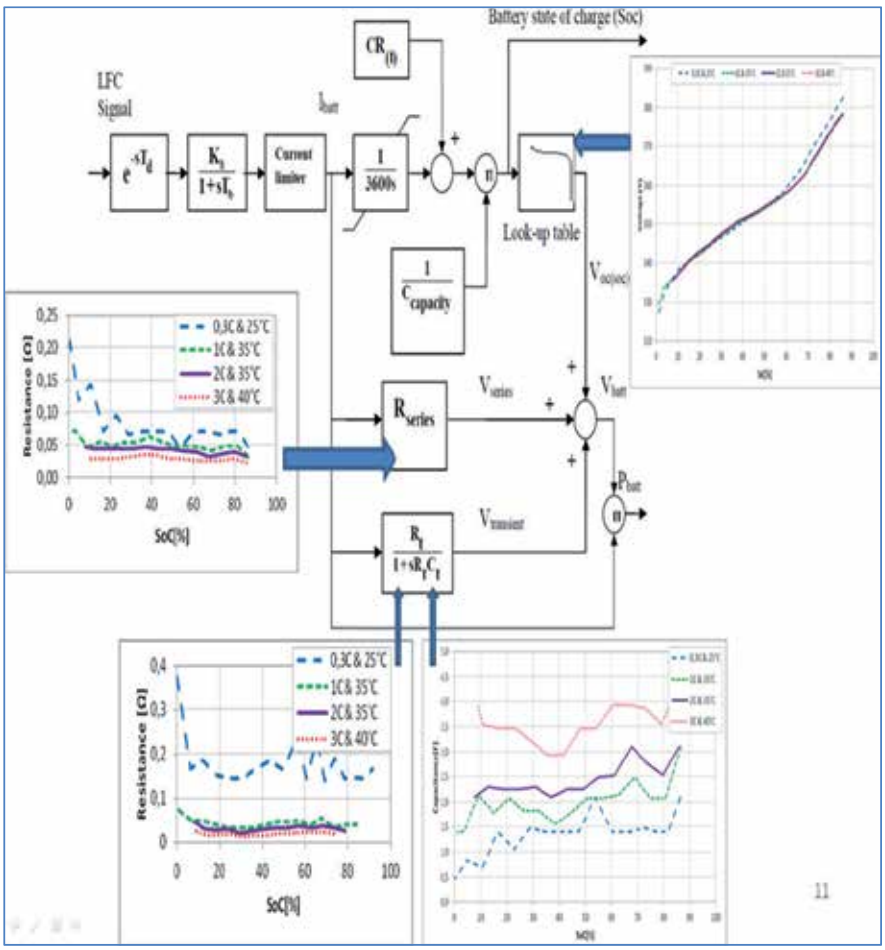

a)

http://dx.doi.org/10.5772/59308

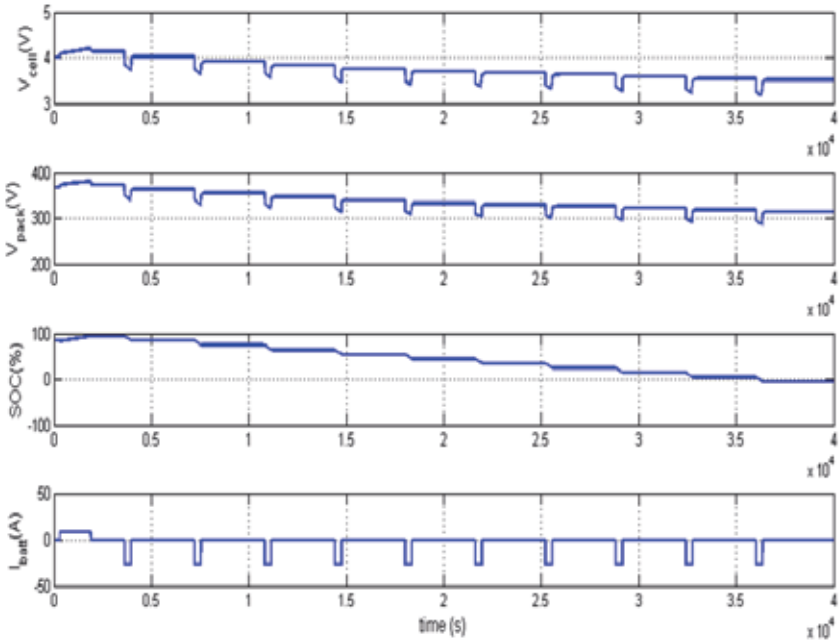

b)

Figure 6. a) Details with EV battery storage simulation model implementation based on equivalent circuit and measurements and b) simulation results of the EV battery pack system with a pulsed current during discharging mode.

In Figure 6b) was shown a time-series simulation with EVs battery cell and package voltage and SOC during the discharging mode when the battery was discharged from full rate to zero, when a battery constant pulsed current of 25 A was applied.

3.3.2. Modeling of the vanadium redox battery system validated by measurements

The VRB model has been implemented in MATLAB/Simulink and DIgSILENTPowerFactory [25]-[26] and is based on the equivalent electrical circuit using the power balance between the input and the stored power.

The power flow is dependent on the efficiency of different components, such as: cell stacks, electrolytes, pumps, power converter and also on the power losses, as it is shown in Figure 7a).

Figure 7b) shows the schematic structure of the simulation model implemented in Power Factory, including Battery Model, charge/discharge controller, PLL block and Static Generator with its Controller. The VRB system frame also contains the measurements blocks, such as voltage, active & reactive power and frequency, used as inputs for different components of the model. The VRB Simulation Model has as outputs cell current and voltage and SOC level, which are the inputs for charge/discharge controller, as can also be seen in Figure 7b).

The simulation model was validated by measurements taken from the DAQ board of the VRB system.

The experiment have been acquired for a time scale of 36 hours considering the starting pointof the SOC=93.5%, meanwhile the battery was discharged with a constant power of P_{AC}=15kW, until the State of Charge decreased to SOC=18%. After that a sequence of charging was considered from SOC=14% until SOC=87% at the constant power of P_{AC}=10kW.

As can be seen in Figure 7c) a comparison between simulation results and experiments of the SOC level of the battery is presented. It is shown a very small difference between curves, which means that the developed simulation model can be consider an accurate tool for studying and analyzing the characteristics of the battery energy storage system in a distributiongrid.

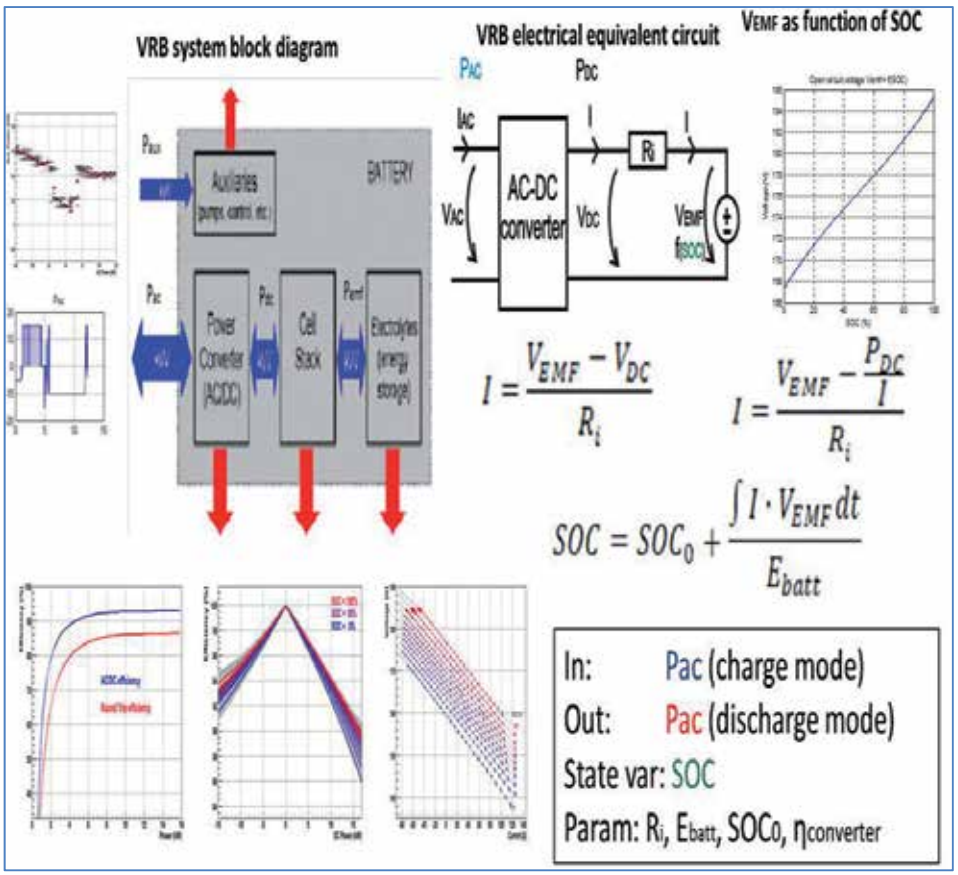

a)

http://dx.doi.org/10.5772/59308

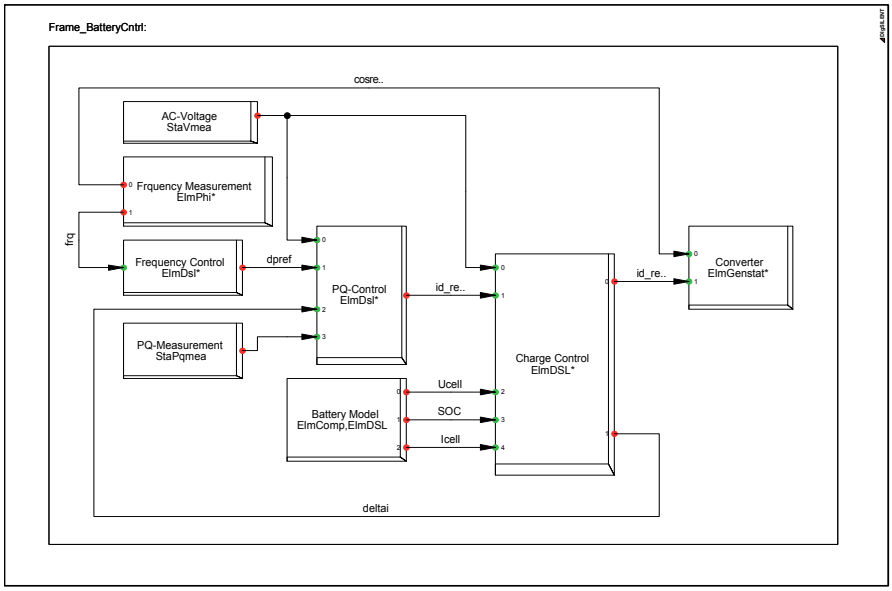

b)

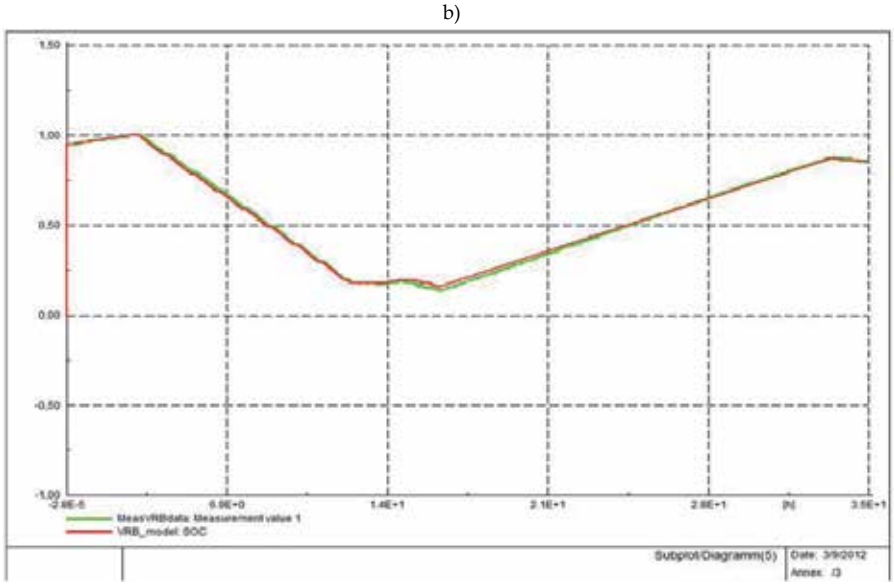

c)

Figure 7. a) VRB simulation model implemented using experimental results based on the equivalent circuit, b) block diagram of the Battery System Simulation Model and c) comparison between simulations and measurements.

These characteristics of the battery have been computed based on the results of experiments [14] where different electric values at different loads and SOC levels were measured. The

simulation model was validated by measurements using experimental facility of the active and distributed power systems laboratory presented in Figure 1 [25-26].

4. Control strategies of DER components in a distribution network

As a part of the power system, the low-voltage distribution grid has the objective to provide energy to the end consumer.

A major objective in a distribution network is to control the voltage due to a large number of factors, such as various load profiles and load types or due to a different number of phases (asymmetrical distribution of DERs in the network).

In Figure 8 a) is depicted the configuration of the consumersalong a feeder in a distribution network with a voltage profile increasing or decreasing in function of the number of active loads (including EVs) and PV systems connected to the distribution network along the feeders.

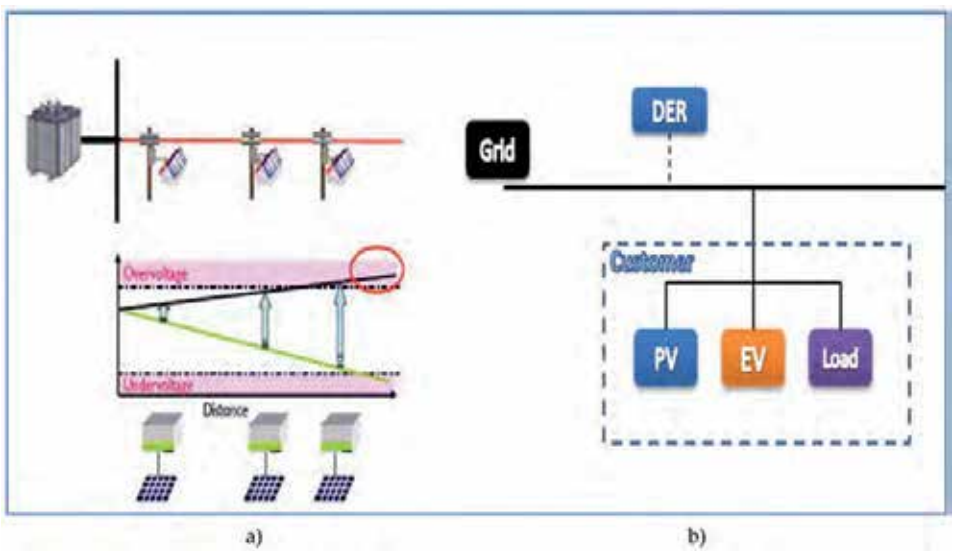

Figure 8. a) Voltage profiles in a low-voltage distribution grid with b) DER components used in this study.

Due to the PV penetration the voltage along the feeders could increase over the admissible limits defined by standards. Also, due to the EVs connected along the feeders the voltages can decreases exceeding the minimum level. In this case a local voltage controller using distributed energy storage and/or a local voltage controller by load shifting could be an option.

Three types of controllers for voltage regulation have been developed and implemented in MATLAB/Simulink and DIgSILENTPowerFactory, for controlling the bus-bar voltage at the connecting point.

http://dx.doi.org/10.5772/59308

One of them is based on local control by load shifting and two of them are controlling the voltage with the help of energy storage systems.

4.1. Voltage control by load shifting

The ability to control active units (only Flex House heaters in our case) will decrease the tension on the low-voltage distribution network by consuming locally the PV production. The energy management systems of the smart houses, such as the SMA Sunny Home Manager [17], can raise the contribution of PV energy being consumed at the distribution customer's site. Therefore decentralized consumption is raised and the stress and losses in the grid are decreased.

4.1.1. Implementation

To test the voltage controller the Flex House has only been connected with the PV system at the same bus-bar, as was shown in Figure 8b).

The simulation model of the intelligent office building, called Flex-House, is based on the equivalent electro-thermal model of the building, presented in (Figure 4) using a stochastic discrete-time linear state-space model (1) combining with physical knowledge regarding heat transfer inside the house together with statistical methods to estimate model parameters [13]-[15], [26].

The model contains 2 subsystems, a thermal model of the building and a voltage controller model. A module to read input data and a load connected to the power system is also included. The input values are measured ambient temperature and solar irradiation. Figure 9a) shows the block diagram of the building model implemented in MATLAB&Simulink with details about the voltage controller implementation using stateflow chart, presented in Figure 9b).

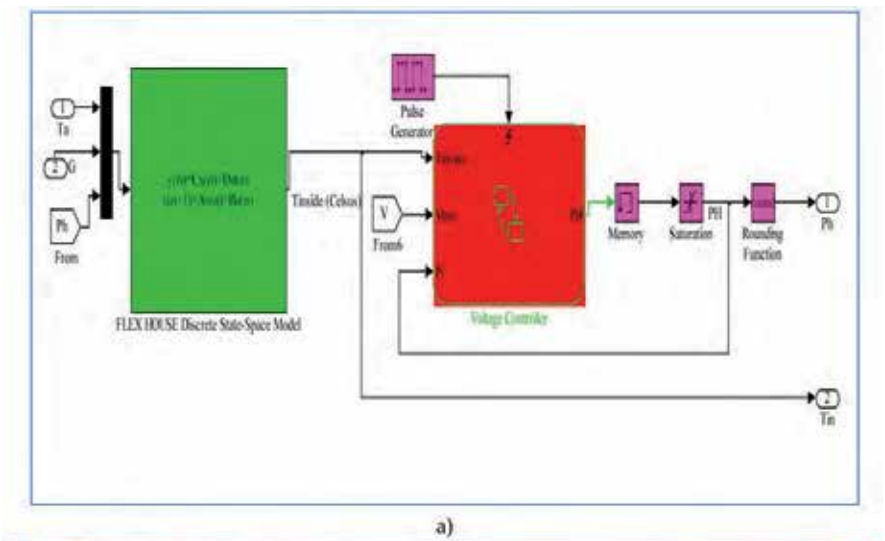

a)

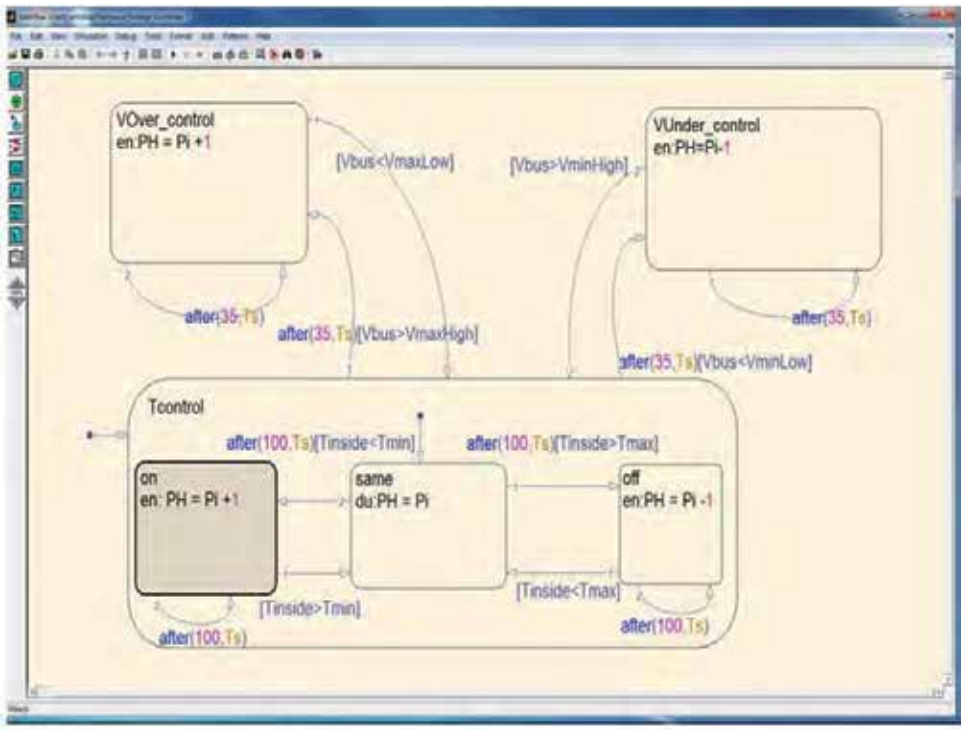

b)

Figure 9. a) Implementation of the Flex House simulation model with voltage controller using stateflow chart and b) details about voltage controller implementation.

The voltage controller was developed using a state flow chart, which is an interactive graphical design tool for developing and simulating event driven system based on finite-state machine theory. It is a thermostatic control for the building, so that when the temperature inside the building is below a certain set point the heaters in the building turn on, and when the temperature is above another set point the heaters turn off.

4.1.2. Simulation results versus measurements

Figure 10 point out the simulation results with a comparison between normal operation (Figure 10 a), when the voltage control is not activated, and the situation when the voltage at the local bus-bar is controlled using the load shifting (Figure 10 b) by consuming the PV energy production. The voltage was kept under a certain level (1.04 in this case) when the PV production growths, increasing the heaters power (FH power) and doing that the inside temperature of the house. As was shown in Figure 10 b) when the power production increased more heaters were switched on by the local controller and the inside temperature was increased from 21 ^{0}C to 27 ^{0}C.

http://dx.doi.org/10.5772/59308

To validate the local voltage controller in Figure 10c) it is shown an experimental test using the distributed power system laboratory presented in Figure 1, when the PV system was connected to the grid together with the Flex House.

The parameters which were monitored are heaters output power, the temperature inside the office building and the voltage, which was measured at the bus-bar where the Flex House was connected. As was shown in Figure 10c), when the voltage overtaken the maximum value, set it up at 398 V in this case, the local controller reacts by modifying the heaters power, and implicitly the inside temperature of the house.

The events that point out the state transitions are marked with colored circles. The marks in the first graphic correspond to the local controller response and are the effect of the voltage limit intersection with the voltage at the bus-bar. This voltage is also plotted in the third window. The red circles point out the events when the bus-bar voltage increases to the upper limit, while the blue circles show the events when safe voltage limits are touched and the local controller turns back to the control state.Finally, the green circles show the events when the lower voltage boundary is touched.

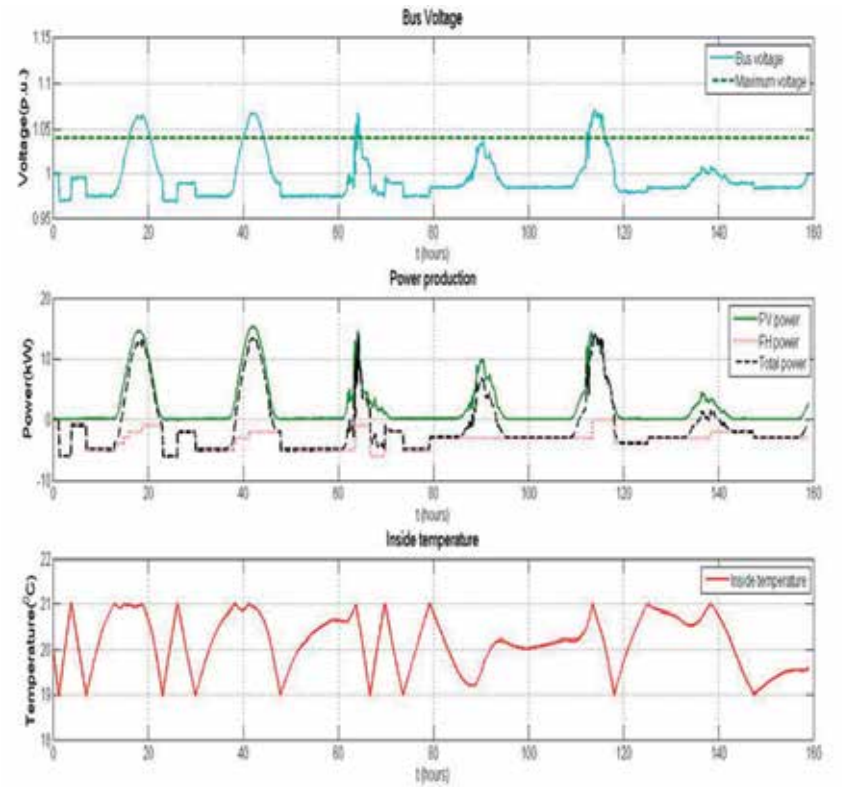

a)

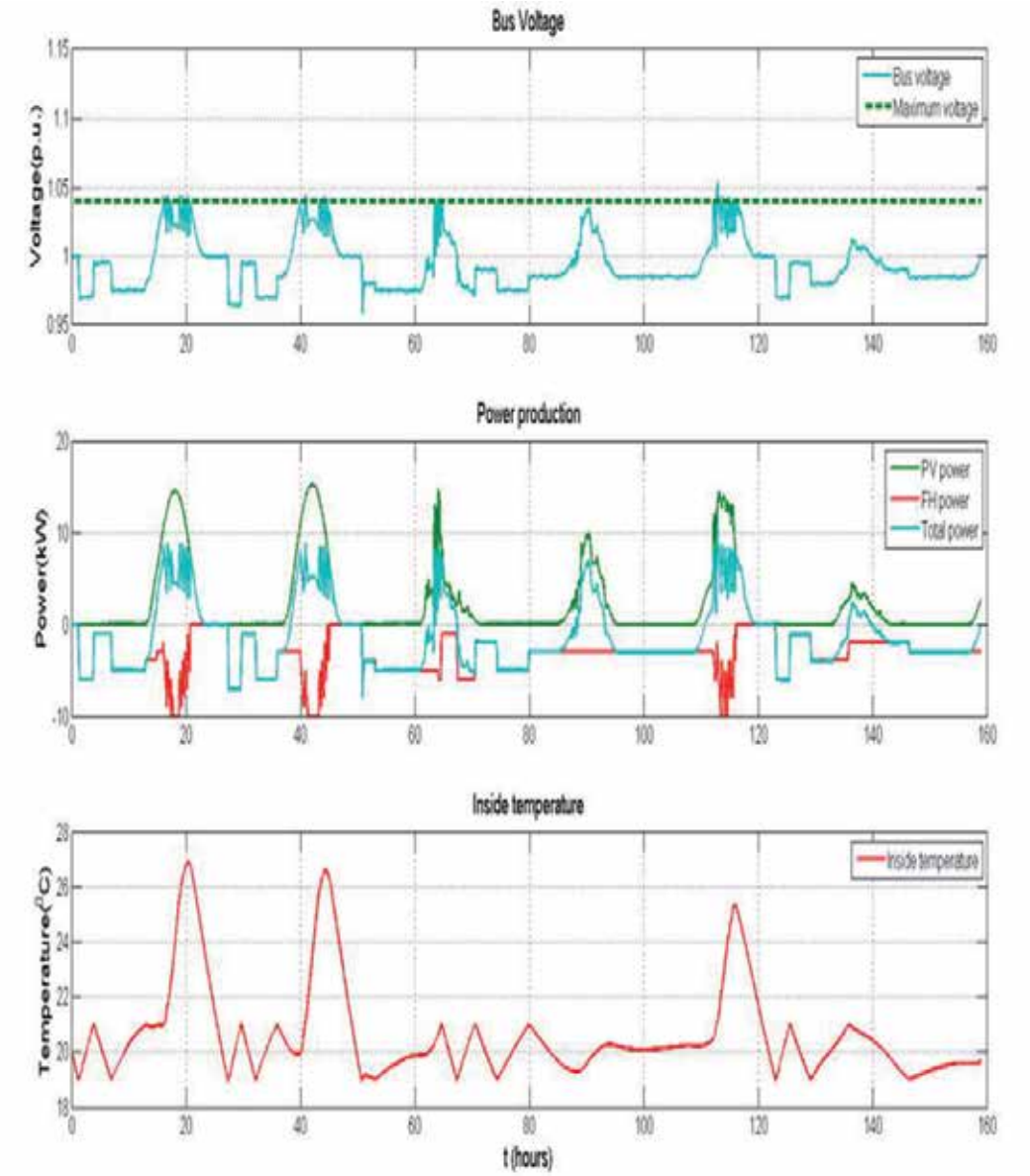
Bus Voltage
Bus voltage
Maximum voltage
Voltage(p.u.)
1.15
1.1
1.05
1
0.95
0
20
40
60
80
100
120
140
160
Power production
PV power
FH power
Total power
Power(kW)
20
10
0
-10
Inside temperature
Inside temperature
Temperature(°C)
28
26
24
22
20
18
t (hours)

b)

http://dx.doi.org/10.5772/59308

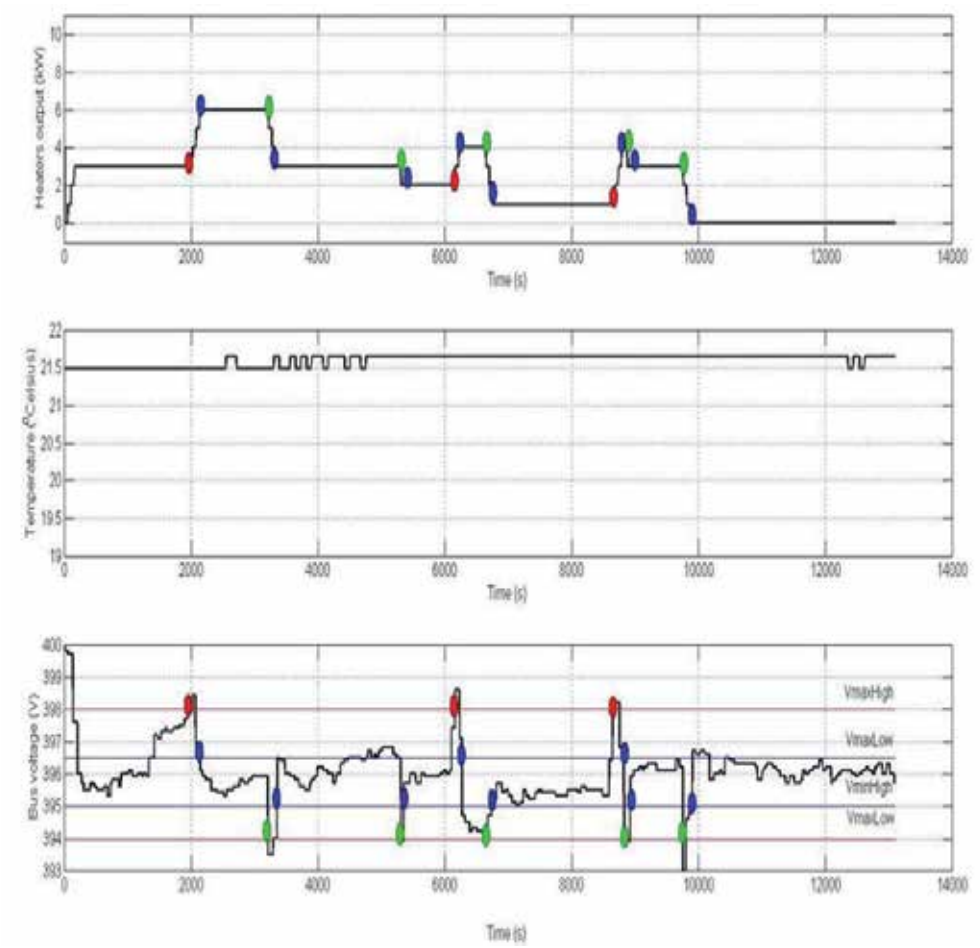

c)

Figure 10. a) Normal operation without any control versus b) local voltage control by load shifting, and c) voltage controller validated by measurements using the distributed power system lab from Figure 1.

4.2. Voltage control using battery energy storage systems

4.2.1. Implementation

Two voltage controllers have been developed and implemented based on finite state machine for controlling the bus-bar voltage at the connecting point (Figure 11).

An overvoltage controller, able to charge the battery when the bus-bar voltage exceeds the limits (Figure 11b), and a voltage controller able to set-up the battery to run in schedule mode (Figure 11c), have been implemented in MATLAB/Simulink and DIgSILENTPowerFactory.

The first controller adjusts the voltage at the bus-bar charging the battery when an overvoltage is detected. That means the voltage is adjusted at the bus bar when exceeds the maximum value (set-up here at 1.1 Un), due to the PV production, modifying the state of the battery (discharging/charging).

Only when an over-voltage is detected the controller will modify the charging state of the battery.

Another method of controlling the voltage with the help of storage energy systems it is to set the EV to run in schedule mode. That means the battery is scheduled to operate during the day in function of the weather conditions, such as PV penetration. This control method doesn't require any voltage measurements on the bus-bar, but it has to be appropriately scheduled for charging with the right amount of energy in the middle of the day.

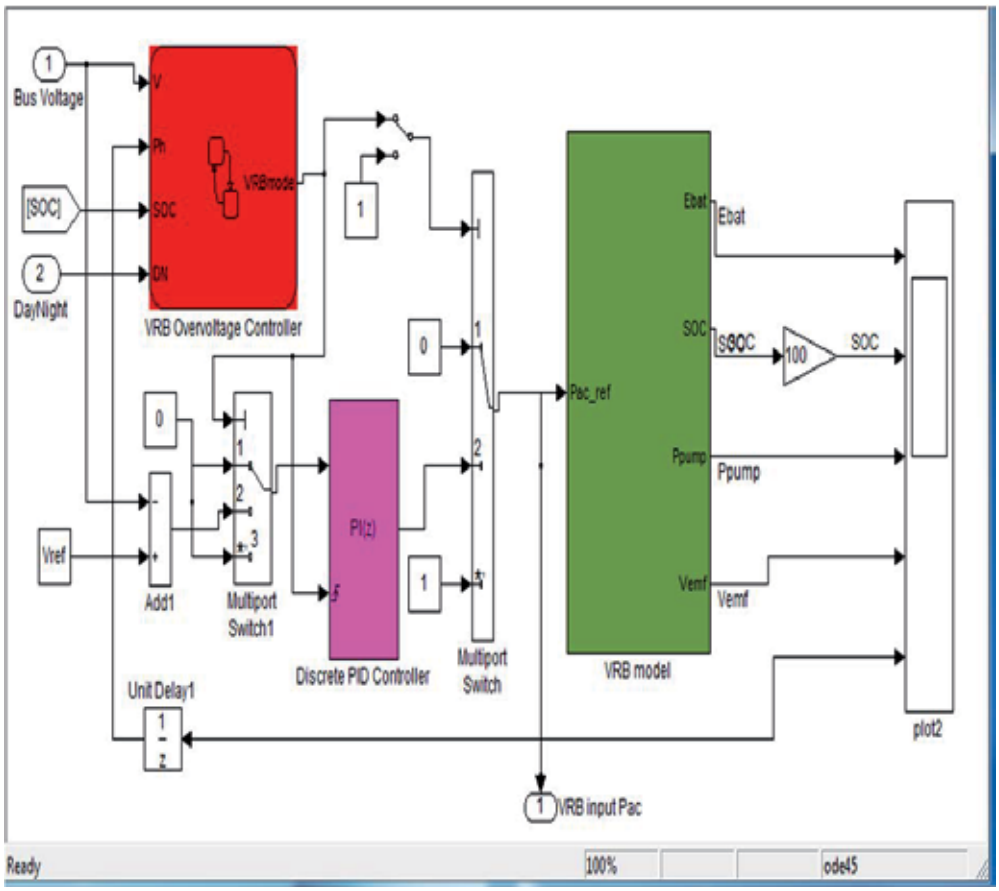

a)

http://dx.doi.org/10.5772/59308

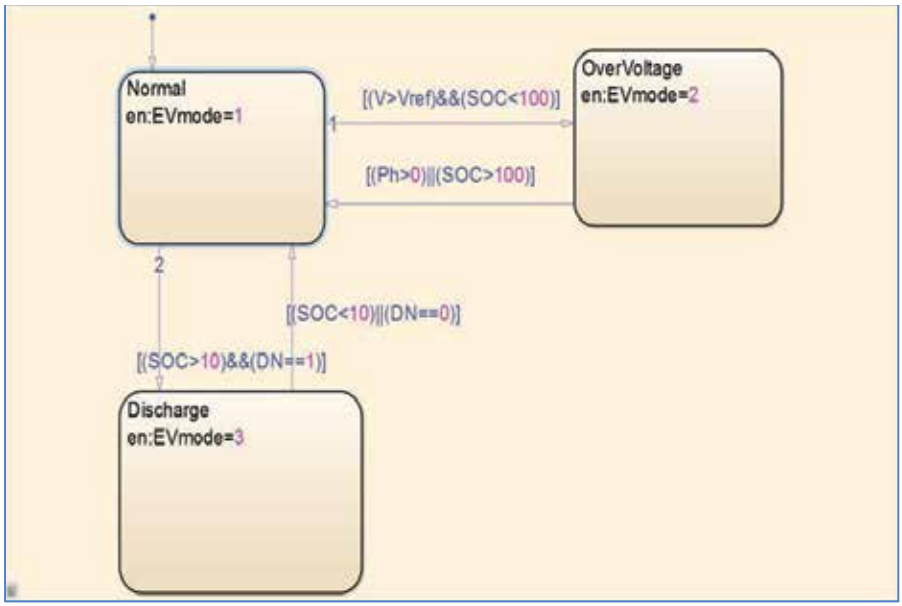

b)

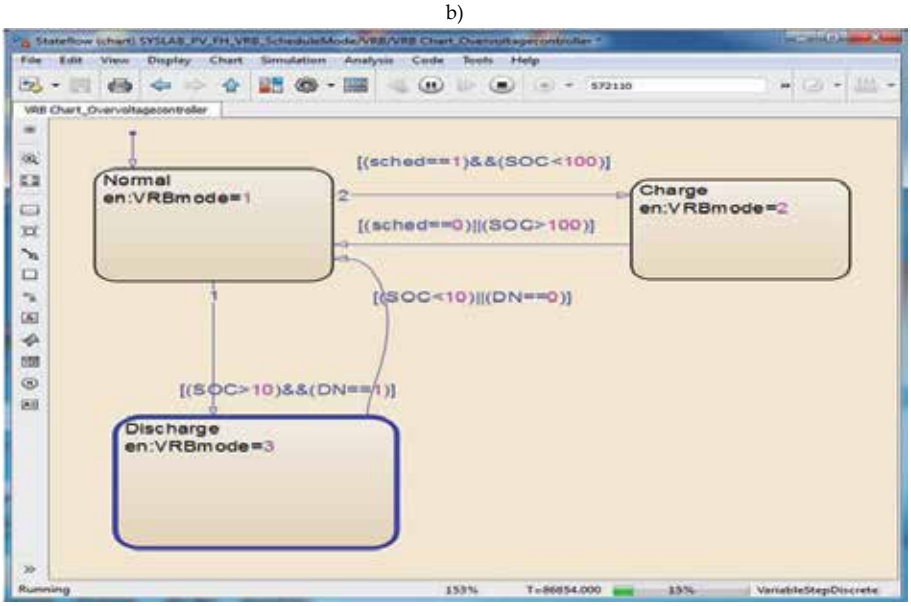

c)

Figure 11. a) Implementation of the EV model with the voltage controller, b) voltage controller developed in state flow for over-voltage control and c) EV controller implementation using schedule mode.

4.2.2. Simulation results

This section shows two study cases with PV production for 1 week. The PV system is connected together with the Smart-House at the same bus-bar, whilst the battery energy storagesystem is connected to a different bus-bar at the same distributionnetwork, as can be seen in Figure 12 a). Due to the PV penetration, voltage at the bus-bar will exceds the upper acceptable value (set-up at 1.1 in this case regarding European norm EN 50160). Integration of energy storage systems in distribution network to store excessive energy can be a solution to alleviate the over-voltage problem.

Figure 12 b) shows the case when the voltage controller (presented in Figure 12 b)) is employed. The EV's operation here is outlined as using the voltage control during the day, when the PV system is producing the power. The EV battery system is connected to the network only when an over voltage exists and it consums the surplus active power until the power injected into the grid is not affecting the voltage to the bus-bar, exceeding the voltage limit, as can also be seen in Figure 12 b).

In Figure 12 c) is shown the simulation results for another case when the voltage is controlled bya static battery storage system (VRB system in our case), arranging the battery to work in scheduling mode. The VRB was programmed to operate (charged) between 10-18 o'clock during the day, when the PV systems produce the active power, and has been discharged during the night, operating in an efficient way. The drawback of this case is that the VRB has to be suitably scheduled of charging itself with the appropriate amount of energy in the daytime.

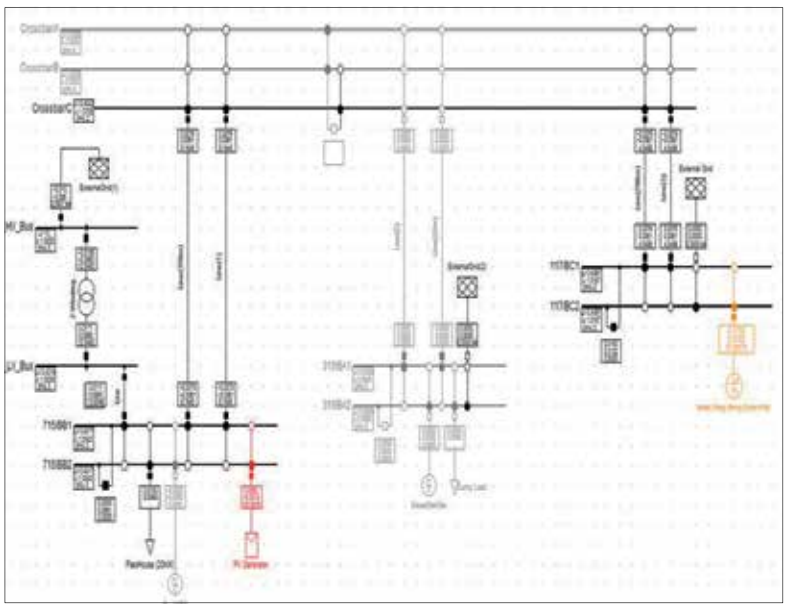

a)

http://dx.doi.org/10.5772/59308

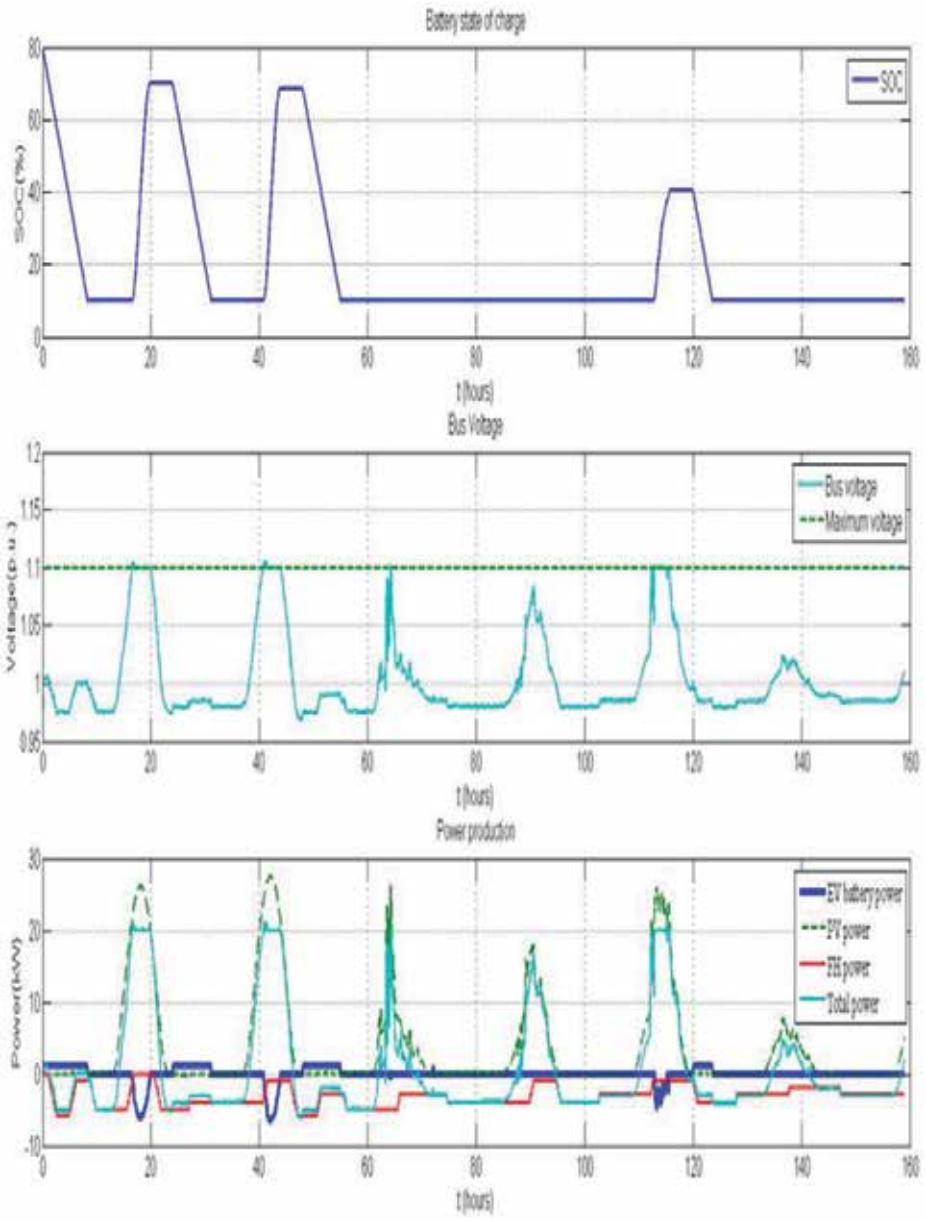

b)

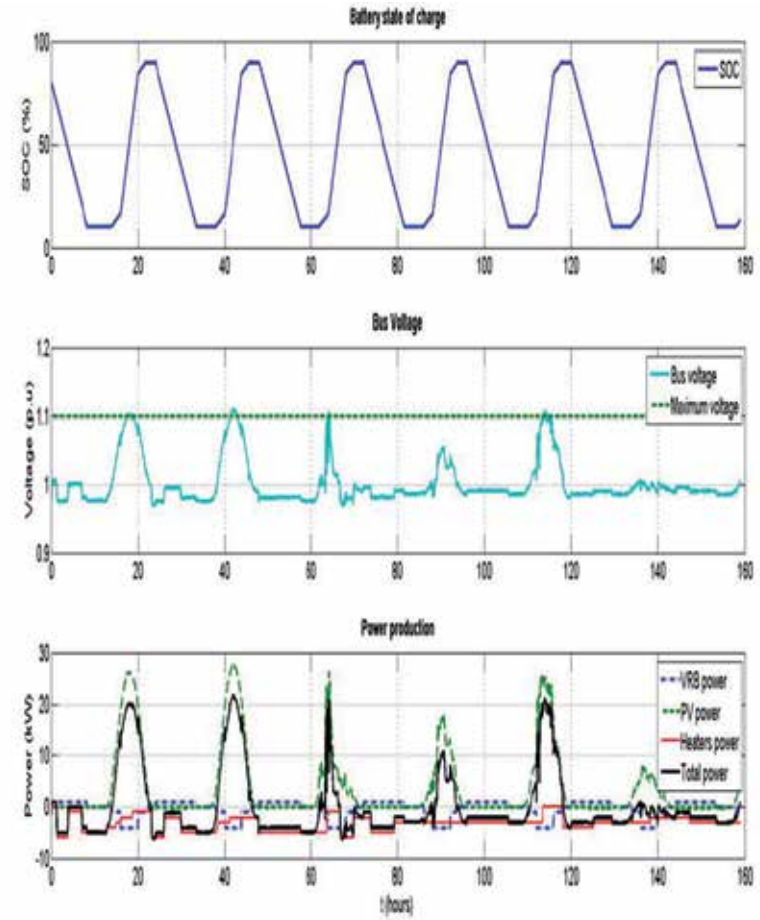

c)

Figure 12. a) Simulation results for normal operation, b) with over voltage control and c) with EV battery control in schedule mode.

5. Conclusion

In this paper we have described the development of simulation tools for DER components in a distribution network. The main focus was on modeling and implementation of the model components and systems with voltage controllers using a smart-house load shifting and using energy storage systems (EV battery), as well, for PV penetration.

The simulation models wereelaborated to simulate and test the growth PV production effects on voltage variations in a distribution network. Another objective has been to use it in simulating distribution system power constraints and methods for assisting high load cases.

http://dx.doi.org/10.5772/59308

The PV, Flex-House, VRB system and EV battery system simulation models have been implemented in two software packages, MATLAB/Simulink and DIgSILENT Power Factory, taking into accounts the characteristics, the efficiency and also the power losses of their components.

The models have been validated using measurements from a dedicated power system research lab with real components.

Comparison with experimental data, acquired using the SCADA system and processed in MATLAB, has shown that the models can be an accurate tool for prediction of energy production with Intelligent Houses and Battery Energy Storage Systems, as well.

Three types of voltage controllers have also been developed and implemented, using a state flow chart and a PI controller, based on finite-state machine. A voltage controller using load shifting (active units), an overvoltage controller, able to charge the battery when the bus-bar voltage exceeds the limits, and a voltage controller able to set-up the battery to run in schedule mode. In the case of the former, the EV battery is connected to the distribution network only when an over voltage appears and consumes the surplus active power until the power injected into the network is not causing the bus voltage to overtaken the limit. It means that the battery requires fewer charging/discharging cycles, leading to increased battery life.

Simulation results and experiments have shown that the controllers have been designed and implemented successfully.

As a future work we will try to develop and implement a coordinated control of DER components to improve the voltage profile of the distribution network.

Author details

Lucian Mihet-Popa[1*] and Voicu Groza[2]

*Address all correspondence to: lucian.mihet@upt.ro; groza@site.uOttawa

1 Politehnica University of Timisoara, Department of Electrical Engineering, Romania

2 University of Ottawa, Department of Information Technology and Engineering, Canada

References

[1] K. Richardson, D. Dahl-Jensen, J. Elmeskov, C. Hagem, J. Henningsen, J. A. Korstgard, N. B. Kristensen, P. E. Morthorst, J. E. Olesen, and M. Wier, "Green energy - theroadto a Danishenergysystemwithoutfossilfuels," DanishCommission on Climate ChangePolicy, 2010.

[2] "Smart Grid i Danmark", joint report by energinet.dk andDanskEnergi, September 2010.

[3] X. Liu, A. Aichhorn, L. Liuand H. Li, "Coordinated control of distributedenergystoragesystemwithtapchangertransformers for voltagerisemitigationunderhighphotovoltaicpenetration", IEEE Transactions on Smart Grid, Vol. 3, No. 2, June 2012, pp. 897-906.

[4] European CommissionDraft, "Energy 2020-A strategy for competitive, sustainableand secure energy", Brussels, September 2010. [Online].Available:http://eur-lex.europa.eu/LexUriServ/LexUriServ.do?uri=COM:2010:0639:FIN:EN:PDF.

[5] Y. Riffonneau, S. Bacha, S. Barrueland S. Ploix, "Optimal Power Management for gridconnected PV Systemswithbatteries", IEEE Transaction on Sustainable Energy, vol. 2, no. 3, pp. 309-320, July 2011.

[6] H. Jiayi, J. Chuanwen, and X. Rong, "A review on distributedenergyresourcesand Micro Grid", ELSEVIER Renewable&Sustainable Energy Reviews, vol. 12, pp. 2472-2483, 2008.

[7] P. C. Loh, L. Zhangand F. Gao, "Compact integratedenergysystems for distributedgenerations", IEEE Transactions on Industry Electronics, Vol. 5, May 2012.

[8] "Smart Grid: Reinventingthe Electric Power System", IEEE Power & Energy Magazine, March 2012.

[9] A. Timbus, M.Larssonand C. Yuen, "Active Management of Distributed Energy ResourcesUsingStandardized Communications and Modern Information Technologies", IEEE Transactions on Industrial Electronics, Vol. 56, No. 10, October 2009, pp. 4029-4037.

[10] J.C. Vasquez, R.A. Mastromauro, J.M. Guerreroand M. Liserre, "VoltageSupportProvidedby a Droop-ControlledMultifunctionalInverter", IEEE Transactions on Industrial Electronics, Vol. 56, No.11, November 2009, pp. 4510-4519.

[11] P. Palenskyand D. Dietrich, "Demand Side Management: DemandResponse, Intelligent Energy Systems, andSmartLoads", IEEE Transactions on Industrial Informatics, Vol. 7, No. 3, August 2011, pp. 381-388.

[12] T. Strasser, F. Andren, F. Lehfuss, M. Stifter, P. Palensky, "Online Reconfigurable Control Software for IEDs", IEEE Transactions on Industrial Informatics, Vol. 9, No. 3, August 2013, pp. 1455-1465.

[13] A.D. Hansen, P. Sorensen, L.H. Hansen, H. Bindner, "Models for a Stand-Alone PV System", Risoe National Laboratory, Roskilde, Risoe-R-1219 (EN) / SEC-R-12, Dec. 2000.

[14] H. Bindner, C. Ekman, O. Gehrkeand F. Isleifsson, "Characterization of Vanadium-FlowBattery", Riso-R-1753 Report, Roskilde, Denmark, October 2010.

[15] W. Wang, B. Ge, D. Bi and D. Sun, "Grid-ConnectedWind Farm Power Control usingVRB-based Energy StorageSystem", IEEE Transaction on Energy Conversion, pp.3772-3777, 2010.

[16] A. C. Hill, M. C. Such, D. Chen, J. Gonzalez and W. M. Grady, "Batteryenergystorage for enablingintegration of distributed solar powergeneration", IEEE Transactions on Smart Grid, Vol. 3, No. 2, June 2012, pp. 850-857.

[17] L. Barote, R. Weissbach, R. Teodorescu, C. Marinescu, M. Cirstea, "Stand-Alone-WindSystemwithVanadiumRedoxBattery Energy Storage", IEEE International Conference on Optimization of Electricaland Electronic Equipments, OPTIM'08, pp. 407-412, 22-24 May 2008, Brasov, Romania.

[18] C. Blanc, A. Ruffer, "Multiphysicsand energetic modeling of a vanadiumredoxflow-battery", in Proc. of IEEE International Conference on Sustainable Energy Technologies (ICSET), November 24, 2008, pp. 696-701.

[19] F. Baccino, S. Grillo, M. Marinelli, S. Massuccoand F. Silvestro, "Power andenergy control strategies for a vanadiumredoxflowbatteryandwind farm combinedsystem", in Proc. of IEEE Power Engineering Society Conf. andExhibition on Inovative Smart Grid Technology (ISGT Europe), December 5, 2011, pp. 1-8;

[20] J. Chahwan, C. Abbeyand G. Joos, "VRB modeling for thestudy of output terminal voltages, internallossesand performance", in Proc. of IEEE Canada Electrical Power Conference (EPC), 2007, pp. 387-392.

[21] S. Teleke, M. E. Baran, A. Q. Huang, S. Bhattacharyaand L. Andersen, "Control strategies for batteryenergystorage for wind farm dispatching", IEEE Transactions on Energy Conversion, Vol. 24, No. 3, September 2009, pp. 725-732.

[22] Z. Feng, W. Ke, C. Jianyeand Z. Hua, "Control strategy for vanadiumredoxbatteryinverter in islandingmicrogrid", AdvancedMaterialsResearch Journal, Vol. 8, pp. 5794-5800, Switzerland 2012.

[23] C. Blanc and A. Rufer, "Optimization of theoperatingpoint of a vanadiumredoxflow-battery", in Proc. of IEEE Energy ConversionCongressandExposition (ECCE) 2009, San Jose, CA, 20-24 September, pp. 2600-2605.

[24] F. Marra, Y. T. Fawzy, T. Bulo and B. Blazic, "Energy storageoption for voltagesupport in low-voltagegridswithhighpenetration of photovoltaic", in Proc. of 3rd IEEE PES InnovativeSmart Grid Technologies (ISGT), Berlin, December 2012.

[25] L. Mihet-Popa, C. Koch-Ciobotaru, F. Isleifssonand H. Bindner, "Development of tools for simulationsystems in a distributionnetworkandvalidatedbymeasurements", IEEE International Conference on Optimisation of Electricaland Electronic Equipment, OPTIM 2012, May 24-26, Brasov-Romania, pp. 1022-1031.

[26] L. Mihet-Popa, C. Koch-Ciobotaru, F. Isleifssonand H. Bindner, "Development of tools for DER Components in a distributionnetwork", in Proc. of the 20th Internation-

al Conference on ElectricalMachines, IEEE ICEM 2012, September 2-5, Marseille-France, pp. 1022-1031.

[27] C. Koch-Ciobotaru, L. Mihet-Popa, F. Isleifssonand H. Bindner, "Simulation Model developed for a Small-ScalePV-System in a Distribution Network", in Proc. of the IEEE 7th International Symposium on AppliedComputational Intelligence andInformatics-SACI 2012, Timisoara-Romania, May 24-26, pp. 257-261.

[28] Y. Zong, L. Mihet-Popa, D. Kullmann, A. Thavlov, O. Gehrkeand H. Bindner, "Model Predictive Controller for Active Demand Side Management with PV Self-Consumption in an Intelligent Building", in Proc. of IEEE PES InnovativeSmart Grid Technologies Europe (ISGT), Berlin-Germany, October 14-17, 2012.

[29] Y. Zong, D. Kullmann, A. Thavlov, O. Gehrkeand H. Bindner, "Application of Model Predictive Control for Active Load Management in a Distributed Power Systemwith-HighWindPenetration", IEEE Transactions on Smart Grid, Vol. 3, No. 2, June 2012, pp. 1055-1062.

[30] L. Mihet-Popa, O.M.F. Camachoand P.B. Norgard, „Charginganddischargingtests for obtaining an accuratedynamicelectro-thermal model of highpowerlithium-ionpack-system for hybridand EV applications", in Proc. of the IEEE PES Power TechConference, Grenoble, June 16-20, 2013.

Chapter 5

Efficiency Boosting for PV Systems- MPPT Intelligent Control Based

Farhat Maissa and Sbita Lassâad

Additional information is available at the end of the chapter

http://dx.doi.org/10.5772/59399

1. Introduction

Nowadays renewable energy techniques for power production are mature and reliable. The photovoltaic (PV) energy is the most promising source of energy since it is pollution free and abundantly available everywhere in the world. PV energy is especially beneficial in remote sites like deserts or rural zones where the difficulties to transport fuel and the lack of energy grid lines make the use of conventional resources impossble. Pumping water in these sites is a vital task that requires a feasible source of energy to supply power to the electrical elements of the pumping structure.

This work analyses the control of a stand-alone PV pumping system. The success of a PV application depends on the effectiveness of the power electronic devices to efficiently operate the photovoltaic generator (PVG) even under variable climatic conditions The big need is to extract the maximum of power from the PVG at any climatic input levels. Therefore, the reliability of the MPPT controller is of paramount importance in successful PV pumping applications.

The MPPT control is a challenge, because the PVG sunshine energy input flux may change at any time. In fact, the PV system is considered as a non-linear complex one. For these reasons, the design of an appropriate setup controller is difficult to build. In the literature, numerous MPPT methods have been developed, among them: The hill climbing, incremental conductance and the P&O [1]. These algorithms consist of introducing a crisp values positive or negative (decrease or increase) all around the actual PVG operating point. From the previous power point position, the trajectory of the new one helps the algorithm to decide on the command output value. This algorithm may fail to act as an accurate MPPT because of the used crisp value (step size) that is mainly fixed by trial and tests running.

The intelligent techniques have recently attracted the interest of engineers due to several facts: as Self-Optimization fast convergence and simplicity of combination with classical extremum seeking [2], [3]. In this work the interest was focus on applying these techniques on the photovoltaic fields. In this work, the control strategy is described and tested in the context of a highly dynamic input.

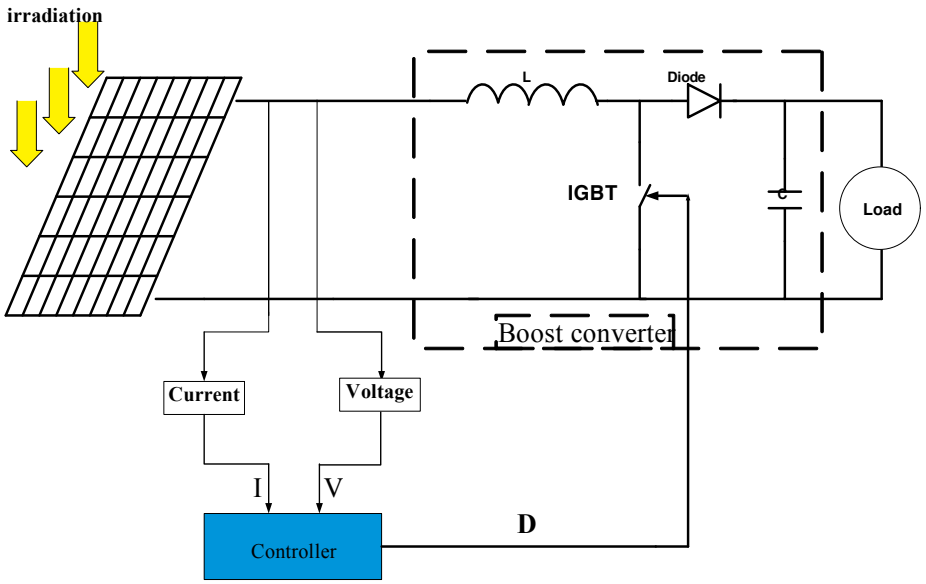

Figure 1. Synoptic diagram of PV system

2. Modeling of photovoltaic system

One can substitute a PV cell to an equivalent electric circuit which includes a power supply, resistors and a diode as shown in figure 2.

The power source generate a current called an I_{ph} current, this last depends on the irradiation amount. [1], [4], [5].

Up on the node law;

$$I_c = I_{ph} - I_d - I_{sh} \tag{1}$$

The current I_{ph} can be evaluated as:

http://dx.doi.org/10.5772/59399

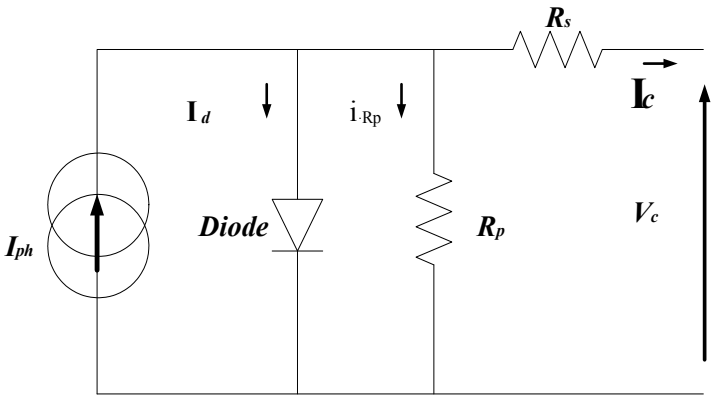

Figure 2. Simplified PV Cell Equivalent Circuit

$$I_{ph} = \frac{G}{G_{ref}}\left(I_{sc\_ref} + K_{SCT}\left(T_c - T_{c\_ref}\right)\right) \tag{2}$$

And the cell current is

$$I_c = I_{ph} - I_{rs}\left(\exp\left(\frac{q}{n\beta T_c}\left(V_c + R_s I_c\right) - 1\right) - \frac{\left(V_c + R_s I_c\right)}{R_p}\right. \tag{3}$$

With I_{rs} reverse saturation current is:

$$I_{rs} = I_{rs\_ref}\left(\frac{T_c}{T_{c\_ref}}\right)^3 \exp\left[\frac{qE_g}{n\beta}\left(\frac{1}{T_c} - \frac{1}{T_{c\_ref}}\right)\right] \tag{4}$$

The modeling of a PV Array depending on Ns and Np is then deduced as [5]:

$$\begin{cases} I_p = N_p I_c \\ V_p = n_s N_s V_c \\ R_s = \dfrac{n_s N_s}{N_p} R_s \\ R_p = \dfrac{n_s N_s}{N_p} R_p \end{cases} \tag{5}$$

Finally the I_p panel current can be given by

$$I_p = N_p I_{ph} - N_p I_{rs}\left(\exp\frac{q}{n\beta T_c}\left(\frac{V_p}{n_s N_s}+\frac{R_s I_p}{N_p}\right)-1\right)-\frac{N_p}{R_p}\left(\frac{V_p}{n_s N_s}+\frac{R_s I_p}{N_p}\right) \quad (6)$$

The cartelistic I-V in various irradiation and temperature is shown in figure 3

It is clear to find the three specific operating points in figure 3(a) [5].

- zone of voltage: characterized by an open circuit voltage V_{OC}.,
- zone of current: characterized by a short – circuit current I_{SC},
- Zone of maximum of power (P_{max}.) It is necessary to operate the PV at the third zone to extract the maximum power from the PVG.

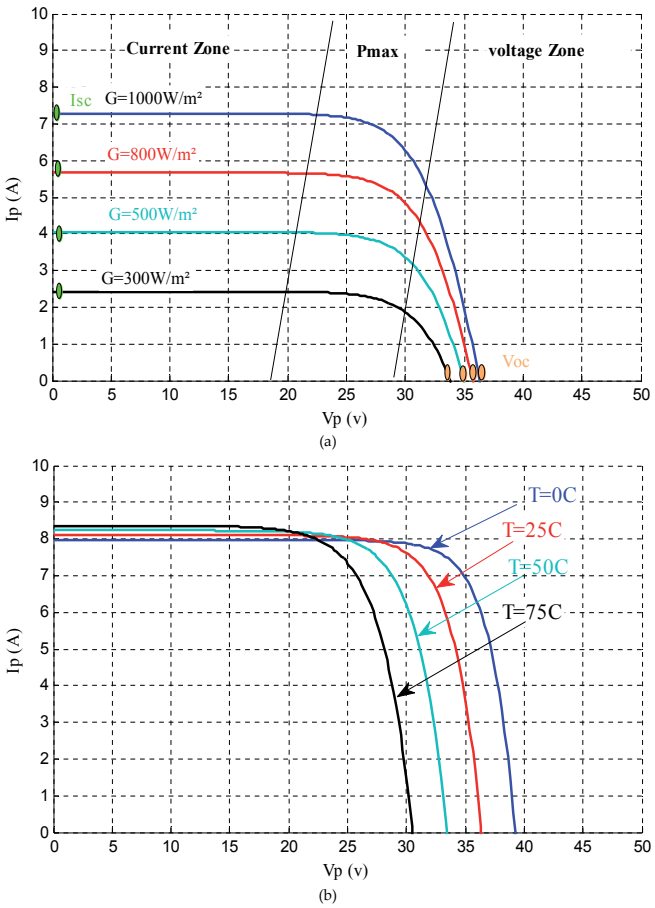

Figure 3. I-V characteristics of the PVG for variable: (a) irradiation at a constant temperature of 25°C, (b) temperature at a constant irradiation (1000W/m²)

http://dx.doi.org/10.5772/59399

3. Boost converter

DC-DC converters are electronic devices used whenever is needed to change DC electrical power efficiently from one voltage level to another. A DC-DC converter is an adapter controlling the load power through a regulated duty cycle. In order to step up the voltage, the operation consists of switching an IGBT (Figure 4) at a high commutation frequency, with output voltage control by varying the switching duty cycle (D) [6] and [7].

$$V_{in} = (1 - D)V_o \tag{7}$$

Where D is the actual duty cycle.

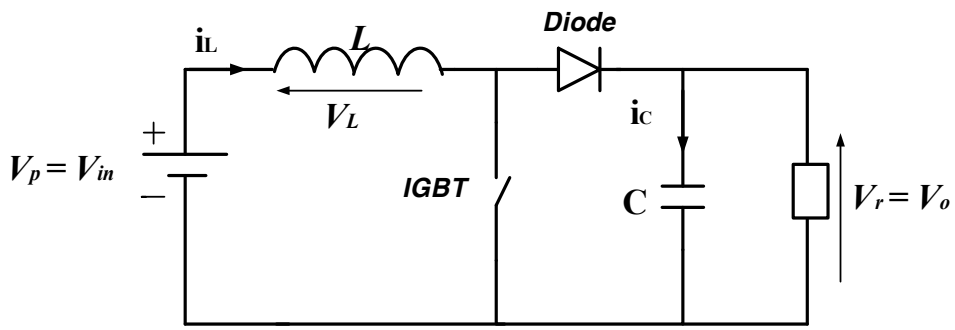

Figure 4. Circuit diagram of the used Boost converter

4. P&O algorithm principle

Due to its simplicity, P&O algorithm is the most popular one [5]. The principle of this scheme is to generate a crisp value by acting (decrease /increase) on the duty cycle actual command (D) and then observe the output power reaction. If the actual power P(k) is lower than the previous one, then the acting direction is inversed otherwise it is maintained [8], [9].

When dP/ dV>0, the voltage is increased, this yields to

D (K)= D (K)+ΔD, (ΔD: crisp value)

When dP/ dV< 0, the voltage is decreased through

D (k) = D (k −1) −ΔD.

The ΔD crisp value is chosen by trial and tests in simulation. The P&O diagram is shown in figure 5:

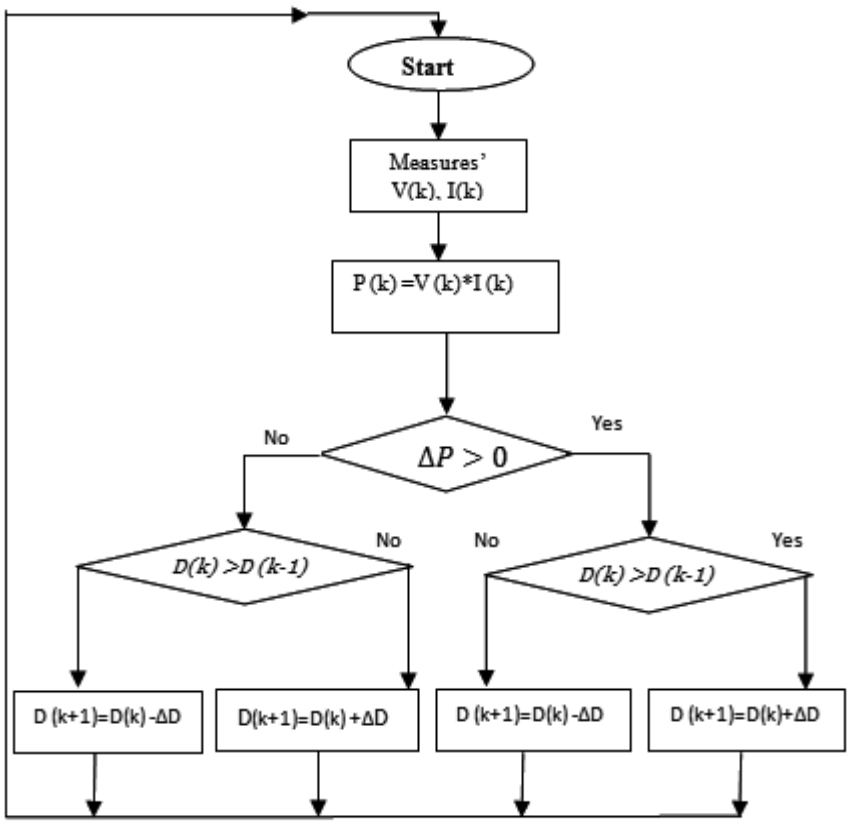

Figure 5. P&O Algorithm structure

If the crisp value ΔD is very big or very small then we may lose information as shown in figure 6. Despite the P&O algorithm is easy to implement it has mainly the following problems [9]:

- the PV system always operates in an oscillating mode.
- the operation of PV system may fail to track the maximum power point.

The ΔD crisp value is chosen by trial and tests in simulation. The P&O diagram is illustrated in fig. 5.

5. Intelligent Artificial MPPT Control technics

In this section, the most investigated Intelligent Artificial control techniques are considered. In particular, The artificial neuronal networks (ANN), the Fuzzy Logic control (FLC), and the adaptive neuro-fuzzy inference system (ANFIS) as the best one that combines the FLC and ANN advantages.

http://dx.doi.org/10.5772/59399

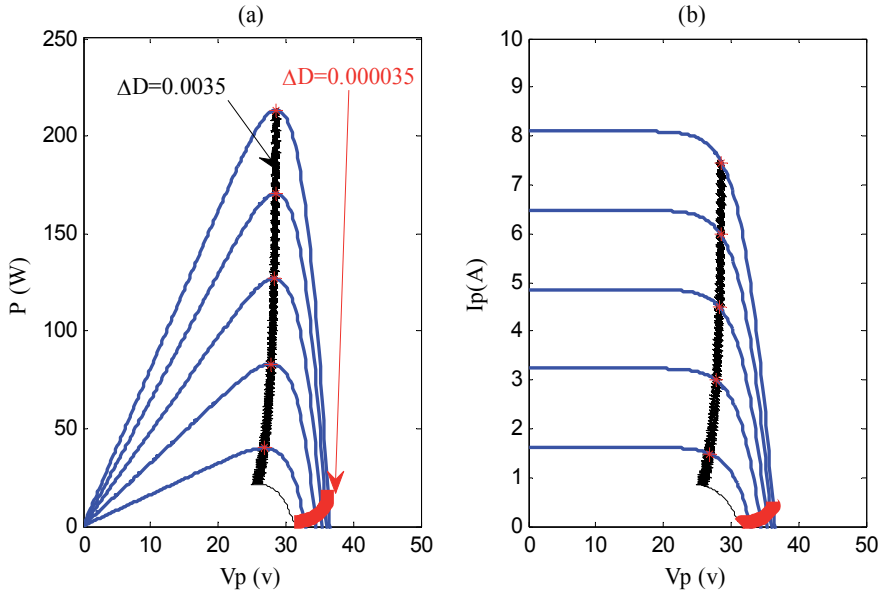

Figure 6. P-V, I-V curves and the MPPT-P&O for ΔD: (a) 0.0035 ET (b) 0.000035

5.1. ANN

Artificial Neural network (ANN) method have been employed successfully in solving problems with a high degree of complexness in various fields and applications including pattern recognition, identification vision, prediction,control systems and classification, [10]. Now the ANN can be used in order to solve a lot of problems that are difficult for conventional computers or even for human beings. ANNs, overcome the limitations of the conventional approaches, and present a solution by extracting the desired information directly from the experimental data. The fundamental element of a neural-network is neurons. The method is based on neurons receiving input from other neurons, after that the ANN combines them in a non-linear operation and then generate outputs as a final result. [11].

Artificial neural network was used as a controller to track the maximum power point by commanding the boost converter. Effectively the MPPT artificial neural controller is composed in general by a three layers, first; an input, then hidden and finally an output layer [12],[13], This connection is characterized respectively by weights, w^I and w^o, like presented in figure 7.

The mathematical expressions define the relation between the input and the output signals are given in equation 8, 9 and 10.

- The output layer :

$$D^{na}(k) = f\left(\sum_{j=1}^{nc} w^{o}{}_{i}(k)\, y_i(k)\right) \tag{8}$$

- The output hidden layer:

$$y_i(k) = f\left(S_j(k)\right) = \frac{1}{1+\exp(-S_j(k))} \tag{9}$$

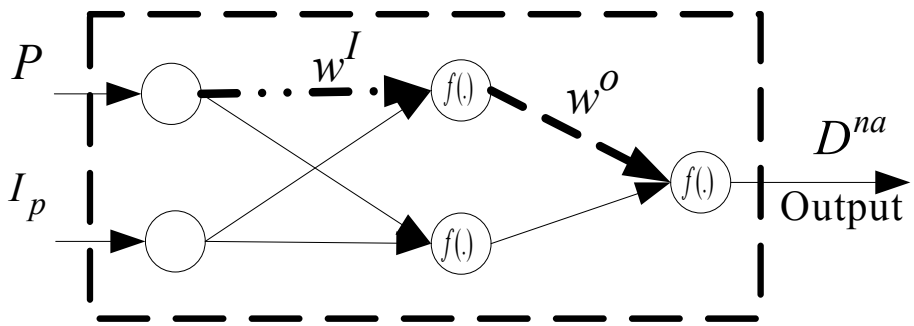

Figure 7. Structure of an artificial neural network

- The hidden layer:

$$H_j(k) = \sum_{i=1}^{ne} w_{j,i}^I(k)\, x_j(k) \tag{10}$$

qWhere '*nc*' represent the neurons number in the hidden and '*ne* ' the output layer. The data vector x_i represents the input signals that are given in equation 11 [11].

$$x_i = \left[D^*(k) \quad P(k-1) \quad I_P(k-1) \right]^T \tag{11}$$

in the ANN_MPPT Controller, an activation function defines each neuron. The sigmoid function has been chosen for this work.

To achieve the required input/output relationship, an adjustment of weights between the output layer and the hidden layer, and the input layer and the hidden layer is required. for the weights updating ;the back propagation algorithm is used, by minimized an error function defined in equation 12 [11].

$$E_{na}\ (k) = \frac{1}{2}\left[D^*(k) - D^{na}(k) \right]^2 = \frac{1}{2} e_{na}^2(k) \tag{12}$$

Where $D^*(k)$ is the desired output, $E_{na}(k)$ is the accrued output, and $e_{na}(k)$ represent the error between the desired and accrued output

The updating of weights is calculated by using the gradient method [11].

$$w_{i,1}^{o}(k+1) = w_{i,1}^{o}(K) + \Delta w_{i,1}^{o}(K) = w_{i,1}^{o}(K) - \eta^{o}(K)\frac{\partial E_{na}(K)}{\partial w_{i,1}^{o}(K)} \tag{13}$$

$$w_{j,i}^{I}(k+1) = w_{j,i}^{I}(K) + \Delta w_{j,i}^{I}(K) = w_{j,i}^{I}(K) - \eta^{I}(K)\frac{\partial E_{na}(K)}{\partial w_{j,i}^{I}(K)} \tag{14}$$

Where $\eta_{na}{}^{o}$, $\eta_{na}{}^{I}$ are respectively the ANN learning rates for the hidden and the output layer.

The quantity $\frac{\partial E_{na}(K)}{\partial w^{I}(K)}$ and $\frac{\partial E_{na}(K)}{\partial w^{o}(K)}$ are respectively calculated by the equation 15 and 16.

$$\frac{\partial E_{na}(K)}{\partial w^{I}(K)} = -e_{na}(k)y_i(k) \tag{15}$$

$$\frac{\partial E_{na}(K)}{\partial w^{o}(K)} = -e_{na}(k)w^{o}{}_{i,1}(k)x_j(k) \tag{16}$$

Figure 8 is the windows given by the Matlab at the starting of learning, where the neural model performance, the structure, the learning function, and the maximum training patterns, are given. It's clear that the ANN performance is good as shown in figure 9 witch present an error of learning equal to 10E-8 the neural architecture used for this model is [11].:

- 2 neurons in the input layer,
- 2 neurons in the first next hidden layer, and 4 neurons in the second one
- 1 neuron in the output layer
- the learning rates is 0.01

The training pattern is 100 epoch.

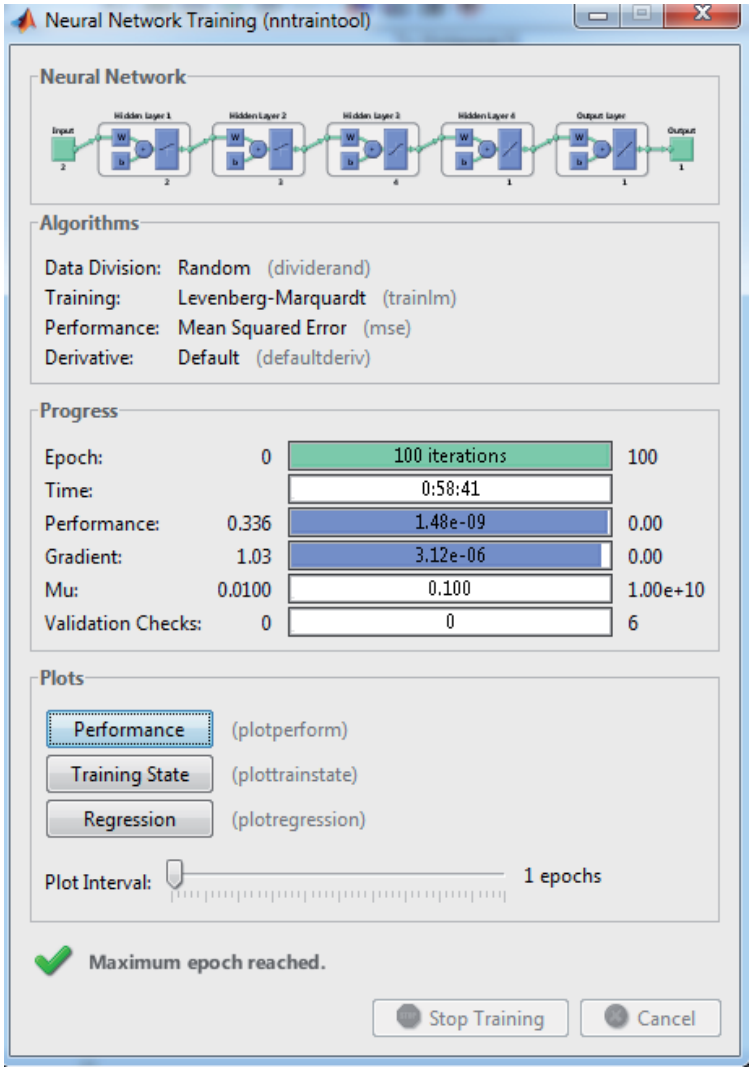

Figure 8. Neuronal network training

For simulation work, the Data Base has been created by using the *Ip*-and *Vp* then calculating the optimal duty cycle eq (21).

$$P_{in} = P_{out} \tag{17}$$

$$V_p \times I_p = V_r \times I_r \tag{18}$$

Utilizing equation (7)

http://dx.doi.org/10.5772/59399

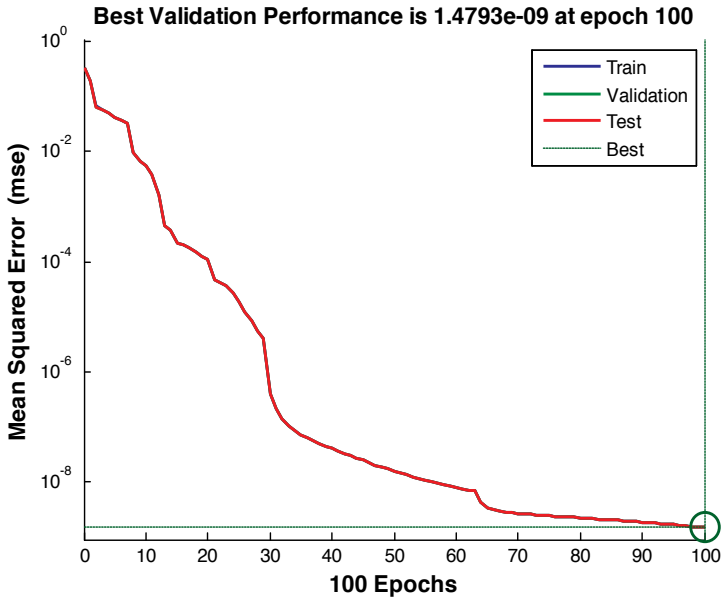

Figure 9. Validation performance

$$V_p \times I_p = \frac{V_r^2}{R} \tag{19}$$

$$V_p \times I_p = \frac{V_p^2}{(1-D)^2 R} \tag{20}$$

$$D = 1 - \sqrt{\frac{V_p}{R \times I_p}} \tag{21}$$

The result obtained using the $D_{opt} = 1 - \sqrt{\frac{V_{opt}}{R \times I_{opt}}}$ will be used as reference for the t other controllers and will be named as $\text{MPPT}_{\text{ideal with}}$ V_{opt} and I_{opt} are respectively the voltage and current of the Maximum power point

5.2. Fuzzy-logic control (FLC)

FLC is a way that mimics the human capability of judgment and reasoning [12]. A typical FLC based approach is composed by three modules [13]. fuzzification, Inference, defuzzification to made a closed-loop system that uses the process of fuzzification to generate fuzzy inputs to

an inference engine processes the fuzzy sets using a library of IF-THEN. The defuzzification is the inverse process, used in a FLC control system in order to generate the create step size real values.

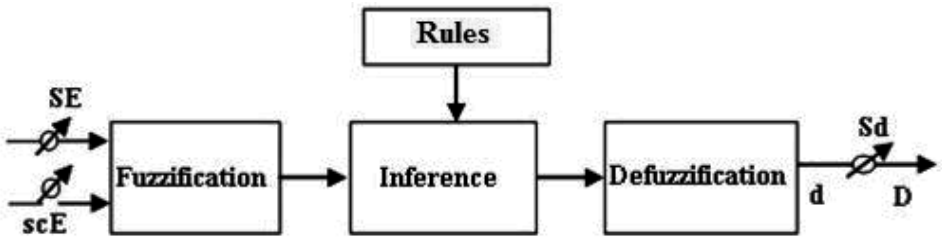

Figure 10. FLC controller structure

To adjust the controller input/output, SE, SCE and Sd gains are introduced. The controller crisp value (ΔD) is the output and the two variables E and CE represent respectively the error and it's derivate as the controller inputs [14].

$$\begin{cases} E(k) = \dfrac{P_{ph}(k) - P_{ph}(k-1)}{V_{ph}(k) - V_{ph}(k-1)} \\ CE(k) = E(k) - E(k-1) \end{cases} \tag{22}$$

With $P_{ph}(k)$ is the PV generator instantaneous power.

The input E (k) shows if the load operating point at the instant k is located on the left or on the right of the maximum power point on the PV characteristic, while the input CE (k) expresses the moving direction of this point.

The fuzzy inference is carried out by using Mamdani method, Table 1, and the defuzzification uses the center of gravity to compute the controller output [14]:

$$\Delta D = \frac{\sum_{j=1}^{n} \mu(\Delta D_j).\Delta D_j}{\sum_{j=1}^{n} \mu(\Delta D_j)} \tag{23}$$

The control rules are indicated in Table 1 with E and CE as inputs and ΔD as output. The corresponding variables member ship functions are given in Figure11.

The membership functions of E, CE and ΔD are depicted in figure 11:

http://dx.doi.org/10.5772/59399

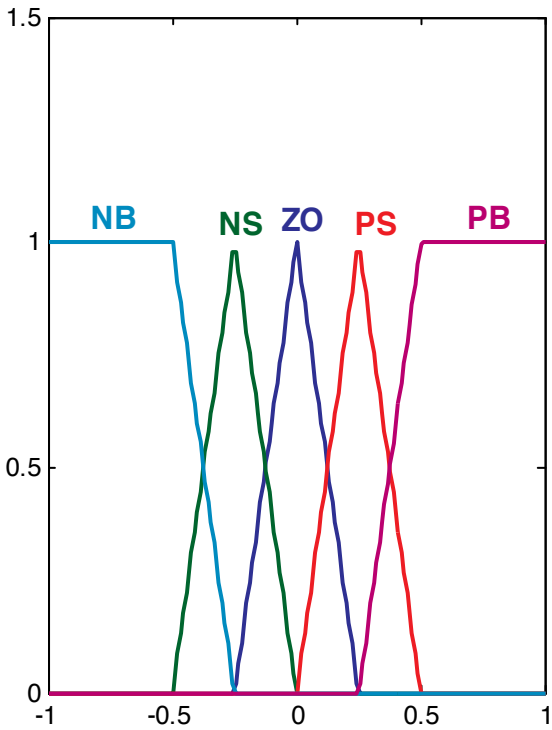

Figure 11. Membership functions of E, CE and D

	CE				
E	*NB*	*NS*	ZO	*PS*	*PB*
NB	ZO	ZO	*PB*	*PB*	*PB*
NS	ZO	ZO	*PS*	*PS*	*PS*
Z0	*PS*	ZO	ZO	ZO	*NS*
PS	*NS*	*NS*	*NS*	ZO	ZO
PB	*NB*	*NB*	*NB*	ZO	ZO

Table 1. Fuuzzy logic controller Rules.

5.3. An adaptive neuro-fuzzy inference contol

Neuro-fuzzy technique is combining the ANN learning methods and the fuzzy inference system (FIS) [15], [16], [17]. In general the FIS structure consists of three important components:

and the rule base one, for rule fuzzy selection [18]; a database, which defines the fuzzy rules MF and a decision generator, that bring up the inference procedure to finally generate an output as shown in Figure 12. The FLC concepts are based on knowledge from expert and in the other hand the neural network models are using a data base. Moreover, neuro-fuzzy approach seems covenant and suitable if both advantages of the tow method are combined. The neuro-fuzzy controller is the called, in this work adaptive network (ANFIS). The structure of the system is an adaptive network running as a first-order Sugeno fuzzy inference system. The hybrid ANFIS learning rule, combine the back-propagation gradient-descent first and second a least-squares algorithm for identification and optimization of the the Sugeno first order system. The the ANFIS working process is simplified by an equivalent ANFIS architecture with two rules are given in Figure 13 [4], [16], [18].

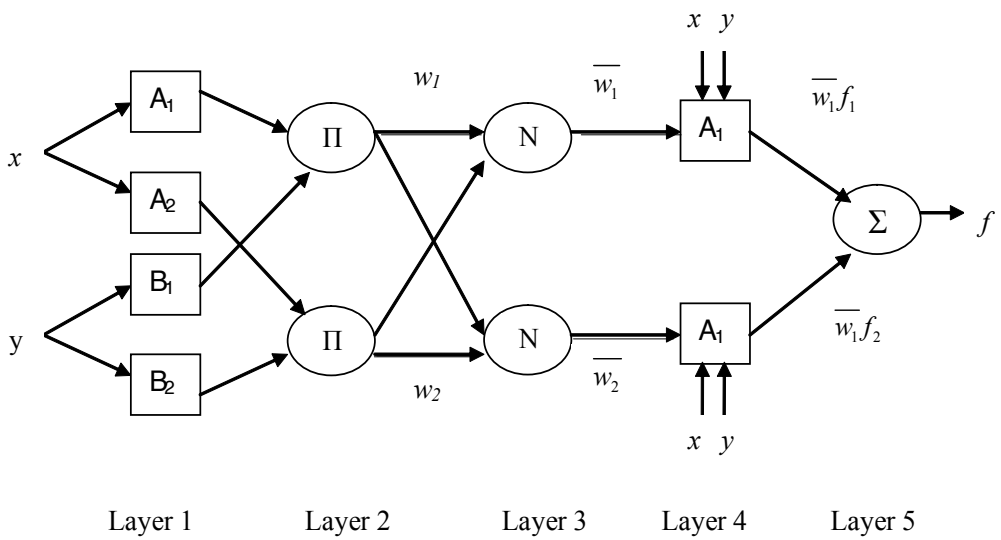

Figure 12. Architecture of The ANFIS model Sugeno's fuzzy inference method

The given architecture has five layers and every node in a layer has a similar function. The two fuzzy rules, in which outputs are dressed as linear combinations of their inputs, are [4]:

$$\text{Rule 1}: \text{ if x is } A_1 \text{ and y is } B_1 \text{ then } f_1 := p_1x + q_1x + r_1 \tag{24}$$

$$\text{Rule 2}: \text{if x is } A_2 \text{and y is } B_2 \text{ then } f_2 := p_2x + q_2x + r_2 \tag{25}$$

Layer 1: consists of adaptive nodes that generate membership grades of linguistic labels based upon premise signals, using any appropriate parameterized membership function such as the generalized bell function given by [4]:

http://dx.doi.org/10.5772/59399

$$O_{1i} = \mu_{A_i}(x) = \frac{1}{1 + \left| \frac{x - c_i}{a_i} \right|^{2b_i}} \tag{26}$$

Where output O1,i is the output of the ith node in the first layer, x is the input to node i, Ai is a linguistic label ("small," "large," etc.) from fuzzy set A =(A1, A2, B1, B2,) associated with he node, and {ai, bi, ci} is the premise parameter set used to adjust the shape of the membership function [4]:.

Layer 2: are fixed nodes designated Π, which represent the firing strength of each rule. The output of each node is the fuzzy AND (product or MIN) of all the input signals [4]::

$$o_{2,i} = w_i = \mu_{Ai}(x)\mu_{Bi}(y) \quad \text{i=1, 2} \tag{27}$$

Layer 3: The outputs are the normalized firing strengths. Each node is a fixed rule labeled N. The output of the ith node is the ratio of the ith rule's firing strength to the sum of all the rules firing strengths [4]::

$$o_{3,i} = \overline{w_i} = \frac{w_i}{w_1 + w_2} \tag{28}$$

Layer 4: the equation gives the rule outputs is:

$$o_{4,i} = \overline{w_i} f_i = \overline{w_i}(p_i x + q_i y + r_i) \tag{29}$$

With $\overline{w_i}$ is the firing strength that is normalized from the layer number 3, p_i, q_i, r_i are the node set parameters.

Layer 5: the ANFIS output is given by:

$$o_{5,i} = \sum_i \overline{w_i} f_i = \frac{\sum_i w_i f_i}{\sum_i w_i} \tag{30}$$

The ANFIS controller developed in this section includes ' Ip ' and ' P ' as inputs and 'D' as output which represent respectively, the PV current, the PV-Power and the converter duty cycle ratio. The input variables allow the ANFIS to generate the converter command. This last is applied to the converter, in order to ensure the adaptation of the power provided by PVG. This controller yields to an automatic fuzzy rules generation based on the Sugeno inference model. The equivalent neural structure of the proposed ANFIS is given in figure 13, figure 14 show the MPPT-ANFIS validation and errors curves.

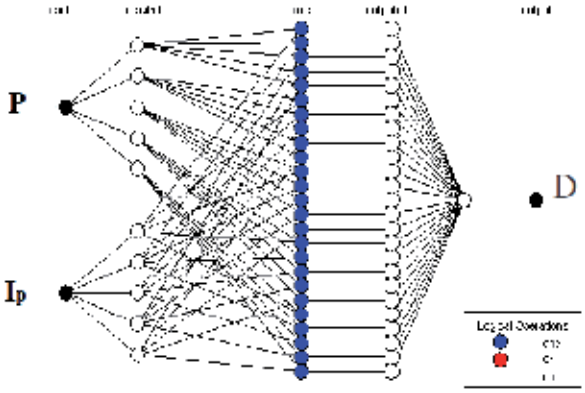

Figure 13. Structure of proposed neuronal model

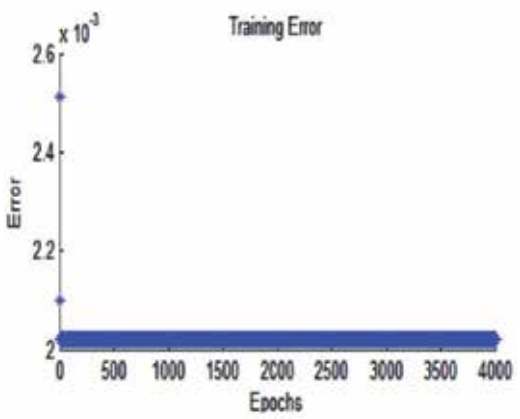

(a)

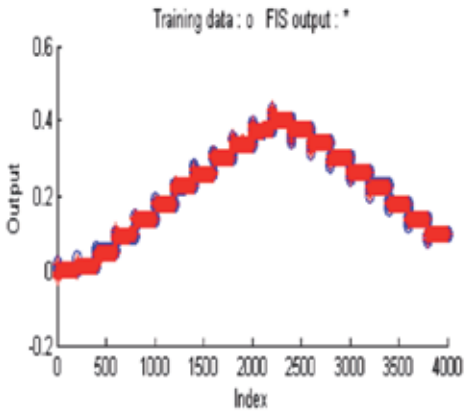

(b)

Figure 14. MPPT-ANFIS validation and errors curves

http://dx.doi.org/10.5772/59399

6. Simulation results

In this section the performance of MPPT controller; Fuzzy, Neuronal, ANFIS will be distingue by the comparison between them and $MPPT_{ideal}$, he signal corresponding to the ideal MPPT present the reference used to compare the performances of various MPPT controllers

6.1. FLC

The figure 15 shows that the Fuzzy flow th $MPPT_{ideal}$, the FLC controllers ensure a good maximum power tracking. Nevertheless, the fuzzy regulator is oscillating around the MPP zone and is not powerful especially on weak irradiation level.

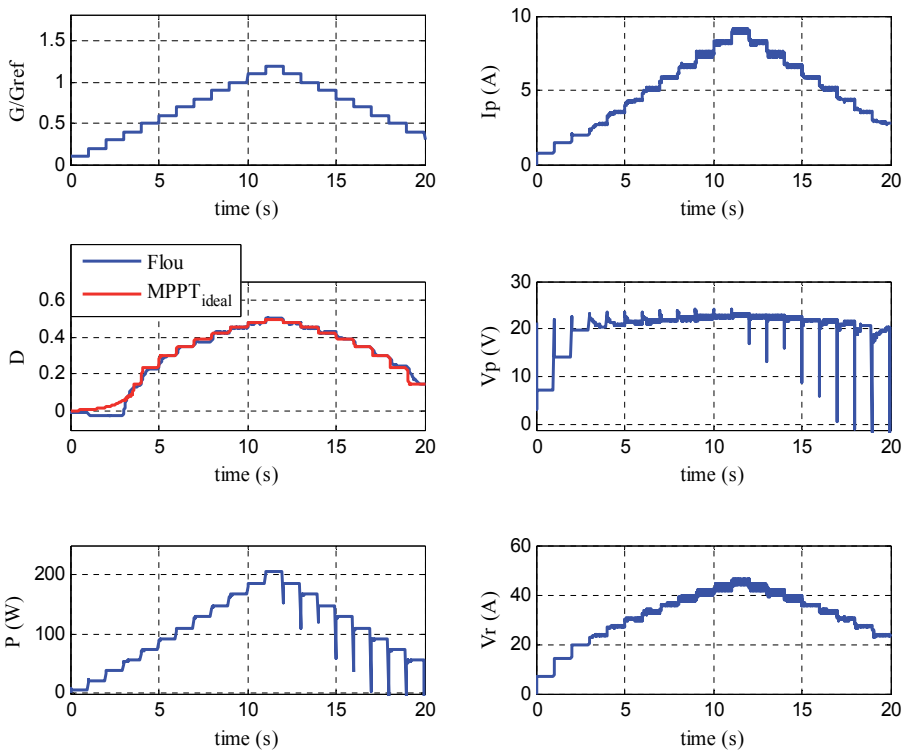

Figure 15. Irradiation, duty cycle, power, Power (FUZZY/$MPPT_{ideal}$), PV current, PV voltage, converter voltage in different values of irradiation (100 to 1200W/m², 25°C)

6.2. Neuronal network

The acquired sizes I_P and P are the input. The output of the controller is the duty cyclic D commanding an MLI block of the controller. The figure 16 contains the data base adopted for the training. This base corresponds to the MPPT ideal.

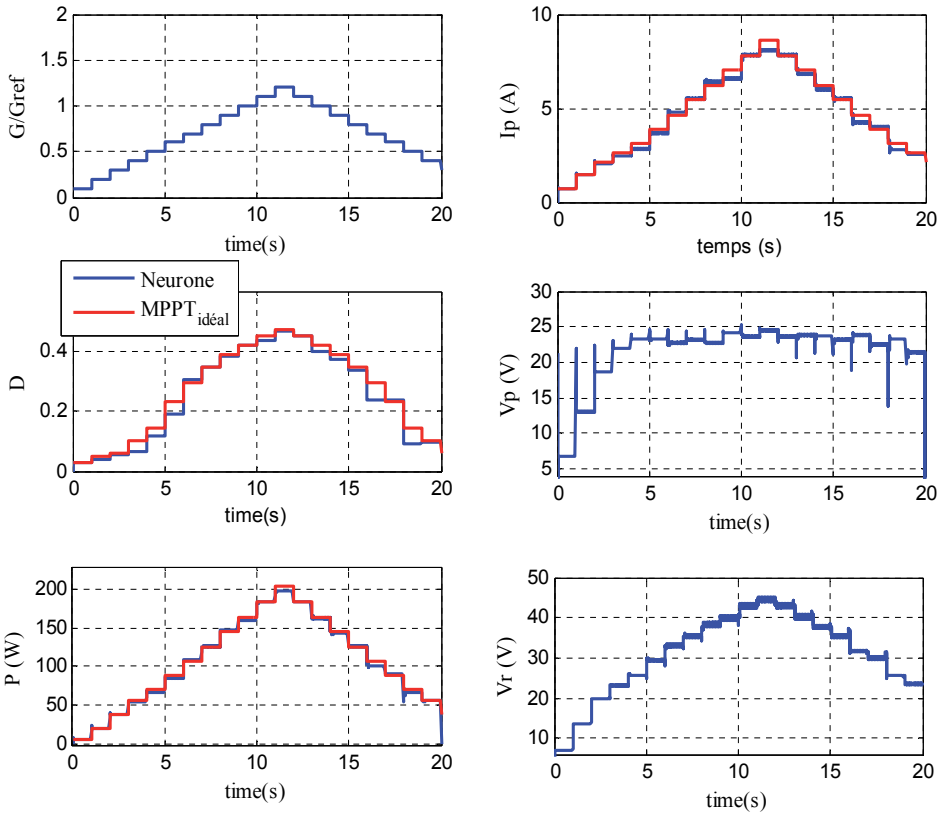

Figure 16. Irradiation, duty cycle, power, Power (Neuron/ $MPPT_{ideal}$), PV current, PV voltage, converter voltage in different values of irradiation (100 to 1200W/m², 25°C)

The figure 16 show well that controller MPPT ANN presents a mediocre performances with respect to the request of the incidental system with precipice irradiation variation. The time and the training memory capacity as well as the heaviness of a significant data base form one huge flexibility handicaps. To overcome these problems, we propose in the following section the algorithm combining the FLC and RNA.

6.3. ANFIS

The acquired sizes I_P and P are the input. The duty cyclic D is the output ordering the MLI block of Boost converter. Figure 17 contains the data base adopted for the training of the ANFIS. This base corresponds to ideal MPPT (MPPT ideal).

6.4. Comparative study

The ANFIS-MPPT Controller ensured the compensation of a reliable tracking on the low values of irradiation as shown in figure 17. The figure 18 confirms this improvement of the tracking

http://dx.doi.org/10.5772/59399

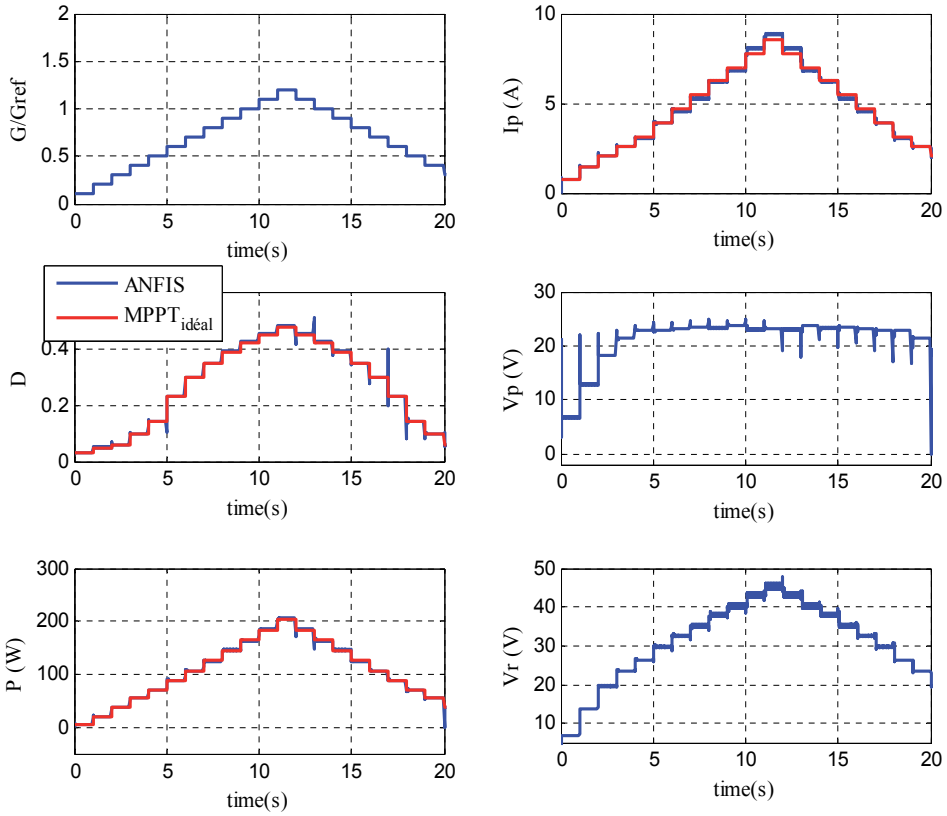

Figure 17. Irradiation, duty cycle, power, Power ratio(ANFIS/MPPT$_{ideal}$), PV current, PV voltage, converter voltage in different values of irradiation (100 to 1200W/m², 25°C)

in term of speed, increasing the step response and decreasing of error. Comparing performance put in evidence that the ANFIS precedes the RNA and the Fuzzy logic on MPPT action.

Figure 19 allows compare the different methods (P&O, Neuron, Fuzzy, ANFIS and MPPT $_{ideal}$) and this for a PV system coupled to a resistive load under a constant temperature and an irradiation (G=1000W / m², T=25C°)

The figure 18 illustrates the dynamic responses of the duty cycle and of the power of the GPV for a step of incidental irradiation of 1000W/m² and a temperature of 25°C. It is to be announced that the fuzzy controller presents a great oscillation beyond and an assailant mode to 0.6 seconds and a static error. The ANFIS and the P&O have the same response time. The RNA and for its parallel structure, justifies well the response time relatively instantaneous. The P&O and the RNA present the same static error which is larger than the fuzzy logic controller. The ANFIS MPPT is presented relatively as the most powerful controller with a static error near to zero. The figure 19 gives the plan of phase of the duty cycle according to the tension of the GPV. It is it should be noted that controller ANFIS-MPPT converges exactly towards the ideal MPPT with good performances superiors to the others.

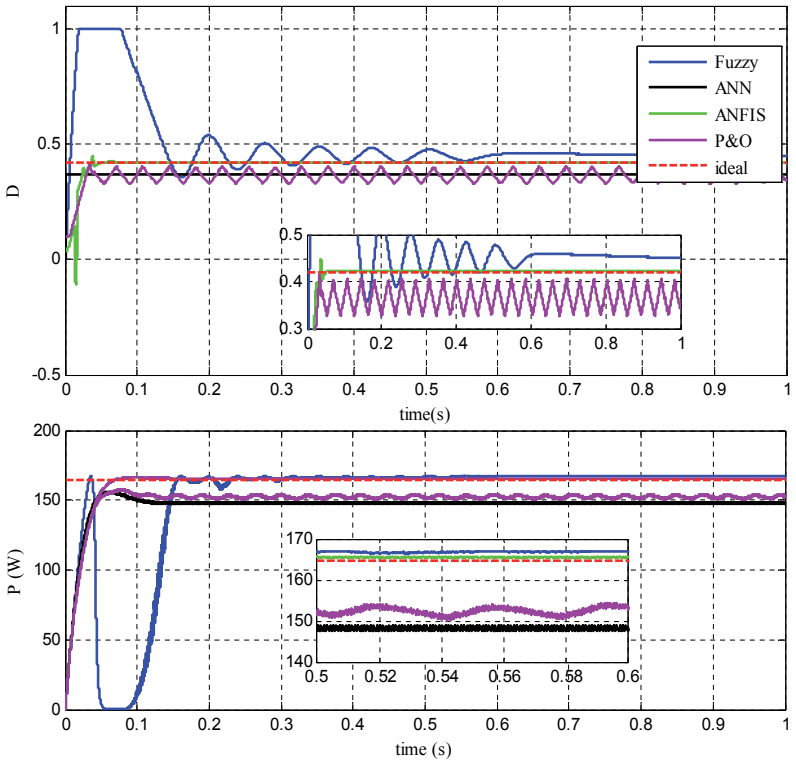

Figure 18. Fuzzy, Neuronal, Anfis and P&O duty cycle and power

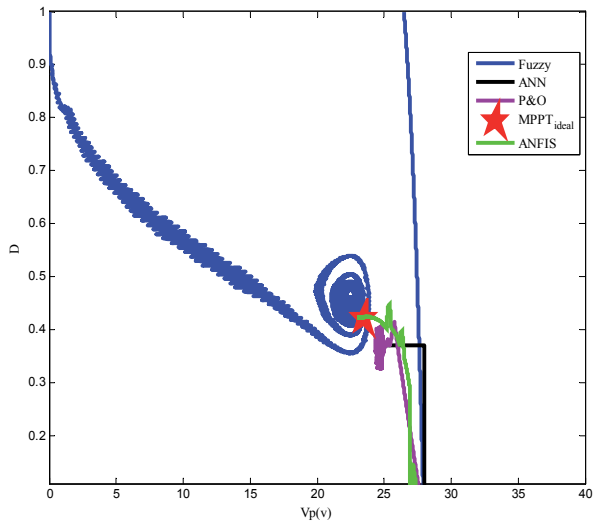

Figure 19. Fuzzy, Neuronal, Anfis and P&O performance

http://dx.doi.org/10.5772/59399

7. Application: Water pumping

7.1. Dc motor model

The mathematical relation that describes the dynamic model of a DC motor is given by [19]:

$$L_a \frac{dI_a}{dt} = U_a - R_a I_a - K_t \omega \tag{31}$$

$$j \frac{d\omega}{dt} = T_{em} - T_l - f\,\omega \tag{32}$$

With, L_a, Kt, V_a and I_a are armature resistance, armature inductance, back emf constant (also motor torque constant), armature voltage and current, f is constant viscous friction coefficient and J the inertia Moment. In the mechanical equation (32) T_{em} and T_L are the motor and the load (pump) torque, respectively [20].

7.2. Modeling of DC Water Pump

Recently, photovoltaic pumps use attracts more and more attention. For a positive displacement pump, the water flow of this type is depending on the drive moto shaft speed.

The piston of the pump uses the volume variations caused by the piston displacement in a cavity. The displacements in a different produce an aspiration or repression phase's dependence on the direction.

The pump piston moves in a first direction, the liquid is compressed: the induction valve is closing and the repression valve will be open. And then the operation will be reversed when the pump piston moves the second direction. This type of pump has the advantage of dry operation. However, the flow generated by this pump is limited. The model of the positive displacement pump load torque with is [21].

$$T_L = K_1 \cdot \omega + K_2 \tag{33}$$

The mathematical model that connects the pump water flow rate to the water column 'h' and power P and is: [22].

$$P(Q,h) = a(h)Q^3 + b(h)Q^2 + c(h)Q + d(h) \tag{34}$$

$$\begin{cases} a(h) = a_0 + a_1 h^1 + a_2 h^2 + a_3 h^3 \\ b(h) = b_0 + b_1 h^1 + b_2 h^2 + b_3 h^3 \\ c(h) = c_0 + c_1 h^1 + c_2 h^2 + c_3 h^3 \\ d(h) = d_0 + d_1 h^1 + d_2 h^2 + d_3 h^3 \end{cases} \tag{35}$$

Figure 19 shows the characteristics of the power according to the flow rate (P=f (Q)). They are dressed according to various heights of the water columns as given by equations 34 and 35, [4].

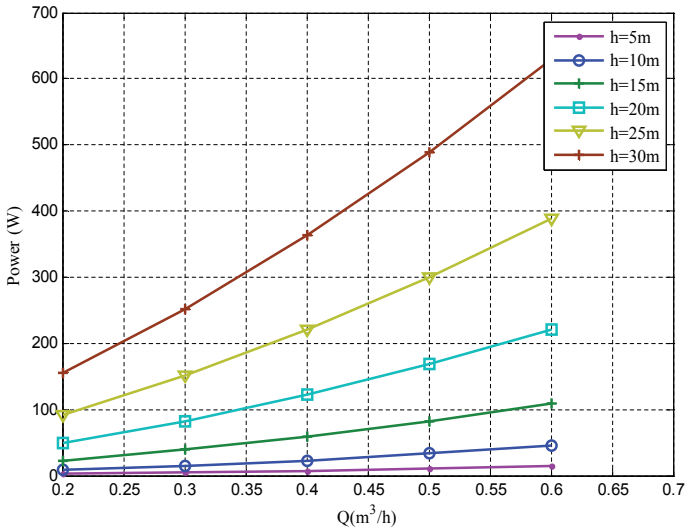

Figure 20. Pump characteristic.

From figure 19 it is easily to deduce that for a water height of 20 m, eq. 12 yields to the pumped water flow rate [11].

$$Flow = \frac{0,6}{220} P \tag{36}$$

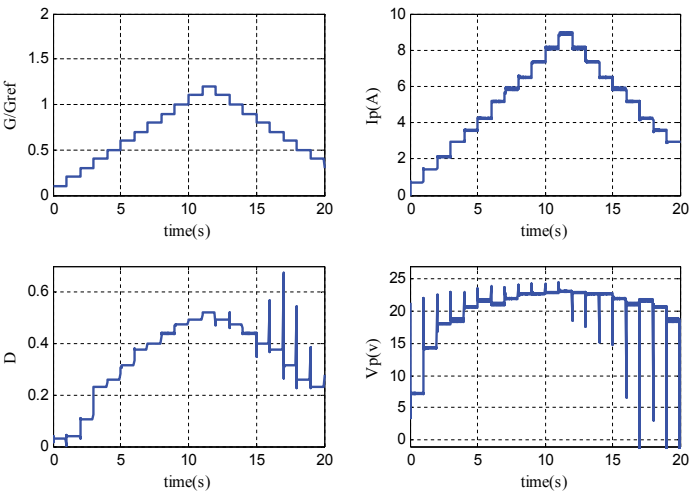

Figure 21. Irradiation, duty cycle, power, PV current, PV voltage

http://dx.doi.org/10.5772/59399

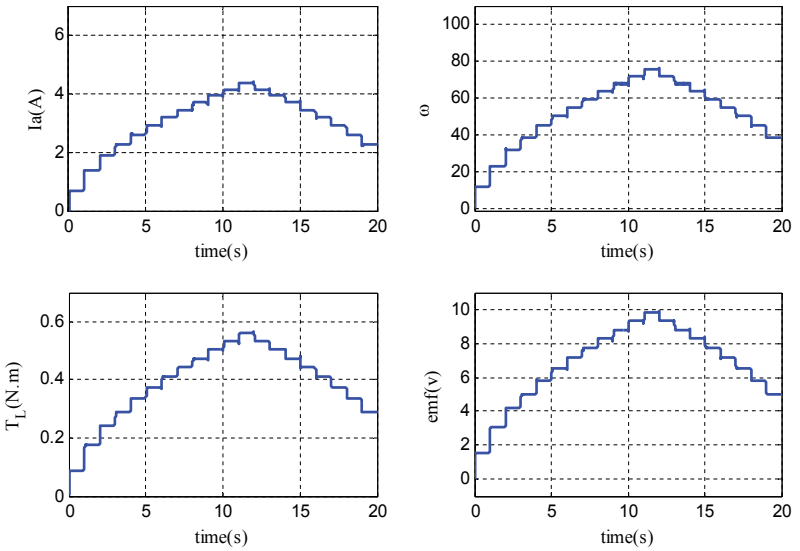

Figure 22. Motor behavouron a temprature of(25°C and various insolation

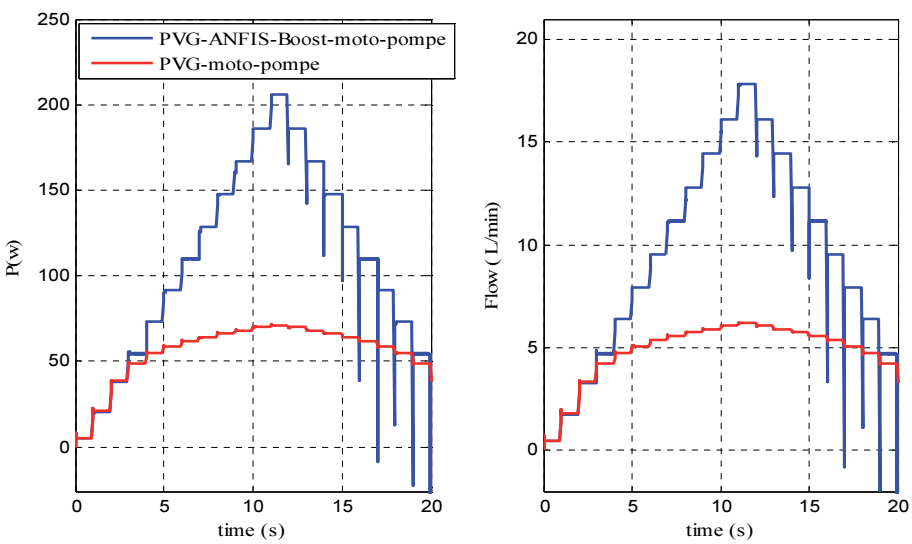

Figure 23. Power and Flow of PV pumping system with and without MPPT controller.

The MPPT ANFIS controller improves the PVG performances as clearly seen in PVG outputs tracking curves. The obtained results confirm the benefit in water flow rate is improved.

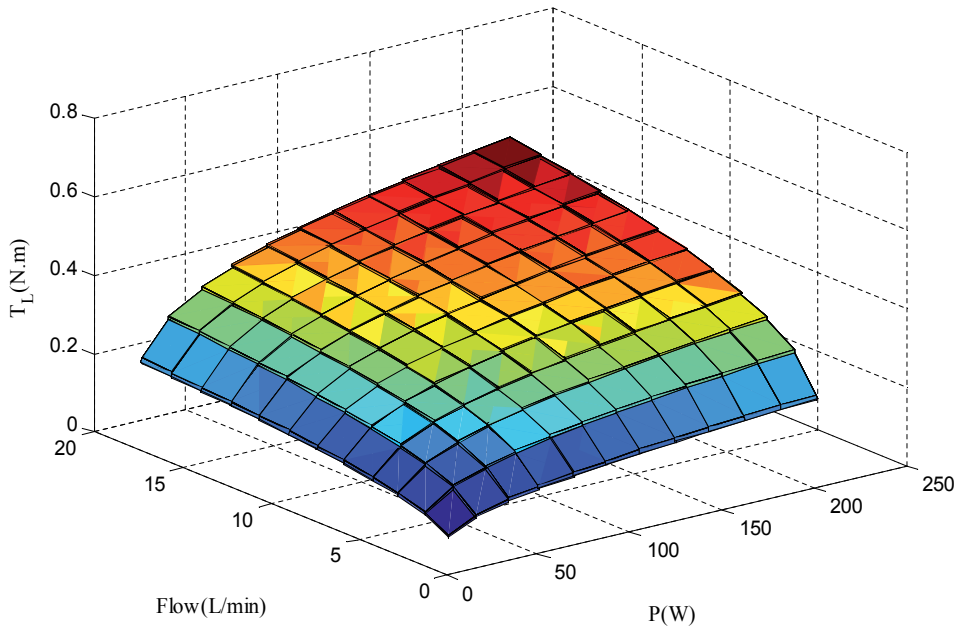

Figure 24. 3D surface of the flow power and load torque.

8. Conclusion

In this work a modeling study of the PV pumping system components is presented. Moreover in order to improve PV system performance, different maximum power point controller was studied and investigated. The system behavior incorporating the P&O, Fuzzy, ANN and neuro fuzzy were investigated and compared based on an extensive simulation work. Finally the Maximum Power Point tracking of PV pumping system is ensured by using an ANFIS controller. Performed simulation tests for the complete system lead to two main conclusions. The proposed PV system performances are highly boosted and the pumping flow rate benefit is going up to three times more [4].

Symbols

G:	Global insulation (W /m²)
Gref :	Reference insulation (W /m2)
I p:	Cell output current
Vp:	Cell output voltage
I :	Light-generated current source (A)

Rs:	cell series resistance (Ω)
Rp	Cell parallel resistance (Ω)
n:	Solar ideal factor
Irs :	Reverse diode saturation current(A)
KSCT:	Short circuit current temperature coefficient (A/°K)
Tc :	Cell junction temperature (°C)
Tc_ref :	Reference cell temperature(°C)
β :	Boltzmann constant (1.38e-23)
Eg:	Band gap energy (ev)
ns	Number of series cells.
D	duty cycle

Author details

Farhat Maissa and Sbita Lassâad*

*Address all correspondence to: lassaadsbita@yahoo.fr

Research Unit of Photovoltaic, Wind and Geothermal Systems, National Engineering School of Gabes, University of Gabes, Rue Omar Ibn-Elkhattab, Zrig, Gabès, Tunisia

References

[1] T. Esram, P. L. Chapman, Comparison of Photovoltaic Array Maximum Power Point Tracking Techniques. IEEE transactions on energy conversion, vol.22, 2007.

[2] D. Nikhitha, J.N.C. Sekhar, Modeling and Simulation of IM Drive Performance Using PI, ANN and FLC, International Conference on IT Convergence and Security (ICITCS), 2013.

[3] L.A. Torres-Salomao, J. Anzurez-Marin, Adaptive Neuro-Fuzzy Inference System Control for a Two Tanks Hydraulic System model, IEEE International Autumn Meeting on Power, Electronics and Computing (ROPEC),pp.1-5, 2013.

[4] M.farhat, L.Sbita, Advanced ANFIS-MPPT Control Algorithm for Sunshine Photovoltaic Pumping Systems, The First International Conference on Renewable Energies and VEhicular Technology, Hammamet, pp. 167- 172, from 26 to 28 March 2012.

[5] M. Farhat, A. fleh, L. Sbita., Influence of photovoltaic DC bus voltage on the high speed PMSM drive, 38th Annual Conference of the IEEE Industrial Electronics Society, 25-28 October, Montreal, Quebec, Canada, 2012.

[6] S.Hamidreza Mohades Kasaei, S. Mohammad reza Mohades Kasaei, S.Alireza Mohades Kasaei, Design and Implementation Solenoid Based Kicking Mechanism for Soccer Robot Applied in Robocup-MSL, International Journal of Advanced Robotic Systems, Vol. 7, no. 4, pp.73-80,2010.

[7] M, Zalani Daud,A, Mohamed, M. A. Hannan, An Optimal Control Strategy for DC Bus Voltage Regulation in Photovoltaic System with Battery Energy Storage The Scientific World Journal, Article ID 271087, 16 pages, 2014.

[8] S. Abouda,, F. Nollet, N. Essounbouli, A.Chaari,Y. Koubaa., Design, simulation and voltage control of standalone photovoltaic system based MPPT: Application to a pumping system, International Journal of Renewable Energy Research, vol. 3, pp. 538-549, 2013.

[9] M. farhat, L. Sbita, ANFIS controlled solar pumping system, i-manager's Journal on Electronics Engineering, Vol. 2, no. 2, march-march 2011.

[10] M. Farhat, A. Flah, L. Sbita, Photovoltaic Maximum Power Point Tracking Based on ANN Control, International Review on Modelling and Simulations (IREMOS), Vol 7, No 3, 2014.

[11] A.Flah, M.Farhat, L. Sbita, A Robust PMSM Speed Control using an Artificial and a Recurrent Neural Network, International Journal of Research and Reviews in Computer Science (IJRRCS),Vol. 2, no. 4,pp. 1023- 1028, 2011.

[12] Trishan.E, Patrick L. C, Comparison of Photovoltaic Array Maximum Power Point Tracking, Techniques, IEEE Trans. on Energy conversion, vol.22,no.2,pp. 439-449, 2007.

[13] A. Mellit, A. Kalogirou, "ANFIS-based modelling for photovoltaic power supply system: A case study, Renewable Energy: 36, pp. 250-258, 2011.

[14] Chokri. B. S, Mohamed. O, Comparison of Fuzzy Logic And Neural Network In Maximum Power Point Tracker For PV Systems, Electric Power Systems Research,.vol.81,pp. 43–50, 2011.

[15] Ollervides.j, Santibáñez..M, Lama.A, Dzul.A,, Aplicación de Control Borroso a un Sistema de Suspensión Magnética: Comparación Experimental, Revista Iberoamericana de Automática e Informática industrial,vol. 7,no3,pp.1697–7912,

[16] M. farhat, L. Sbita, ''ANFIS controlled solar pumping system, '' i-manager's Journal on Electronics Engineering, Vol. 2, no. 2, march-march 2011

[17] S. Thiruvenkadam, A. N. Kumar, and A. Sakthivel, "Distribution feeder energy conservation by using hybrid Neuro-Fuzzy approach," I-manager's Journal on Electrical Engineering, Vol.1, no. 3, pp. 45-52, 2008.

[18] S. Sankar," Simulation and Application of ANN in Fuzzy logic System, " I-manager's Journal on Future Engineering and Technology, Vol. 6, No. 1.pp 44-50, 2010.

[19] M. Alata, M. A. Al-Nimr, "Developing a multipurpose sun tracking system using fuzzy control, Energy Conversion and Management: 46, pp. 1229-1245,2005.

[20] C. T. Chi, S.A. Yin, Speed measurement of a general DC brushed motorbased on sensorless method,IEEE Conference on Power & Energy IPEC, 2012

[21] K. Niruba, S.Boopathi, Advanced power window motor using permanent Magnet DC motor, IEEE Power and Energy Systems Conference: Towards Sustainable Energy, 2014

[22] A. Hamidat, B. Benyoucef, M.T. Boukadoum,"New approach to determine the performances of the photovoltaic pumping system," Revue des Energies Renouvelables ICRESD, Tlemcen, pp. 101-107, 2007.

[23] M. Asim, A.Tariq & A. Sarwar, "Simulation and Analysis of a Directly Coupled Solar PV Based Water Pumping System," Journal on Electrical Engineering, Vol.2, no.3, 2009

Chapter 6

Energy Efficiency of Electric Vehicles – Energy Saving and Optimal Control Technologies

Guoqing Xu, Chunhua Zheng, Yanhui Zhang,
Kun Xu and Jianing Liang

Additional information is available at the end of the chapter

http://dx.doi.org/10.5772/59420

1. Introduction

Electric vehicles (EVs), including pure electric vehicles (PEVs or EVs), hybrid electric vehicles (HEVs), and fuel cell vehicles (FCVs), have attracted worldwide attention increasingly from governments, industry, and public. Though EVs have shown advantages over internal combustion engine (ICE) vehicles in terms of environmental friendliness and energy efficiency, there are still many technical challenges impeding the market share growth.

In this chapter, the energy-related issues for EVs will be discussed in detail. The primary aim of this chapter is to give a clear and systematic understanding of the energy processing and control for EVs and to introduce some latest energy saving and optimal control technologies and present the key results regarding this area. The overall technical architecture and the overview of the state of the art will be introduced. Then some advanced and newest technologies of energy savings and optimal control for EVs, such as the high-efficiency traction motor, intelligent battery management system, regenerative braking with high energy recovery, and the vehicle energy management, will be included and discussed as well as the key results. The detailed contents of this chapter are as follows:

2. Introduction of EVs

2.1. EVs

The transportation sector is the largest consumer of oil and it has grown at a higher rate than any other sector in recent decades [1]. Increases in transportation have caused pollution

emissions because of the utilization of ICEs, and that have consequently caused some environmental problems, which must be prevented to maintain the quality of life. Thus, many governments have developed more stringent standards for the pollution emissions of vehicles. In order to achieve better fuel economy and lower emissions, both academia and automotive industry have conducted research on improving the efficiency of powertrains, developing other energy sources, and changing the concept of the conventional powertrains to EVs including PEVs, HEVs, and FCVs. Among them, PEVs use electric motors for traction and batteries or supercapacitors for energy storage systems. FCVs take the fuel cells as the energy sources, however, the fuel cells do not have the energy recovery function which the batteries and the supercapacitors have. PEVs and FCVs have many outstanding advantages over ICE vehicles such as zero emission, independence from petroleum, higher efficiency, and quiet operation [2]. As a power source, a fuel cell system (FCS) has a relatively slow power response and the ICE or the fuel cell cannot recover the vehicle braking energy. Thus, the size of the FCS or the ICE will be increased if the FCS or the ICE is the only power source in a vehicle. The secondary power source which has a relatively quick power response and can recuperate the braking energy is needed, and a battery or a supercapacitor could be one of the candidates for the secondary power source. Hybrid powertrain structure is the solution of the above requirements. A fuel cell hybrid vehicle (FCHV) or an HEV can provide sufficient power during its acceleration and can recuperate the kinetic or potential energy of the vehicle during braking by the hybridization.

2.2. The state of the art of energy saving and optimal control technologies for EVs and the technical challenges

For the traction motors, the optimization of different machines is still the most important means to pursue higher power density and higher efficiency. In order to reduce the overall weight, volume, and cost, the integrated motor drive becomes more and more popular which integrates the circuit of the charger into other power electronic circuits existing in EVs. In addition to the three-phase AC motors, switched reluctance motor (SRM) has attracted increasing attention recently due to its low cost, simple structure, good controllability, high efficiency, and wide operation range. SRMs have been extensively applied to the electric drive systems of EVs.

For the BMS of EVs, the main and key difficulties are the voltage balance and the battery SOC estimation. The voltage balance is dependent on the accurate estimation of the battery SOC. Thus, the battery SOC estimation is not only for the voltage balance but also for achieving a good energy management result. Currently, the ampere-hour (Ah) model is one of the most widely used methods in this area.

For the RBS, in spite of the significant benefits of RBS, there are still technical challenges. The battery conditions, including the SOC and temperature, affect the energy recovery. When the SOC is too high, the regenerative braking energy may not be fed back to the battery. The hydraulic braking system functions instead of the RBS in such case. Additionally, the hydraulic braking system is reserved in case of failure of the electric braking actuator. Therefore, the hybrid brake system (HBS) that consists of both the hydraulic and the regenerative braking

http://dx.doi.org/10.5772/59420

systems is the main architecture in this area, which is further divided into the parallel type and the series type. The HBS needs an appropriate coordination mechanism between the two subsystems to achieve multi-objectives, i.e., safety, energy efficiency, and brake comfort. Various control methodologies including the rule-based, fuzzy logic-based, robust control-based, and neural network-based approaches have been proposed and investigated in the literature. Nevertheless, the HBS needs further studies due to the model nonlinearity, parameter uncertainty, external disturbances, and the interaction with the driver's operation on the brake pedal. From the point of view of the safety and energy savings, emphasizing the electric braking force is a significant trend in future.

For the energy management of EVs, rule-based energy management strategies are usually used currently because of the simplicity. Other advanced strategies, for example optimal control theory-based energy management strategies, are still on the research step due to several unsolved problems such as lack of the memory for big data saving and low speed of the processor. In addition, the research on the energy management strategies using the prediction of future driving condition is active currently, as the driving route of the vehicle is not fixed in the real-world driving.

3. Electric driving technologies

3.1. Introduction of EV traction motors

The traction motors, working as the heart of powertrains, are the most important key components of modern EVs. Unlike conventional motors, traction motors and drive systems for EVs are under special demands, such as compact structure, light weight, high reliability, high efficiency, low noise, low vibration, wide operating range, and most importantly, low cost. With the harsh requirements, innovative concepts are used to design the EV traction motors, which include the innovations on conventional motor structure, principle, design, performance, and manufacturing technology. In order to achieve high power/torque densities, high reliability, and wide operating range, a lot of new technologies such as water-cooled frame structure, internal oil-cooled stator structure, thin-shell frame, and ultra-short and solid filled-in end-turns will be utilized. Due to the natural disadvantages, such as complicated brush assembly, poor reliability, and the need of maintenance, conventional brushed DC machines are not suitable for larger scale commercial application in vehicle business. Modern vehicles normally use AC machines without brushes, namely, induction machines, switched reluctance machines, and permanent magnet AC machines.

To pursue a high power density of machines, the major task is to increase the peak output torque, rather than the rotating speed, because the speed may be limited by applications and manufacturing technology of the powertrain. The size and weight of machines are mainly related to the peak output torque, not peak output power. The peak torque depends on the saturating level of magnetic path and the current in the winding. Designers have to endlessly optimize the structure of magnetic path to achieve better usage of ferromagnetic materials and search for peak torque with smaller winding current. For the similar heat dissipation condition,

the smaller winding current results in less conductor materials and the ferromagnetic materials surrounding them and consequently leads to less resistance losses in the conductor and less iron losses in the ferromagnetic materials. Hence, the higher power density requires the higher efficiency, while the higher efficiency normally results in the higher power density. Under certain situations, the higher power density can also be achieved with higher current density, which requires promotions on the heat resistance of materials and improvements of heat dissipations. However, such solutions demand for better materials and manufacturing technologies. The total power loss will be the largest in induction machines, smaller in reluctance machines, and the smallest in permanent magnet (PM) machines. The efficiency of the machines will follow the reverse sequence. Thus, the PM machines come with the most potential for higher power density. In fact, the optimization of different machines is still the most important means to pursue higher power density and higher efficiency.

3.2. Electric drive based on integrated technology

Transport electrification has been considered as one of the most promising solutions to the urgent challenges facing our human beings, such as global warming, environmental pollution, energy crisis, and so forth [3]. Most recently, with the advent of the vehicle-to-grid (V2G) technology [4], the gridable EVs that can be directly connected to the utility grid have been expected to function as distributed energy storage system during the parking period, so as to balance the demand and supply of the electricity market in the future. Generally, gridable EVs include battery EVs, plug-in hybrid EVs [5, 6], and range-extended EVs [7].

In contrary to the traditional EVs, the gridable EVs are equipped with plugs and on-board chargers. By connecting the plug to the utility grid, the electrical energy can flow into the on-board batteries through the on-board charger. Moreover, the energy deposited in EVs can also be fed back to power grid when the bi-directional on-board charger is engaged.

In gridable EVs, the high power energy conversion systems are installed, for example, motor drive system, low voltage DC/DC converter, electrical air conditioning system, battery charger system, and grid-connect inverter shown in Figure 1. Many complex power electronics and electrical systems bring the serious challenges from system layout, installation, weight, cooling, electromagnetic compatibility, and cost, etc. The diverse needs for the electromechanical systems of EVs can be satisfied by the development of integrated technology.

In order to reduce the overall weight, volume, and cost, integrated motor drive becomes more and more popular to integrate the circuit of the charger into other power electronic circuits existing in EVs. In the previous publications, the circuits of motor drive and the motor are involved to construct integrated on-board chargers [8, 9]. Due to the neutral point of AC motors, one terminal of AC line can be conveniently connected to the neutral point, and the three-phase windings can function as the couple inductances in the boost converter circuit. However, the boost converter topology requires the input voltage lower than the output voltage. Thus, such kind of integrated charger is more feasible in countries and regions where 110 V AC power is adopted. In order to extend the range of the input voltage, the buck converter has been added to the battery side.

http://dx.doi.org/10.5772/59420

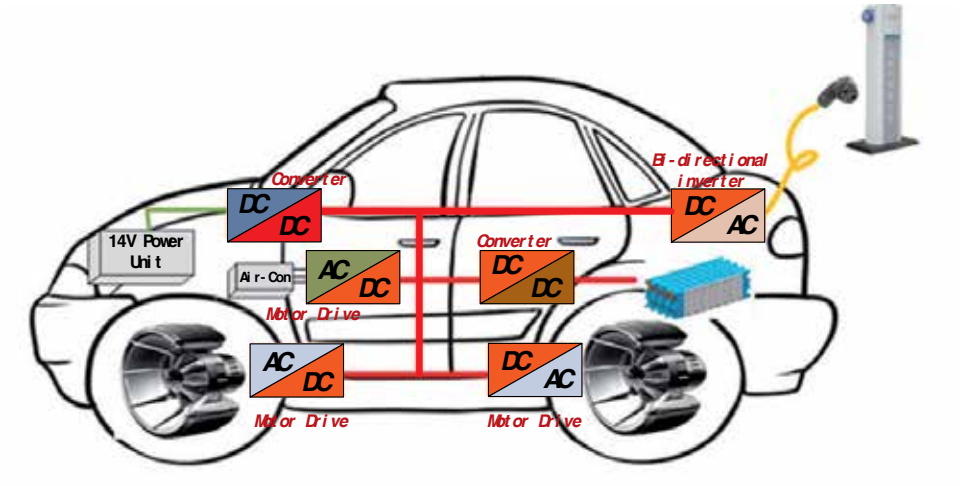

Figure 1. Main electrical energy conversion system in EVs

In addition to the three-phase AC motor, SRM has attracted increasing attention recently due to its low cost, simple structure, good controllability, high efficiency, and wide operation range [10, 11]. SRMs have been extensively applied to the electric drive systems of EVs. The purpose of this study is to propose a novel integrated SRM drive with the bi-directional inverter to reduce the cost, volume, and weight for EV applications.

3.3. Integrated technology of switched reluctance motor drive

3.3.1. Conventional SRM and its converter

SRMs, which are non-rare earth permanent magnet motor, have been recognized as the considerable candidates for EV and HEV applications. It has salient poles on both rotor and stator, but only the stator carries windings. The torque is produced by the alignment tendency of poles. The rotor will shift to a position where the inductance of the excited winding is maximized. Therefore, the advantages of SRMs can be summarized as simple construction, low manufacturing cost, and outstanding torque characteristics. The structure of SRMs is shown in Figure 2.

When the rotor position enters into inductance increasing region, this phase winding is injected with the phase current. SR motor operates at motoring mode and produces positive torque. Contrarily, SR motor operates at regeneration mode and produces negative torque. Motoring and regeneration modes of SRM are shown in Figure 3.

For EV applications, the conventional SRM drive uses a battery source and a large capacitor in the front-end as shown in Figure 4. This capacitor helps the battery to keep a steady DC-link voltage, acting as a low-pass filter. Another function of DC-link capacitor is to store the magnetic field energy when the SR motor is demagnetized.

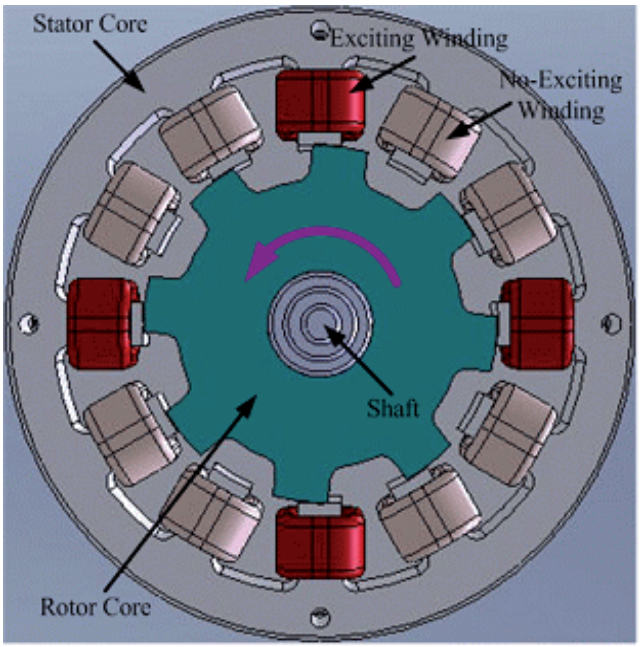

Figure 2. Excited phase winding in 12/8 3-phase SRM

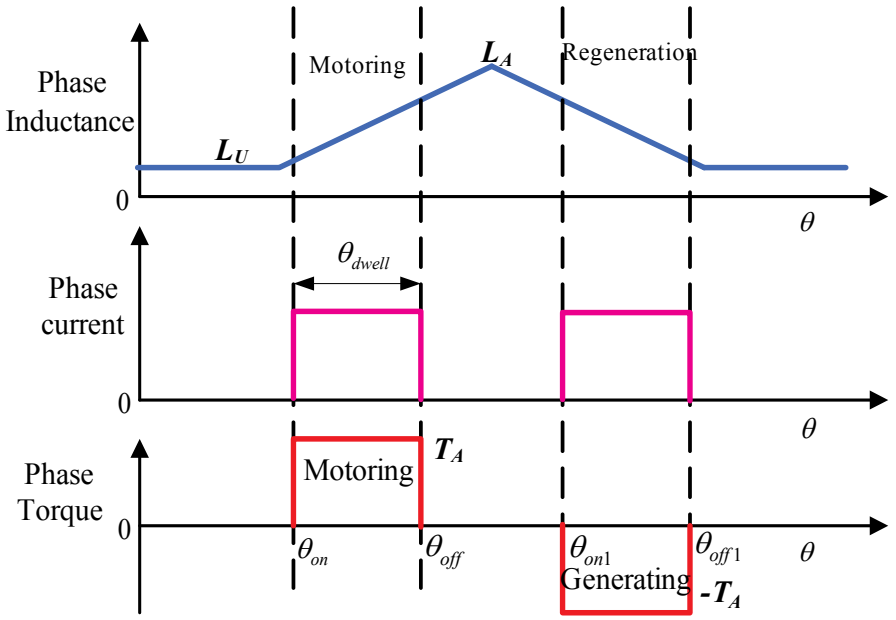

Figure 3. Motoring and regeneration modes of SRM

http://dx.doi.org/10.5772/59420

The asymmetric bridge converter consists of two power switches and two diodes per phase, which can support independent control of each phase and handle phase overlap. The asymmetric converter has three modes, which are defined as magnetization mode, freewheeling mode, and demagnetization mode as shown in Figure 4 (b-d).

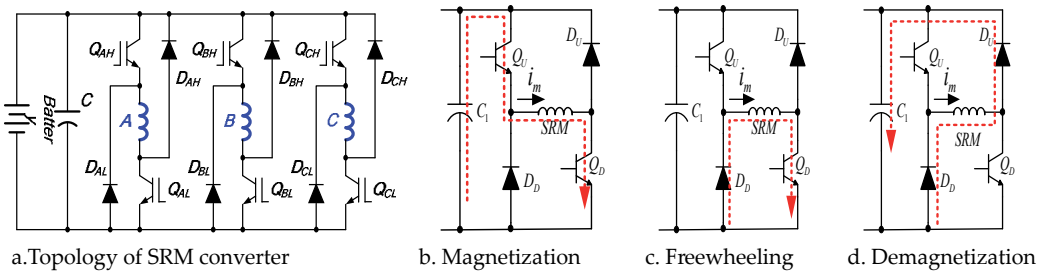

Figure 4. Conventional 3-phase SRM drive and its operation modes

3.3.2. Integrated switched reluctance motor converter

In the conventional EV application, the on-board battery charge and the grid-connect inverter are independent devices. To reduce the size, weight, and cost, the integrated SRM drive with the bi-directional inverter is introduced [12]. The integrated converter can be operated as: SRM drive, battery charger, and grid-connect inverter. In order to improve the coefficient of utilization, the power switches, inductors, capacitors, and controller are multiplexed in the same circuit. For city vehicle application, the operation of driving mode, battery charging mode, and grid-connect mode can be divided by Time-Division Multiplexing (TDM) method. The integrated drive system can be served the activity plan of daily as shown in Figure5. The integrated system can be seamless transferred to each application. Of course, more complicated case can be supported by this method.

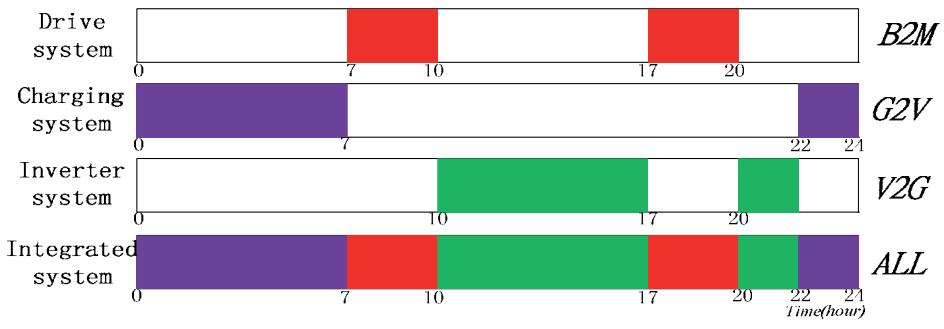

Figure 5. The activity plan of different application in working day

The battery charger is a device used to put grid energy into the battery by forcing an electric current through it. It consists of the rectifier, the boost converter, and the buck converter. The grid connect inverter is a device used to put battery energy into the grid. It is made up of the boost converter and inverter bridge. Due to the power factor requirement, the power factor correction is required to perform. The topology of three circuits is shown in Figure 6. In order to build the integrated motor drive, all the functions of the three devices should be included.

A novel integrated SRM drive with the bi-directional inverter is introduced in Figure 7 [12]. Compared with the conventional asymmetric converter, the two lines from the plug outlet are connected to the cathode of the lower diode in phase A and B. A relay is added between the switch Q_{CH1} and the switch Q_{CH2} to divide the voltage stage of DC-link and battery. In order to reconstruct the bi-directional converter, two free-wheeling diodes of phase C's are replaced by two power switches with parallel protection diodes.

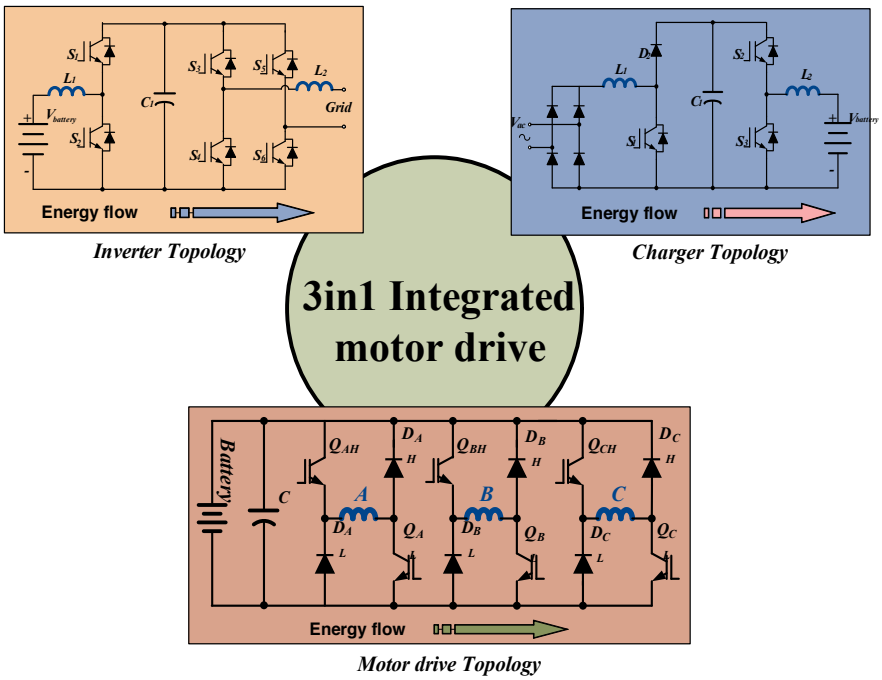

Figure 6. The circuit topology of motor drive, charger, and inverter

Obviously, two stages of the bi-directional converter are suitable for the battery charger application due to the wide range of the battery voltage. The bulk capacitor of the motor drive is designed to separate two parts and serve two independent voltage stages. In the driving mode, the two capacitors are paralleled to increase the capacitance value. In the bi-directional converter mode, the two capacitors are divided: one is for the boost voltage stage, and the other is for the battery voltage stage. In the battery charger mode, the relay is opened and the proposed integrated SRM drive is constructed by the bridgeless power factor correction (PFC)

http://dx.doi.org/10.5772/59420

front-end and the buck-boost converter. The bridgeless PFC front-end can improve the efficiency of AC-DC conversion. The key point of this integrated SRM drive is that it applies the motor winding as the boost inductance and the buck inductance [12]. In the grid-connected inverter mode, the relay is similarly opened. The bridgeless PFC frond-end is operated as a single phase inverter, and the full bridge converter of the phase C is run as a boost converter in the opposite direction [12].

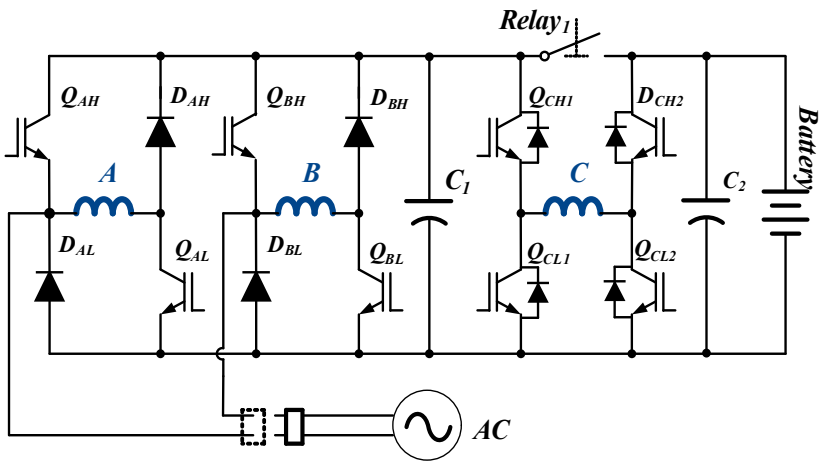

Figure 7. A novel integrated SRM drive with the bi-directional converter

3.3.3. Control strategy of the integrated motor drive

For the normal inverter, the inductance is only like a static transformer. However, in the novel integrated drive system, the inductance of the integrated inverter is related to the phase winding of SRM, which varies according to the rotor position and phase current. In this application, the phase inductance is limited by the primary characteristic of the SRM drive. Thus, three problems can be found: the first is that the inductance of the SRM is changed by the rotor position; the second is that the relative space angle between phase windings is 120 electrical degrees; and the last is that the phase inductance has effects of magnetic saturation.

In the motor driving mode, the rotor performs the rotational motion according to the instructions. However, unlike the driving mode, the rotor position of the battery charging mode and the grid-connect mode prefers not to rotate. The rotation and vibration only increase the loss of energy conversion. Two questions appear: how to fix the rotor at still and how to find the suitable position.

For the fixed position, two methods can be selected: the mechanical brake method and the zero torque control method [11]. For the mechanical method, the rotor will be locked by the mechanical structure. The motor torque will be counteracted, but the mechanical components increase the cost and space. Due to satisfy the power factor correction and battery charging,

the sine wave current is injected in the phase A or B, and phase C is flown in the direct current. Therefore, the zero torque control method cannot be applied in this converter topology [13]. Thus, the mechanical method is used, and the advantage is that the rotor position is easy to set to any position.

For finding the suitable rotor position, the aligned position of the phase A is defined as zero. Ignoring the influence of mutual inductance, the inductance of the SRM is a periodic function of the rotor position, and it can be simplified and expressed using Fourier series as follows:

$$L(\theta,i)=\sum_{n=0}^{\infty}L_n(i)\cos(n\theta)\qquad(n=0,1,2...) \tag{1}$$

where *Ln* (i) is the amplitude of the Fourier components, whereas θ_A, θ_B, and θ_C are electrical degrees of each phase. In a three phase SRM, the axes of the three-phase windings are spaced 120° electrical degrees from one another, that is

$$\theta_A=\theta \tag{2}$$

$$\theta_C=\theta+2\pi/3 \tag{3}$$

$$\theta_B=\theta+4\pi/3 \tag{4}$$

For the bridgeless PFC front-end circuit, a boost inductor is needed to boost-up the DC-link voltage. However, in the novel integrated drive system, the winding of phase A or B is alternated to replace the boost inductor in the different half-cycle of sinusoidal voltage. Obviously, the inductor of the phase A and B should be equal in value to make the circuit symmetrically. Therefore, the charging position of the novel integrated system must meet the inductor requirement.

$$L(\theta_A,i)=L(\theta_B,i) \tag{5}$$

The inductance of the phase A and B can be calculated from (1), (4), and (5):

$$\theta_A=-\frac{2\pi}{3}+k\pi,\qquad(k=0,1,2..) \tag{6}$$

So, meet the conditions in case of rotor position is

http://dx.doi.org/10.5772/59420

$$\theta_A = \frac{\pi}{3}, or \quad \theta_A = \frac{4\pi}{3}. \tag{7}$$

In both cases, the difference between the inductance of the phase A and B is clearly indicated in Figure 8. The inductance of the phase A and B at π/3 is higher than that at 4π/3. However, the inductance of the phase C reaches the maximum value at 4π/3 and the minimum value at π/3. The selection of the charging position should be decided by the real application. Due to the phase C winding used by DC/DC converter, the inductance of the phase C will affect the dynamic response ability.

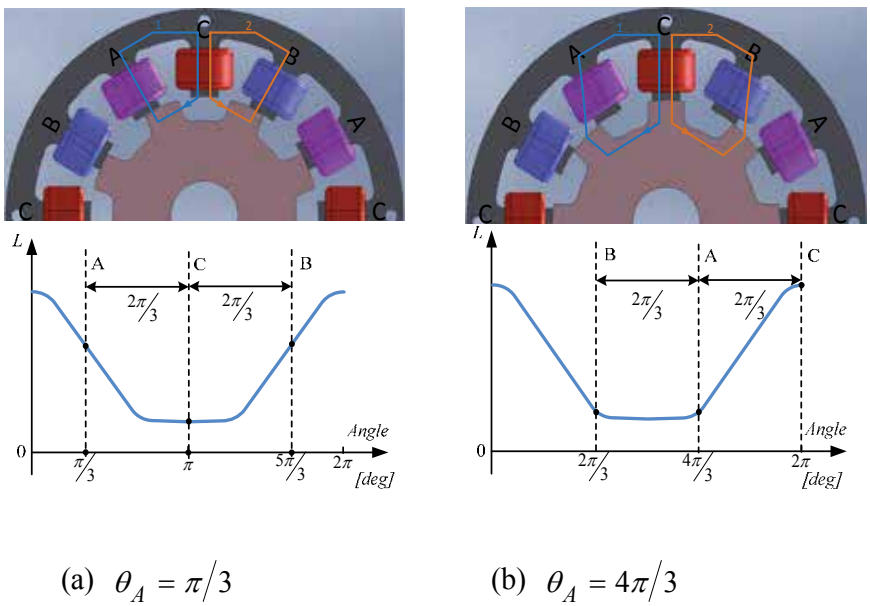

Figure 8. Rotor position of phase A in the bi-directional inverter mode

The block diagram of the novel integrated SRM drive system is shown in Figure 9. In the driving mode, the battery supplies the stored energy to drive SR motor, and the power flow is through the battery, integrated converter, and SR motor. When the outlet is connected to the grid, the vehicle management system should decide operation mode of the integrated drive system. If charging mode is executed, the asymmetric converter of the phase A and B is operated as a bridgeless PFC converter to meet the requirement of the PFC and DC-link voltage. And the full bridge converter of the phase C is implemented as a buck converter to manage the battery charging strategy. The power flow is followed the grid, SR motor, proposed converter, and the battery.

Due to the topology of the bridgeless front-end, the positive half cycle of the line current is injected into the winding of the phase A, and the negative half cycle of the line current is

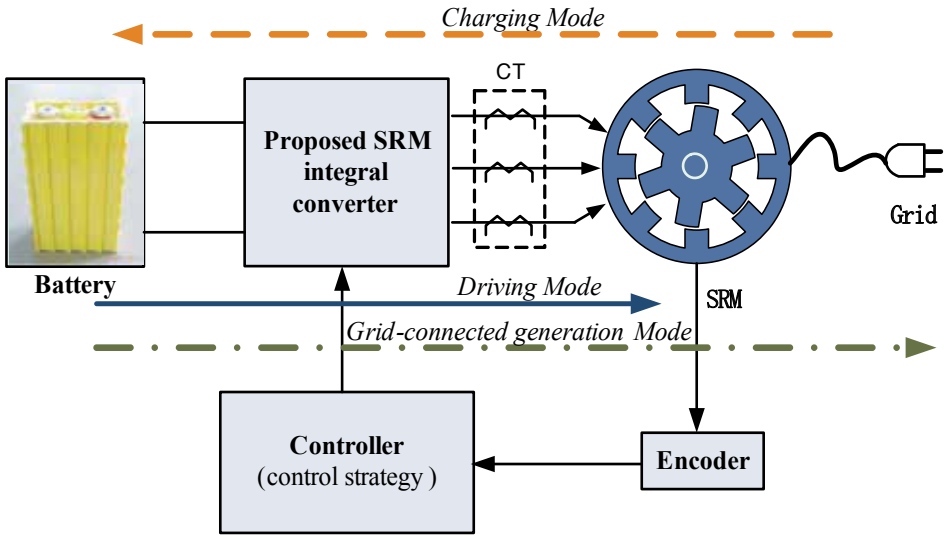

Figure 9. Block diagram of the integrated system

injected into the winding of the phase B. However, the input line current waveform is also sinusoidal. At the rotor position of $4\pi/3$, the inductance of the phase C reaches the maximum value and the torque of the phase C is zero. Because the phase A and B are conducted in turn, the total torque of the rotor is not equal to zero in Figure 10. The power factor of 220Vac input is 0.99.

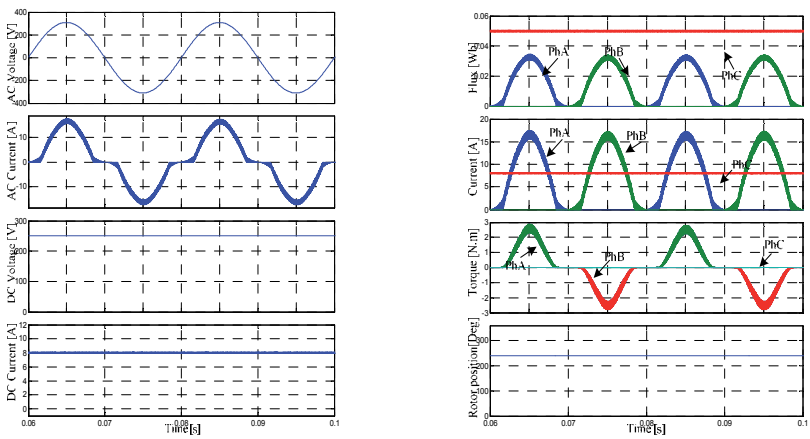

(a) Voltage and current (220[*Vac*]) (b) Current, flux and torque (220[*Vac*])

Figure 10. Simulation results of novel integrated system in charging function (220V)

http://dx.doi.org/10.5772/59420

If the inverter mode is carried out, the quadrant DC/DC converter of the phase C is implemented as a boost converter which meets the DC-link voltage requirement. The asymmetric converters of the phase A and B are acted as the inverter bridges. The power flow passes the battery, converter, SR motor, and the grid.

In the inverter function (Figure 11), the current of the phase C is the reverse direction of charging function's. Thus, the phase current and flux of the phase C are negative. Since the current of the phase A and B is unidirectional, the flux of them is positive. For the battery side, the battery discharges the energy to the DC-link. The current and voltage of power grid have 180 degrees.

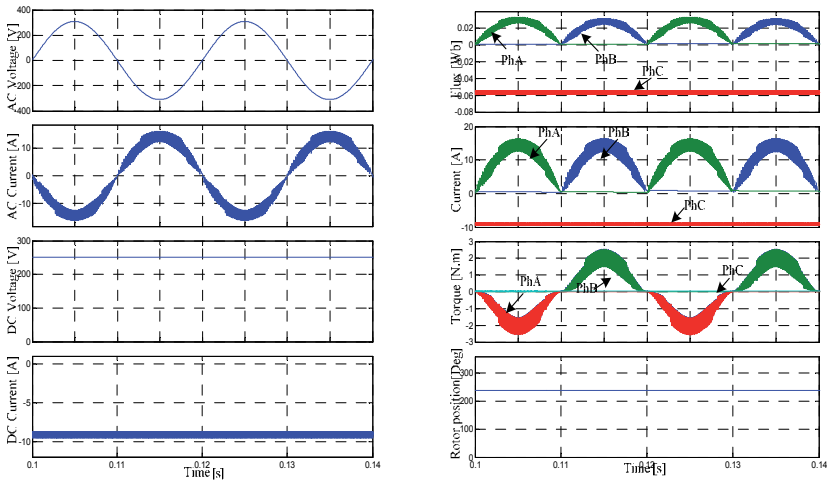

(a) Voltage and current(220V) (b) Current, flux and torque(220V)

Figure 11. Simulation result of proposed integrated system in inverter function (220V)

4. Advanced battery management technologies

4.1. Introduction of battery management system (BMS)

The lithium-ion battery has attracted special attention for HEVs and EVs owing to its advantages of high specific power, high energy density, no memory effect, and long durability. What is more, research is yielding a series of improvements to traditional manufacturing technology focusing on power density and intrinsic safety of battery.

A BMS is an important means for raising the intrinsic safety and durability of batteries. The main parameters of the batteries are monitored with the BMS including the voltage, current, temperature, and also the leakage detection and SOC & state of health (SOH) condition. The maximum mileage and the charging control algorithm can be achieved based on the battery

voltage, current, and temperature under the maximum output power control algorithm. The real-time communication is achieved between the CAN bus interface and the vehicle master controller, motor controller, energy control system, and automotive display systems. The BMS is a bridge between the battery and drivers, and it plays a critical role for the EV performance. The diagram of the BMS is shown as Figure 12.

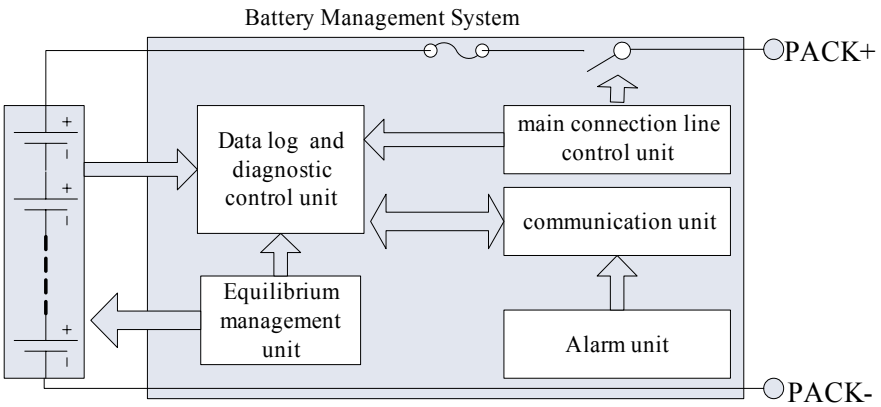

Figure 12. Diagram of the BMS

4.2. SOC estimation of Lithium-ion batteries

Many ways of SOC estimation have been proposed in the literature [14]. According to the main detection parameters, they are classified into voltage model, resistance model, current model, and intelligent algorithm model [15]. The open circuit voltage (OCV) provides the useful information on the intrinsic characteristics of the battery and it declines proportionately with the energy expenditure [16]. However, it does not apply to frequent repeated conditions of charge/ discharge. Moreover, this similarly situation also occurs in the resistance model. Ah model is one of the most widely used methods, and it is an iterative algorithm of dynamic current with time integral. The main drawback is the initial SOC (SOC0) cannot be estimated. Additionally, the intelligent algorithm model, such as Kalman filter model, Extended Kalman filter model, and Artificial neural network model, is highly dependent on the quantity of battery model and input variables, which greatly influences the accuracy and computational complexity. The hybrid model of OCV model and Ah model is considered to be easy to accomplish. Additionally, it is easily implemented in EVs and it needs uncomplicated hardware.

4.2.1. Definition of terms related to SOC

Accordingly, when a battery is in discharging step, the formula to calculate SOC as the ratio of releasable capacity, $Q_{releasable}$, relative to the rated capacity, Q_{rated}, during the profiles is as follows:

http://dx.doi.org/10.5772/59420

$$SOC = \frac{Q_{releasable}}{Q_{rated}} \times 100\% = (1 - \frac{Q_{consumption}}{Q_{rated}}) \times 100\% \quad (8)$$

If the discharging step is not from the rated energy, the Ah model of SOC estimation could be expressed as (9) and shown as Figure 13. The real time SOC estimation (SOC (t)) is equal to the plus of the initial SOC (SOC0) and the ration of the consumption capacity with the rated capacity in an operating period τ. I is positive for discharging and negative for charging. To enhance the accuracy of SOC estimation, the energy efficiency denoted as η is considered.

$$SOC(t) = SOC_0 + \Delta SOC = SOC_0 + \eta \frac{-\int_{t_0}^{t_0+\tau} Idt}{Q_{rated}} \times 100\% \quad (9)$$

4.2.2. The function of OCV to SOC0

The lithium-ion battery used in the investigation is $LiFePO_4$/graphite battery. A $LiFePO_4$ battery with nominal voltage of 3.65 V and nominal capacity of 20 Ah is selected.

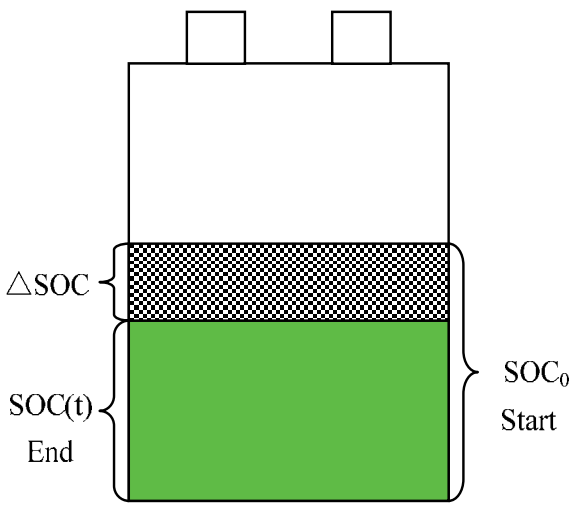

Figure 13. Diagram of relative locations of the initial SOC (SOC0), real time SOC (SOC (t)), and the ration of energy discharged ΔSOC

The OCV is the equilibrium potential difference of an electrode, which depends on the temperature and the amount of active material left in the electrolyte. The OCV can be calculated by Nernst equation [17]. However, the measured voltage at the breaking of the current cannot be denoted as OCV because of the presence of polarization and the relaxation of solid particles. In fact, after the short discharge, the terminal voltage is gradually increased due to relaxation

of over potentials and eventually leveled off to an equilibrium potential. Figure 14 illustrates the OCV as a function of SOC after discharging at a room temperature. The verification experiment is conducted to calculate the accuracy of the above estimation method of OCV (see the circles in Figure 14).

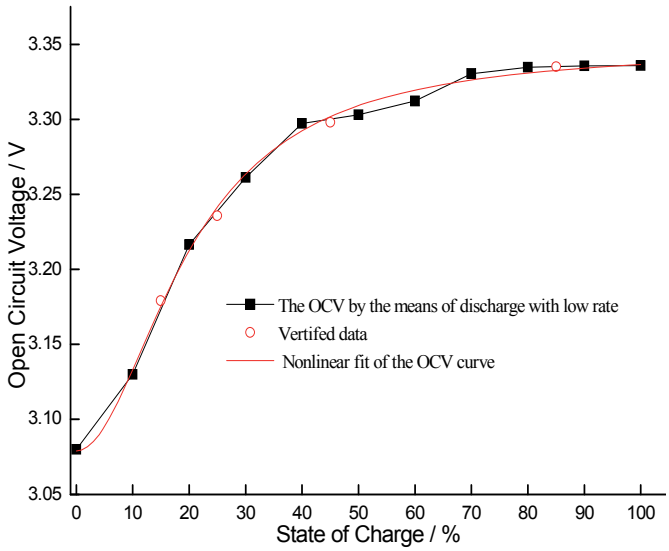

Figure 14. The comparison profiles of the measured voltage and the nonlinear fit

In this study, the quantitative relationship between the SOC and OCV as the logistic function (equation (10)) is proposed. The values of b and p are 20.12155 and 1.97038, respectively, and the correlation coefficient of the fit is 0.997.

$$U = \frac{U(SOC0\%) - U(SOC100\%)}{1 + (SOC_0 / b)^p} + U(SOC100\%) \tag{10}$$

4.2.3. The function of temperature to SOC0

To mitigate the estimation error, the following technique is used in this work. At a certain temperature, the relationship between SOC0 and OCV is obtained and can be established using nonlinear function. dV0 /dT is proportional to the entropy of reaction by the relation dV0 / dT=ΔS/nF, where n is the number of electrons passed in the reaction and F is Faraday's constant, and reflects the influence of the incremental lithium atoms on the ordering of lithium-ion in the host lattice [18].

The battery is discharged to a designed SOC and kept to a temperature of 30°C for 20 hours. This is to impel the degradations of diffusion and migrant to obtain a steady voltage. The

http://dx.doi.org/10.5772/59420

temperature experiments focus on the changes of OCV under different ambient temperature conditions of 3°C, 15°C, 25°C, 35°C, and 45°C for 0.5h [19]. The result is shown in Figure 15. The results reveal that the temperature affects the changes of OCV. To reduce the error of temperature upon the SOC0 estimation, the voltage is calculated according to a unified energy unit under a constant temperature, which selects 25°C as a base.

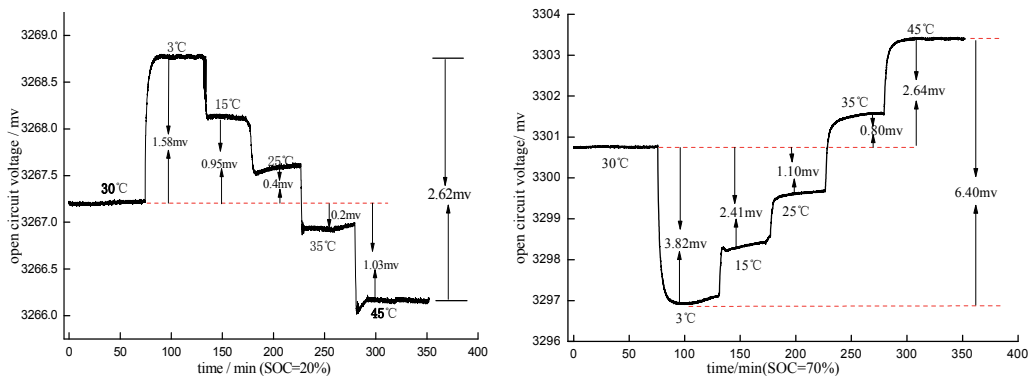

Figure 15. OCV under different temperature (the first and the second subplots respectively correspond to the cases in which SOC=20% and SOC=70%)

Through the above analysis, we can see that the temperature and resting time have significant impacts on the SOC0 estimation. In the present study, the quantitative relationship (equation (11)) exhibits the functions of terminal voltage u, resting time t, and temperature T to SOC0 based on the theory above.

$$SOC_0 = f_3(\Delta t)\exp\frac{1}{f_4(\Delta t)}\left(\frac{f_2(\Delta t)}{u - f_1(\Delta t) - \Delta u(T)} - 1\right) \tag{11}$$

Meanwhile, the temperature correction factor Δu (T), which reflects the influence of the temperature variation on the OCV, is also considered when estimating SOC0.

4.3. Energy Efficiency for intermittent charging-discharging

In order to fully explore the effect of thermal characteristics of lithium-ion battery on the energy efficiency under the continuous process of charging and discharging, the energy balance model under the heat generation behavior is investigated. The energy balance for batteries consists of chemical reactions, ionic mixing, electrical work, and heat transfer with surroundings [20]. Assuming that the temperature distribution in the battery is uniform and the enthalpy of ionic mixing and the radiation between the battery and the environment are neglected, the energy balance function can be written as:

$$q = I^2R + I(\eta + T\frac{\partial V_0}{\partial T}) + MC_p\frac{dT}{dt} \tag{12}$$

$$\eta = V_0 - V \tag{13}$$

Where V0 is the OCV, V is the terminal voltage, q is the heat transfer rate between battery and the surrounding environment, I is the current, R is the resistance, η is the over potential, $IT^{\partial V_0}\big/_{\partial T}$ is the reversible heat, and Cp is the heat capacity of the battery.

In the charge/discharge cases, we are interested in evaluating how much energy is lost due to the thermal characteristics as a function of internal feature in the battery. If the irreversible reaction energy is ignored and considering the battery back to the initial state after the cycle, the energy balance function can be expressed as follows:

$$e_{charge} + TI_1\frac{\partial V_0}{\partial T} = I_1^2R + \eta I_1 + e_{discharge} + TI_2\frac{\partial V_0}{\partial T} + I_2^2R + \eta I_2 \tag{14}$$

To create an energy efficiency model for the charge/discharge cases, we similarly ask what percent of energy loss E_{loss} will be existed in a battery if the battery is charged or discharged at a given current I and a variable power P. The relative definitions of power P, energy loss E_{loss}, and energy stored E_{charge} or discharged $E_{discharge}$ can be visualized in Figure 16.

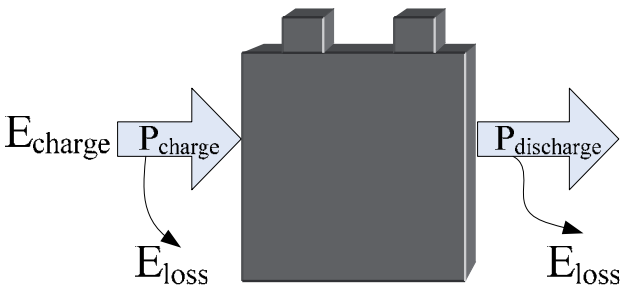

Figure 16. Diagram of relative locations in charge/discharge cases

In the process of charging and discharging, the energy lost caused by the battery thermal characteristics can be written as follows:

$$\begin{aligned}\Delta E &= E_{charge} - E_{discharge} \\ &= \int_0^{t_1}(I_1^2R + \eta I_1 - TI_1\frac{\partial V_0}{\partial T})dt + \int_0^{t_2}(TI_2\frac{\partial V_0}{\partial T} + I_2^2R + \eta I_2)dt\end{aligned} \tag{15}$$

http://dx.doi.org/10.5772/59420

By using the above function, the energy efficiency of the battery, which is dependent on the thermal feature during constant charge/discharge cycles, is determined by the following:

$$Eff = \left(1 - \frac{\Delta E}{\int_0^{t_1} P_{charge} dt + \int_0^{t_2} P_{discharge} dt}\right) \times 100\% \tag{16}$$

The main parameters of the energy efficiency, resistance, and entropy change coefficient can be determined by experiments. The experiments mainly focus on the thermal characteristics of the lithium-ion battery and the analysis of their effect on the energy efficiency under different depth of discharge (DOD) values, as shown in Table 1.

DOD	SOC	Current (charge)	Current (discharge)
20	40-60	0.3C	0.3C,0.5C,1C
40	30-70	0.3C	0.3C,0.5C,1C
60	20-80	0.3C	0.3C,0.5C,1C
80	10-90	0.3C	0.3C,0.5C,1C

Table 1. Battery test cycle under different DOD values

The experimental results are as follows:

i. Resistance

The discharge test at constant current is performed in the experimental setup and a few representatives are selected at 25°C as shown in Figure 17. The results of the resistance obtained for the SOC values are shown in Figure 17.

ii. Entropy change

Regarding entropy change, there have been many investigations and it is another factor contributing to heat generation in the energy balance. In general, the entropy change ΔS can be estimated from the temperature gradient of OCV, dV0 /dT. dV0 /dT is proportional to the entropy of reaction by the relation $dV_0/dT=\Delta S/nF$, where n is the number of electrons passed in the reaction and F is Faraday's constant, and reflects the influence of the incremental lithium atoms on the ordering of lithium-ion in the host lattice [18].

The entropy change of the lithium-ion battery is positive in the SOC regions of 30%-90%. This means that the thermal behavior of the battery is mainly endothermic during the discharge cycle even if there is no over-potential loss. Different entropy change under different temperature cycle is resulted from the phase change of active material, as shown in Figure 18.

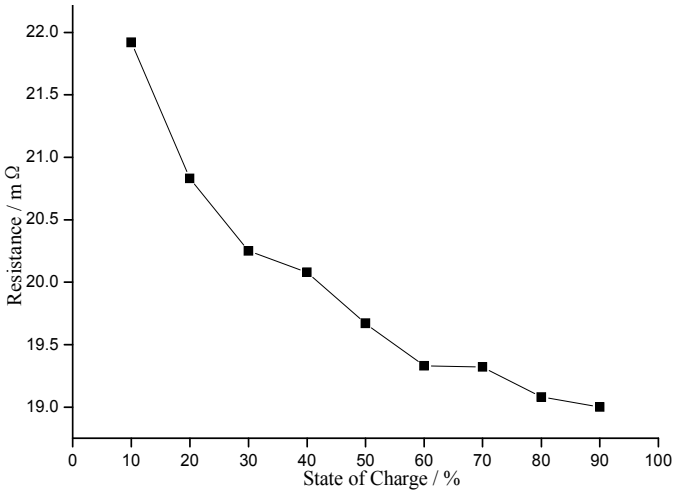

Figure 17. Resistance as a function of SOC

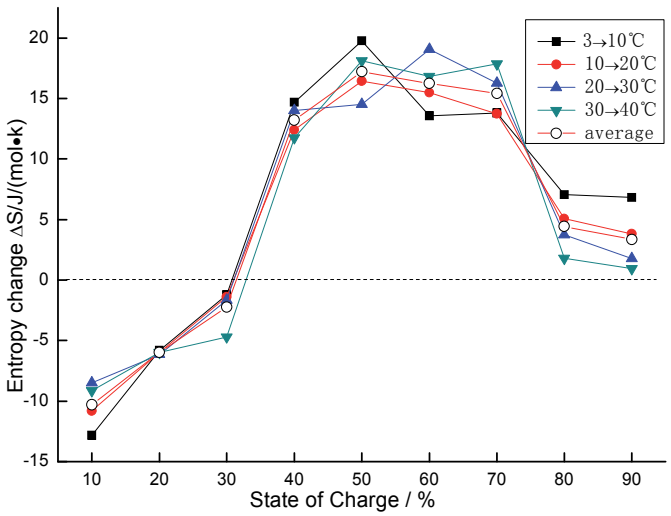

Figure 18. Entropy change for SOC and temperature

iii. Energy efficiency

The battery energy efficiency under the process of shallow charge/discharge is influenced by two factors: (1) External influence factor, such as the DOD, the ambient temperature, and the battery temperature. (2) The energy loss caused by the self-performance, for example, the increasing of resistance, the change of over-potential and the entropy. The above factors cause the energy loss and eventually reduce the battery energy efficiency.

http://dx.doi.org/10.5772/59420

In order to evaluate the contribution of thermal characteristics to the energy efficiency, we explore the effect under discharge and charge process by plotting the energy efficiency as a function of the DOD as shown in Figure 19. By examining the energy loss, we can determine the influence of the heat generation on the battery energy efficiency. The effects of the DOD, current rate, and temperature on energy loss are explored under different discharging interval. The results are shown in Figure 19.

The result of correlation analysis shows that there is a parabola relationship between energy efficiency and depth of discharge under the constant current rate. In addition, the lower the current rate, the higher the energy efficiency. It should be pointed out that the intercept for the minimum energy efficiency at 60% DOD reaches 85.7% at 1C. This may be related to the active material utilization at the above DOD (SOC 20%-80%).

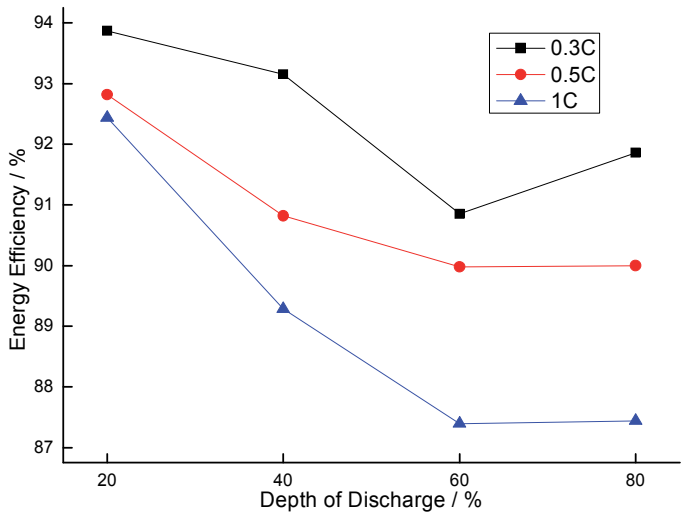

Figure 19. Energy efficiency versus DOD for lithium-ion cells

5. Advanced Regenerative Braking System (RBS) of EVs

5.1. Introduction of RBS

RBS converts part of the mechanical energy into electric energy during braking. The drive motor functions as a generator to provide the brake torque when the vehicle brakes. The potential energy, e.g., the kinetic energy, is converted into electric energy that is then stored in an energy storage system (ESS), e.g., power battery pack, supercapacitor or their combination. When a vehicle starts or accelerates, the drive motor receives the electric energy from ESS to propel vehicle. Utilizing such energy consumption-recycling mechanism, EV recycles a significant amount of energy that is consumed in conventional vehicles [21]. The total energy efficiency and the drive range are thus improved. Recent studies indicate that the energy

savings are completed from 8% to 25% of the total energy use [22-24], depending on the drive cycles and RBS performance. Additionally, the electric brake force generated from the motor is superior to the frictional brake force from the hydraulic brake actuator in terms of precision, accuracy and bandwidth for the torque control and measurement [25].

Maintaining brake safety under various braking conditions is the primary consideration when designing a vehicle brake system. The commercialized EVs/HEVs that utilize RBS still reserve the conventional hydraulic brake device in case of possible failure of the RBS. Another reason for employing the hydraulic brake is the rechargeable capacity of power battery pack. For example, when the SOC is high, the regenerative electric energy may not be fed into the battery, and thus the regenerative brake does not function. In this case, the conventional hydraulic brake is required to provide the brake force alone. The brake system with both the hydraulic brake and regenerative brake is the HBS, which has two architectures, i.e., parallel and series architectures [26]. In parallel braking architecture, both the regenerative torque and the friction torque are exerted on the same drive axle directly, while series braking allows independent modulation of the hydraulic brake torque of each axle according to the regenerative torque, and thus more kinetic energy can be recovered potentially than that with parallel braking.

Controlling the RBS involves multiple objectives, e.g., the total efficiency, brake safety, and comfort. As a RBS is an uncertainty system with parameter perturbation, strong nonlinearity and uncertain external disturbances, the classical control methods that adopt the rule based strategies [27, 28] are ineffective to guarantee the performance. Hence, researchers have studied and proposed advanced methodologies on the RBS control in the literature recently, including the fuzzy control strategies [29, 30], H∞ control [31], and neural network approaches [32]. The studies mostly focused on improving the energy recovery performance based on common factors. However, the vehicle drive safety and ride comfort, which are strongly influenced by the braking performance due to various uncontrollable phenomena by the driver's brake pedal operations [33], need sufficient considerations in the RBS control.

5.2. Regenerative Braking Control Design Based on Fuzzy Control (RBS-FC)

We propose a control methodology based on fuzzy logic for series RBS architecture to facilitate EV's energy-savings and brake safety. The RBS control aims at: 1) preventing wheel's excessive slip and lock via brake torque distribution between the front and rear axles; 2) achieving nearly the optimal regenerative efficiency under normal brake condition.

5.2.1. Braking Force Distribution

The total vehicle brake force F_{car} that is estimated via vehicle acceleration α_{car}, consists of the front brake force F_f and the rear brake force F_r exerted on the front and rear wheels, respectively, which is shown in (17) and the first subplot of Figure 20, where M is the total vehicle mass. However, the load movement during braking may induce wheel lock and the consequent vehicle instability using average torque distribution between the front and rear wheels. Therefore, RBS needs appropriate brake torque distribution law to ensure the braking safety.

http://dx.doi.org/10.5772/59420

$$F_{car} = M \cdot \alpha_{car} = F_f + F_r \tag{17}$$

The ideal distribution curve is represented in (18) and the second subplot of Figure 20, where the symbols are indicated in the first subplot of Figure 20. When RBS control distributes the brake forces to the front and rear axles according to the ideal curve at each friction coefficient, the front and rear wheels do not lock simultaneously. The vehicle handling and stability are thus maintained.

$$F_r = \frac{1}{2}\left[\frac{G}{h_g}\sqrt{b^2 + \frac{4h_g L}{G}F_f} - \left(\frac{Gb}{h_g} + 2F_f\right)\right] \tag{18}$$

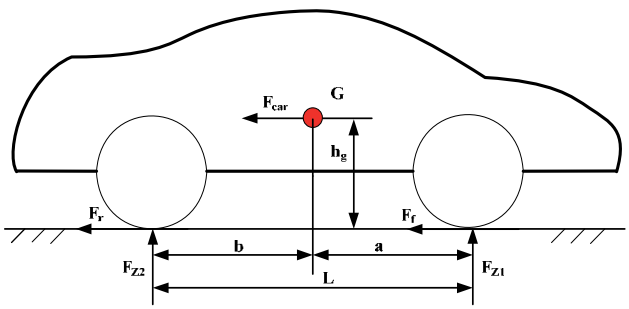

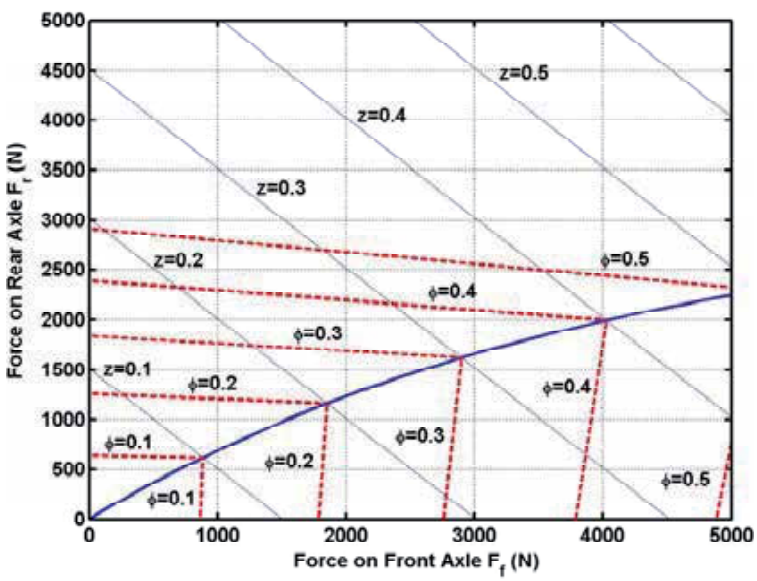

Figure 20. Vehicle braking dynamics on flat road and the ideal distribution curve

5.2.2. RBS based on Fuzzy Control (RBS-FC)

Vehicle speed and the driver's brake force command have large impacts on brake safety. The battery limitations including the battery capacity and the maximum permissible charging current protect the battery cell from damage. The capacity of the batteries is indicated with battery SOC. The maximum permissible charging current is a function of battery capacity Q, battery temperature T, battery SOC, and battery SOH, i.e., $I = f(Q, T, SOC, SOH)$. SOH is hard to determine and has little direct impact on calculating the maximum permissible charging current. Therefore, we only take SOC and battery temperature into consideration here.

The RBS-FC that uses a Takagi-Sugeno model is shown in Figure 21. There are four inputs including battery temperature, SOC, vehicle speed and driver's brake force command. The output is the regenerative brake force. The controller obtains the driver's brake force command from the pedal sensor, the vehicle speed from onboard sensor or speed estimator, and the battery SOC and temperature from the BMS. The ideal braking force distribution law gives the front brake force and the rear brake force in real time, respectively. Then, the controller determines the desired regenerative brake force according to the fuzzy rules.

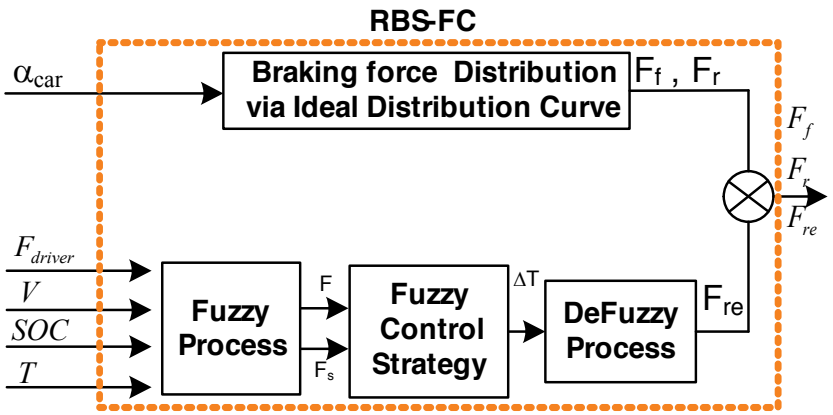

Figure 21. Structure of the control strategy system

5.2.3. Results

The proposed RBS-FC was verified in an EV prototype [22] (see Figure 22). In the test, we drove the EV on an urban road without and with RBS-FC function, respectively. The comparative results are shown in Figure 23 and Table 2, which verify that both the component efficiency and the maximum driving range are improved significantly with the proposed RBS-FC compared to the non-RBS-FC operation. The overall energy efficiency is improved from 0.341 to 0.417, i.e., an improvement of about 22%. The immediate benefit is that the maximum driving range of LF620 EV is extended from 163 kilometers to 205 kilometers for a single charge, i.e., a 26% improvement.

http://dx.doi.org/10.5772/59420

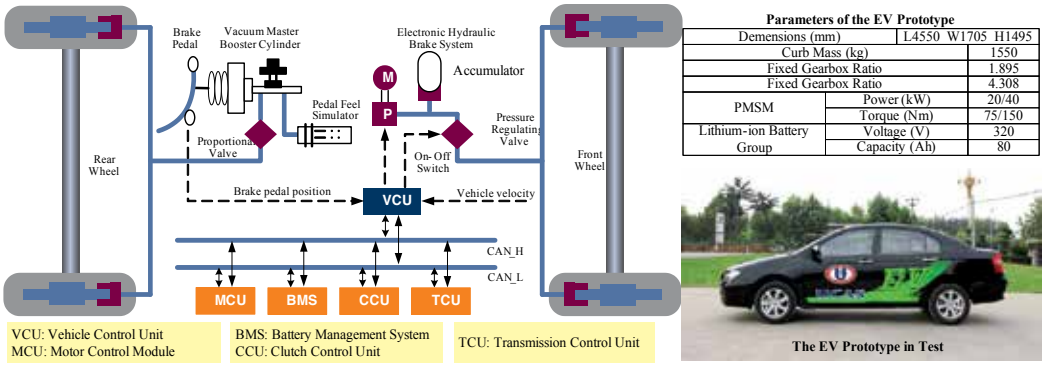

Figure 22. The test EV prototype

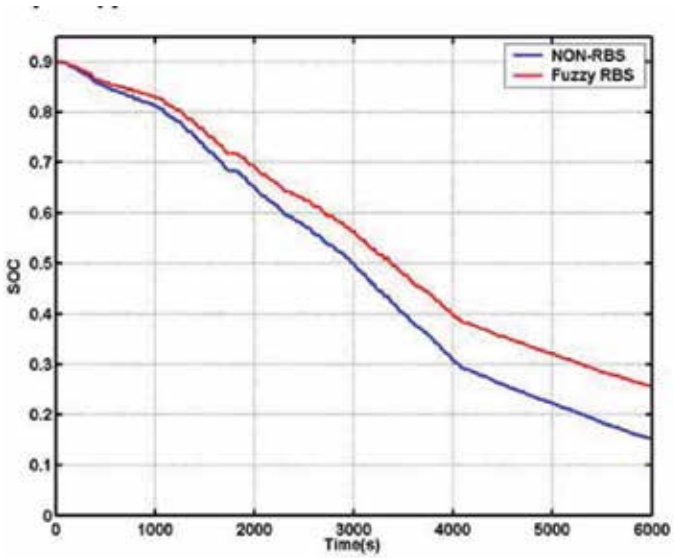

Figure 23. Comparative result of the SOC

	WITHOUT RBS-FC	WITH RBS-FC	Improvement
Motor/Controller Efficiency	0.67	0.78	16.4%
Overall Energy Efficiency	0.341	0.417	22.2%
Maximum Driving Range (km)	163	205	25.7%

Table 2. Comparison of the experimental results

6. EV energy management and optimization

6.1. Introduction of EV energy management

The energy management here is mainly targeted at the hybrid vehicles. Hybrid vehicles use two or more than two kinds of power sources, thus the energy management strategy of hybrid vehicles is one of the most important and popular research topics, as it determines the power split between power sources and because it is related to the fuel economy of the hybrid vehicles. Several types of energy management strategies for hybrid vehicles have been developed during last few decades. These strategies can be divided into two major groups: one is on the basis of the heuristic concept; the other is based on the optimal control theory. The former mainly includes rule-based algorithms and fuzzy logic algorithms [2, 34]. Earlier in the development of hybrid vehicles, energy management strategies were dominated by these types of strategies owing to their simplicity when actually realizing them. These types of strategies, however, cannot guarantee the optimal power distribution between power sources and the optimal fuel economy as well. In addition, the rules and fuzzy logics need expert knowledge. To remedy this problem, the optimal control theory was introduced as part of the energy management strategy of hybrid vehicles, including both Dynamic Programming (DP) as developed by R. E. Bellman [35] and Pontryagin's Minimum Principle (PMP) [36-38]. The DP approach examines all admissible control inputs at every state, thus guaranteeing global optimality if the driving cycle information is given in advance [35]. However, the DP approach cannot be used directly for the real-time control of hybrid vehicles due to the backward-looking calculation process and the long calculation time. Being confronted with the drawbacks of the DP, some researchers have proposed stochastic dynamic programming (SDP) [39, 40] to overcome these problems. The PMP-based energy management strategy optimizes the power distribution between power sources and minimizes the performance measure by instantaneously providing the necessary optimality conditions. One of the major advantages of the PMP-based strategy is that there is usually one parameter to be tuned in this strategy in order to obtain optimal results over a specific driving cycle [36]. Moreover, the core of this strategy is implementable in a real-time controller, even if the driving cycle information is not known in advance [37]. Furthermore, previous research [41] proved from a mathematical point of view that the PMP-based energy management strategy can serve as a global optimal solution (DP) under the assumption that the OCV and the internal resistance of a battery are independent of the battery SOC. This assumption is reasonable for charge-sustaining types of hybrid vehicles, especially for those which use lithium-ion batteries.

6.2. Energy management based on optimal control theory

In this sub-section, two types of optimal control theory-based energy management strategies of hybrid vehicles are introduced which are the DP approach and the PMP-based strategy, respectively. The simulation results regarding the two energy management strategies are also presented.

http://dx.doi.org/10.5772/59420

6.2.1. The vehicle model

An FCHV is selected as an example to introduce the two energy management strategies. Figure 24 [42] shows the block diagram of an FCHV in which an FCS and a battery are the two power sources. The electrical energy provided by the FCS and the battery is converted to the mechanical energy through the electric motor to propel the vehicle. Meanwhile, the electric motor can be controlled to work as a generator to convert a part of braking energy of the vehicle to electrical energy and store it into the battery. A group of vehicle parameters are selected by consulting the available literature [43] for the simulation study as listed in Table 3. The powertrain information is also summarized in Table 3. Details on this vehicle model can be found in the literature [42, 44, 45].

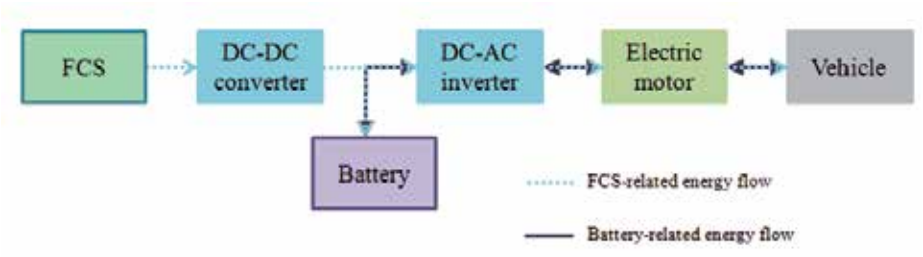

Figure 24. Configuration and energy flow of an FCHV

Parameter	Value
Vehicle total mass (kg)	1500
Final drive gear efficiency (%)	95
Tire radius (m)	0.29
Aerodynamic drag coefficient	0.37
Vehicle frontal area (m^2)	2.59
Air density (kg/m^3)	1.21
Rolling resistance coefficient	0.014
Electric motor (kW)	75
FCS (kW)	45
Battery (kWh)	1.9
Efficiency of converter and inverter (%)	95

Table 3. Vehicle parameters and powertrain information of the FCHV

6.2.2. DP approach

The DP examines all possible control inputs at every state [46]. Thus, the optimal trajectory to the final state can be obtained for every state in the DP. The DP needs much more calculation time compared to the PMP due to above characteristics.

The objective of the optimal control problem here is to find an optimal power split ratio trajectory during driving which brings the minimum fuel consumption. Here, we define the battery power P_{bat} as the control variable and the battery SOC as the state variable. The state equation of the optimal control problem expresses the dynamic behavior of the battery as shown in (19), in which Q_{bat} is the capacity and V is the open circuit voltage and R is the internal resistance of the battery.

$$\begin{aligned} \dot{SOC} &= -\frac{1}{Q_{bat}} \frac{V(SOC) - \sqrt{V(SOC)^2 - 4R(SOC) \cdot P_{bat}}}{2R(SOC)} \\ \dot{SOC} &= f(P_{bat}, SOC) \end{aligned} \tag{19}$$

Now, we rewrite (19) in a discrete form as (20):

$$x(k+1) = x(k) + \Delta t \cdot f(u, x) \qquad k = 0, 1, \cdots, N-1 \tag{20}$$

Here, x is the state variable and u is the control variable. N is the number of time steps and f is the same function as in (19).

The performance measure J to be minimized here is the total fuel consumption. Optimal performance measure from every possible state at every time step to the designated final state can be expressed as follows:

$$\begin{aligned} &J^*_{N-k,N}(x(N-k)) = \min_{u(N-k)} (\Delta t \cdot \dot{m}_{h_2}(x(N-k), u(N-k)) + J^*_{N-(k-1),N}(x(N-(k-1)))) \\ &x(N-(k-1)) = x(N-k) + \Delta t \cdot f(u(N-k), x(N-k)) \\ &k = 0, 1, \cdots, N-1 \end{aligned} \tag{21}$$

Here, $\dot{m}_{h_2}$ is the fuel consumption rate of the FCS. $J^*_{N-k,N}$ represents the optimal performance measure from $N-k$ time step to the final time step N for every possible state at $N-k$ time step. The DP examines all possible control variables at every state and selects the optimal one to every state. $J^*_{N-(k-1),N}$ represents the optimal performance measure from $N-(k-1)$ time step to the final time step N for every possible state at $N-(k-1)$ time step.

Due to the calculation characteristics of the DP, the optimal results can be acquired only when the DP calculation is finished. The results of the DP form a field which is defined as the optimal field here. The optimal field includes not only the optimal state trajectory information but also the optimal performance measure information. Figure 25 illustrates an example of the optimal field of the FTP72 urban driving cycle. Here, the initial battery SOC and final SOC are all set to 0.6, and the line on the optimal field indicates the optimal trajectory of the battery SOC.

http://dx.doi.org/10.5772/59420

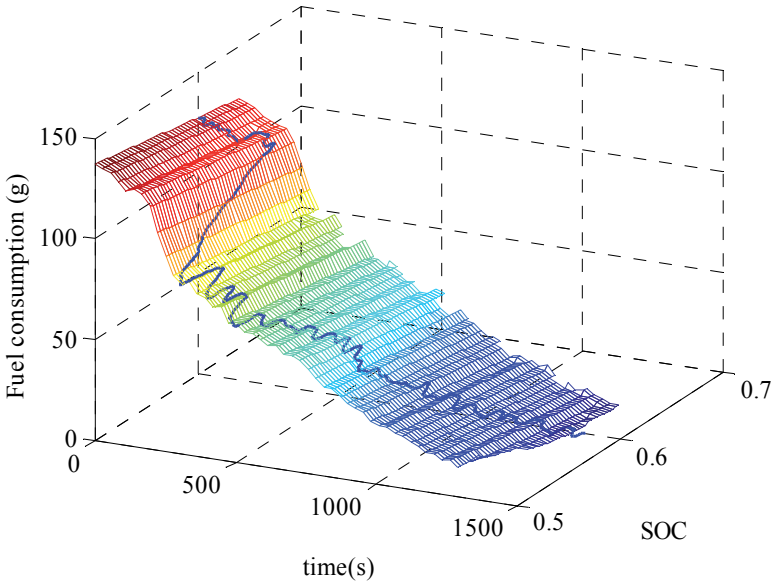

Figure 25. The optimal field of the FTP72 urban driving cycle

6.2.3. PMP-based strategy

The PMP-based energy management strategy optimizes the power distribution between the FCS and the battery instantaneously by providing the necessary optimality conditions. Here, we define the FCS net power P_{fcs} as the control variable, whereas the control variable in 5.2.2 is the battery power P_{bat}. The state equation of the control system is given in equation (19). Here, the time derivative of the battery SOC is expressed by P_{fcs} and the battery SOC instead of P_{bat} and SOC, as the total power requirement of the vehicle can be obtained when a driving cycle is given in advance. Therefore, the state equation of the optimal control problem is transformed using another function F, as follows:

$$\dot{SOC} = F(P_{fcs}, SOC) \tag{22}$$

Considering the state equation (22), which is also a constraint on the optimal control problem, and the relationship between P_{fcs} and $\dot{m}_{h_2}$, the performance measure is as follows:

$$J = \int_{t_0}^{t_f} \left\{ \dot{m}_{h_2}(P_{fcs}) + p \cdot \left(F - \dot{SOC} \right) \right\} dt \tag{23}$$

Here, p is the Lagrange multiplier, which is also defined as the co-state in the PMP and is an equivalent parameter between the fuel usage and the electric usage.

According to the optimal control theory based on the Calculus of Variation, the necessary conditions of the optimal control problem can be obtained when the variation of the performance measure δJ is zero [46]. If we introduce a Hamiltonian H, which is defined as

$$H = \dot{m}_{h_2}(P_{fcs}) + p \cdot F(P_{fcs}, SOC), \tag{24}$$

then the necessary conditions that minimize the performance measure (23) from time t_0 to time t_f are as follows:

$$\begin{aligned} \frac{\partial H}{\partial p} &= \dot{SOC} \\ \frac{\partial H}{\partial SOC} &= -\dot{p} \\ \frac{\partial H}{\partial P_{fcs}} &= 0 \end{aligned} \tag{25}$$

The first necessary condition in (25) is the state equation. The second necessary condition is the co-state equation, which determines the optimal trajectory of the co-state p. The third necessary condition determines the optimal trajectory of the control variable P_{fcs} by minimizing the Hamiltonian H.

The PMP is the general case of the Calculus of Variation, in which the third necessary condition in (25) is expressed as follows:

$$H(P_{fcs}^*, SOC^*, p^*) \le H(P_{fcs}, SOC^*, p^*) \tag{26}$$

The advantage of this form is that it can be applied to non-linear or non-differentiable or non-convex function [41].

Figure 26 [47] illustrates an example of solving the optimal solution according to the PMP. From the shape of the third subplot, it can be observed that the optimal FCS net power can be obtained at this moment, which minimizes the Hamiltonian. The similar process is repeated at every calculation time step, and the optimal solution trajectory can be obtained finally.

6.2.4. Comparison of PMP-based strategy and DP approach

Simulation results of the above two energy management strategies are compared on three typical driving cycles here. The first subplot in Figure 27 [48] illustrates the optimal battery SOC trajectories on the FTP72 urban driving cycle solved by the PMP and the DP. As we can

http://dx.doi.org/10.5772/59420

see, the two trajectories overlap each other most of the time. However, the two trajectories are not perfectly the same. Different calculation environment for each energy management strategy may have influence on this fact. The trajectories will be closer to each other if the same calculation environment is used. The second and the third subplots in Figure 27 are for the cases of the NEDC 2000 and the Japan 1015 driving cycle, respectively. Table 4 [48] shows the fuel economy comparison of the two energy management strategies. As we can see, the discrepancy between the two strategies is within 0.5 % for the three driving cycles.

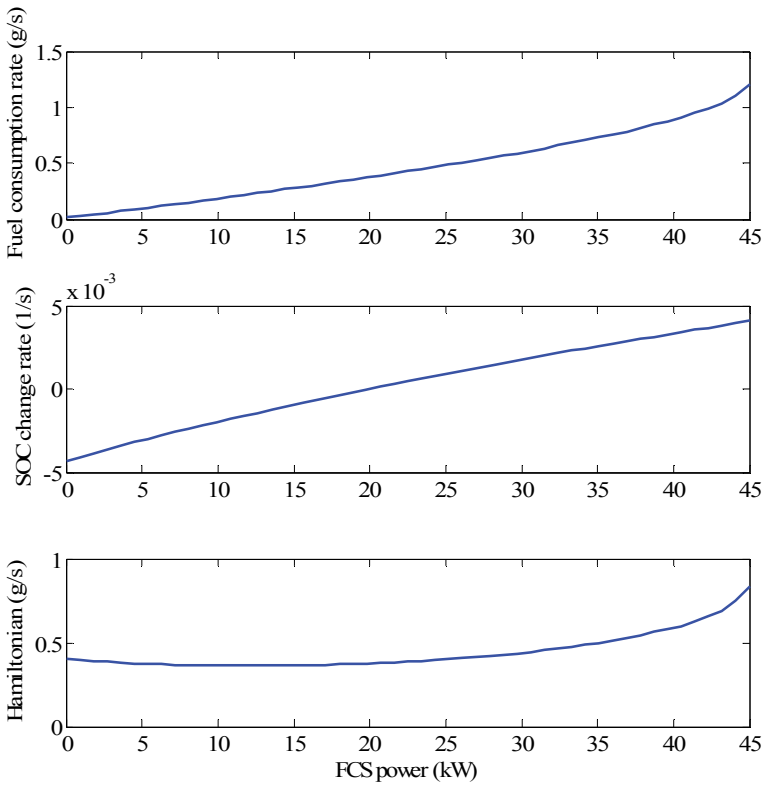

Figure 26. An example of solving the optimal FCS net power according to the PMP

	FTP72 urban	NEDC 2000	Japan 1015
DP (kg/100 km)	1.063	1.195	1.012
PMP (kg/100 km)	1.064	1.195	1.017
Discrepancy (%)	0.094	0	0.494

Table 4. Fuel economy comparison between DP and PMP

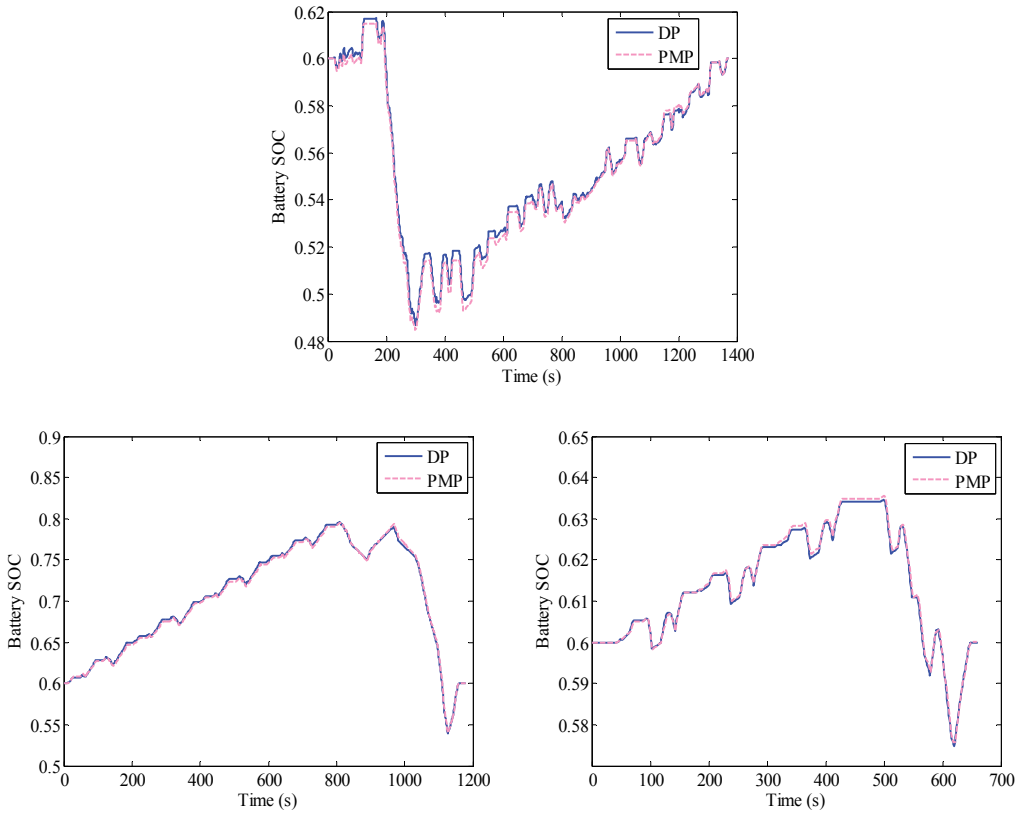

Figure 27. Comparison of DP and PMP on the optimal battery SOC trajectories

6.3. Energy management using prediction of future driving condition

In 5.2, the energy management strategies are evaluated on some specific driving cycles. However, the driving cycle is not fixed in the real-world driving. Currently, the vehicle telemetry, such as the Global Positioning System (GPS) and the Intelligent Transportation System (ITS), is actively used to vehicles in order to provide traffic preview information to the drivers. This information can be used when constructing energy management strategies of hybrid vehicles. In this section, the PMP-based energy management strategy introduced in 5.2.3 is extended in order to optimize the power distribution and as well as the vehicle driving route based on the traffic preview information.

The control objective here is to optimize the vehicle driving route and the power split ratio at the same time using the traffic preview information, so that the fuel consumption is further minimized. There are two state variables in this control problem, which are the battery SOC and the vehicle velocity v_{veh}. The two state equations are as follows:

http://dx.doi.org/10.5772/59420

$$\begin{aligned} \dot{SOC} &= f\left(SOC, P_{fcs}, v_{veh}, a_{veh}\right) \\ \dot{v}_{veh} &= a_{veh} \end{aligned} \tag{27}$$

The first equation in (27) is the dynamic behavior of the battery, and the second equation represents the vehicle dynamic behavior. Here, the FCS net power P_{fcs} and the vehicle acceleration a_{veh} are two control variables of the control problem.

Constraints on the state variables and on the control variables are as follows:

$$\begin{aligned} &SOC_{\min} \le SOC(t) \le SOC_{\max} \\ &v_{\min}(t) \le v_{veh}(t) \le v_{\max}(t) \\ &P_{fcs,\min}(t) \le P_{fcs}(t) \le P_{fcs,\max}(t) \\ &a_{\min}(t) \le a_{veh}(t) \le a_{\max}(t) \\ &\int_{t_0}^{t_f} v_{veh}(t)dt = L \end{aligned} \tag{28}$$

Here, t_0 and t_f are the initial time and final time of the preview length, and L is the preview length. L, $v_{\min}$, and $v_{\max}$ can be obtained from the GPS and ITS devices. The battery SOC constraint is time-invariant, and the maximum and minimum values of other cases are time-variant.

The application process of the PMP for the two-state variable system is similar to that for a single state variable system. According to the PMP, when a Hamiltonian is defined as follows

$$H\left(SOC, P_{fcs}, v_{veh}, a_{veh}\right) = \dot{m}_{h_2}\left(P_{fcs}\right) + p_1 \cdot f\left(SOC, P_{fcs}, v_{veh}, a_{veh}\right) + p_2 \cdot a_{veh}, \tag{29}$$

the necessary conditions that can achieve the goal of this control problem are as follows:

$$\begin{aligned} \dot{SOC}^* &= \frac{\partial H}{\partial p_1}\left(SOC^*, P_{fcs}{}^*, v_{veh}{}^*, a_{veh}{}^*\right) \\ \dot{v}_{veh}{}^* &= \frac{\partial H}{\partial p_2}\left(SOC^*, P_{fcs}{}^*, v_{veh}{}^*, a_{veh}{}^*\right) \\ \dot{p}_1{}^* &= -\frac{\partial H}{\partial SOC}\left(SOC^*, P_{fcs}{}^*, v_{veh}{}^*, a_{veh}{}^*\right) \\ \dot{p}_2{}^* &= -\frac{\partial H}{\partial v_{veh}}\left(SOC^*, P_{fcs}{}^*, v_{veh}{}^*, a_{veh}{}^*\right) \\ H\left(SOC^*, P_{fcs}{}^*, v_{veh}{}^*, a_{veh}{}^*, p_1^*, p_2^*\right) &\le H\left(SOC^*, P_{fcs}, v_{veh}{}^*, a_{veh}, p_1^*, p_2^*\right) \end{aligned} \tag{30}$$

Here, the first two necessary conditions are the two state equations, which are also constraints on the optimal control problem. p_1 and p_2 are two co-states which can be determined based on the third and the fourth necessary conditions. At every calculation time step, the optimal FCS net power and the optimal vehicle acceleration can be found by the fifth necessary condition.

Figure 28 [49] illustrates an example of simulation results. A FCHV with the total mass of 1700kg is used in this simulation. This figure shows the maximum and the minimum vehicle velocities along the preview driving which are assumed to be provided by the GPS and ITS devices. This figure also shows a benchmark vehicle velocity profile, which is within the above two velocity profiles, and the optimal vehicle velocity profile derived from the proposed energy management strategy. The length discrepancy between the optimal and the benchmark vehicle velocity profiles is around three meters here. The fuel economy is improved through the proposed energy management strategy compared to the benchmark case. In the benchmark case, the vehicle velocity profile is fixed and only the power split ratio is optimized. Table 5 [49] shows the fuel consumption information of the two vehicle velocity profiles. This table reflects that the fuel consumption is improved around 10.4 % by the proposed energy management strategy.

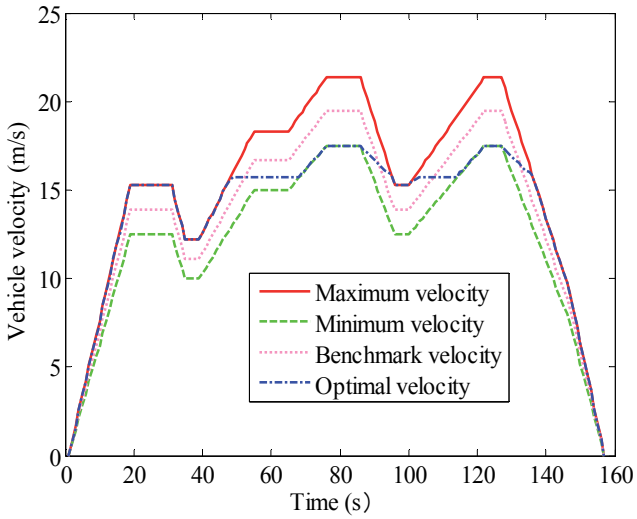

Figure 28. The optimal vehicle velocity profile and the benchmark velocity profile

	Fuel consumption (kg/100km)	Driving distance (m)
Benchmark velocity profile	1.030	2173
Optimal velocity profile	0.923	2170

Table 5. Fuel consumption of the optimal vehicle velocity profile and the benchmark velocity profile

7. Conclusions

This chapter deals with the energy processing and control of EVs. The latest energy saving and optimal control technologies are introduced and the key results contributed by the authors on the high-efficiency traction motor, intelligent battery management system, regenerative braking with high energy recovery, and the vehicle energy management are presented. The following points are drawn from this chapter:

1. For the integrated motor drive study, the integrated SRM drive obtains the battery charger and grid-connected inverter functions, whereas it saves the cost, space, and weight. The TDM method is used to improve the coefficient of utilization of the components. The suitable parking position is discussed for the stable working in the bi-directional mode. The power factor correction is considered and well worked in the integrated SRM drive.

2. For the BMS study, the proposed quantitative relationship exhibits the functions of the terminal voltage, resting time, and temperature to the initial battery SOC. This achievement raises the accuracy of the battery SOC estimation system and improves match flexibility between the battery SOC and the power output. The correlation analysis result of the energy efficiency shows that there is a parabola relationship between the energy efficiency and the DOD under the constant current rate. The battery energy conversion efficiency is less influenced by the thermal effect under the smaller current rate.

3. For the RBS study, the comparative results verify that both the component efficiency and the maximum driving range are improved significantly with the proposed RBS-FC compared to the non-RBS-FC operation. The overall energy efficiency is improved around 22%. The immediate benefit is that the maximum driving range of LF620 EV is extended from 163 kilometers to 205 kilometers for a single charge, i.e., a 26% improvement.

4. For the energy management and optimization study, the PMP-based strategy obtains almost the same optimal trajectories with the DP approach, while it saves much more computation time compared to the DP approach. The extended PMP-based strategy, which optimizes the power distribution and as well as the vehicle driving route based on the traffic preview information, improves the fuel economy around 10.4 % compared to a benchmark case studied in this chapter.

Acknowledgements

This work was supported by National Natural Science Foundation of China (Grant No. 51305437 and No. 51107142), Shenzhen Basic Research Fund (JCYJ20130401170306801, JCYJ20120617121836364, JCYJ20130401170306854), and Guangdong Innovative Research Team Program (No. 201001D0104648280).

Author details

Guoqing Xu[1,2], Chunhua Zheng[1,2*], Yanhui Zhang[1], Kun Xu[3] and Jianing Liang[1]

*Address all correspondence to: ch.zheng@siat.ac.cn

1 Automotive Electronics Research Center, Shenzhen Institutes of Advanced Technology, Chinese Academy of Sciences, Shenzhen, China

2 Department of Mechanical and Automation Engineering, The Chinese University of Hong Kong, Hong Kong, China

3 Shenzhen College of Advanced Technology, University of Chinese Academy of Sciences, Shenzhen, China

References

[1] Chan CC, Bouscayrol A, Chen K. Electric, Hybrid, and Fuel-cell Vehicles: Architectures and Modeling. IEEE Transactions on Vehicular technology 2010; 59(2) 589-598.

[2] Ehsani M, Gao Y, Emadi A. Modern Electric, Hybrid Electric, and Fuel Cell Vehicles. Boca Raton: CRC Press; 2010.

[3] Chan CC. The State of the Art of Electric, Hybrid, and Fuel Cell Vehicles. Proceeding of the IEEE 2007; 95(4) 704-718.

[4] Dyke KJ, Schofield N, Barnes M. The impact of transport electrification on electrical networks. IEEE Trans. Ind. Electron. 2010; 57(12) 3917-3926.

[5] Mapelli FL, Tarsitano D, Mauri M. Plug-in hybrid electric vehicle: modeling, prototype, realization, and inverter losses reduction analysis. IEEE Trans. Ind. Electron. 2010; 57(2) 598-607.

[6] Saber AY, Venayagamoorthy GK. Plug-in vehicles and renewable energy sources for cost and emission reductions. IEEE Trans. Ind. Electron. 2011; 58(4) 1229-1238.

[7] Wieringen V, Pop-Iliev R. Development of a dual-fuel power generation system for an extended range plug-in hybrid electric vehicle. IEEE Trans. Ind. Electron. 2010; 57(2) 641-648.

[8] Sul SK, Lee SJ. An integral battery charger for four wheel drive electric vehicle. IEEE Trans. Ind. Appl. 1995; 31(5) 1096-1099.

[9] Pellegrino G, Armando E, Guglielmi P. An integral battery charger with power factor correction for electric scooter. IEEE Trans. Pow. Electron. 2010; 25(3) 751-759.

[10] Liang J, Lee DH, Xu G, Ahn JW. Analysis of passive boost power converter for three-phase SR drive. IEEE Transactions on Industrial Electronics 2010; 57(9) 2961-2971.

[11] Chang HC, Liaw CM. Development of a compact switched-reluctance motor drive for EV propulsion with voltage-boosting and PFC charging capabilities. IEEE Transactions on Vehicular Technology 2009; 58(7) 3198-3215.

[12] Liang J, Xu G, Wang B, Wang H. A Novel Integrated Switched Reluctance Motor Drive with Bi-directional Inverter: proceedings of IEEE International Conference on Industrial Technology, 26 Feb.-1 Mar. 2014, Busan, Korea.

[13] Liang J, Xu G, Jian L, Chang M. Analysis Parking Position of Integrated Switched Reluctance Motor Drive System with On-board Charger for EV: proceedings of the 8th IEEE Vehicle Power and Propulsion Conference, 9-12, Oct. 2012, Seoul, Korea.

[14] Li JH, Barillas JK, Guenther C, Danzer MA. A Comparative Study of State of Charge Estimation Algorithms for LiFePO4 Batteries Used in Electric Vehicles. Journal of Power Sources 2013; 230 244-250.

[15] Zhang YH, Song WJ, Lin SL, Lv J, Feng ZP. A Critical Review on State of Charge of Batteries. Journal of Renewable and Sustainable Energy 2013; 5(2) 021403-1-021403-10.

[16] He HW, Zhang XW, Xiong R, Xu Y, Guo Hq. Online Model-Based Estimation of State of Charge and Open Circuit Voltage of Lithium Ion Batteries in Electric Vehicles. Energy 2012; 39(1) 310-318.

[17] He HW, Xiong R, Guo HQ. Online Estimation of Model Parameters and State-of-Charge of LiFePO4 Batteries in Electric Vehicles. Applied Energy 2012; 89(1) 413-420.

[18] Thomas KE, Bogatu C, Newman J. Measurement of the Entropy of Reaction as a Function of State of Charge in Doped and Undoped Lithium Manganese Oxide. Journal of the Electrochemical Society 2001; 148(6) A570-A575.

[19] Onda K, Kameyama H, Hanamoto T, Ito K. Experimental Study on Heat Generation Behavior of Small Lithium-Ion Secondary Batteries. Journal of the Electrochemical Society 2003; 150(3) A285-A291.

[20] Bandhauer TM, Garimella S, Fuller TF. A Critical Review of Thermal Issues in Lithium-Ion Batteries. Journal of the Electrochemical Society 2011; 158(3) R1-R25.

[21] Gao YM, Chen LP, Ehsani M. Investigation of the effectiveness of regenerative braking for EV and HEV. SAE Trans 1999; 108 3184-3190.

[22] Xu GQ, Li WM, et al. An Intelligent Regenerative Braking Strategy for Electric Vehicles. Energies 2011; 4(9) 1461-1477.

[23] Yao J, Zhong ZM, Sun ZC. A fuzzy logic based regenerative braking regulation for a fuel cell bus: proceedings of the IEEE International Conference on Vehicular Electronics and Safety, 13-15 December 2006, Beijing, China.

[24] Zolot M, Markel T, Pesaran A. Analysis of fuel cell vehicle hybridization and implications for energy storage devices: proceedings of the 4th Advanced Automotive Battery Conference, 2-4 June 2004, San Francisco, CA, USA.

[25] Yin GD, Jin XJ. Cooperative Control of Regenerative Braking and Antilock Braking for a Hybrid Electric Vehicle. Mathematical Problems in Engineering 2013; 1-9.

[26] Guo HQ, He HW, et al. A Combined Cooperative Braking Model with a Predictive Control Strategy in an Electric Vehicle. Energies 2013; 6(12) 6455-6475.

[27] Zhang CW, Bai ZF, Cao BG, Li JC. Study on regenerative braking of electric vehicle: proceedings of the 4th International Power Electronics and Motion Control Conference, 14-16 August 2004, Xi'an, China.

[28] Guo JG, Wang JP, Cao BG. Regenerative braking strategy for electric vehicles: proceeding of the 2009 IEEE Intelligent Vehicles Symposium, 3-5 June 2005, Xi'an, China.

[29] Zhang JM, Song BY, Cui SM. Fuzzy logic approach to regenerative braking system: proceedings of the International Conference on Intelligent Human-Machine Systems and Cybernetics, 26-27 August 2009, Hangzhou, China.

[30] Paterson J, Ramsay M. Electric vehicle braking by fuzzy logic control: proceedings of the IEEE Industry Applications Society Annual Meeting, 2-8 October 1993, Toronto, Canada.

[31] Ye M, Bai Z, Cao B. Robust Control for Regenerative Braking of Battery Electric Vehicle. IET Control Theory and Applications 2008; 2(12) 1105-1114.

[32] Gao HW, Gao YM, Ehsani M. A neural network based SRM drive control strategy for regenerative braking in EV and HEV: proceedings of the Electric Machines and Drives Conference, 17-20 June 2001, Cambridge, MA, USA.

[33] Mutoh, N, Hayano Y, Yahagi H, Takita K. Electric braking control methods for electric vehicles with independently driven front and rear wheels. IEEE Transactions on Industrial Electronics. 2007; 54(2) 1168-1176.

[34] Gao DW, Jin ZH, Lu QC. Energy Management Strategy Based on Fuzzy Logic for a Fuel Cell Hybrid Bus. Journal of Power Sources 2008; 185(1) 311-317.

[35] Lin CC, Peng H, Grizzle JW, Kang J. Power Management Strategy for a Parallel Hybrid Electric Truck. IEEE Transactions on Control Systems Technology 2003; 11(6) 839-849.

[36] Serrao L, Rizzoni G. Optimal control of power split for a hybrid electric refuse vehicle: proceedings of American Control Conference, 11-13 June 2008, Washington, USA.

[37] Chasse A, Sciarretta A. Supervisory Control of Hybrid Powertrains: an Experimental Benchmark of Offline Optimization and Online Energy Management. Control Engineering Practice 2011; 19(11) 1253-1265.

[38] Kim NW, Cha SW, Peng H. Optimal Equivalent Fuel Consumption for Hybrid Electric Vehicles. IEEE Transactions on Control Systems Technology 2012; 20(3) 817-825.

[39] Lin CC, Peng H, Grizzle JW. A stochastic control strategy for hybrid electric vehicles: proceedings of American Control Conference, 30 June-2 July 2004, Boston, USA.

[40] Kim MJ, Peng H. Power Management and Design Optimization of Fuel Cell/Battery Hybrid Vehicles. Journal of Power Sources 2007; 165(2) 819-832.

[41] Kim NW, Cha SW, Peng H. Optimal Control of Hybrid Electric Vehicles Based on Pontryagin's Minimum Principle. IEEE Transactions on Control Systems Technology 2011; 19(5) 1279-1287.

[42] Zheng CH, Xu GQ, Cha SW, Park YI, Lim WS. PMP-Based Power Management Strategy for Two-State Variable FCHV Systems and Its Optimality. International Journal of Precision Engineering and Manufacturing 2014; 15(4) 769-776.

[43] Bernard J, Delprat S, Buechi F, Guerra TM. Fuel-Cell Hybrid Powertrain: Toward Minimization of Hydrogen Consumption. IEEE Transactions on Vehicular Technology 2009; 58(7) 3168-3176.

[44] Zheng CH, Kim NW, Cha SW. Optimal Control in the Power Management of Fuel Cell Hybrid Vehicles. International Journal of Hydrogen Energy 2012: 37(1) 655-663.

[45] Zheng CH, Xu GQ, Park YI, Lim WS, Cha SW. Prolonging Fuel Cell Stack Lifetime Based on Pontryagin's Minimum Principle in Fuel Cell Hybrid Vehicles and Its Economic Influence Evaluation. Journal of Power Sources 2014; 15 533-544.

[46] Kirk DE. Optimal Control Theory. New York: Prentice-Hall; 1970.

[47] Zheng CH, Oh CE, Park YI, Cha SW. Fuel Economy Evaluation of Fuel Cell Hybrid Vehicles Based on Equivalent Fuel Consumption. International Journal of Hydrogen Energy 2012: 37(2) 1790-1796.

[48] Zheng CH, Park YI, Lim WS, Cha SW, Xu GQ. Comparison of PMP and DP in Fuel Cell Hybrid Vehicles. International Journal of Automotive Technology 2014: 15(1) 117-123.

[49] Zheng CH, Xu GQ, Cha SW. A power management strategy of hybrid vehicles using traffic preview information: proceedings of Vehicular Technology Conference 2014-Spring, 18-21 May 2014, Seoul, Korea.

Energy Efficiency Improvements in Smart Grid Components - Optimization in Electrical Power System

Chapter 7

Optimization of Hybrid Energy Efficiency in Electrical Power System Design

Kenneth E. Okedu, Roland Uhunmwangho,
Ngang Bassey Ngang and Richard Azubuike John

Additional information is available at the end of the chapter

http://dx.doi.org/10.5772/59017

1. Introduction

Evaluation of economic and technical feasibility of a large number of technology options, accountability for variations in technology costs and energy resource availability, could easily be carried out using the hybrid optimization model for electrical renewable (HOMER). A power system designer can use HOMER to provide an important overview that compares the cost and feasibility of different configurations and evaluate the technical performance of the power system [1]. A hybrid system is an electricity generation system, based on the integration of various energy sources (such as photo voltaics, wind turbines, small hydro power or diesel generators) [2]. Hybrid configurations can potentially deliver improved performance and better economic values for a given electrification situation [3].

Among the various energy modeling software available, the capabilities provided by the HOMER software is the best option for modeling and investigating various hybrid systems. The program first runs an hourly simulation of all possible configurations of system types. Due to the speed of processing these simulations, there is room for the evaluation of thousands of combinations. This hourly simulation also provides improved accuracy over statistical models that typically evaluate average monthly performance of a system. HOMER also models the partial load efficiency of diesel generators. This more accurately simulates the lower efficiency of a generator when it is not operating at full capacity. When the simulations have be run, HOMER sorts the feasible cases in order of increasing net present (or lifecycle) cost. This cost is the present value of the initial, component replacement, operation, maintenance, and fuel costs. HOMER lists the optimal system configuration, defined as the one with the least net present cost, for each system type. The sensitivity analysis of HOMER then repeats this optimization as user-defined factors, such as fuel price, load size, reliability requirement, and

resource quality [4, 5]. Furthermore, the HOMER analysis simplifies the task of evaluating designs of both off-grid and grid-connected power systems for a variety of applications. In designing a power system, many decisions about the configuration of the system are to be made: components to include in the system design, size of each component to use etc. The large number of technology options and the variation in technology costs and availability of energy resources make these decisions difficult [6].

In [6-8], the authors limited the use of the HOMER software to only the solar resources, while in [8, 9], an analysis was carried out proposing an optimization solution of a hybrid system of renewable energy by using the Homer software for remote areas. The Hybrid systems reported in these papers involve combination of different energy sources like wind/battery, PV/battery, wind/PV/battery, wind/PV /diesel/battery. However, various sizes of the system configurations were not taken into account and the focus was not on the best operating conditions and combination of the power systems, in terms of optimized energy efficiency. This chapter presents the use of HOMER software in the analysis of a power system comprising a wind turbine, solar photo voltaic, AC generator, converter, primary load and battery system. Various sizes of the sources were considered for all possible configurations of system types. The optimized energy efficiency based on the least net present cost was used as the basis for the selection of the best operating condition of the power system. Also, a further investigation was carried out considering two cases with two different load profiles to show that the load profiles affects the responses of the renewable energy system and the cash flow summary of some of the system equipments. In light of this, a wind turbine is integrated into the PV, battery, converter and AC diesel generator system.

2. System model considered

The model system used for this study is shown in Figure 1, where a primary load of 157kwh/d, 22kW peak is connected to the AC bus. The ENAIR 70 wind turbine type and a diesel generator (Keno) used in the study are connected to the AC bus. A converter system is in between the AC and DC bus, while the photo voltaic (PV) solar panel and battery H1500 are connected to the DC bus respectively. A brief detailed presentation of the model system parameters is given in subsequent section of this chapter. Table 1 shows some of the merits and limitations of using the HOMER software [10].

Merits	Limitations
Simulates a list of real technologies, as a catalogue of available technologies and components	Quality input data needed (sources)
Very detailed results for analysis and evaluation.	Detailed input data (and time) needed
Determines the possible combinations of a list of different technologies and its size.	An experienced criterion is needed to converge to the good solutions
It is fast to run many combinations.	HOMER will not guess key values or sizes if there are missed.

http://dx.doi.org/10.5772/59017

Merits	Limitations
Results could be helpful to learn a system configuration and optimization.	Could be time consuming and onerous

Table 1. Merits and limitations of HOMER

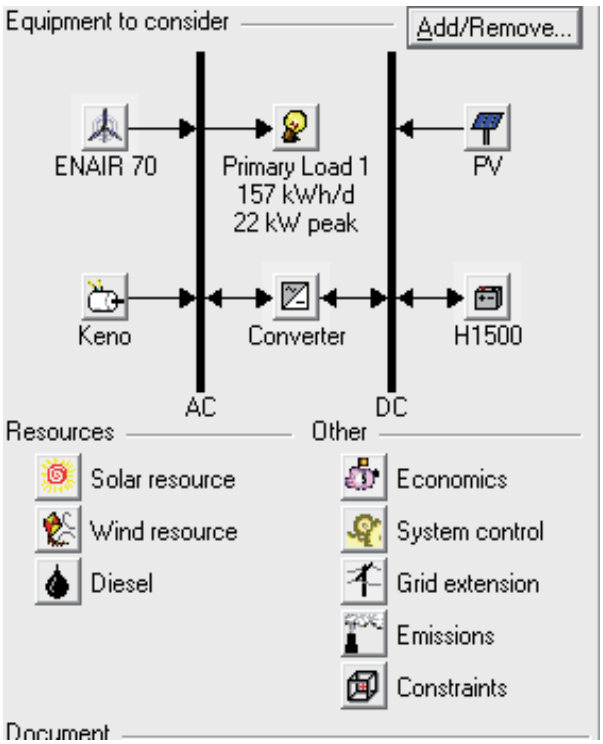

Figure 1. Model system

3. Inputs and assumptions of system model

AC load: Primary **load 1**

The load profile used for this study is shown in Figure 2, where there was a peak of 8.2kW at the early hours of the morning and dropped to 4kW until around 6am, where a slight peak of above 6kW was observed. Just before noon and after noon, the load profile slightly increased and decreased respectively and a gradual peak was observed in the evening between 6pm and about 11pm going as high as 13kW. A scaled annual average of 160, 147kWh/d, scaled peak load of 12.8, 11.7kW and a load factor of 0.522 was considered in this study as shown in Table 2.

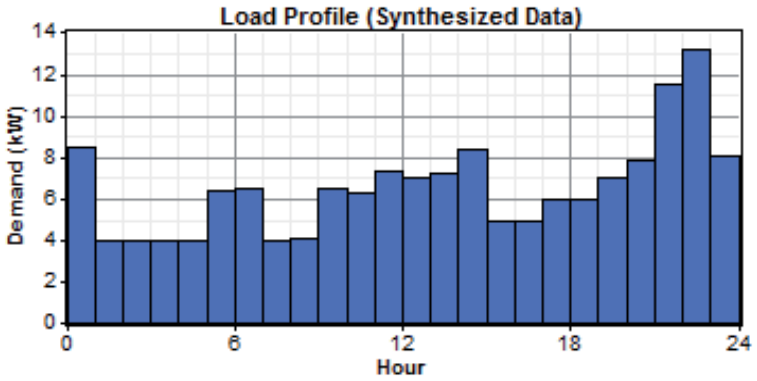

Figure 2. Load profile of study

AC Load: Primary Load 1

Data source:	Synthetic
Daily noise:	15%
Hourly noise:	20%
Scaled annual average:	157 kWh/d
Scaled peak load:	21.6 kW
Load factor:	0.303

Table 2. AC Load Parameters

PV

The detail of the PV system is shown in Table 3. A 20 year lifetime and derating factor of 80% were considered. The slopes were 14, 24 degs, with a ground reflectance of 20%.

PV

Size (kW)	Capital ($)	Replacement ($)	O&M ($/yr)
0.240	420	420	42

Sizes to consider:	21, 22, 23, 24, 25, 30, 40, 50 kW
Lifetime:	20 yr
Derating factor:	80%
Tracking system:	No Tracking
Slope:	14, 24 deg
Azimuth:	0 deg
Ground reflectance:	20%

Table 3. PV Parameters

http://dx.doi.org/10.5772/59017

Solarresource

Table 4 shows the parameters of the solar resource, where the maximum average radiation occurred in the month of April. The scaled annual average is 6.04kWh/m^2/day.

Solar Resource

Latitude: 14 degrees 0 minutes North
Longitude: 23 degrees 0 minutes West
Time zone: GMT -1:00

Data source: Synthetic

Month	Clearness Index	Average Radiation (kWh/m^2/day)
Jan	0.611	5.100
Feb	0.632	5.790
Mar	0.670	6.720
Apr	0.668	7.050
May	0.660	7.030
Jun	0.622	6.590
Jul	0.598	6.330
Aug	0.587	6.180
Sep	0.590	5.990
Oct	0.608	5.700
Nov	0.609	5.180
Dec	0.598	4.820

Scaled annual average: 6.04 kWh/m²/d

Table 4. Solar Resource Parameters

The daily radiation and clearness index of the solar resource is shown in Figure 4.

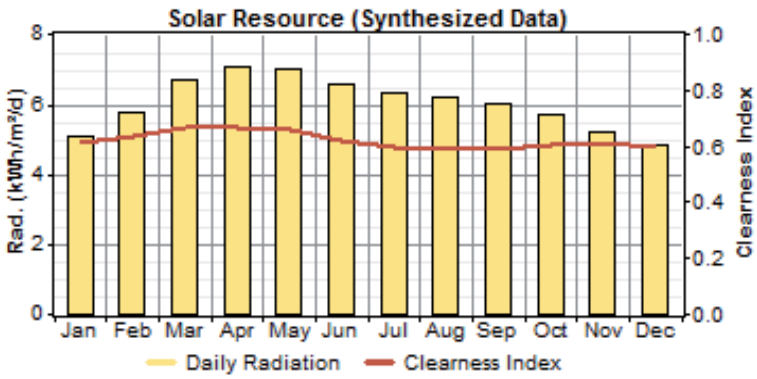

Figure 3. Solar resource radiation and clearness index

AC wind turbine**: ENAIR7**0

ENAIR wind turbine with different quantities and hub height of 15m was used in this study. The details and power curve of the wind turbine are shown in Table 5 and Figure 4 respectively.

AC Wind Turbine: ENAIR 70

Quantity	Capital ($)	Replacement ($)	O&M ($/yr)
1	16,000	16,000	160

Quantities to consider: 1, 2, 3
Lifetime: 15 yr
Hub height: 15 m

Table 5. Details AC Wind Turbine

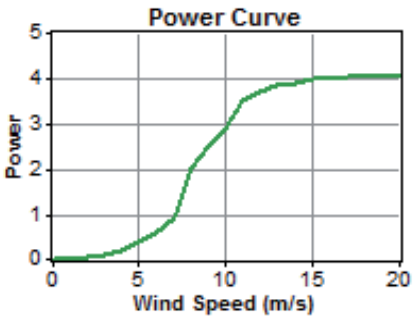

Figure 4. Power Curve of ENAIR 70 Wind Turbines

Windresource

The wind resource data used for this study is shown in Tables 6 and 7, with the peak wind speed occurring in January, while the least wind speed in August, while a plot of the wind speed for the various months is shown in Figure 5.

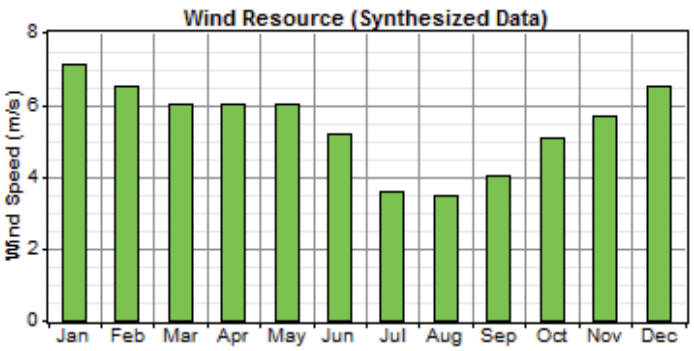

Figure 5. Wind Resource

http://dx.doi.org/10.5772/59017

Wind Resource

Data source: Synthetic

Month	Wind Speed (m/s)
Jan	7.1
Feb	6.5
Mar	6.0
Apr	6.0
May	6.0
Jun	5.2
Jul	3.6
Aug	3.5
Sep	4.0
Oct	5.1
Nov	5.7
Dec	6.5

Table 6. Wind speed distribution

Weibull k:	2.00
Autocorrelation factor:	0.850
Diurnal pattern strength:	0.250
Hour of peak wind speed:	15
Scaled annual average:	5.43 m/s
Anemometer height:	10 m
Altitude:	0 m
Wind shear profile:	Logarithmic
Surface roughness length:	0.01 m

Table 7. Details of Wind Resource

ACgenerator:Keno

The details of the AC generator details are given in Table 8, while its efficiency is shown in the simulation results.

AC Generator: Keno

Size (kW)	Capital ($)	Replacement ($)	O&M ($/hr)
36.000	6,000	6,000	2.000

Sizes to consider:	36 kW
Lifetime:	15,000 hrs
Min. load ratio:	30%
Heat recovery ratio:	0%
Fuel used:	Diesel
Fuel curve intercept:	0.08 L/hr/kW
Fuel curve slope:	0.25 L/hr/kW

Table 8. Details of AC Generator

Fuel:Diesel

The fuel details are shown in Table 9.

Fuel: Diesel

Price:	$ 1.6/L
Consumption limit:	5,000 L
Lower heating value:	43.2 MJ/kg
Density:	820 kg/m3
Carbon content:	88.0%
Sulfur content:	0.330%

Table 9. Details Fuel Type

Battery:Hoppecke12OPzS 1500

The Hoppecke 12 OPzS 1500 battery parameters used are shown in Table 10. A battery spring of 24 was considered in the study.

http://dx.doi.org/10.5772/59017

Battery: Hoppecke 12 OPzS 1500

Quantity	Capital ($)	Replacement ($)	O&M ($/yr)
1	1,369	1,369	50.00

Quantities to consider:	1, 2
Voltage:	2 V
Nominal capacity:	1,500 Ah
Lifetime throughput:	5,136 kWh

Table 10. Battery Parameters

Converter

Table 11 shows the parameters of the converter system.

Converter

Size (kW)	Capital ($)	Replacement ($)	O&M ($/yr)
15.000	5,975	5,975	50

Sizes to consider:	15 kW
Lifetime:	15 yr
Inverter efficiency:	90%
Inverter can parallel with AC generator:	Yes
Rectifier relative capacity:	100%
Rectifier efficiency:	85%

Table 11. Converter Parameters

4. Grid extension/ economics/generator control

A grid extension was compared to stand alone system to know if it is cheaper to use the grid or the stand alone system. Details of the grid extension, economics of the system and generator control are shown in Table 12.

Grid Extension

Capital cost:	$ 15,000/km
O&M cost:	$ 160/yr/km
Power price:	$ 0.134/kWh

Economics

Annual real interest rate:	6%
Project lifetime:	20 yr
Capacity shortage penalty:	$ 0/kWh
System fixed capital cost:	$ 0
System fixed O&M cost:	$ 0/yr

Generator control

Check load following:	No
Check cycle charging:	Yes
Setpoint state of charge:	80%
Allow systems with multiple generators:	Yes
Allow multiple generators to operate simultaneously:	Yes
Allow systems with generator capacity less than peak load:	Yes

Table 12. Grid Extension/Economics/Generator Control Parameters

5. Emissions/Constraints

The emissions and constraints in running the system are described in Table 13. It would be discovered that the emissions are zero due to the renewable energy level of operation.

Emissions

Carbon dioxide penalty:	$ 0/t
Carbon monoxide penalty:	$ 0/t
Unburned hydrocarbons penalty:	$ 0/t
Particulate matter penalty:	$ 0/t
Sulfur dioxide penalty:	$ 0/t
Nitrogen oxides penalty:	$ 0/t

Constraints

Maximum annual capacity shortage:	2%
Minimum renewable fraction:	0%
Operating reserve as percentage of hourly load:	10%
Operating reserve as percentage of peak load:	0%
Operating reserve as percentage of solar power output:	25%
Operating reserve as percentage of wind power output:	50%

Table 13. Emissions and Constraints of the System

http://dx.doi.org/10.5772/59017

6. Simulation results and analysis

Simulations were run in the HOMER software for various configuration system types of the power system, in order to obtain the most efficient system configuration that would give the lowest net present cost to determine the basis of energy efficiency. Figure 6 shows all the possible configurations and results that can be obtained using the various power sources.

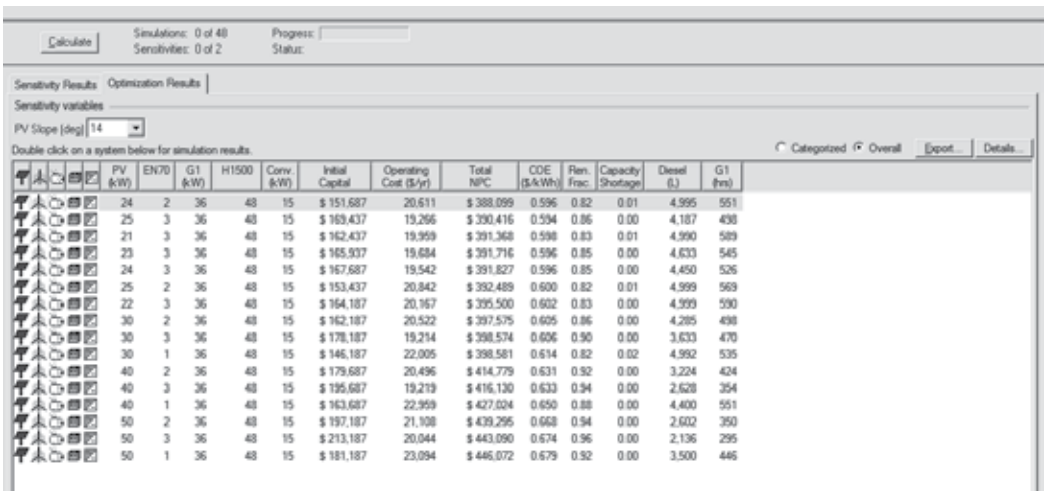

PV (kW)	EN70	G1 (kW)	H1500	Conv. (kW)	Initial Capital	Operating Cost ($/yr)	Total NPC	COE ($/kWh)	Ren. Frac.	Capacity Shortage	Diesel (L)	G1 (hrs)
24	2	36	48	15	$ 151,687	20,611	$ 388,099	0.596	0.82	0.01	4,995	551
25	3	36	48	15	$ 169,437	19,266	$ 390,416	0.594	0.86	0.00	4,187	458
21	3	36	48	15	$ 162,437	19,959	$ 391,368	0.598	0.83	0.01	4,990	589
23	3	36	48	15	$ 165,937	19,684	$ 391,716	0.596	0.85	0.00	4,633	545
24	3	36	48	15	$ 167,687	19,542	$ 391,827	0.596	0.85	0.00	4,450	526
25	2	36	48	15	$ 153,437	20,842	$ 392,489	0.600	0.82	0.01	4,999	569
22	3	36	48	15	$ 164,187	20,167	$ 395,500	0.602	0.83	0.00	4,999	590
30	2	36	48	15	$ 162,187	20,522	$ 397,575	0.605	0.86	0.00	4,285	498
30	3	36	48	15	$ 178,187	19,214	$ 398,574	0.606	0.90	0.00	3,633	470
30	1	36	48	15	$ 146,187	22,005	$ 398,581	0.614	0.82	0.02	4,992	535
40	2	36	48	15	$ 179,687	20,496	$ 414,779	0.631	0.92	0.00	3,224	424
40	3	36	48	15	$ 195,687	19,219	$ 416,130	0.633	0.94	0.00	2,628	354
40	1	36	48	15	$ 163,687	22,959	$ 427,024	0.650	0.88	0.00	4,400	551
50	2	36	48	15	$ 197,187	21,108	$ 439,295	0.668	0.94	0.00	2,602	350
50	3	36	48	15	$ 213,187	20,044	$ 443,090	0.674	0.96	0.00	2,136	295
50	1	36	48	15	$ 181,187	23,094	$ 446,072	0.679	0.92	0.00	3,500	446

Figure 6. Display of all Possible System Configuration

From Figure 6, HOMER has been able to optimize the energy efficiency of the system using various conditions, by displaying the results from the most cost effective system to the least cost effective configuration. The best solution obviously is the first array, where the most effective system of the solar panel, wind turbine, ac generator, battery and converter configuration, would use 24kW PV system, 2 wind turbines, 36kW AC generator, 48 H1500 battery system, and 15kW converter system. The initial cost of the optimized system is $151,687, with an operating cost per year of $20,611, giving a total net present cost (NPC) of $388,099 and cost of energy per kWh of 0.596 and renewable fraction of 0.82.

6.1. Details of optimized results

From Figure 6, the details of the optimized results are shown in Figures 7 to 20.

Figure 7 shows the cash flows for the system. The negative values indicate expenditures, while the positive value is the salvage value of the system in the expected life of the project. The battery state of charge is shown in the frequency histogram in Figure 8, while Figures 9 and 10 show the battery bank state of charge on an hourly basis for the various months of operation. The AC generator output is shown in Figure 11 in the course of operation, while Figure 12 displays its response of efficiency.

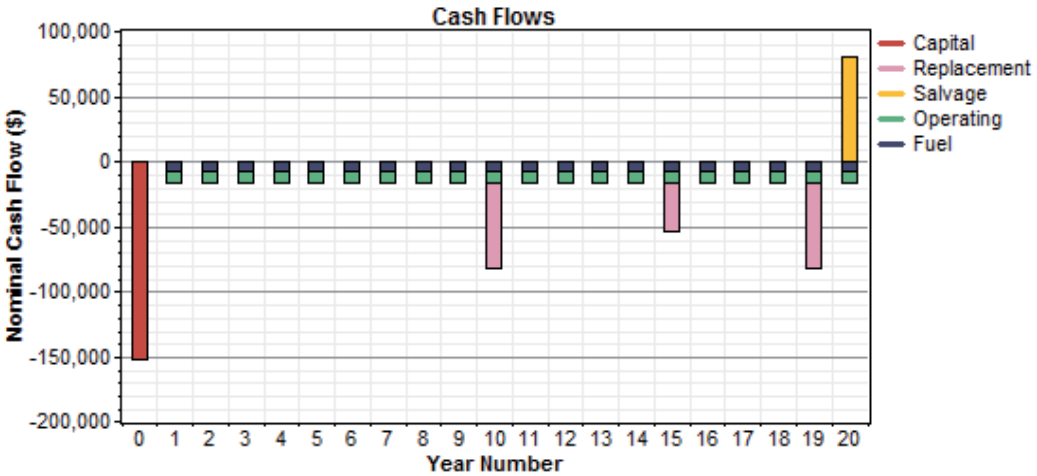

Figure 7. Cash flows

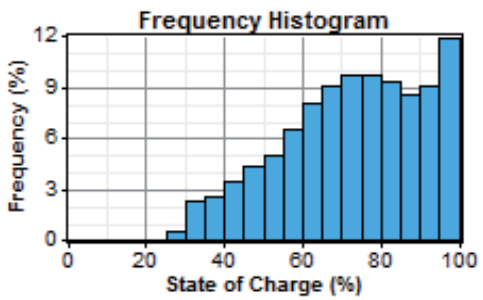

Figure 8. Battery state of charge

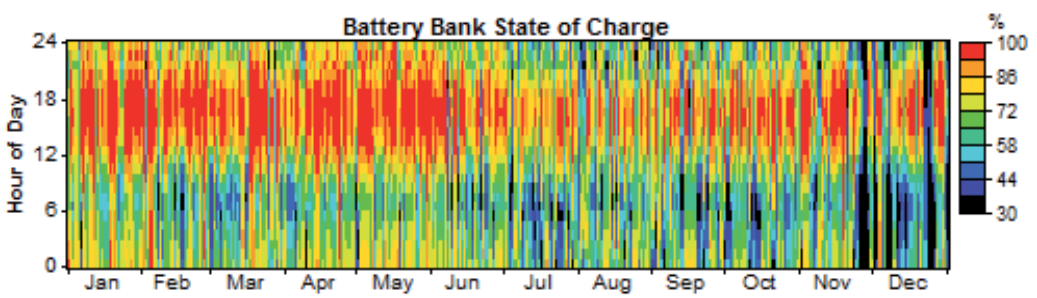

Figure 9. Battery bank SOC

http://dx.doi.org/10.5772/59017

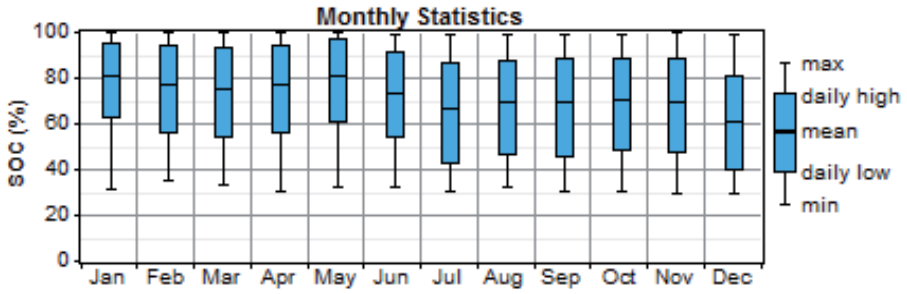

Figure 10. SOC monthly statistics

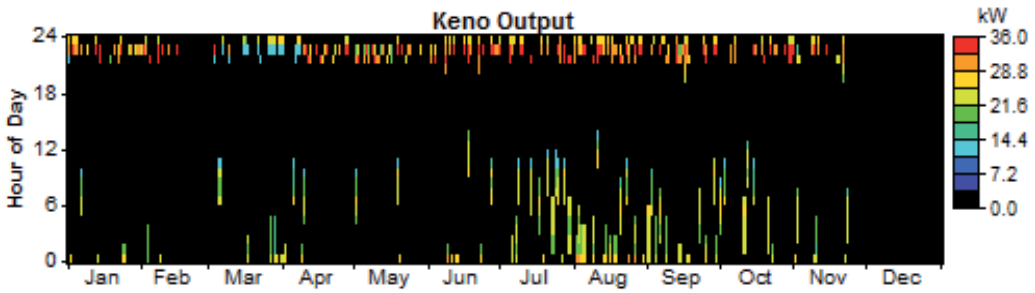

Figure 11. Generator Output

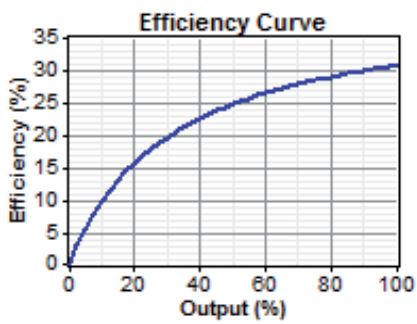

Figure 12. Efficiency curve of the generator

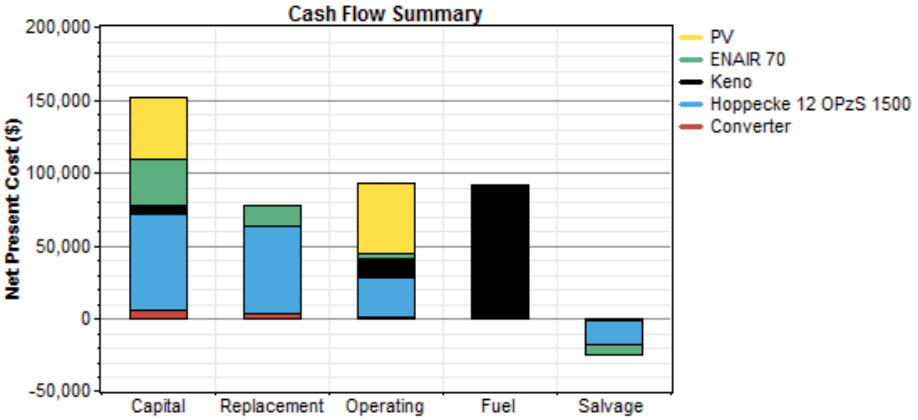

Figure 13. Cash flow summary

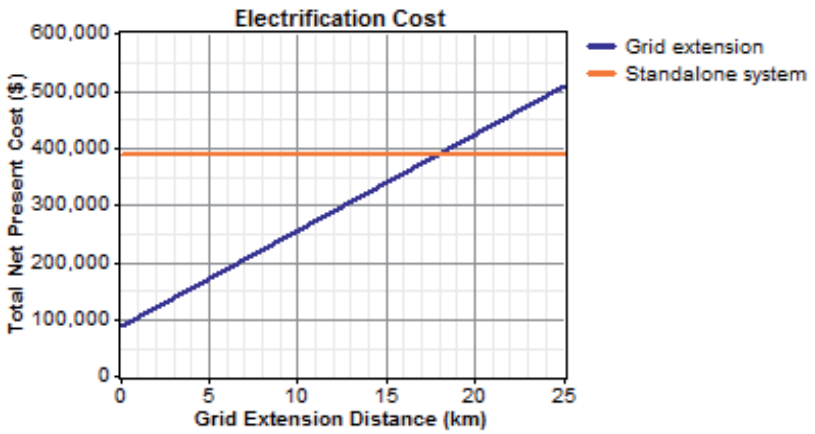

Figure 14. Grid system

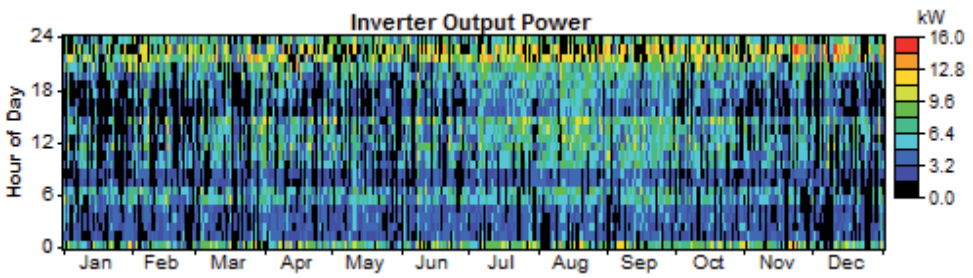

Figure 15. Inverter output power

http://dx.doi.org/10.5772/59017

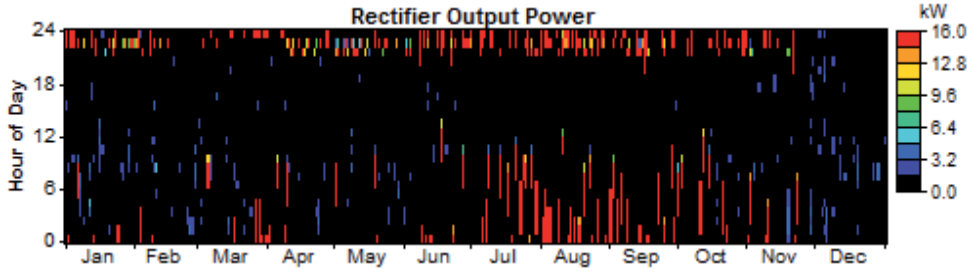

Figure 16. Rectifier output power

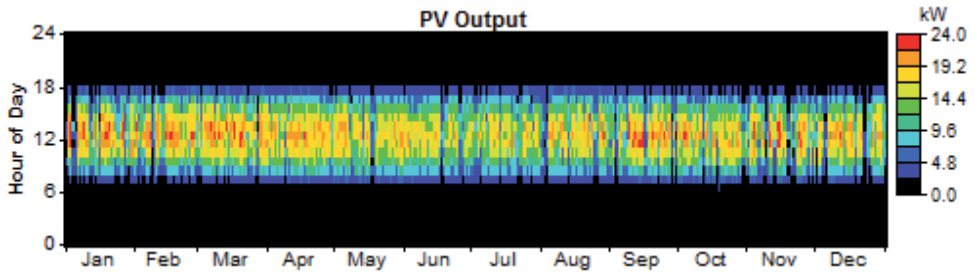

Figure 17. PV output

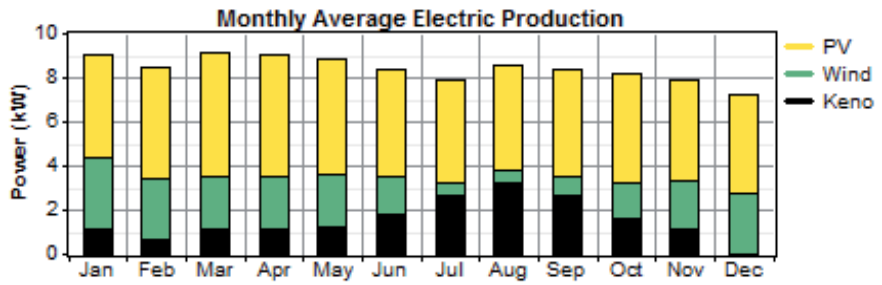

Figure 18. Monthly average electric production

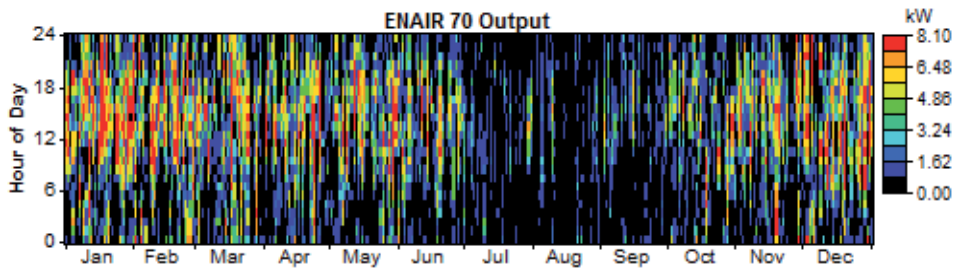

Figure 19. Wind turbine output

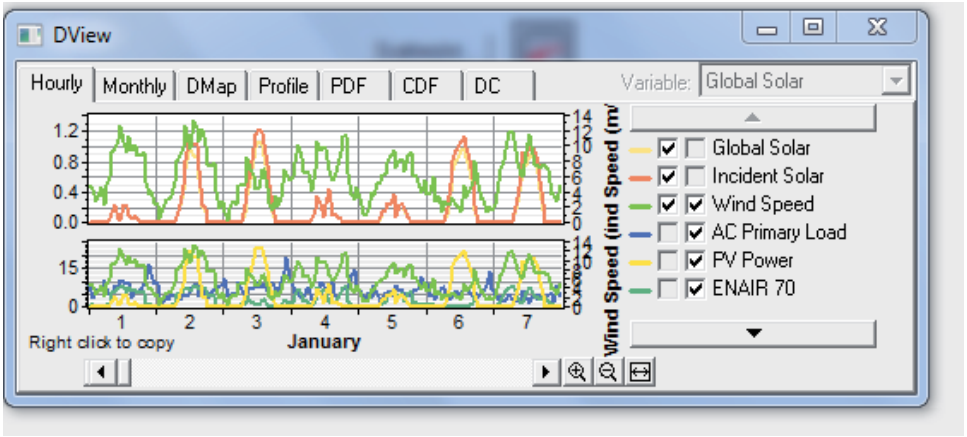

Figure 20. Hourly plot for sources for the month of January

A detailed cash flow summary of the PV, wind turbine, AC generator, converter and battery system is shown in Figure 13, with much consumption coming in from the use of the diesel fuel. Figure 14 shows the electrification cost of using the grid or stand alone system. It can be deduced from Figure 14 that the use of the grid system is more economical than the stand alone system until a grid extension distance of 17.8km, after which a break even occurs and is more economical to use the stand alone system. The inverter, rectifier and PV output are shown in Figures 15 to 17 respectively. The monthly average electric production for the wind, solar and AC generator are shown in Figure 18, with more power been produced by the PV system due to high average radiations. The wind turbine output power is shown in Figure 19, while an hourly plot DView of the wind speed, PV, wind turbine and AC primary load for the month of January is shown in Figure 20. Due to the fact that the wind speed is highest in January for the wind resource used in this study, its effect has greater impact than the other power sources for that particular month.

7. Investigating the effects of different load profiles on the system

Two cases using two load profiles shown in Figures 2 and 21 respectively were also considered with the model system shown in Figure 1. A comparison and investigation of the effects of the two load profiles on the equipments in the model system was carried out. Load profile 2 shown in Figure 21 is skewed towards the right where a maximum load of about 17kW is used towards the late hour of the evenings, while the load profile in Figure 2 is roughly and evenly distributed with a peak load of 13kW observed also in the late evenings.

From Figures 22 and 23, it is seen that the load profile has a great influence in the cash flow summary of the system. Lower load profile shown in Figure 21 requires lower capital, replacement, and operating, fuel and salvage value of the project for the PV, wind turbine, diesel and battery system as compared to higher load profile shown in Figure 2. However, the

http://dx.doi.org/10.5772/59017

cost of operating the converter system remains the same despite the variation in the load profiles.

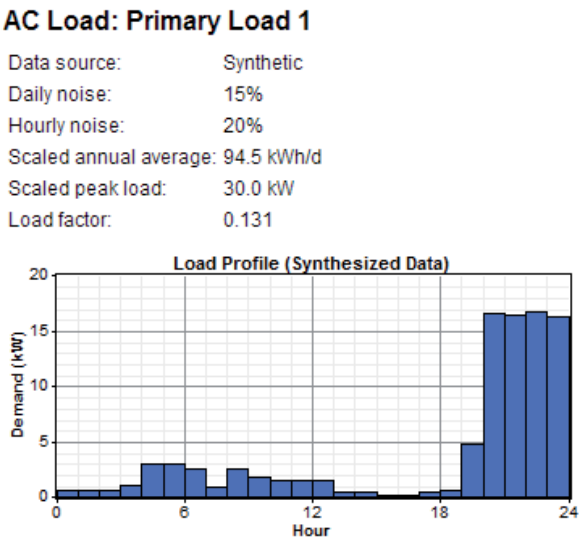

Figure 21. Load profile 2

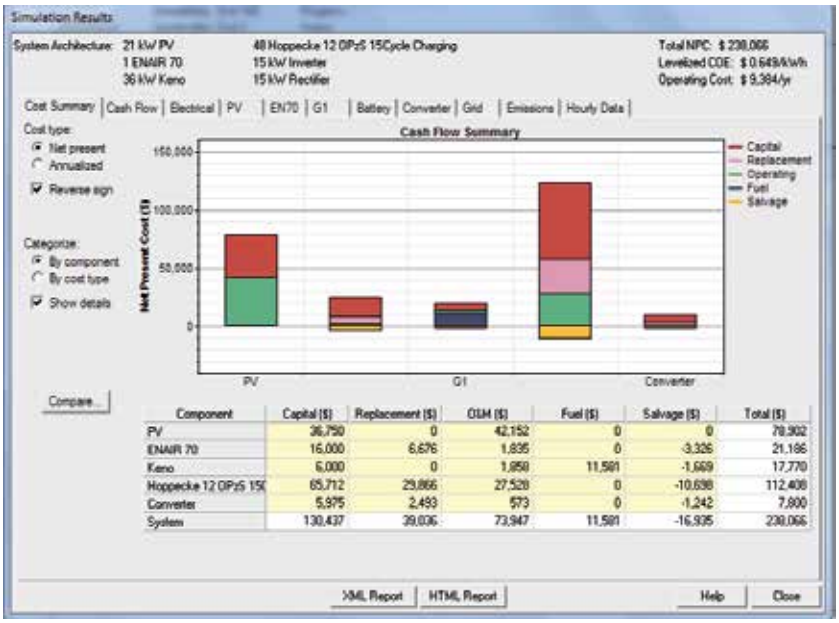

Figure 22. Cash flow summary of lower load profile

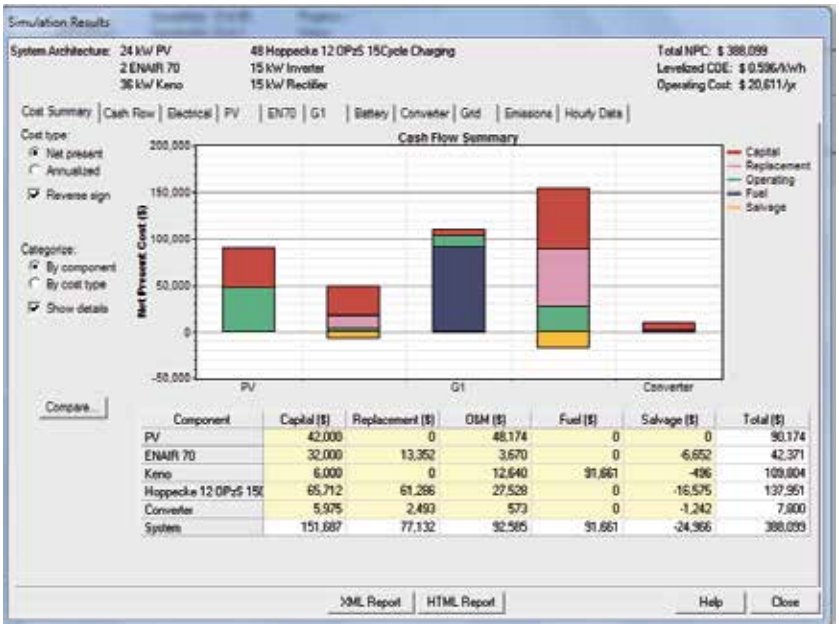

Figure 23. Cash flow summary of higher load profile

8. Levelized cost of electricity and demand side management loading scheme

The Levelized cost of electricity (LCOE) is also the levelized cost of energy (LCOE) or the levelized energy cost (LEC). It is a common metric for comparing power generating technologies as used in the model system of this study. The full life-cycle costs (fixed and variable) of a power generating technology per unit of electricity (MWh) are often called levelized costs of electricity. In contrast to the tendency of increasing energy prices for conventional power sources, like the AC diesel generator used in this study, the levelized cost of electricity of all renewable energy technologies (the PV and wind turbine) have been falling continuously for decades. This development is driven by technological innovations such as the use of less expensive and better performing materials, reduced material consumption, more-efficient production processes, increasing efficiencies as well as automated mass production of components [11, 13]. It can be defined with the following equation [10, 12, and 14].

$$LEC = \frac{\sum_{t=1}^{n} \frac{I_t + M_t + F_t}{(1+r)}}{\sum_{t=1}^{n} \frac{E_t}{(1+r)^t}} \tag{1}$$

http://dx.doi.org/10.5772/59017

Where

- LEC is the average lifetime levelized electricity generation cost
- I_t is the investment expenditures in the year t
- M_t is the operations and maintenance expenditures in the year t
- F_t is the fuel expenditures in the year t
- E_t is the electricity generation in the year t
- r is discount rate
- n is life of the system

The LCOE of this study, for the best HOMER configuration option are shown in Figure 6 with value range of $0.596/kWh to 0.679/kWh. The LCOE, as shown in Figures 22 and 23 respectively are $0.649/kWh and $0.596kWh. It could be observed that the lower load profile gives a higher LCOE, lower net present cost of $238.066, and lower operating cost of $9,384/yr compared to results obtained in the higher load profile, with higher net present cost and operating cost.

Moreover, the costs of constructing and operating a new capacity generation unit are increasing everyday as well as transmission and distribution and land issues for new generation plants. This leads to the utilities to search for another alternative without any additional constraints on customers comfort level or quality of delivered product. Demand side management (DSM) therefore encompasses load reduction strategies as well as load growth strategies and flexible energy service options. This can be defined as the selection, planning, and implementation of measures intended to have an influence on the demand or customer-side of the electric meter, either caused directly or stimulated indirectly by the utility. DSM programs are peak clipping, valley filling, load shifting, load building, energy conservation and flexible load shape [15, 16]. Considering the model system of study, with respect to the two load profile scenarios, the second load profile in Figure 21 is said to have a better demand side management compared to first load profile of Figure 2. Thus, more energy would be saved in the lower load profile, with less pressure on the renewable energy sources based on effective load or energy management system.

9. Conclusion

The use of hybrid optimization model for electrical renewable (HOMER) software has been presented in this chapter for design of a power system mainly composed of electric renewables. Hybrid Optimization Model for Electrical Renewable (HOMER), is a micro power optimization model, that simplifies the task of evaluating designs of both off-grid and grid-connected power systems for a variety of applications. The HOMER Hybrid Optimization Modeling Software is used for designing and analyzing hybrid power systems, which contain a mix of conventional generators, cogeneration, wind turbines, solar photovoltaic, batteries, fuel cells and other inputs. In order to determine the optimized system configuration that would be

more energy efficient, the net present cost was used as the basis for the selection of the best operation conditions considering a system made up of a PV, wind turbine, AC diesel generator, battery and converter systems. The lowest net present cost of the various solutions was chosen as the optimized configuration.

Also, HOMER would give idea of the best rating of the PV, the number of wind turbines, the rating of the AC diesel generator, number of battery springs, rating of the converter system, initial cost, operating cost, total net present cost, cost of energy per kWh, renewable energy fraction, capacity storage, diesel consumption in liters, and the generator hours of operation. HOMER contains a powerful optimizing function that is useful in determining the cost of the various energy project scenarios as shown in the text of this chapter. This functionality allows for minimization of cost and optimization of scenarios based on various factors.

Furthermore, a model system consisting of wind turbine, PV system, diesel ac generator, battery and converter system was investigated using different load profiles. The cash flow summary results demonstrates that increase load profile leads to more capital, operating, replacement, increase fuel, and salvage value of the project for the wind turbine, PV, diesel and battery systems. However, the converter system was found to be independent of the load profiles.

Author details

Kenneth E. Okedu[1*], Roland Uhunmwangho[1], Ngang Bassey Ngang[2] and Richard Azubuike John[3]

*Address all correspondence to: kenokedu@yahoo.com; Kenneth.okedu@uniport.edu.ng

1 Department of Electrical Engineering, College of Engineering, University of Port Harcourt, Nigeria

2 Exxon Mobil Production and Exploration Company, Nigeria

3 Jobaz Engineering Services Limited, Port Harcourt, Nigeria

References

[1] National Renewable Energy Laboratory. Energy Efficiency and Renewable Energy, USA, 2008.

[2] ECOWAS Center for Renewable Energy and Energy Efficiency (ECREEE). HOMER Software for Renewable Energy Design, 2013.

[3] ESMAP Technical Paper 121/07 Technical and Economic Assessment of Off-grid, Mini-grid and Grid Electrification Technologies. The World Bank, Washington, 2007. http://www.ecowrex.org/document/technical-and-economic-assessment-grid-mini-grid-and-grid-electrification-technologies.

[4] Givler T, and Lilienthal P. Using HOMER Software, NREL's Micro power Optimization Model, to explore the Role of Gen-sets in Small Solar Power Systems; Case Study: Sri Lanka Technical Report. National Renewable Energy Laboratory, USA, 2005.

[5] Kassam A. HOMER Software Training Guide for Renewable Energy Station Base Design. Green Power for Mobile. 2010.

[6] Alabdul Salam M. et al. Optimal sizing of photovoltaic systems using HOMER for Sohar, Oman. International Journal of Renewable Energy Research. 2013; 3(2):301 – 307.

[7] Al-Karaghouli A., Kazmerski L.L Optimization and Life-Cycle Cost of Health Clinic PV System for a Rural Area in Southern Iraq using HOMER Software. Solar Energy. 2010; 84: 710-714.

[8] Ajao K. R., Oladosu O.A and Popoola O.T. Using HOMER Power Optimization Software for Cost Benefit Analysis of Hybrid-Solar Power Generation Relative to Utility Cost in Nigeria. IJRRAS. 2011; 7(1): 96-102.

[9] Ahmed S., Hasnaoui Othman, Sallami Anis. Optimal Sizing of a Hybrid System of Renewable Energy for a Reliable Load Supply without Interruption. European Journal of Scientific Research. 2010; 45(4): 620-629.

[10] Okedu K.E and Roland Uhunmwangho. Optimization of Renewable Energy Efficiency using HOMER. International Journal of Renewable Energy Research. 2014; 4(2): 421-427.

[11] Ahmed S., Hasnaoui Othman, Sallami Anis. Optimal Sizing of a Hybrid System of Renewable Energy for a Reliable Load Supply without Interruption. European Journal of Scientific Research. 2010; 45(4): 620-629.

[12] Fraunhofer Institute for Solar Energy System (ISE). Levelized Cost of Electricity Renewable Energy Technologies. November 2013.

[13] Ueckerdt F., Hirth L., Luderer G., and Edenhofer O. System LCOE: What are the Costs of Variable Renewables. Postdam – Institute for Climate Impact Research. Germany. 2013.

[14] Ocampo M. T. How to Calculate the Levelized Cost of Energy-a Simplified Approach. Energy Technology Expert. 2009.

[15] AboGaleela M., El-Marsafaway M., and El-Sobki M. Optimal Scheme with Load Forecasting for DSM in Residential Areas. Energy and Power Engineering. 2013; 5: 889-896.

[16] Gellings C.W, Smith M.W. Integrating Demand Side Management into Utility Planning. Proceedings of the IEEE. 1989; 77(6); 908-918.

Chapter 8

Increasing Energy Efficiency by Reducing Losses and Promoting Value Propositions

Rune Gustavsson and Leif Marcusson

Additional information is available at the end of the chapter

http://dx.doi.org/10.5772/59343

1. Introduction

Energy is the base of our society and is the precondition of almost all human activities since at least a couple of centuries. Besides the benefits of energy usage we also have severe drawbacks related to negative effects on our environment. Manifested by, e.g., the climate change due to increased carbon dioxide emissions and scars and waste from coal mining and oil digging.

Energy efficiency has at least the following interpretations.

- Diminishing losses in generation, transmission and distribution of energy. It is estimated that we today have about 10% energy losses in the transmission and distribution grids of Alternating Current (AC) energy.
- Increasing performance of equipment and processes
- Increasing comfort and well being of humans

By increasing the performance of equipment we get 'more mileage' from each unit of energy. Better support tools for human activities in different areas, e.g., by smart robots, will increase the demand of energy as well as provide increased quality of work. Novel tools and techniques increase comfort and well being of humans in areas such as ´smart cities' and/or individual health-care and monitoring systems.

The following *conceptual energy triangle*, from AC technologies, supports discussions on different energy efficiency issues (Figure 1).

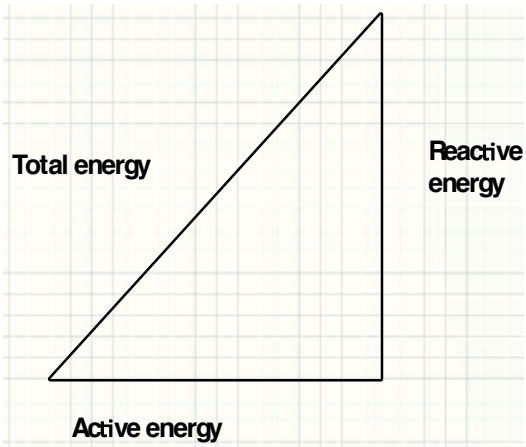

Figure 1. Conceptual energy triangle

In the case of AC generated power, *Active power* represents the power consumed by loads at customer's premises. That is, the power measured and paid for by customers. *Reactive power* is needed to continuously keep the electric balance of the power systems. Keeping this balance needs supporting equipment and real time monitoring and control provided by SCADA systems.

The following Figure 2, adopted from[1], captures the basic notations related to AC systems.

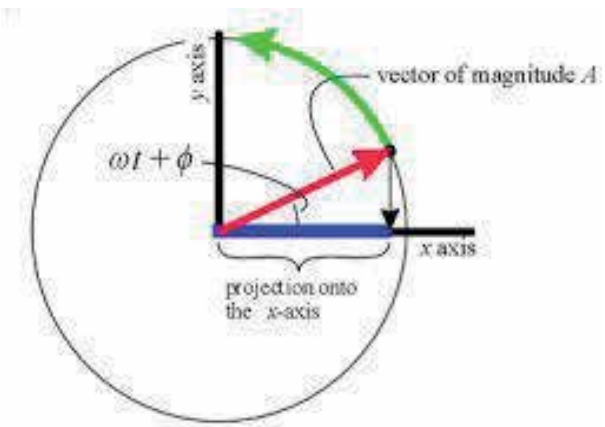

Figure 2. AC generation parameters at generators

Generators driven by an external energy source such as waterfalls typically generate AC power. The rotation in the generator causes AC generated by *interactions between magnetic and electric fields*. In Figure 2 this phenomenon is illustrated by rotations of the red total vector. Its

1 http://en.wikipedia.org/wiki/AC_power

http://dx.doi.org/10.5772/59343

projection on the x-axis is the *active power generated (KWs),* whence the projection on the y-axis is the *Reactive Energy (VARs).* The *sinusoidal waveform* of both projections have a phase angle of ($\omega t + \Phi$), where ω is the angle speed (radians/second), t denotes the time and Φ determines the Phase Factor (PF).

A sinusoidal alternating voltage applied to a *purely resistive* load results in an alternating current that is *fully in phase* ($F = 0$) with the voltage. However, in many applications it is common to also have a *reactive component* in the system, that is, due to the fact that the system possesses *capacitance*, *inductance*, or both. These electrical properties cause the current to *change phase* (Φ) with respect to the voltage: capacitance tending the current to lead the voltage in phase, and inductance to lag it.

Reactive power (measured in VARs) is present in a system containing reactive (induc-tive or capacitive) components and can be either produced or consumed by different load/generation elements. Though 'imaginary', the reactive power has great physical significance and is essential to the operation of the electrical system as a whole.

While the real power P is used to supply the energy required to perform actual work (such as running a motor), the *reactive power regulates the voltage* in the system. If the reactive power is too low, inductive loads such as transformers will be unable to maintain voltages necessary for the generation of electromagnetic fields, leading to a 'voltage collapse' that create blackouts.

Transmission line impedances also make it necessary to provide reactive power to maintain voltage levels necessary for active power to flow through. Therefore *reactive power is essential to move active power through transmission and distribution systems* to the customer. However if reactive power in a system is too high, there is *increased heat loss in transmission lines and loads as the current flowing through the system is much higher*, creating a potentially hazardous breakdown situation. The power factor (PF) of a load tells us what *fraction* of the *apparent power* (red in Figure 2) is in the form of real power and performs actual work. A high power factor is desirable since it minimizes the amount of reactive power needed by the load, reducing heat losses and maximizing efficiency (Section 2.3 and Section 5).

In the case of vehicles the *total energy* corresponds to the distance travelled whence reactive energy corresponds to energy needed to overcome different kinds of resistance (wind, road, engine) during the journey. The demand from customers to have more energy efficient vehicles has forced manufacturers to improve the efficiency by reducing the need of total energy in driving vehicles.

The customer costs are thus, as we know, different in those two cases. In the electrical power case the customer only pays for active energy, whence reactive energy has implicit costs for the end customer and is, at present, provided by grid operators. The two energy cost models; total costs versus partial cost paid by customers, have led to different focus of transport and energy system developments [Section 6].

The total cost model has led to customer driven demands of increased energy efficiency in design and maintenance of vehicles and a transport market with transparent total cost of ownership as well as clear roles of public and private stakeholders.

In AC energy systems the increased demands by authorities to include vast amounts of *Renewable Energy Sources* (RES), e.g., by wind farms or solar cells have stressed the transmission and distribution system abilities to keep the energy balance. That is, increased the costs for maintaining necessary (not billable) reactive power. The *only incentive* for customers of emerging Smart grids, however, so far is to save *active* energy.

In short, in order for future Smart grids to really take off to meet the societal expecta-tions we have to *reconsider current cost and revenue models (CMs and RMs)* to meet the emerging market demands, not the least from future customers [Section 5].

Energy as such has different interchangeable forms and sources. We focus on electricity markets, as it is arguably the most versatile form of energy.

The remainder of the chapter is organized as follows. In Section 2 *Introduction to Smart grids* we outline the motivations and approaches towards Smart grids. We specifically address challenges such as:

- Estimated increased demands of energy
- Meeting environmental challenges
- Reducing losses in power generation and distribution
- Architectural principles of Smart Grids

The *Smart Grid Architecture Model (SGAM)* supports design and implementation of different energy models. The business view of those can be analysed and modelled using the complementary *Business Model Framework eTransit* described in Section 4 *eTransit Framework*.

Key components of the eTransit framework are *Value Propositions (*VPs) and *Revenue Models and Cost Structures* (RMs). A given *Business Case* can be mapped onto the Layers of the SGAM Framework identifying *relevant stakeholders and infrastructures* to deliver the chosen services related to the selected VP. Issues related to *coordination and monitoring* of tasks and stakeholders are handled by design and implementation of *Service Level Agreements* (SLAs). Identification, design, implementation and monitoring of SLAs are addressed in Section 3 *Trustworthy Service Level Agreements*. Specific challenges are related to *interoperability*, assuring that stakeholders have a *shared understanding* of the monitored state of operations, and that *high-level business concepts are supported in real time while maintaining the energy balance* of the system. To specifically support *empowerment of customers* we are addressing issues related to *Cognitive Interaction Patterns* in Section 4.1.

We have now a necessary toolbox to address the issues raised earlier. That is, suitable Cost and Revenue models to meet future market demands of Smart grids. This challenge is the topic of Section 5 *Suitable Cost and Revenue models for future Smart grids*. We exemplify our findings by introducing:

- Power Quality markets (Section 5.1)
- Cutting losses in power distribution grids (Section 5.2)
- Smart Home services enabled by Service Level Agreements (Section 5.3)

http://dx.doi.org/10.5772/59343

The Chapter concludes with Section 6 *Conclusions and Future Work* and Section 7 *References*.

2. Introduction to smart grids

Current energy systems are under preasure of three challenges. *Firstly*, they must meet the expected increasing demands on energy globally (Section 2.1). *Secondly*, they must meet the demands of decreasing the negative effects on our environment (Section 2.2). Here we must, however, establish better models for evaluating and comparing *different approaches*. *Thirdly*, they have to be more efficient (Section 2.3). To meet those challenges the concept of *Smart grids* have been introduced (Section 2.4)

2.1. Estimated increased demands on energy

There are several prognoses of future energy demands. A recent one is provided by *U.S. Energy Information Administration* [1] In their *International Energy Outlook (IEO) 2013* the following Figure 12 is presented. According to the IEO2013 Reference case, world energy consumption has increased from 524 quadrillion (10^{15}) Btu (Brittish thermal unit) in 2010 to expected 630 quadrillion Btu in 2020 and 820 quadrillion Btu in 2040, hence a 30-year estimated increase of 56 percent. More than 85 percent of the increase in global energy demand from 2010 to 2040 occurs among the developing nations outside the *Organization for Economic Cooperation and Development* (non-OECD), driven by strong economic growth and expanding populations. In contrast, OECD member countries are, for the most part, already more mature energy consumers, with slow anticipated economic growth, and little or no anticipated population growth.

Many economic and geopolitical circumstances add considerable uncertainty to any long-term assessment of world energy markets. Currently, there is a wide variation in the economic performance of different countries and regions around the world. In the United States and Europe, short- and long-term debt issues remain largely unsolved and are key obstacles of future growth.

2.2. Meeting the environmental challenges

Governments in both Europe and the United States have implemented CO_2 emission policies of the following three types:

1. *Renewable Incentives*. Renewable initiatives are generally not available for non-carbon initiatives such as nuclear, large-scale hydro or gas combined cycles. Yet results from a recent report, below, demonstrate clearly that these three alternatives are far more cost effective per MW or capacity in reducing carbon dioxide emissions than wind or solar. In both the United States and Europe, there is, however, political opposition to all three of these alternatives on environmental and safety grounds, despite their cost-effective superiority in reducing carbon dioxide emissions

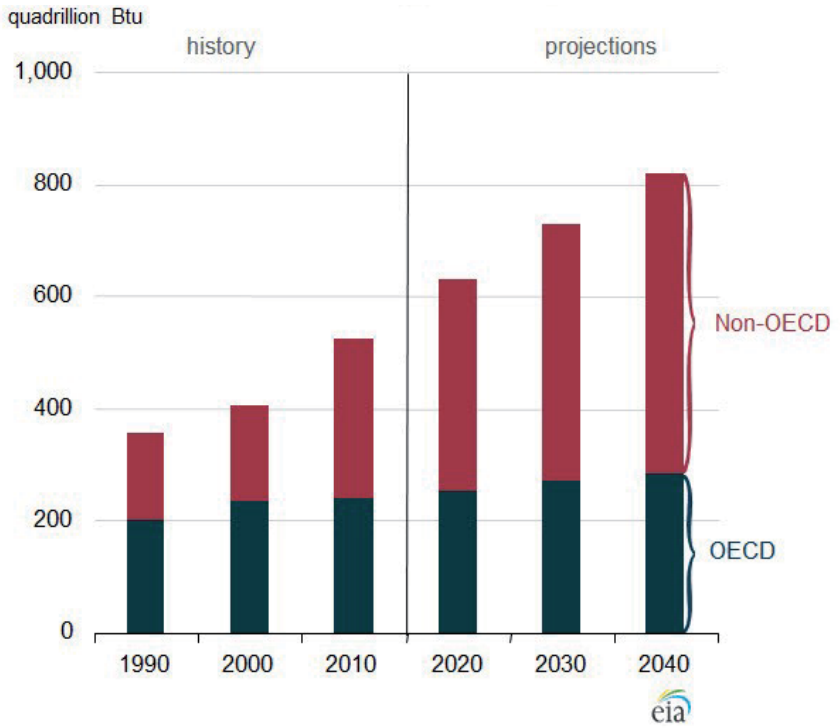

2. *Carbon Trading Systems.* There is two generally recognized methods of introducing a price for carbon dioxide emissions: (1) a *carbon tax*, or (2) a *cap-and-trade system*[2] for enforcing lower carbon dioxide emissions. The price of carbon emissions on the *European Trading System* (ETS) reached a peak of 30 euros in 2006 but was settled at 5 euros 2013. The reduction in the ETS carbon emission price, along with increases in the price of natural gas in Europe has *made coal more attractive* as an energy source

3. *Tighter Regulations*. The United States has failed to adopt a national carbon emission trading system because of political opposition in the U.S. Congress. However, the U.S. *Environmental Protection Agency* (EPA) is planning tighter regulations under the Clean Air Act of 1990. The proposed regulations would, in effect, have same of the same effects on coal-fired plants as a carbon price

It is likely to be *far less costly* to achieve reductions in carbon dioxide emissions through a effective carbon trading system that allows the market to determine the most effective way to reduce emissions rather than through establishment of EPA standards for emissions.

To address the environmental challenges we must *model and analyse* different aspects of energy production. The most common method for comparing cost of different electricity technologies is to compute the *Levelized Energy Cost* (LEC[3]). It can be defined in a single formula as:

2*http://www.edf.org/climate/how-cap-and-trade-works*

http://dx.doi.org/10.5772/59343

$$LEC = \frac{\sum_{t=1}^{n} \frac{I_t + M_t + F_t}{(1+r)^t}}{\sum_{t=1}^{n} \frac{E_t}{(1+r)^t}}$$

where;

- LEC = Average lifetime levelized electricity generation cost
- I_t = Investment expenditures in year t
- M_t = Operations and maintenance expenditures in the year t
- F_t = Fuel expenditures in year t
- E_t = Electricity generation in the year t
- r = Discount rate
- n = Life of the system

However, there are convincing arguments that levelized costs are not appropriate for *ranking technologies*. The trouble is that levelized costs do not take account of the costs of intermittency. Wind power is not generated on a calm day, nor solar power at night, so conventional power plants must be kept on standby—but the *associated costs* are not included in the levelized cost of renewables. Electricity demand also varies during the day in ways that the supply from wind and solar generation may not match, so even if renewable forms of energy have the same levelised cost as conventional ones, the value of the power they produce may be lower. In short, levelized costs are *poor at comparing different forms* of power generation.

In a recent report from Booking; *The Net Benefits of Low and No-Carbon electricity Technologies*, different approaches supporting comparisons of different forma of power generation are introduced and discussed [2]. The report examines five different low and non-carbon electricity technologies and present the net benefits of each under a range of assumptions. It estimates the costs per megawatt per year for wind, solar, hydroelectric, nuclear, and gas combined cycle electricity plants. To calculate these estimates the paper uses a methodology based on *avoided* emissions and *avoided* costs. Rather than comparing the more prevalent levelized costs.

The following three findings are reported:

1. *First* – assuming reductions in carbon emissions are valued at €50 per metric ton and the prize of natural gas €16 per million Bty or less – Finding: nuclear, hydro, and natural gas combined cycle have far more net benefits than either wind or solar. This is the case because solar and wind facilities suffer from very high capacity cost per megawatt, very low capacity factors and low reliability, which result in low avoided emissions and low avoided energy cost per dollar invested.
2. *Second*, low and non-carbon energy projects are most effective in avoiding emissions if a price for carbon is levied on fossil fuel energy suppliers. In the absence of appropriate

3 http://en.wikipedia.org/wiki/Cost_of_electricity_by_source

price for carbon, new non-carbon plants will tend to displace low-carbon as combined cycle plants rather than high-carbon coal plants and achieving only a fraction of the potential reduction in carbon emissions. The price of carbon should be high enough to make production from gas-fired plants preferable to production from coal-fired plants, both in the short term, based on relative short-term energy costs, and in the longer term, based on relative energy and capacity costs combined.

3. *Third*, direct regulation of carbon dioxide emissions of new and existing coal-fired as proposed by the U.S. Environmental Protection Agency, can have some of the same effects as a carbon price in reducing coal plant emissions, both in the short term and in the longer term as old, inefficient coal plants are retired. However, a price levied on carbon dioxide emissions is likely to be a less costly way to achieve reduction in carbon dioxide emissions.

The findings of the report is summarized in the following Figure 3 from *The Economist* July 26th – August 1st 2014, page 20.

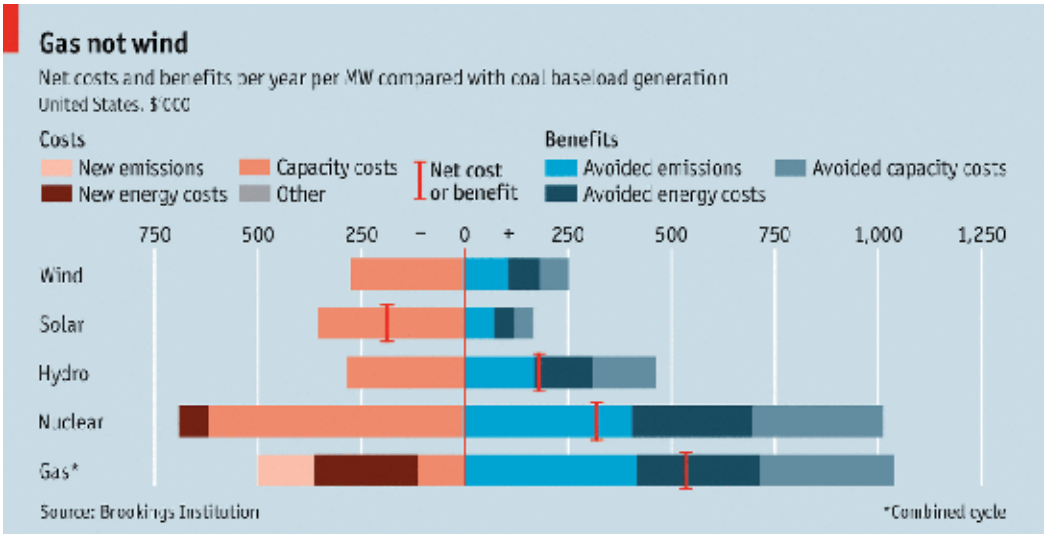

Figure 3. Cost-benefit analysis of different energy sources

If all the costs and benefits are added up using the model given in the report, solar power is by far the most expensive way of reducing carbon emissions. It costs $189,000 to replace 1MW per year of power from coal. Wind is the next most expensive. Hydropower provides a modest net benefit. But the most cost-effective zero-emission technology is nuclear power. The pattern is similar if 1MW of gas-fired capacity is displaced instead of coal. And all this assumes a carbon price of $50 a tonne. Using actual carbon prices (below $10 in Europe) makes solar and wind look even worse. The carbon price would have to rise to $185 a tonne before solar power shows a net benefit.

http://dx.doi.org/10.5772/59343

There are, of course, all sorts of reasons to choose one form of energy over another, including emissions of pollutants other than CO_2 and fear of nuclear accidents. Still, the findings have profound policy implications. At the moment, most rich countries and China subsidize solar and wind power to help stem climate change. Yet this is the most expensive way of reducing greenhouse-gas emissions. Meanwhile Germany and Japan, among others, are mothballing nuclear plants, which (in terms of carbon abatement) are cheaper. The implication of the research reported is clear: *governments should target emissions reductions from any source rather than focus on boosting certain kinds of renewable energy!*

2.3. Reducing losses in power generation and distribution

Power generated in power stations pass through large and complex networks of transformers, overhead lines, cables and other equipment before reaching the end users. It is fact that the Unit of electric energy generated by Power Station does not match with the units distributed to the consumers! Some percentage of the units is lost in the transmission and distribution networks. This difference in the generated and distributed units is known as *Transmission and Distribution (T&D) losses*[4].

- Transmission and Distribution losses, of AC systems, are not paid by users. They only pay for the received power (part of the Active energy, Figure 1).
- The Distribution sector is considered as the weakest link in the entire power sector efficiency measurement chain. Transmission Losses is approximate 17% while Distribution Losses is approximate 50% of the generated AC power.

There are two identified types of T&D losses. The losses are identified as *Technical losses* or *Non-technical losses*.

2.3.1. Technical losses[5]

The technical losses are due to energy dissipated in the conductors, equipment used for transmission Line, Transformer, sub- transmission Line and distribution Line and magnetic losses in transformers. Technical losses are normally 22.5%, and directly depend on the network characteristics and the mode of operation. The major amount of losses in a power system is in primary and secondary distribution lines. While transmission and sub-transmission lines account for only about 30% of the total losses. Therefore the primary and secondary distribution systems must be properly planned to ensure within limits. Losses are inherent to the distribution of electricity and cannot be eliminated [3].

Variable losses vary with the amount of electricity distributed and are, more precisely, proportional to the square of the current. Consequently, a 1% increase in current leads to an increase in losses of more than 1%. Between 2/3 and 3/4 of technical (or physical) losses on distribution networks are variable Losses. By increasing the cross sectional area of lines and

4*http://en.wikipedia.org/wiki/Electric_power_transmission*

5 http://electrical-engineering-portal.com/

cables for a given load, losses will fall. This leads to a direct trade-off between cost of losses and cost of capital expenditure. It has been suggested that optimal average utilization rate on a distribution network that considers the cost of losses in its design could be as low as 30 percent.

2.3.2. Main reasons for technical losses

The main reasons for technical losses are:

- Lengthy Distribution lines
- Inadequate Size of Conductors of Distribution lines
- Installation of Distribution transformers away from loads centers
- Low Power Factor (PF) of primary and secondary distribution systems
- Bad Workmanship
- Feeder Phase Current and Load Balancing

One of the easiest loss savings of the distribution system is *balancing current* along three-phase circuits. Feeder phase balancing also tends to balance voltage drop among phases giving three-phase customers less voltage unbalance. Amperage magnitude at the substation doesn't guarantee load is balanced throughout the feeder length. Feeder phase unbalance may vary during the day and with different seasons. Feeders are usually considered "balanced" when phase current magnitudes are within a specified interval. Similarly, balancing load among distribution feeders will also lower losses assuming similar conductor resistance. This may require installing additional switches between feeders to allow for appropriate load transfer.

Power Load Factor (PF) [Figure 2] has several effects on losses. Power consumption of Customer varies throughout the day and over seasons. Residential customers generally draw their highest power demand in the evening hours. Same commercial customer load generally peak in the early afternoon. Because current level (hence, load) is the primary driver in distribution power losses, keeping power consumption more level throughout the day will lower peak power loss and overall energy losses. Load variation is denoted load factor and it varies from 0 to 1. *Power and energy losses are reduced by raising the load facto*, which, evens out feeder demand variation throughout the feeder.

The load factor can be increased by offerings to customer *time-of-use rates*. Companies use similar pricing power to influence consumers to shift electric-intensive activities during off-peak times (such as, electric water and space heating, air conditioning, irrigating, and pool filter pumping).

With financial incentives, some electric customers are also allowing utilities to interrupt large electric loads remotely through radio frequency or power line carrier during periods of peak use. Utilities can try to design in higher load factors by running the same feeders through residential and commercial areas.

http://dx.doi.org/10.5772/59343

To decrease T&D losses we need to be able to optimize the grid structure dynamically. To that end we need to implement a *suitable information processing system by monitoring relevant system parameters and take appropriate actions*. This is one of the goals of future Smart grids! Obviously, in reducing losses we also improve the environmental effects of power production.

In Section 5 we give an example of reducing losses in power distribution by installing 'smart equipment' and by empowerment of customers.

2.4. Architectural principles of smart grids

Smart Grids are in focus of several international R&D past and present efforts since at least a decade. The EU *Smart Grids Technology Platform* [4] has recently published *SmartGrids SRA 2035* outlining R&D efforts to be met 2035 [5]. Smart Grids is a well-known metaphor for future power grids. However, the meaning, or semantics of the concept has, naturally, changed due to increased understanding of the inherent complexities of the subject matter.

The driving forces behind the efforts on Smart Grids include:

- Demands of increased energy efficiency to meet the 20-20-20 EU goals
- Demands of integrating new energy sources such as *Distributed Energy Sources* (DES) and *Renewable Energy Sources* (RES) in a massive way into generation and transmission grids of future energy systems.
- Establishment of a de-regulated customer oriented energy market, including new types of energy based service markets.

The transition from today's mostly hierarchical power grids towards tomorrow´s Smart Grids poses several challenges to be properly addressed and harnessed.

Among the challenges we have systems of systems requirements such as:

- Supporting information protection and security, as well as maintaining trustworthiness of services and systems by involved stakeholders in different use cases.
- Supporting interoperability and flexibility of involved systems.

Introduction of 'Smartness' of systems, such as classical power system, requires some new views and designs of systems to be implemented in a proper way. Some decades ago those systems were mainly hierarchical stovepipe hardcoded systems with SCADA systems monitoring and controlling the generation, transmission and distribution of energy. The SCADA systems enabled operators to maintaining agreed upon Quality of Service (QoS) to the sockets at customer´s premises.

A first step to allow for flexibility across and between stovepipe systems is to *decouple* hierarchical systems into open *Service- Oriented Systems* (SOS), and to introduce *open reconfigurable interfaces* between the components. That is, standard interfaces sup-ported by tools and methods to *inspect and assess data-flows* across those interfaces (Section 4.1). Those methods also allow design and implementation of *defence-in-depth* to carter for increased system- and data security [6, 7].

A second step is to *decouple and supplement* the traditional SCADA and Protection systems into SOS and to introduce *dedicated* Information Processing Systems supplementing the SCADA systems. Its purpose is to Monitor and Control information flows supporting integration of new types of energy sources and flows of business transactions. In effect, future Smart Grids will consist of three *interconnected* types of systems:

- Systems supporting *Energy management*
- Systems supporting *information management*
- Systems supporting *Business management*

The first two types of systems are specified in Figures 4 – 7. However, the related Busi-ness management systems have so far *not been explicitly specified* to the same extent. This complementary view on Smart grid has also to be in focus in order to assess specific challenges related to *market models* of The Smart grids. We introduce to that end the *eTransit Business Model Framework* in Section 4! This allows us to specifically model *user centric case models* where we can illustrate *interdependence between all three views* of Smart grids (Section 5). In short, introduction of the eTransit Framework complements the Smart Grid Architecture Models, below, in a *crucial* aspect!

Different architectures of Smart grids have been proposed. For instance the *Smart Grid Architecture Model (SGAM*) outlined in Figure 4 and Figure 5 below [8].

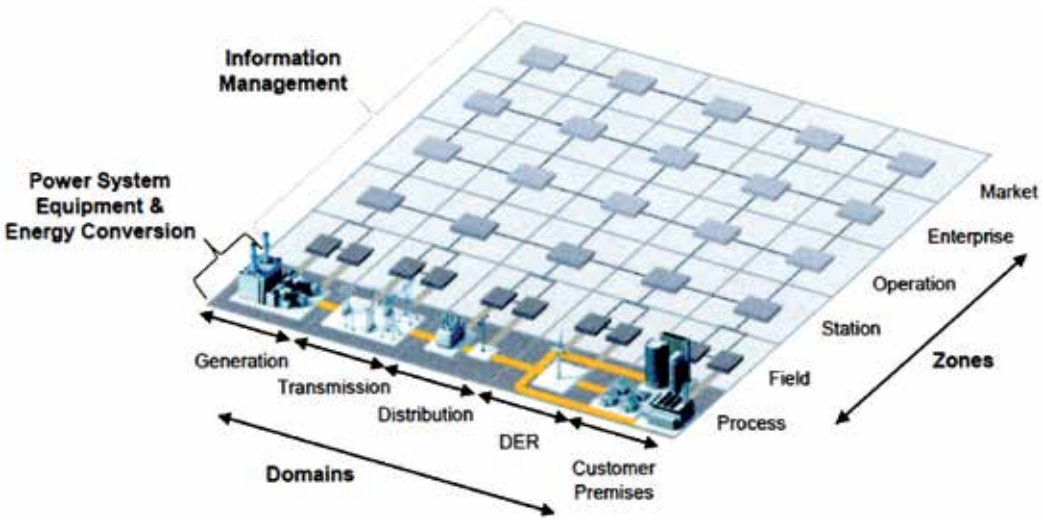

Figure 4. Smart Grid plane of SGAM

The Smart Grid plane consists of a grid with two axes of *Domains* and *Zones*. The Domain consist of components related to *Power System Equipment & Energy Conversion*, e.g., *Generation*, *Transmission* and *Distribution* as in classical power systems. However, and important *added* feature of Smart grids are the explicit components of *DER and Customer Premises*. The Zones

http://dx.doi.org/10.5772/59343

consists of the complementary axis to Domains, that is, generalizations of the classical components *Processes*, *Field*, *Station*, *Operation* complemented with *Enterprise* and *Market*.

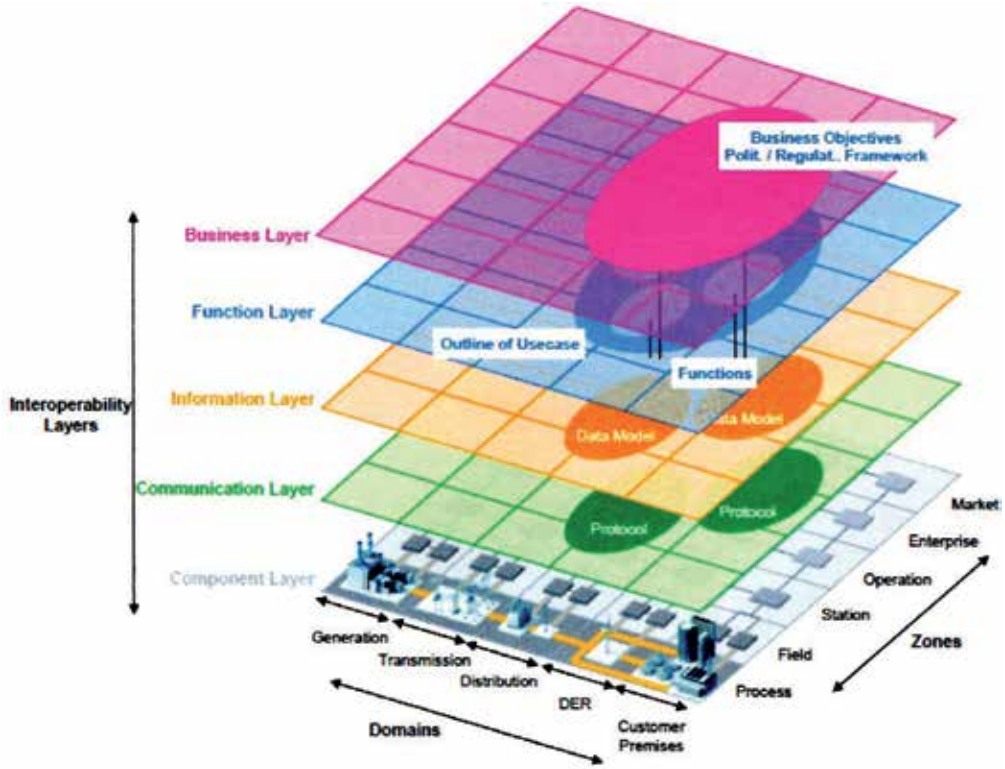

Figure 5. Layers of SGAM framework

The purpose of this Smart Grid plane is to implement and support the related *Information Management* of the individual and integrated three Infrastructures of Smart grids mentioned above. In order to carter for this very complex task we need to introduce a third axis, vertical and above, the Smart Grid plane. This axis of *Interoperability layers* is depicted in Figure 5, above.

The Interoperability layers are from bottom to top: *Component*, *Communication*, *Information*, *Function*, and *Business* layers. In Figure 5 we also have depicted a *projection from a Business Case* with stated objective down onto the SGAM framework cube.

In order to proper address issues related to Interoperability, the *Interoperability Framework* proposed by *GridWise Architecture Council*, (Figure 6), is incorporated in SGAM.

Interoperability issues are treated in some detail in Section 5.3 *Smart Home Services enabled by Service Level Agreements.*

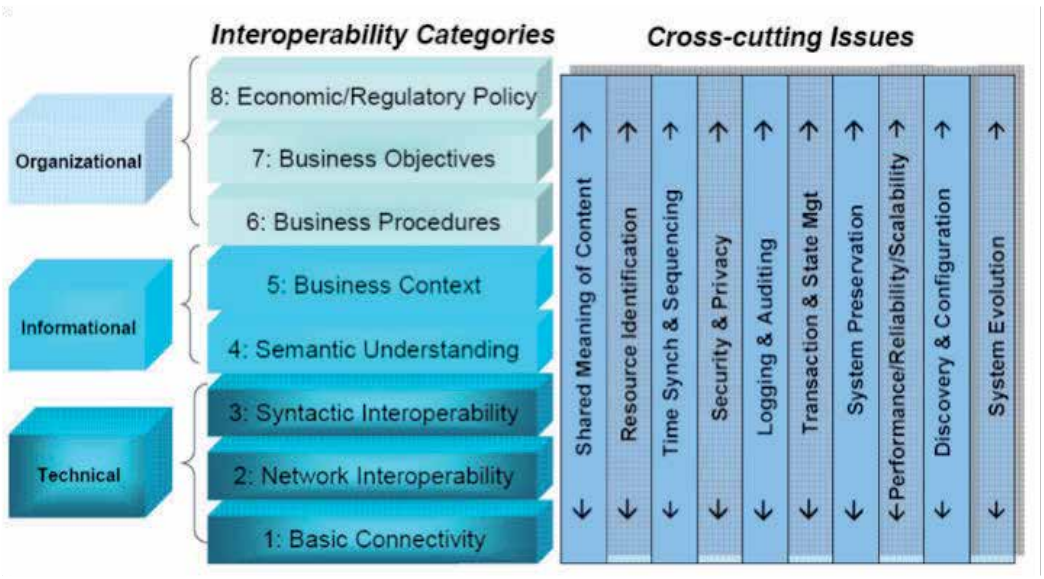

Figure 6. GWAC Interoperability Framework with a layered set of Categories and non-functional Cross-cutting Issues

In a classical power system the relevant Doman Component were *hierarchically integrated* with relevant zones into a *closed system* delivering and billing power to the customer according to relevant regulations and tariffs. The customers were just loads or ´two holes in the wall´. The necessary monitoring, control, and billing were supported by SCADA systems.

Transitions towards flexible and resilient Smart grids pose several basically hitherto unknown challenges. We know that power system engineering has been very successful during the last century in designing and maintaining the most complex human engineered infrastructures worldwide today. However, from Figure 5 and Figure 6 we can infer that this well renowned competence has to be *suitable complemented* with other competencies to meet the new challenges. Candidates include areas of computation and information sciences as well as competencies from economics and behavioral sciences and from psychological insights (Section 4.1).

Furthermore, to meet the societal demands we have to develop *suitable roadmaps* guiding political decisions related to procurement and evaluation towards understanding of relevant *socio-technical-economic* issues [5].

An illustrative example is the current focus of exploring RES to lower the CO_2 emissions causing the expected global warming. As we know those efforts are heavily subsided by governments worldwide. However, *the economic and environmental end results of those efforts are still not sufficiently understood and need more modeling and analysis* (Section 2.2).

http://dx.doi.org/10.5772/59343

In this chapter we focus on *Empowerment of customers* as a mean to increase energy efficiency in Smart grids as well as promoting environment protection. We know that introduction of massive amounts of DER and RES, e.g., by wind farms, will demand complementing by reactive power to keep the needed energy balance of AC systems. At the moment R&D efforts on RES and DER are heavily subsidized in several countries. This might lead to unsustainable market in the near future. To that end, there are ongoing discussions to implement some full-cost services in *Ancillary Service Markets* on:

- Operation Reserve
- Frequency Control
- Reactive Power and Voltage Control
- Short – Circuit Capacity
- Voltage Quality
- Black-Start
- Island Operation of the Grid
- Inertia
- Stability

Those markets are necessary to address, for instance, reducing losses in power generation and distribution (Section 2.3) and will be further discussed in Section 5.

Empowerment of customers might also support new *energy based services* that will increase several kinds of Energy efficiency aspects mentioned above (Section 6).

3. Trustworthy service level agreements

Present power systems have a straightforward business model. The generation and distribution is in accordance with rules and *regulations set up and monitored by regulators*. The customers sign standardized documents and are billed based on the KWh consumption measured by meters installed at customer site and owned by a distributor. In liberated markets the bills *separates the costs into two parts* for (active) energy and for the corresponding use of network (net tariffs). The customer can choose between different energy providers and/or price incentives aiming at matching the supply/demands at peak hours (Section 2.3). The customers can also be compensated according to fixed rules in case of, for instance, blackouts.

Obviously, this simple business model cannot meet the requirements of future Smart grids! The standardized contract has to be replaced with a more flexible and market oriented concept.

We will, to that end, identify and establish a *Trustworthy Service Level Agreement* (SLA) based on a *selected Use Case* (UC) at the Business Layer in Figure 5.

Projections of a selected use cases onto lower Layers of SGAM (Figure 5) will determine:

- Relevant *stakeholders* and their concerns related to the chosen use case
- Identification of *Key Performance Indicators* (KPIs) to be monitored
- Identification of relevant functions (*business services*) at the Function layer
- Identification of supporting *information models* and *information exchange mechanisms* at the Information Layer
- Selecting relevant *communication systems and protocols* at the Communication Layer
- *Connecting and interfacing* the communication layer with selected components from the Component Layer

This process will design a business case as a *set of information processing boxes* from the Function-, Information-, and Communication Layers connecting the Use Case with components from the Component Layer. The information processing boxes (*information services*) have to be implemented and loosely coupled, to allow inspection and re-use, into a reliable information system that meet *Interoperability* (semantic) requirements as well as trustworthiness requirements from stakeholders in the use case.

The purpose of a SLA is to *coordinate and monitor* the business services and information services to meet the agreed upon requirements of the use case. We have proposed a validated methodology to negotiate and establish suitable SLAS for Smart grids [9].

From the analysis above it follows that a use case can be modeled as a *set of vertical and horizontal workflows* (*business channels*) built from *chains of services* and *connecting components* from the Component Layer *with stakeholders* at the Business Layer (Section 5). To support analysis and modeling of the relevant *flexible* information systems we need a set of *meta models* as those defined by the eTransit Framework in the next section, Section 4.

The following Figure 7 captures the contexts of SLAs. The design and implementation of SLAs are based on *Drivers and opportunities* formulated as *requirements* related to Use cases. Those requirements have to be *matched against affordances* from the infrastructures.

A *challenge is to match the high-level business requirements with low-level affordances*. Specifically *real time* constraints related to energy management sub-systems with *high-level business concepts*. To that end we have suggested a *layered structure* of the SLAs as bundles of sub-SLAs. The high-level SLAs are *coordinated, via message exchanges*, with low-lever SLAs at the Information Layer of Figure 5. Some technological challenges are further discussed below (Section 5.3).

In present power systems the ICT system is mainly the SCADA system monitoring and controlling production and distribution of power. The SCADA system *integrates information from the component Domain with the Operation Zone for monitoring and contro*l. The operators react on information given to them with control signals down the zones. Since the use case at the business layer is a point – *a fixed contractö* between customer and distributor - we do not have to consider specific business information at the operator level. Use cases where we really need more complex SLAs are further discussed in Section 5.

http://dx.doi.org/10.5772/59343

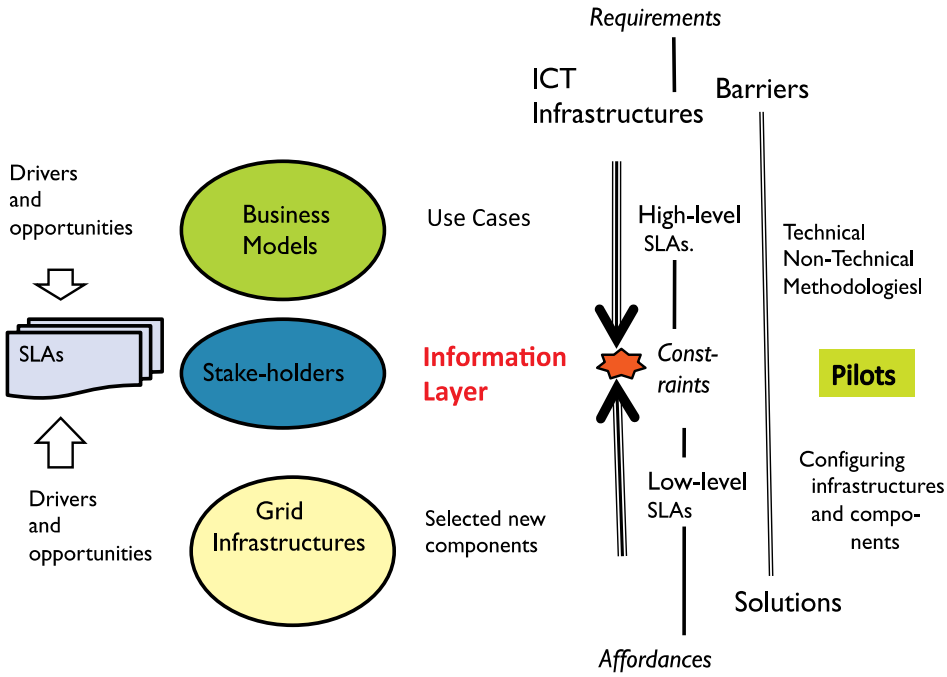

Figure 7. SLA context as coordination of bundles of high-level and low-level SLAs

4. eTransit business model framework

From Section 2.4 we have seen that Smart grids can be modeled as *three* interconnected types of systems. The Energy management and Information management systems are the focus of SGAM frameworks Figures 4 – 6. To *complement* those views with a focus on *Business management* we suggest add to those these models the *eTransit Business Model Framework*. This framework was a result of the eTransit project in Sweden and Finland 2013-14 [10].

The focus of the eTransit project was to investigate the effects on the business processes of the rapidly expanding e-Commerce sector, specifically the role of mobile access points and its mutual dependencies with more traditional points of sale. A specific focus of the project was to investigate drivers and obstacle related to *transitions* between different business channels. To support those investigations we proposed the following eTransit Framework (Figure 8).

The eTransit Framework identifies a set, the *eTransit Views*, of useful aspects on Business Models (BMs). The Framework, with associated Methodology, is supporting *Requirements Engineering*, *Design*, *Implementations* and *Validation of* Business support systems. The *usefulness and adequacy* of the model was validated in the project as well. Since the Business management view of Smart grids, addressing energy based markets and empowerment of customers, is important, we suggest that the eTransit framework is a natural and necessary complement to the other two views of Smart grids given by SGAM (Section 2.4).

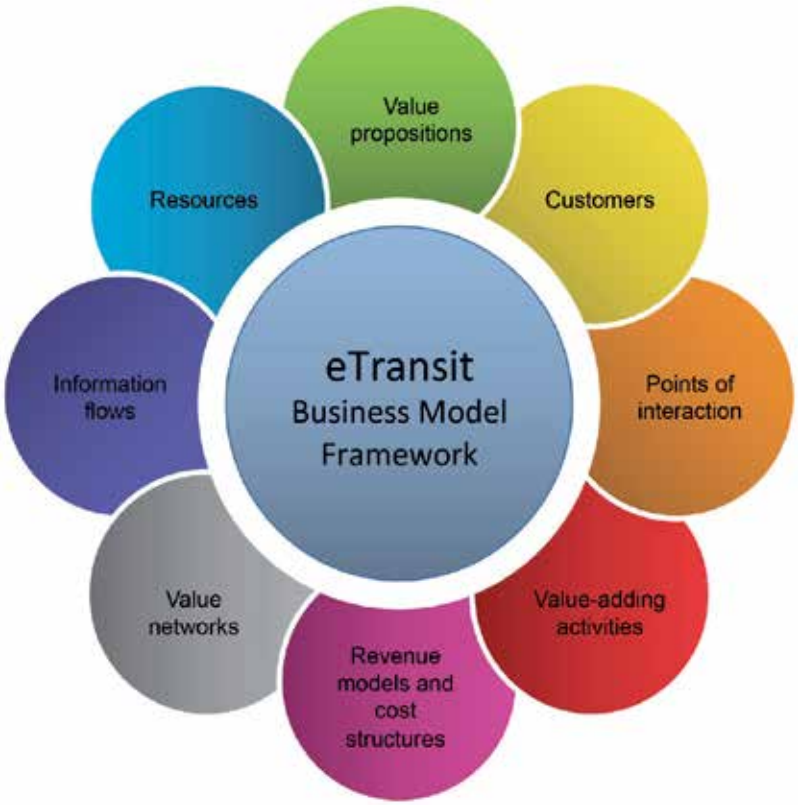

Figure 8. The eTransit Busness Model Framework

The Framework is an extension of BMs put forward by *Place to Space* [11], *Canvas*[6] and *Visor*[7], to allow a deeper investigation and modeling of transitions between different *business channels, or implemented workflows. Viewpoints* of the Framework are:

- Value Propositions
- Revenue models and cost structures
- Value network
- Value adding activities
- Information flows
- Resources
- Points of Interaction
- Customers

6*http://www.businessmodelgeneration.com/canvas*

http://dx.doi.org/10.5772/59343

In our supplementary methodology we *configure* a selection of the eight different viewpoints into a solution of a given use case. This configuration constitutes *design and implementation of the corresponding SLA* of previous section.

The starting subset of eTransit supporting our specification of SLAs is (Section 3 and Section 5) is:

- *Value proposition* (VP): A package of a solution and a product / service offered to a specific customer segment of a use case
- *Revenue Model* (RM): Sources of revenue for a VP
- *Points of Interaction* (PI): Workflows related to a VP are implemented as different *channels* with information check points at PIs (Figure 9)
- *Resources* (Rs): Critical tools for a company in order to create and deliver its VP

The workflows are determined by the SLA of the use case. A workflow is a *chain of service*s connected at PIs (Figure 9). The corresponding *information flow* has *inspection points* at PIs that are monitored and controlled by the SLA. Information related to *revenue models and cost structures,* of each workflow, is *collected for each stakeholder* of the SLA at the PIs.

We have suggested *separating the design and implementation of workflows in channels* (Figure 9), by using the identified BM models as *meta-models* for the channels. Specific *implementation models* for each channel are refinements of those meta-models meeting specific requirements for the selected channel (Figure 5 – 7). This allows *reuse and reconfigurations* of workflows in *different channels* with *invariant* meta-models (Figure 9). In short, it allows *cost efficient and reliable management and change of business channels*.

The starting points for design and implementation of SLAs are:

- *Identification from the use case* the related Value Proposition (VP), Revenue Models (RM), and Customer views (C)
- *Identification of* Value Network (VN) and Resources (R)
- *Identification of Information flow*s (IFs), workflows (WFs) and Points of Interaction (PIs)

Key issues related to the translation of meta-models onto suitable implementation models include (Figure 6 and Figure 7):

- *Identification of suitable goal architectures* supporting flexible use
- *Identification of suitable sets of protocols* to support implementation, testing and validation
- *Agreements* on suitable *Key Performance Indicators* (KPIs) to be monitored
- *Selection* of suitable protocols and inspection methods at PIs to ensure *interoperability* and *trustworthiness* (Figure 9 and Figure 10)
- Selection of proper services to be trustworthy outsourced, e.g., payment services

7*http://classic.marshall.usc.edu/ctm/research/visor-business-model.htm*

The methodology has to be refined and tested but is based on similar methodologies supporting implementations of *Service Oriented Systems (*SOS) such as *Multi Agent Systems* (MAS) [6].

It is important to note that the identification of a VP, together with Revenue Models and Cost Structures, will provide a 'skeleton model' as a starting point. It should also be noted that *payment solutions* and the *roles and status of suppliers* are of big concerns for seller – buyers and should therefore be specifically addressed by the SLAs.

Related works in other domains are reported in [12]. In this case health care systems supporting patient oriented decision-making aiming at increasing patient safety.

4.1. Cognitive interaction patterns

The following Figure 9 illustrates a VP with associated WFs, implemented as channels, with PIs generating and controlling the related information flows. The information collected and processed will monitor and control the execution of a use cases in accordance with agreed upon SLAs. Related costs and revenues are collected and distributed among stakeholders.

Our findings from evaluations of the interviews in the project eTransit [10] suggest the following two complementary strategies to implement cost efficient and resilient e-Commerce solutions:

- Preparedness for flexibility and trustworthiness
- Minimizing costs for maintenance

The separation of meta-models and implementation models also allows assessments of *transitions* between different channels (for example mobile/stationary solutions) meeting different customer needs.

A closer analysis of different policies that can be implemented at PIs of different channels can greatly influence the decisions made by customers at those points.

The purpose of our design and implementation of Cognitive Interaction Patterns is to translate a VP into Workflows to be assessed by potential customers. The goal is, of course to guide the customer to make an educated decision on the proposed VP! The next issue is thus related to decision support.

Classical Decision support systems are based on models of *Rational Reasoning.*

This subject has ben investigated from a computational point of view since 1950's. Research areas include *Artificial Intelligence* (AI), *Agent technologies* (AT) and *Multi-Agent Systems* (MAS). Rational reasoning is based on formal (mathematical) models such as different logics or statistical models. The strength is that we can reason about the reasoning (proofs or validations) [13, 14]. A weakness is that human decision-making is not always rational in the objective sense but often *subjective rational*.

There is at present high international focus on developing 'smart' distributed networked systems in areas such as Smart grids and Smart healthcare. Those kinds of 'smartness' can be

http://dx.doi.org/10.5772/59343

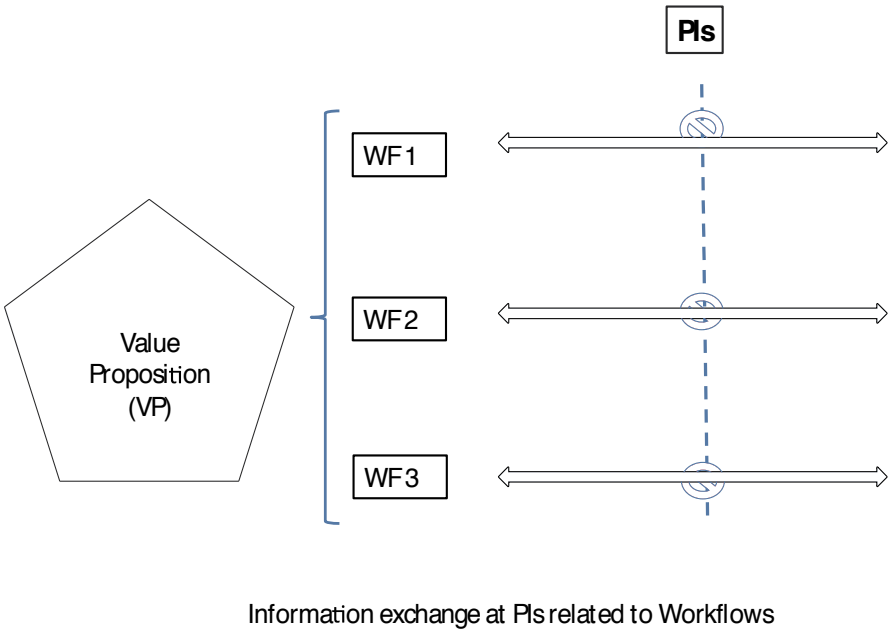

Figure 9. Some relations between VP, WFs and PIs

modelled as service oriented systems (Multi-agent Systems) with intelligent interfaces (APIs) implemented using AI technologies [15].

Behavioural and experimental economists have in recent years successfully challenged the conventional view that individual actors make decisions purely by trading off expected costs and benefits (i.e., the "unbounded rationality" model) and suggested that behavioural predictions should be based on a *bounded rationality* framework instead [16]. The bounded rationality framework has generated a range of insights that apply to design and implementations of suitable PIs related to selected VPs!

By definition a *default* is a condition that is imposed when an individual fails to make a decision. Research and practice show that it is possible to *significantly impact people's behaviour* by carefully setting the default. For example, when asking for consent to store personal data online for marketing purposes, consent rates are higher when consent is the default (i.e., a "presumed consent" model) compared to a situation where the default is no consent (i.e., an *explicit consent* model) [17, 18, 19].

The bottom line is that designers of IP policies for e-Commerce applications should learn how to *customize* Interaction Patterns in a proper way to empower and learn more about their customers. In short we can combine rational information sharing between system components and bounded rational information sharing with or between human actors while maintaining interoperability assuring *shared and common understanding* of states of a use case [20, 21]. These insights are important in addressing Increasing Energy Efficiency by Reducing Losses and Promoting Value Propositions in future Smart grids.

5. Suitable cost and revenue models for future smart grids

Value Propositions and related workflows are illustrated in the following Figure 10. Inspection of message contents and distribution of messages to involved stakeholders of a VP is taken place at *Points of Interaction* (PIs) along the workflow. The workflow is implemented on suitable channels of the information systems.

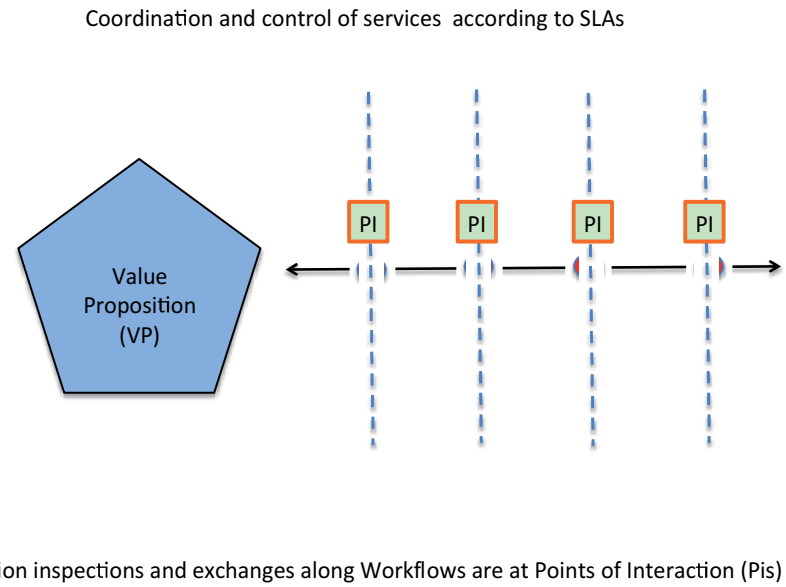

Figure 10. A VP of a use case involves stakeholders and services and information flows defined by the SLA.

The information monitoring and control of the workflow, governed by the SLA, is managed at the Points of Interaction (PIs) along the workflow (Figure 10). The infor-mation managementto all stakeholders of the VP is supported by suitable cognitive interaction patterns (Section 4.1).

There are different aspects of customer oriented Value Propositions. *Firstly*, we have VPs in application areas directly related to energy services. *Secondly*, we have VPs of services utilising parts of the Smart grid infrastructures to support, for example, comfort of living and/or health care.

In this chapter we focus on the following customer oriented VPs related to energy services:

- Power Quality (Section 5.1)
- Cutting losses in power distribution (Section 5.2)
- Smart Home Services enabled by Service Level Agreements (Section 5.3)

http://dx.doi.org/10.5772/59343

5.1. Power quality

In order to maintain the grid and to meet system performance requirements, the following set of ancillary services have been identified and implemented:

- Operational reserve
- Frequency control
- Reactive power and voltage control
- Short-circuit capacity
- Voltage quality
- Black-start
- Island operation of the grid
- Inertia
- Stability

The responsible stakeholders for quality and efficiency of the traditional regulated power systems are the utilities (TSOs and DSOs). Besides the main tasks of generation, transmission and distribution of power, the utilities also are responsible for *ancillary services related to system protection, Supervision and Control (SCADA), and billing*. Today, most of the ancillary support systems are hence *closed and proprietary*. In the traditional regulated power market those ancillary services were provided by the (state-own) utilities. The specific costs were implicit and as such hidden from the customers.

One of the main traits that differentiate existing power markets from the vertically integrated monopoly of the past is the *changing ownership of the product*, electric energy, as it moves from the generating plants (sources) to users premises. Although ownership changes hand with price variations, electrical energy is regarded as a homogenous product irrespective of which generating source it comes from and what resources are used to produce it. This is fortunately a sufficient definition for the power market to operate on as it is not necessary to have any differentiation when dealing with units of energy only.

However, this model is not suitable for handling power quality by itself. Power quality is classically not a sellable product. It is an attribute or value-added feature of another product, electrical energy. On the other hand, modern industrial processes with new types of electrical equipment are *increasingly adversely affected by poor power quality* than the traditional equipment. In addition integrated manufacturing supported by extensive automations and our today's individual way of life are more dependent on good quality of electricity than ever.

The goal of deregulation is to enhance competition and to bring to customers new choices and economic benefits. We argue that *Markets of Services based on power quality* could be based on *generalized* bilateral agreements between customers and providers. Those Service Level Agreements (SLAs) could become an *coordination and monitoring* mechanism between stakeholders of different energy based markets [27]. In the paper *A conceptual view of Power Quality*

Regulation Using Market-Driven Mechanism [25] the authors suggest to employ market mechanisms to regulate power quality. However, in order to successfully identify and sell power quality services we have to identify and market value added Value Propositions (VPs) to customers. Those issues are treated in Section 4 and later in this section.

Challenges related to Ancillary services of Smart grids are mainly due to the distributed character of such systems involving new types of stakeholders and Distributed and Renewable resources (DER/RES) supporting active *prosumers (producers – consumers)* in agile and changing energy based business processes. The roles, stakeholders, responsibilities and business models of Smart grids are evidently completely different from those homogenous utility-based models of classical power grids. Focus of current R&D on Smart grids have been on energy-centric services and related smart energy markets. *Market models* related to *ancillary services* of Smart grids, e.g., business and cost models, remains to be identified and implemented. This will, of course, require changes of the corresponding regulatory frameworks. This necessary transition also requires deeper insights in the economic, societal, technical and environmental constraints to be assessed and resolved [23, 24].

Future smart grids will be based on two key ingredients: *intelligence* and *power electronics*. Intelligence or 'smartness' will be based on *agent technologies* applied to *components and interfaces* to allow context dependent con-figurations and instantiations of service based systems coordinated by Service Level Agreements [9].

Energy losses in the present power grid T&D are typically around 10%. Those losses are mainly due to resistance and imbalance of active and reactive power. The use of *FACTS* (Flexible AC Transmission Systems) has been successful for the Transmission net [22] and are now also investigated for the Distribution nets.

The importance of issues related to Power Quality (PQ) is mainly due to the increasing number of disturbing loads and increasing number of RES/DER. Main references are *Power Quality Indices in Liberalized markets* [23], *A Conceptual View of Power Quality Regulation Using Market Driven Mechanism* [25] and *Quality of Electricity Supply as a Service* [26].

We adopt the following definition of PQ [27]:

- The ability of power systems to operate loads without disturbing or damage them.
- The ability of loads to operate without disturbing or reducing the efficiency of the power system.

That is: PQ is a *common concern* between producers and consumers of power. That is, *suitable to address* as SLAs!

Power quality disturbances defined by *indices and objectives* are important tools in our demonstrators supporting Power quality Markets [23]. PQ indices represent a *compact way* to describe the characteristics of PQ disturbances as single numbers

An important class of PQ disturbances is due to voltage sags. Identifying and detecting voltage sags are therefore an important issue in identifying and monitoring SLAs between producers and consumers in a PQ Market. Proposed methods identifying sources of voltage sags

http://dx.doi.org/10.5772/59343

(inferring responsibilities in cases of low probability of simultaneous disturbances) are based on, e.g., the following models [23]:

- Disturbance power and energy approach
- Slope of the system trajectory approach
- Real current component approach
- Resistance relay approach

As a case study we shortly describe the main features of the *Resistance sign* approach. The following Equivalent circuit for sag source detection is from [23].

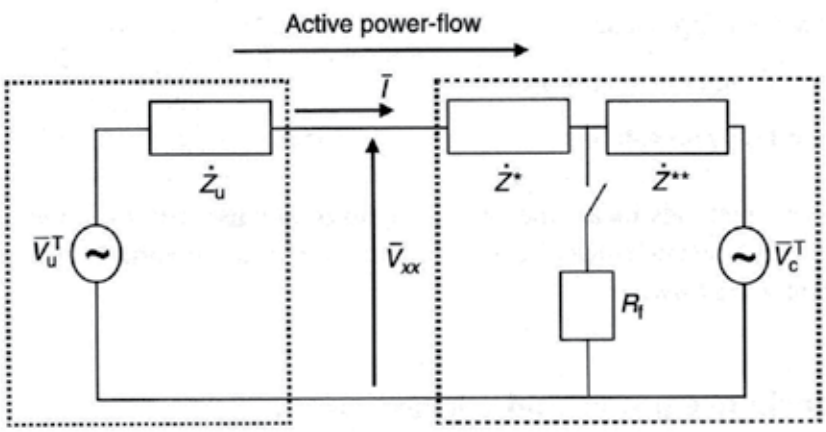

Figure 11. Equivalent circuit for voltage sag detection

Let us refer to Figure 11 in which the right side represents the customer installation ($Z^* + Z^{**} = Z_c$), while the left side represents the utility supply system. Setting up the equa-tions *at the customer side*, before and after a fault, and performing some calculations ([23] pp. 128 -129), we can deduce that:

- If Real (Z_c) < 0, the impedance (multiplied by -1) is the *utility impedance* and the *fault is on the customer side*.
- If Real (Z_c) > 0, the impedance is the *customer impedance* and the *fault is on the utility side*.

More examples of modelling and detecting responsibilities, related to Power Quality indices, between customer and utility are given in [24].

Economic aspects of PQ disturbances, based on economic schemes, have become increasingly important due to the current capability to quantifying the economic consequences associated with disturbances in power systems [23]. The true economic value of PQ markets is linked to the effects that PQ disturbances have on equipment and other loads:

- Downtime disturbances causing lost production

- Additional costs related to maintaining equipment and reducing the effects of disturbances
- Existing methods for economic evaluation of PQ disturbances are mainly focused on voltage dips and harmonics

We argue that SLAs are useful tools to set up and maintain PQ markets. The PQ concerns between stakeholders in a use/business case can be expressed as SLAs using suitable indices and concerns. We can use our frameworks (Chapters 4 and 5) for setting up and monitoring suitable SLAs. In short:

- PQ agreements establish a *common concern* between producers and consumers of power. For example settling the investment costs on either side.
- Those concerns related to power disturbances can be expressed by selections of *suitable indices* and objectives
- The indices are composed by *measurable attributes* of the indices

The following Figure 12 captures the main ideas. The red rectangle illustrates the footprint of a SLA Coordinating services and stakeholders of a given use/business case (e.g., Power Quality markets). The footprint identifies interoperability Categories, layers of the GSAM framework (Figure 6), and selected Cross-cutting Issues identified by the SLA. The SLAs orchestrates Coordination, Monitoring and QoS of the services. Proper data aggregation, handling and transformations support semantic interoperability across the Smart Grid plane (Figure 5 and Figure 7).

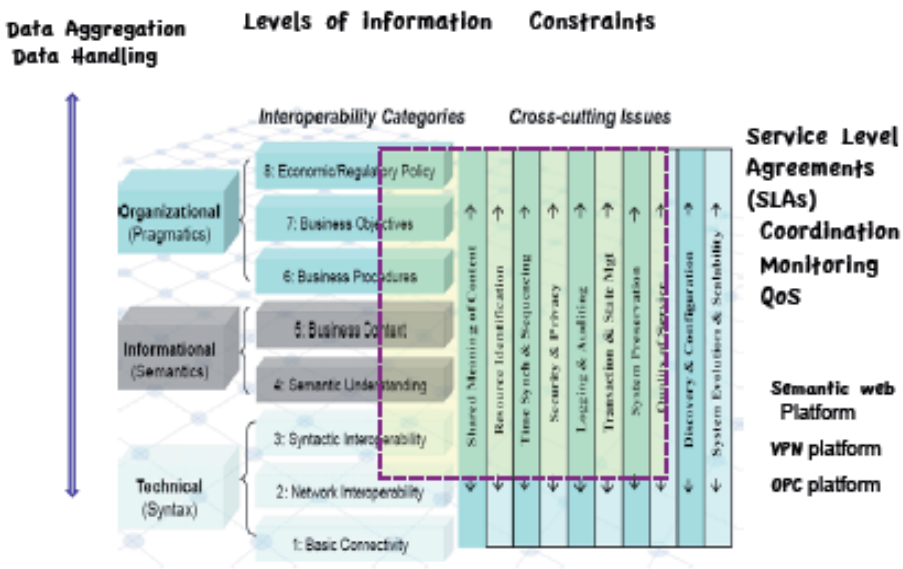

Figure 12. Footprint of SLA in the Interoperability framework

http://dx.doi.org/10.5772/59343

Furthermore, during the different development phases the components of the SLA have been addressed. Specifically, issues related to *resolving potential conflicts* (investments) or interoperability issues.

5.2. Cutting losses in power distribution grids

State estimation of the power system from real-time measurements is one of the most important elements of modern Energy Management Systems and are currently deployed and used by electric utility companies.

A promising technology to cut losses in power systems is to introduce *Phasor Measure-ment Units* (PMUs) to enhance efficiency, performance, and reliability in existing electric power system infrastructure [8]. A *Phasor* refers to *measurable AC power components* of Figure 2. The PMUs are connected in *Wide Area Networks* (WAN) to allow for large area views of the network. Comparing data between points on an electric system is a good way to reveal stress on the system and home in on the source of the problem. PMUs *monitor the characteristics of electricity flowing through a particular location*, for instance, at the point where a generator connects to the bulk power system, or at a substation. The ability to compare *time-synchronized* data on the same timescale, among widely separated locations, is a relatively new achievement, based on:

- *Speed.* PMUs make measurements at short time intervals – typically 30 times per second – significantly faster than traditional SCADA systems
- *Synchronization.* All PMUs across an interconnection are kept in precise time synchronization using GPS. This synchronization provides the capability to easily compare systems data among geographically dispersed units, creating wide-area visibility across large power systems. This was not previously possible using older technology

The synchronized phasor measurement (PMU) technology is relatively new, and consequently several research groups around the world are actively developing applications of this technology. It seems clear that many of these applications can be conveniently grouped as follows:

- Power system monitoring
- Advanced network protection
- Advanced control schemas

The *North American SynchroPhasor Initiative* (NASPI) supervises instalments and assessments of several PMU installations [28].

A PMU collects and time-stamps data at a point. This data is then *processed and reacted on* according to a selected application.

In a *self-healing system* we have to implement the following cycle of tasks:

1. *Detection* of a fault

8 http://en.wikipedia.org/wiki/Phasor_measurement_unit

2. *Localisation* of the fault
3. *Repairing* of the fault
4. *Restart* of system

The PMUs can directly assist in the first two steps for grids. The remaining steps have to be addressed as add-ons to the PMU system.

We have designed and implemented a pilot of self-healing on Smart grids in the EU Project INTEGRAL [29].

5.2.1. Microgrids and renewable energy sources

We can think of the *Microgrid* as the great equalizer between consumers and the electrical companies. With centralized local power generation, businesses, communities and even towns can have a say in the generation and distribution of local energy.

A Microgrid is a scaled down version of the traditional power grid that most people are familiar with. A Microgrid can be as simple as having a power source like a generator hooked up to a load like a commercial business. A Microgrid can also consist of distributed energy resources (DER) like solar PV systems and wind turbines that have several electrical loads. These Microgrids can operate independently or in parallel with the traditional power grid.

Because Mirogrids can rely on local sources of power generation and also pose a lower demand on the grid infrastructure, large institutions like prisons, campuses and military operations, large commercial and industrial markets or remote settings that are off grid are realizing the benefits of building and maintaining their own Microgrid.

Benefits of Microgrids include:

- Increased efficiency – with the source of generated electricity so close to the use, very little energy is lost in transmission
- With fewer load sources, demand on the Microgrid infrastructure is less than a typical grid
- By being smaller and closer to source and demand and being able to use power generation more specific to the location, the system has higher reliability and is able to respond to demand more quickly
- Microgrids are laid out in a modular manner making expansion and updating more efficient
- With local control, both design and future planning are specific to the needs of the entities participating in the Microgrid
- Because the Microgrid can shut itself off from the main grid (islanding) it is less vulnerable to outside attacks, being cyber or physical

Barriers to the development and running Microgrids include:

- Lack of standards from operations, safety and integration to data on power quality from different sources.

http://dx.doi.org/10.5772/59343

- Legislation and regulations need to be addressed for regulating the operation of Microgrids in many countries.
- Installation costs of distributed energy resources such as solar and wind, may be too great for some areas.
- Lack of technical experience, infrastructure and communication protocols.
- Possibility of market monopoly if no infrastructure is in place to guard against pricing abuse.

Microgrids have to be fitted into the modernization of the current electrical grids that service the world. With increasing volatility to brown or black outs and physical or cyber attacks, Microgrids can keep important services running during any disruptions to the main grid.

We are presently testing technologies of Microgrids with basic components delivered by Hughes Power Systems [30]. We will implement a *Tests site* aiming at implementing smart protection and detection systems enabling, for instance, cutting losses in the distribution system. Specifically by installing products for minimising the number of interruptions (SAFI), the number of interruption minutes (SAIDI) and distribution losses.

We aim at implementing *self-healing capabilities of faults*. That is, *Smart Protection Systems for Microgrids*. Detection and Localisation is facilitated by new 3-Phase *Autoreclosers* (Vacuum Interupter Modules). Smart *automatic sectionalising* is enabled by Autoreclosers together with *distribution transformers* (with very low losses and with on-load tap). We will address a selected subset of the Technical losses listed in Section 2.3.2. Specifically losses related to:

- Lengthy Distribution lines
- Inadequate Size of Conductors of Distribution lines
- Installation of Distribution transformers away from loads centers
- Low Power Factor (PF) of primary and secondary distribution systems
- Bad Workmanship
- Feeder Phase Current and Load Balancing

The configuration of the Test site is given in Figure 13.

The *Repair, Restoring and Reporting* services will be implemented as a set of suitable smart knowledge bases enabling collecting and handling the local information generated by the Autoreclosers.

Repairing might include reconfiguration of the distribution net to cut losses or increase performance. The reporting module also incorporates a learning mechanism to improve the total performance.

The experimental environment will also be a test bed for selected business cases related to energy based service markets.

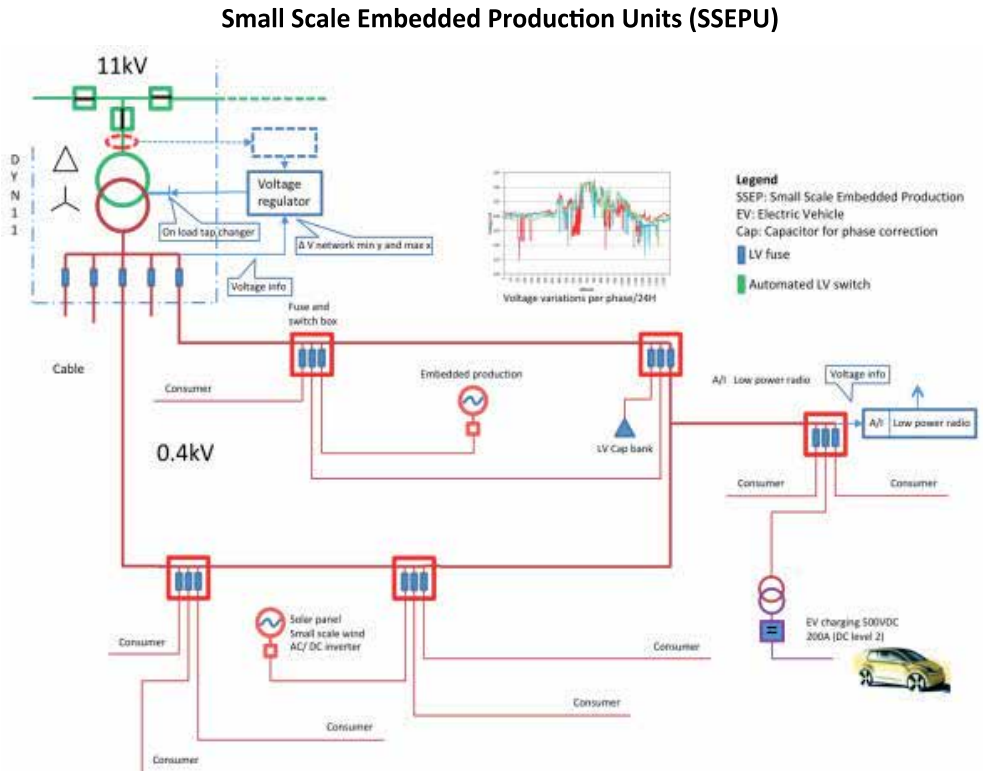

Figure 13. Smart equipment supporting cutting losses in distribution grids

5.3. Smart home services enabled by service level agreements

Smart and Green Building are active areas of R&D related to future Smart grids and active customers[9] (Figure 14). We will select a use case illustrating *Comfort management* in Smart buildings, main own reference are [9, 31 and 32].

The concepts of Service Level Agreements (SLAs) have gain recognition and acceptance with the increasing demand of services in our societies. It is noticeable from ICT business offers, that tariffs are regarded as an old inflexible generic form of service level agreements. The deregulation of the telecommunication sector highlights the issues related to services and related technologies to meet the demands of new business opportunities. As a consequence, the organization *TeleManagement Forum* (TM Forum) has developed a set of technologies and tools, such as *Frameworks*, to support running and renewing service businesses in that sector.

Understandably, the work and results from TM Forum, including SLA management, are valuable inputs to design and implementation of SLAs for Smart grids. For instance, Smart grids presuppose a deregulation of the electric power market towards a service-oriented

9 http://ec.europa.eu/information_society/activities/sustainable_growth/docs/sb_publications/smartbuildings-ld.pdf

http://dx.doi.org/10.5772/59343

market, similar to de deregulation of the telecommunication market. However, there are some fundamental differences between the domains.

TM Forum work on SLAs is an important input to SLAs supporting Smart grids. How-ever, due to the different nature of smart grid we have to address the following specific additional challenges:

- SLAs between different groups of multiple stakeholders
- SLAs involving different sets of real-time constraints. That is, interactions between high- and low-level SLAs.
- SLAs supporting setting up and validating interoperability in Smart grids.

Firstly, formulation of agreements needs business cases with identified stakeholders (roles, capabilities and responsibilities). Secondly, relevant tasks to be coordinated among stakeholders should be identified. Thirdly, non-functional constraints (perfor-mance, security, Quality of Service, etc.) should be identified and taken into account. To do that, the stakeholders should agree upon KPI (Key Performance Indicators) to be implemented and monitored according to the agreements.

Important application areas of Smart Grids are Smart and Green Buildings, Figure 14.

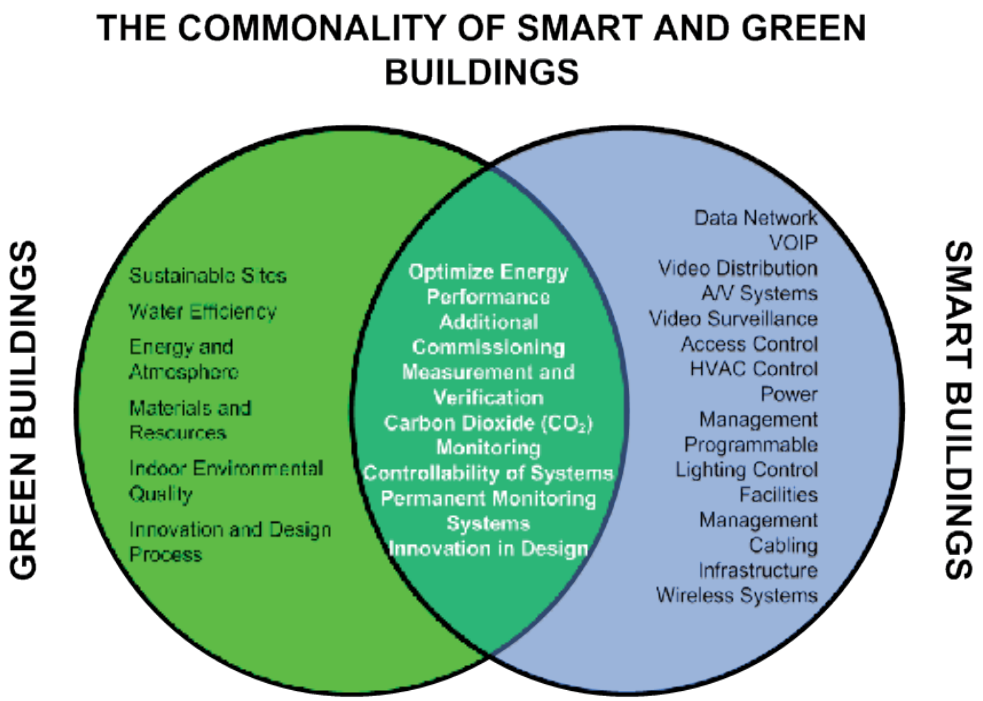

Figure 14. Common application areas of Smart and Green Buildings

Our selected use case, smart home services, is a typical example where we need coordination between high-level and low-level SLAs (Figure 7). The high-level SLA guarantees that the *user perceives and accepts* the desired comfort level, set by the control system. The low-level SLA monitors and *controls the settings of the associated physical system*. Thus we have to address and solve the *challenge of trustworthy translation between perceived subjective parameters* and *settings of physical objective parameters*.

As presented in Figure 7, the key drivers in more complex business cases of Smart grids are SLAs that holds a strong interaction between the higher-level business cases and low-level affordances of the infrastructure.

We model our use case as follows:

Stakeholders

- Customer (C)
- Smart house agent (SHA)
- Market aggregator (MA)
- Operation agent (DSO)
- Service provider (SP)

Scenario

The Market Aggregator (MA) offers a range of services (VPs Figure 8) to the Customer (C). Among those is Comfort management. This service is delivered to C by the SHA in cooperation with SP. SP is responsible for instalment, monitoring and control of smart equipment at customer premises. DSO, together with SHA and MA monitor and control the energy flow associated with a given service. The MA is also responsible for the monitoring and billing of the services to C.

Implementation

The Comfort management systems is modelled and implemented as a *Multi Agent System* (MAS) consisting of the agents C, MA, SHA, DSO and SP. The coordination and control of the MAS is governed by the factual set of High-level and Low-level SLAs. Agents are grouped into the two bundles of SLAs. Firstly, a high-level business related set, SLA-high, between the agents C, SHA, SP, and MA. Secondly, a real-time constrained set represented as SLA-low, between agents MA, DSO, SP, and SHA. SP runs coordination between the SLA sets.

Challenges

The comfort level identified by the customer is represented in a *set* {good, acceptable, not acceptable, not-good}. The following physical (objective) parameters of the customer premises are monitored and controlled by SP:

- Temperature
- Lighting

http://dx.doi.org/10.5772/59343

- Sound
- Humidity
- Air circulation
- Allergy indicators
- Movement indicators

A design challenge is to *identify, implement and validate* an *accepted translation* between the objective sensor readings and the subjective customer values (Figure 5 and Figure 7). This implemented mechanism provides *trustworthy interoperability* of meaning and fulfilment of services according to the SLA (Figure 6).

Requirement Engineering and Validation

Negotiation of a SLA provides a methodology supporting requirement engineering of SLAs. SLA negotiation tools provides a mechanism to *identify* the concerns of the involved stakeholders in a given use case. Typically, those concerns are expressed in *stakeholder case specific concepts* (ontologies). The next step is to negotiate a common understanding among stakeholders of related concepts.

There are in principle two ways to discover and validate this pattern-matching; *model based* or *experimental based*.

A model-based approach is based on establishing a *formal function* between the different types of parameters. That is:

Comfort is defined by an analytic function F:

F(objective_parameters) with value-set {Good, Acceptable, Not acceptable, Not good}

However, this approach is *neither easy nor flexible*. In an *experimental setting* we provide a flexible front-end to the customer with the SP operating the sensor net at the premises of C. By performing a rich enough *calibration* between sets of objective parameters and the customer perceived comfort level we derive a set of tuples Σ, or patterns, connecting objective parameter settings and subjective comfort levels.

Σ(objective parameter values, comfort levels)

Proper analysis of this set will reveal *sufficient rich patterns to support design of corresponding SLA rule sets.* Setting up the front-end to the customer can *support validation* of the rule sets (Figure 6). Maintenance of the rule sets could also be supported with a similar set up.

Management of SLAs

After calibration and validation, the system build substantial knowledgebase that can facilitate decision-making based on historic data of the user's behaviour further supporting negotiations of the corresponding SLAs. The customer is given a set of choices to select the desired type of SLA related to comfort levels and price. That is, the *Value Proposition*!

After the negotiation, the system provides monitoring mechanism of SLA to ensure proper QoS of the service (Figure 10).

Exception Handling: In case of indication of system comfort output of "Not acceptable" or "Not good", generate alerts. The same holds if there is detection of malfunctions of system components.

6. Conclusions and future work

This chapter is about Increasing Energy Efficiency by *Reducing Losses* and *Promoting Value Propositions* in AC power systems. *Reducing losses* relates to the *physical processes* of generating, transmission and distribution of electric power. *Promoting Value Propositions* relates to identifying customer oriented value added business cases and processes based on energy based services.

The core of the emerging Smart grid [5] is addressing the challenges of balancing a very complex physical system in real time while meeting customers and societies expectations on energy and energy related reliable services. The overall constraint, however, is meeting the environmental challenges!

In order to give perspectives on those societal challenges we have given some technological as well as business and societal backgrounds and illustrated our suggested solutions with some implemented examples.

Future Smart grids will consist of the following three interconnected types of systems:

1. Systems supporting *Energy management*
2. Systems supporting *Information management*
3. Systems supporting *Business management*

The technological background of systems of types I and 2 are grounded in *Smart Grid Reference Architecture* (SGAM) Figure 4, Figure 5 and Figure 6 [4]. Those architecture models illustrate the *inherent complexity* of designing, implementing and maintaining Smart grid solutions.

To complement the views of the SGAM architectures of system 1 and 2 we suggest an *extension* of the SGAM model sets with the *eTransit Business Model framework* (Section 4). This enables modelling the views of System 3 and but also the *interactions* between all three types of system (Section 5).

To deal with this complexity, in *time, space and cyberspace*, we propose *Service Level Agreements* (SLAs) as a *coordinating and monitoring mechanism of business cases*. Figure 7 illustrate how bundles of SLAs can manage the different aspects and types of business use cases.

SLAs can be properly identified and modelled by a vertical and horizontal mapping of a use case onto the SGAM (Section 3). To proper model business cases from different viewpoints we

http://dx.doi.org/10.5772/59343

propose the eTransit Business Model, Figure 8. This framework allows for implementing SLAs into Workflows, Channels and Information flows (Figure 9 and Figure 10).

In this chapter we focus on models supporting *trustworthy information exchange between stakeholders in a business case*. In coordination of a use case interoperability is the *shared understanding by stakeholders of the state of the executed use case.* This requirement is extremely important [20, 21]. A key technology is here designing and implementing *Cognitive Interaction Patterns* (Section 4.1)

Societal demands on Smart grids include requirements on *inclusion of Renewable Energy Resources (RES*) and efforts to decrease the environmental negative effects of energy production. To illustrate some of the challenges we indicate the expected total energy consumption 1990-2040 (Section 2.1). *Challenges and problems in comparing* different energy sources are discussed in Section 2.2.

In Section 5 we give some examples of customer centric use cases (Value Propositions) to increase energy efficiency and/or to add customer value:

- *Power Quality* (Section 5.1)
- *Cutting losses in power distribution* (Section 5.2)
- *Smart home Services* (Section 5.3)

Future work includes investigations of *Value Propositions* (VPs) in areas of comfort or Health. Those VPs can be based on energy systems such as Microgrids (Section 5.2.1 and Section 5.3) as in Figure 14.

In defining and discussing proper *Cost and Revenue Models* we refer to Figure 1 with the interpretations; *Total Cost*, *Customer paid cost* (Value Proposition) and *Investment cost* (Private & Public) giving a balance that drives societal acceptable products and services.

Finally, it should be observed that future Smart grids have some commonalities and differences with systems classified as instances of *Cloud computing*[10]. In this setting Smart grids could be modelled *three interacting Platform –as – a – Service* (*PaaS*) cloud systems. That is, as we earlier have stated: Energy system management, Information management systems and Business management systems. Having said that, we believe that Smart grids and Cloud computing systems could benefit from sharing lessons learned.

This observation is enforced by the *Report on the public consultation for the EU H2020 Work Programme 2016-17: Cloud Computing and Software*, Final version 2014-12-04[11] , that states:

> "Attention should be placed on the non-functional aspects of cloud-based applications and services including SLAs and performance optimisation of real-time, cloud based applications and services, and increased energy efficiency through the exploitation of hardware advances, lightweight virtualisation techniques, and intelligent auto-scaling algorithms."

10*http://en.wikipedia.org/wiki/Cloud_computing*

11 EGI recommendations for the Horizon 2020 Work Programme 2016-2017, https://documents.egi.eu/document/2320

Acknowledgements

We gratefully acknowledge the cooperation in the eTransit project with our colleagues from the School of Business and Economics at Linneaus University in Sweden and Institute for Advanced Management Systems Research (IAMSR) at Åbo Akademi University in Finland with the support from Peter Wallenbergs Foundation.

Author details

Rune Gustavsson[1*] and Leif Marcusson[2]

*Address all correspondence to: rune.gustavsson@lnu.se

1 KTH, Stockholm, Sweden

2 Linneaus University, Kalmar, Sweden

References

[1] U.S. Energy Information Administration (2013): *International Energy Outlook 2013*. DOE/EIA 0484(2013)

[2] Frank, C. R (2014): *The Net Benefits of Low and No-Carbon Electricity Technologies*. Global Economy and Development at Brookings. Working Paper 73, May 2014.

[3] Parmar, J (2013): Total losses in Power Distribution and Transmission Lines. In *Transmission and Distribution Electrical Engineering Portal (EEP).* Posted August 19, 2013

[4] European Smart GridsTechnology Platform: Home page http://cordis.europa.eu/technology-platforms/smartgrids_en.html

[5] European Technology Platform (2012): S*martGrids SRA 2035* – Strategic Research Agenda. Update of the SmartGrids SRA 2007 for the needs by the year of 2035

[6] Gustavsson, R. and Hussain, S. (2014): The Proper Role of Agents in Future *Multi-Agent Systems PAAMS 2014 International Workshops*, pp. 226 – 237. Springer Verlag.

[7] Gustavsson, R. (2012): Promoting Increased Energy Efficiency in Smart Grids by Empowerment of Customers. Invited book chapter in *Modeling and Optimization of Renewable Energy Systems*. InTech Open Access Publisher, 2012, ISBN 7978-953-308-487-9

[8] CEN-CENELEC-ETSI Smart Grid Coordination Group (2012): Smart Grid Reference Architecture (SGAM), v 3.0. November 2012

[9] Gustavsson, R., Hussain, S. and Nordström, L (2011): Engineering of Trustworthy Smart Grids Implementing Service Level Agreements. In *Proceedings of 16th Conference*

on Intelligent System Applications to Power Systems. September 25 – 28, 2011, Greece, 2011

[10] The eTransit project (2013): A collaboration project between School of Business and Economics Linneaus University in Sweden and Institute for Advanced Management Systems Research (IAMSR) Åbo Akademi University in Finland with a grant from Peter Wallenbergs Foundation

[11] Weill, P. and Vitale, M. (2001): *Place to Space. Migrating to eBusiness Nodels*. Harvard Business School Press; Boston, Massachusetts

[12] Ådahl, K. and Gustavsson, R. (2011): Decision Support by Visual Incidence. Invited book chapter in *Efficient Decision Support Systems: Practice and Challenges – From Current to Future.* InTech Open Access Publisher

[13] Shapiro, S.C (Editor) (1992): *Encyclopedia of Artificial Intelligence*. John Wiley & Sons, Inc.

[14] Pearl, J. (2000): *Causality Models, Reasoning, and Inferences*. Cambridge University Press.

[15] Wooldridge, M. (2002): *An introduction to MultiAgent Systems*. John Wiley & Sons Ltd.

[16] Kahneman, D., (2011): Thinking Fast and Slow. Pinguin Books.

[17] Brown, C., and Krishna, A. (2004): The skeptical shopper: A metacognitive account for the effects of default options on choice. *Journal of Consumer Research*, 31, 529-539.

[18] Herrmann, A., Goldstein, D.G., Stadler R., Landwehr, J.R., Heitman, M., Hofstetter, R., and Huber, F. (2011): He effect of default options on choice – Evidence from online product configuration. *Journal of Retailing and Consumer Services*, 18, 483-491.

[19] Menzel, S. (2013): Are emotions to blame? – The impact of non-analytic information processing on decision-making and implications for fostering sustainability. *Ecological Economics*, 96, 71-78

[20] Lundberg, J. and Gustavsson, R. (2009): Robust approach toward context dependent information sharing in distributed environments. In *Proceedings of 11th International Conference on Enterprise Information Systems,* Milan, Italy, 2009

[21] Lundberg, J. and Gustavsson, R. (2011): Challenges and opportunities of sensor based user empowerment. In *Proceedings of 8th International Conference on Networking, Sensing and Control ICSNSC 2011,* Delft, The Netherlands, 2011

[22] P.K Steimer, P.K. (2011): Enabled by High Power Electronics – Energy efficiency, Renewables and Smart Grids. *Proceedings* of *The 2011 International Power Electronics Conferenc*e.

[23] Pierluigi, C., Carpinelli, G., and Verde, P. (2009): *Power Quality Indices in Liberalized Markets*. Wiley 2009. ISBN: 978-0-47003395-1

[24] Caramia, P., Carpinelli, G., and Verde, P. (2009): Assessing Responsibilities between Customer and Utility. Book Chapter in *Power Quality Indices in Liberalized Markets*. Wiley 2009.

[25] Chen, S., Wang, C.J., and Lie, L.T. (2006): A Conceptual View of Power Quality Regulation Using Market Driven Mechanism. *Proceedings of PowerCon 2006.*

[26] E. Sersen, E. Vorsic, J. (2008): Quality of Electricity Supply as a Service. In *Proceeding of International Conference on Renewable Energy and Power Quality (ICREPQ-08),* 2008

[27] Gustavsson, R., Hussain, S. and Saleem, A. (2013): Ancillary Services for Smart Grids – Power Quality Markets. In *Proceedings of PowerTech 2013*, Grenoble

[28] NASPI homepage: https://www.naspi.org/

[29] INTEGRAL Report: http://www.integral-eu.com/fileadmin/user_upload/downloads/Presentations/E-Energy2010_-_Integral__Oct-2010_.pdf

[30] Hughes Power Systems. Home page: http://www.hughespowersystem.com/en/

[31] Hussain, S., Gustavsson, R., and Nordström, L. (2012): Smart Home Services Enabled by Service Level Agreements. In *Proceedings of First International Workshop on Intelligent Agent Technology. Power Systems and Energy Markets (IATEM 2012).* Vienna 4th September 2012.

[32] Gustavsson, R. and Hussain, S: (2014): The Proper Role of Agents in Future Resilient Smart Grids. In *Proceedings of Multi-agent Applications for Smart Grids and Sustainable En*ergy Systems (MASGES 14). Salamanca 4 – 6 June 2014.

Chapter 9

Heuristic Optimization Method for Power System Protection Coordination — An Intelligent Tool for Energy Efficiency Improvement

Rabah Benabid and Mohamed Boudour

Additional information is available at the end of the chapter

http://dx.doi.org/10.5772/59713

1. Introduction

The electric protection system plays an important safety function for the industrial installations. Its main purpose is to detect and clear the occurred faults rapidly and isolate only the faulted part of the system. The electric protection system performances are mainly depending on the type, setting and coordination of protective devices. A good electric protection design and setting improve the energy efficiency of the industrial installations in terms of ensure service continuity, decrease the outage time, prevents the devices damage, and lifetime extension. In this context, the nuclear event that has been occurred at the nuclear power plant of Forsmark in July 2006 it is mainly due to an incorrect tuning of a protective relay [1]. However, due to the complex topology of the modern interconnected power systems and the operation close to its limits, the setting and coordination of protective relays have become a very complex and tedious operation.

In order to ensure the reliability of the protective system, the tuning and coordination of protective relays require that the relays closes to the fault must trip faster than the others relays, in order to isolate only, the faulted part of the power system. Furthermore, each main relay has a backup relay acts after a certain time delay known as coordination time interval (CTI), giving the chance for the main relay to operate [2]. Therefore, the reliability and the efficiency of the protective relays depend greatly on theirs setting and coordination with the adjacent equipments [3].

In recent years, the optimal setting of protective relays has been reported in the literature based on various methods and techniques. The linear optimization of protective relays is proposed in [4-7] based on linear programming and simplex method. Furthermore, the non linear

formulation of the optimal coordination of the overcurrent relays has been presented and solved using non linear optimization methods such as: random search technique [8], Genetic Algorithms and its variants [9-11], Differential Evolution method [12, 13], Seeker algorithm [14], Teaching learning-based optimization [15], and Hybrid methods [16, 17].

Based on the previous works in this field, it is clear that the overcurrent relay coordination problem is mainly modeled as continuous optimization problem, i.e. considering only the continuous decision variables. In addition, the relays characteristics and standards are usually chosen arbitrarily or by trial and error method. Furthermore, the violation constraint handling strategy was not presented in the most of the published papers.

On the other hand, the setting and coordination of protective relays is mainly based on the short circuit current seen by the relays. However, the short circuit current value seen by the relays can be varied according to various parameters such as: FACTS devices [18-20], current limiters, resistance faults, series compensation, wind turbines, and power system topology variation. In this case, the setting and coordination of protective relays must be recomputed.

In this chapter, the directional overcurrent relays (DOCR) setting and coordination problem is formulated as non-linear mixed integer constrained optimization problem considering various scenarios related to the power system topology and operation. The objective function of this optimization problem is the minimization of the operation time of the associated relays in the systems. Both real and integer decision variables are considered; where the real variables are the time dial setting (TDS), the pickup current (Ip), and the integer variables are the relay characteristics and standards. Where, these last are usually chosen arbitrarily or by trial and error method. To solve this constrained Mixed Integer optimization problem, an improved version of Biogeography-based optimization (BBO) able to manage the combinatory and constrained optimization problems is proposed. The BBO is validated on 3-bus, and 8-bus power systems test. Furthermore, an impact study of the fault resistance and the power system series compensation on the DOCR performances is presented. Various optimization scenarios are carried out considering the impact of resistance fault and power systems series compensation.

2. Overcurrent relays characteristics and standards

The overcurrent relays characteristics are divided on two types namely, independent and dependent tripping time characteristics. These characteristics could be used in the same time in the same relay.

2.1. Independent tripping time characteristic

In this type of characteristic, the tripping time of the relay is independent of the fault current value (see figure 1). This characteristic is easy to be set and understand, but their drawbacks are the relay tripping time is independent to the fault current, and sometimes the coordination is difficult to achieve with fuses. This type of characteristic is very used in France.

http://dx.doi.org/10.5772/59713

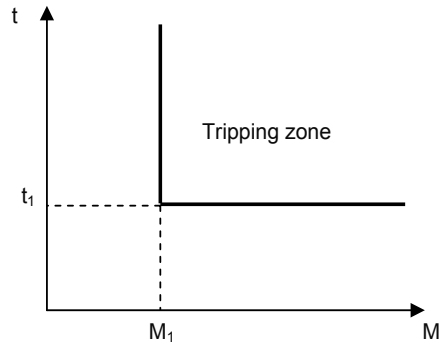

Figure 1. Dependent tripping time characteristic.

2.2. Dependent tripping time characteristic

Figure 2 presents the independent tripping time characteristic. From this figure, it is clear that the greater the fault current; the smaller the tripping time. This type of characteristic is widely used in Anglo-Saxons countries. Their advantages are: flexibility (various characteristic curves), small tripping time for large fault current, and the compatibility with the tipping curves of magneto-thermal circuit breakers and fuses. However, its setting is relatively difficult to achieve.

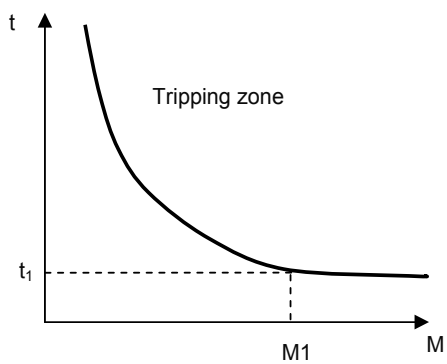

Figure 2. Independent tripping time characteristic

For each protective relay the operating time t is defined as follows [21, 22]:

$$t(s) = TDS \times \left(\frac{K}{\left(\frac{I_F}{K_{CT} \times I_P} \right)^{\alpha} - 1} + L \right) \tag{1}$$

where, t is the relay operating time (sec), TDS is time dial setting (sec), I_F is the fault current (A), Ip is pickup current (A), K_{CT} is ratio of the current transformer. The constants K, α and L depend to the characteristic curve of the relay.

Figure 3 depicts the impact of the TDS on the characteristic curve. From this figure, it is clear that when TDS increases, the curve moves from bottom to top, therefore the relay tripping time increases for the same fault current.

Figure 4 presents the impact of pickup current on the relay characteristic curve. From this figure, it is clear that when pickup current increases, the characteristic curve moves from left to right.

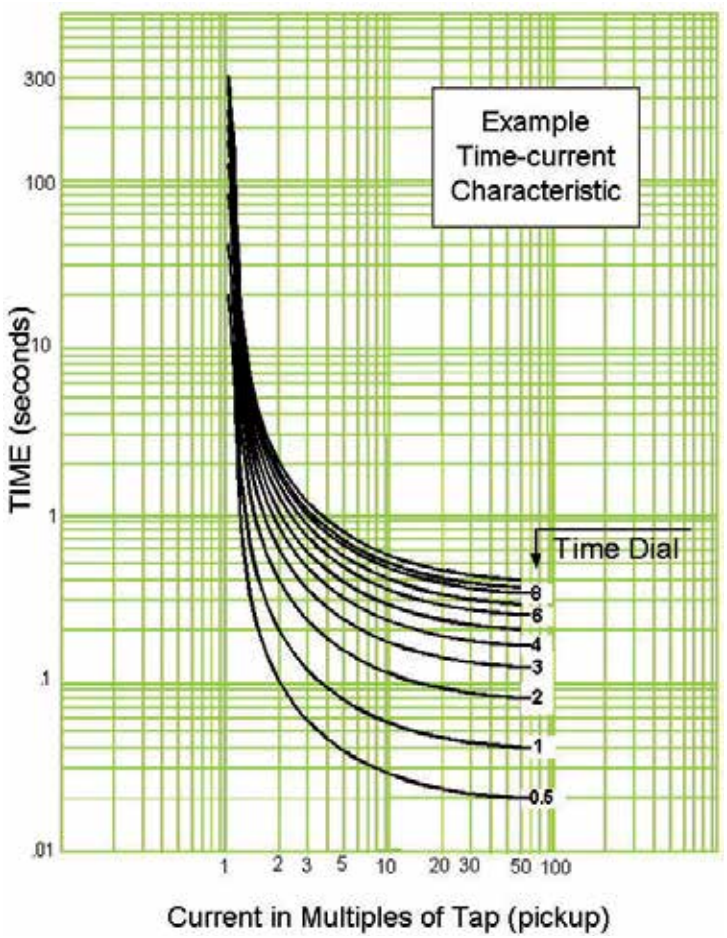

Figure 3. Impact of TDS value on the relay characteristic curve.

http://dx.doi.org/10.5772/59713

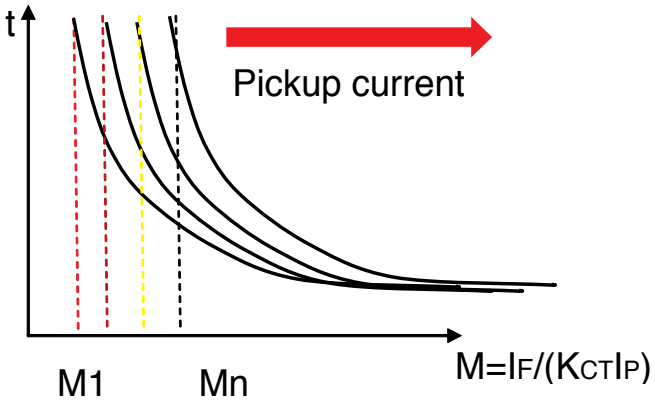

Figure 4. Impact if pickup current value on the relay characteristic curve.

Table 1, presents the constants values of the overcurrent relay characteristic considering AREVA, IEC, and ANSI/IEEE standards [9].

Type of characteristic	Standard	K	α	L
Short time inverse	AREVA	0.05	0.04	0
Normal inverse	IEC	0.14	0.02	0
Very inverse	IEC	13.5	1	0
Extremely inverse	IEC	80	2	0
Long time inverse	AREVA	120	1	0
Moderately Inverse	ANSI/IEEE	0.0515	0.02	0.114
Very Inverse	ANSI/IEEE	19.61	2	0.491
Extremely inverse	ANSI/IEEE	28.2	2	0.1217

Table 1. Constants values of the overcurrent relays characteristics and standards

3. Energy efficiency and protective relays coordination

The energy efficiency is a generic topic that deals with a large range of subjects such as building design, domestic appliances, vehicles, energy transmission and distribution systems, distributed and micro generation. In this chapter, an intelligent strategy is proposed to improve the energy transmission efficiency based on protective relay coordination. It is well known that the energy transmission efficiency requires that the electrical energy must be transmitted to the consumers with low cost, best quality (voltage and frequency), and in continuous manner. For doing so, the transmission grid must be well protected against various kinds of perturba-

tions and contingences that have the negative impacts on energy transmission efficiency in terms of electricity cost increase due to the equipment renovation and maintenance, long time outage of the system, power quality degradation, and so on.

On the other hand, an appropriate design of electrical protective system can improve the energy transmission efficiency by rapid detection of any abnormal situation in the system and isolate only the faulted part, preventing the propagation of the fault and the total blackout of the system. To fulfill this purpose, the protective relays must be well tuned, selected and coordinated. An incorrect setting and coordination of protective relays can cause an extensive damage to the electrical components, outage of large part in the transmission system and may be the total blackout of the electrical grid.

However, the protective relays coordination in the interconnected power systems is very complex and must satisfy the various constraints related to the equipment protection, and coordination requirements.

In the electrical power system, there are several types of protection: namely distance protection mainly used in transmission networks, overcurrent protection used in distribution networks and differential protection for sensitive equipment such as electrical machines, buses, transformers and cables. Furthermore, in order to improve the electrical protection system reliability and efficiency, each electrical component in the system must be protected by two relays: main relay and backup relay; so that if the main relay fails; the backup relay trip after a predefined time delay.

On the other hand, the design and setting of electrical protection system represent a big challenge to the electrical engineers. Figure 5 depicts the main constraints and challenges related to this task. From this figure, it is clear that the protective relays setting requires the definition of pickup current, time dial, characteristic curve (e.g. Normal inverse, Very inverse, Extremely inverse, …etc.) and standard (e.g. AREVA, IEC, IEEE). Furthermore, these setting parameters must satisfy the equipment operation and relays coordination constraints. However, it should be noted that the protective relays setting is mainly based on the short circuit currents seen by the relays. However, several parameters have a great impact on the fault current seen by the relays and therefore on the protective relay efficiency and reliability. Some of these parameters are related to the control devices such as: FACTS devices, Series compensation, Faults current limiter, Wind turbine and the others parameters are related to the power system operation such as: power system operation near to its limits, power system topology variation, and fault resistance value. Therefore, it is clear that the setting and coordination of protective relays in the modern power systems become a difficult task with a big challenge.

4. Setting and coordination of overcurrent relays using heuristic optimization

The coordination of the overcurrent relays is formulated as a constrained optimization problem, where the optimization function and the constraints are presented as follows:

http://dx.doi.org/10.5772/59713

4.1. Objective function

The aim of this function is to minimize the total operating time of all DOCR relays in the system with respect to the coordination time constraint between the backup and primary relays.

$$F = Min\left\{\sum_{i=1}^{NR}(t_i)\right\} \tag{2}$$

where, t_i represents the operating time of the relay *i*, *NR* is represents the number of IDMT relays in the power system.

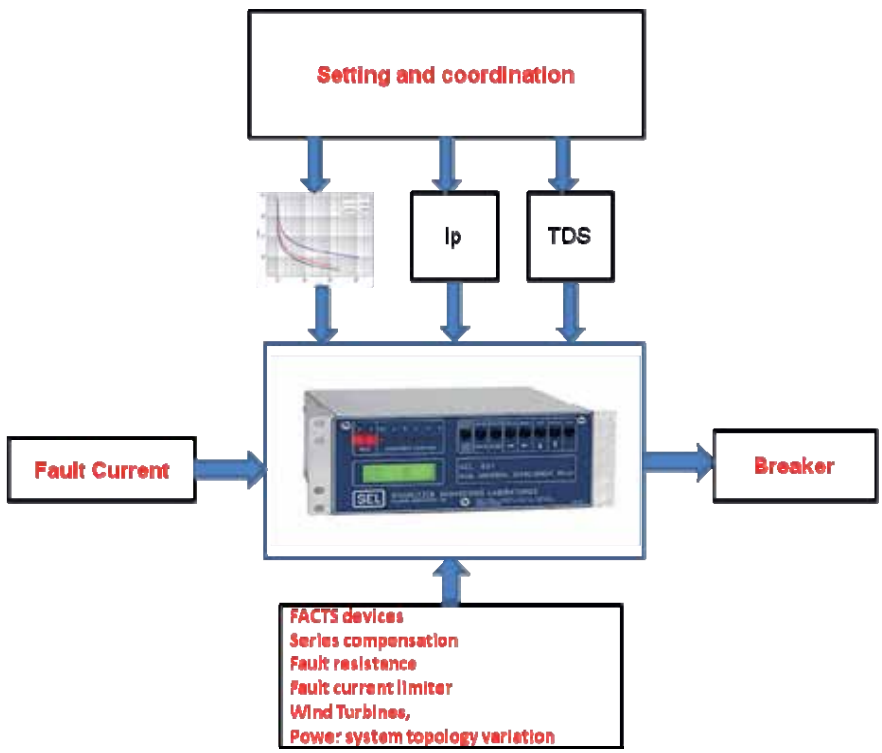

Figure 5. Illustration of protective relays setting challenge;

4.2. Optimization constraints

4.2.1. Coordination time interval

During the optimization procedure, the coordination between the primary and the backup relays must be satisfied the following constraint:

$$t_{\text{backup}} - t_{\text{primary}} \geq CTI \tag{3}$$

where, t_{backup} and t_{primary} are the operating time of the backup relay and the primary relay respectively, CTI is the minimum coordination time interval. For the electromechanical relays, the CTI is varied between 0,30 to 0,40 sec, while for the numerical relays it's varied between 0,10 to 0,20 sec [15].

4.2.2. Time Dial Setting (TDS)

The TDS adjusts the time delay before the relay operates when the fault current reaches a value equal to, or greater than, the relay current setting Ip.

$$TDS_{\min} \leq TDS \leq TDS_{\max} \tag{4}$$

where, $TDS_{\min}$ and $TDS_{\max}$ are the minimum and the maximum limits of TDS respectively.

4.2.3. Pickup current (Ip)

The pickup current Ip represents the set point of the relay. During the optimization process IP is limited as follows:

$$I_{\text{Pmin}} \leq I_{\text{P}} \leq I_{\text{Pma x}} \tag{5}$$

where, $\text{Ip}_{\min}$ and $\text{Ip}_{\max}$ are the minimum and the maximum limits of Ip respectively.

4.2.4. Tripping time of the primary relays

In order to ensure a fast clearing of the fault, the tripping time of the primary relays must be limited as follows:

$$t_{\text{primary\_min}} \leq t_{\text{primary}} \leq t_{\text{primary\_max}} \tag{6}$$

where, $t_{\text{primary\_min}}$ and $t_{\text{primary\_max}}$ are the minimum and the maximum limits of the tripping time of the primary relays.

4.2.5. Type of relays characteristics (RT)

The eight relays characteristics presented in table 1 are considered in the optimization process, and the coding of RT variable is presented in table 2. During the optimization process, the variable *RT* is limited as follows:

http://dx.doi.org/10.5772/59713

$$1 \leq RT \leq RT_{\max} \tag{7}$$

where, RT_{max} is the maximum limit of RT.

Type of characteristic	RT
AREVA Short time inverse	1
IEC Normal inverse	2
IEC Very inverse	3
IEC Extremely inverse	4
AREVA Long time inverse	5
ANSI/IEEE Moderately Inverse	6
ANSI/IEEE Very Inverse	7
ANSI/IEEE Extremely inverse	8

Table 2. Coding of the relay characteristic (RT).

5. Biogeography-Based Optimization (BBO)

5.1. Principle

The Biogeography-based optimization (BBO) is a population based, stochastic optimization technique developed by Dan Simon in 2008, which deals with the geographical distribution principle of biological organisms [23].

A solution in BBO is called habitat, and its performance is assessed by Habitat Suitability Index (HSI) which is equivalent to the fitness in other population-based optimization algorithms like Genetic Algorithms (GAs). The decision variables that characterize habitability are called suitability index variables (SIVs). SIVs can be considered as the independent variables of the habitat and HSI calculation is carried out using these variables.

In BBO, the high HSI solutions represent habitats with many species, and low HSI solutions represent habitats with few species.

Figure 6, illustrates a model of species behavior in a single habitat. From figure 3, λ and μ represent the immigration and emigration rates respectively. Furthermore, it is clear that, when the habitat is empty (there are zero species), λ reaches its maximum value I, and μ is zero, and when the habitat reaches its maximum number of species (Smax), λ is zero and μ equals to its maximum value E.

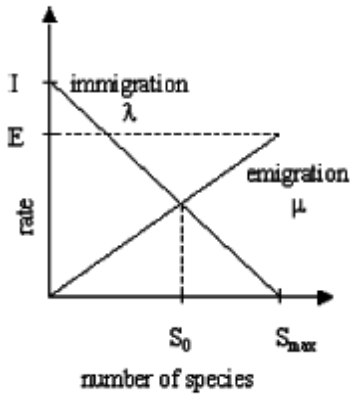

Figure 6. Illustration of species model in a single habitat [23].

The Ps(t) denotes the probability that a habitat contains exactly S species at time t, at time t+Δt the probability is computed as follows:

$$P_s(t+\Delta t) = P_s(t)\left(1-\lambda_s\Delta t-\mu_s\Delta t\right) + P_{s-1}\lambda_{s-1}\Delta t + P_{s+1}\lambda_{s+1}\Delta t \tag{8}$$

where, λs and μs are the immigration and emigration rates when there are S species in the habitat.

If time Δt is small enough so that the probability of more than one immigration or emigration can be ignored then taking the limit of equation (8) as $\Delta t \to 0$ gives the following equation:

$$\dot{P}_s = \begin{cases} -\left(\lambda_s+\mu_s\right)P_s + P_{s+1}\mu_{s+1}, & S=0 \\ -\left(\lambda_s+\mu_s\right)P_s + P_{s+1}\mu_{s+1} + P_{s-1}\mu_{s-1}, & 1 \le S \le S_{\max}-1 \\ -\left(\lambda_s+\mu_s\right)P_s + P_{s-1}\mu_{s-1} & S=S_{\max} \end{cases} \tag{9}$$

For k number of species in habitat, the emigration rate μk and the immigration λk are computed as follows:

$$\mu_k = \frac{E.k}{n} \tag{10}$$

$$\lambda_k = I\left(1-\frac{k}{n}\right) \tag{11}$$

http://dx.doi.org/10.5772/59713

where, E and I are the maximum emigration and immigration rates respectively, n is the total number of species in the habitat. If E=I:

$$\lambda_k + \mu_k = E \tag{12}$$

The BBO is mainly based on two operators which are the migration and the mutation defined as follows [23].

5.2. Migration

In BBO, the migration is used to modify the existing solution based on other solutions with a probability of Pmod. If a given solution Si is selected to be modified, then its immigration rate λi is used to probabilistically decide whether or not to modify any SIV in that solution. After selecting any SIV of that solution for modification, emigration rates μ_j of other solutions Sj (Sj is j-th solution set other than Si, i.e. $j \neq i$) are used to select which solutions among the population set will migrate randomly to chosen SIVs to the selected solution Si [23].

5.3. Mutation

Mutation rate of each set of solution can be calculated in terms of species count probability presented in (9) using the following equation [23]:

$$m(S) = m_{max}\left(\frac{1-P_s}{P_{max}}\right) \tag{13}$$

where, $m_{\max}$ is a user-defined parameter, Ps is the species count probability, and Pmax is the maximum species count probability

5.4. Improvements of the BBO base algorithm

As reported above, the optimal relay coordination problem is formulated as a mixed integer constrained optimization problem. For doing so, the following improvements are carried out on the base algorithm of BBO.

5.4.1. Mixed Integer coding of the solution

In order to solve the above combinatorial optimization problem, the BBO must be able to manage both real and integer decision variables. The real decision variables are represented by TDS and Ip as real decision variables and the integer variables are represented by the relay characteristic type (*RT*). This last, is usually chosen arbitrarily or by trial and error method.

Figure 7, illustrates the coding principle implemented in BBO for *N* relays. From this figure, it is clear that there are 2*N* real decision variables and *N* integer decision variables.

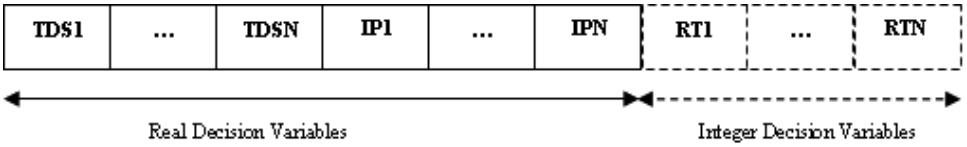

Figure 7. Mixed integer coding of a solution in BBO.

5.4.2. Constraints violation handling

During the optimization process, the coordination constraint presented in (3) could be violated. In this case, the penalty function presented in (14) is used to penalize the violated solutions.

$$F_{penalyzed} = F + PF \tag{14}$$

where, F is the objective function presented in (1) without penalization; and PF is the penalty function defined as follows:

$$PF = \sum_{i=1}^{NR} Viol(i) \tag{15}$$

The Viol parameter is computed as follows:

- Set Viol [1: NR]=0
- For each pair of primary relay i and backup relay j
- If, $t_i - t_j \geq$ CTI
- Viol(i)=Viol (i)+constant.

6. Case studies and simulation results

During this study, the overcurrent relays parameters are limited as presented in table 3.

Decision Variable	Type	Minimum value	Maximum Value
TDS	Real	0.1	1.1
Ip	Real	0.5	2
tprimary	Real	0.05	1
RT	Integer	1	8

Table 3. Limits of the optimization variables

http://dx.doi.org/10.5772/59713

6.1. Test systems

6.1.1. 3-bus test system

The 3-bus test system is presented in figure 8 has three generators, three buses, and six overcurrent relays. The detailed data of this system are presented in appendix.

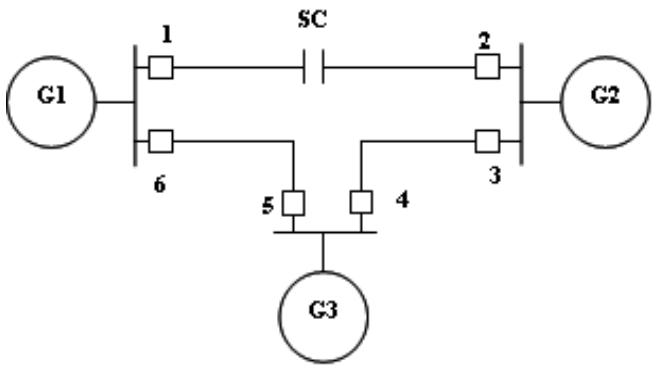

Figure 8. Single line diagram of the 3-bus test system.

6.1.2. 8-bus test system

The 8-bus system presented in figure 9 has two generators and with six buses, seventh lines and four loads. The power system study is compensated with Series capacitor located at middle of the transmission line 1-6. The series capacitor is installed in line 1-6. The 8-bus system has a link to another network, modeled by a short circuit power of 400 MVA. The transmission network consists of 14 numerical DOCRs relays. The detailed system data are given in the appendix.

6.2. Short circuit current computing methodology

The optimization of the overcurrent relays need, at first, the identification of the primary/backup (P/B) relay pairs for each faulted bus. After that, for each P/B relays pairs, the fault currents passing through the relays are calculated for a worst three phase faults applied near the bus as presented in figure 10.

6.3. Impact of resistance fault on the overcurrent relay performances

In this section, the impact of resistance fault value on the overcurrent relays performances is presented. The relays performances are measured by checking the violation of the constraints represented by the primary relays tripping time and the coordination time between the primary and backup relays. Three scenarios are considered in this study namely:

- Base case,

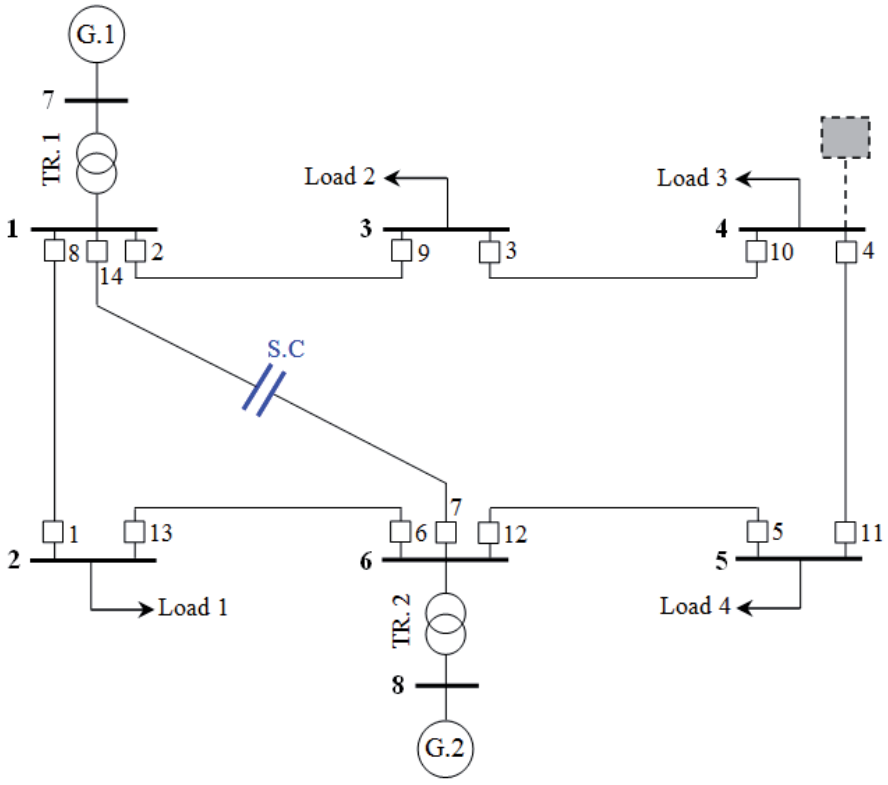

Figure 9. Single line diagram of the 8-bus test system.

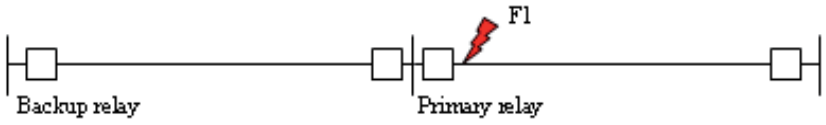

Figure 10. Presentation of near fault.

- R=50 ohms,
- R=100 ohms.

6.3.1. 3-bus test system

Table 4 presents the fault currents seen by the primary and backup relays in the 3-bus test system considering the resistance fault impact. Figures 11 and 12 present the evolution of fault currents seen by the primary and backup relays respectively with respect to the resistance fault value. From these figures, it is clear that the resistance fault has a great impact on the fault

http://dx.doi.org/10.5772/59713

currents seen by the primary and backup relays, such a way, when the resistance value increases; the fault current decreases.

Table 5 presents the best overcurrent relays setting and coordination for the base case obtained by BBO. In this case the characteristic curves of the relays are fixed as IEC normal inverse (i.e. RT=2).

Table 6 presents the impact of resistance fault value on the tripping time of the primary relays. From this table, we can remark that the tripping time of the primary relays satisfy the constraint presented in (6) for R=0 ohms and R=50 ohms. But for R=100 ohms, the primary relays 1, 3, 4 and 6 violate this constraint and their tripping time exceeds the maximum limit fixed as 1s. From these results, we can conclude that when the resistance fault value increases the tripping time of the primary relays increases and may exceeds its maximum limit.

Another parameter used for the assessment of the impact of resistance fault on the overcurrent relays performances, which is the CTI between the P/B relays presented in table 7. From this table, we can remark that the resistance fault causes a miss of coordination between the primary relay N°4 and its backup N° 6 for R=50 ohms and R=100 ohms. The mines sign of the CTI means that the back relay trips before the primary relays. Thus, from the obtained results we can conclude that the resistance fault has a great impact on the relays performances and could cause a miss of coordination between the primary and the backup relays.

P/B pair N°	PR N°	BR N°	Three phase fault current (kA)					
			R=0 ohms		R=50 ohms		R=100 ohms	
			PR	BR	PR	BR	PR	BR
1	1	5	4.2336	0.6651	0.6737	0.1058	0.3424	0.0538
2	2	4	2.7391	1.1056	0.5550	0.2240	0.2849	0.1150
3	3	1	2.7929	1.1063	0.5562	0.2203	0.2852	0.1130
4	4	6	3.1340	0.9223	0.5918	0.1742	0.3026	0.0891
5	5	3	3.0325	0.9669	0.5993	0.1911	0.3076	0.0981
6	6	2	4.1044	0.6864	0.6757	0.1130	0.3442	0.0576

Table 4. Short circuit current of P/B relays of 3-bus test system.

Relay N°	TDS	Ip
1	0.44977	0.96948
2	0.37812	0.9805
3	1	0.5
4	0.50507	0.92512
5	0.36898	1
6	0.1	2.5
F(s)		0.51479

Table 5. Best relays coordination for original case.

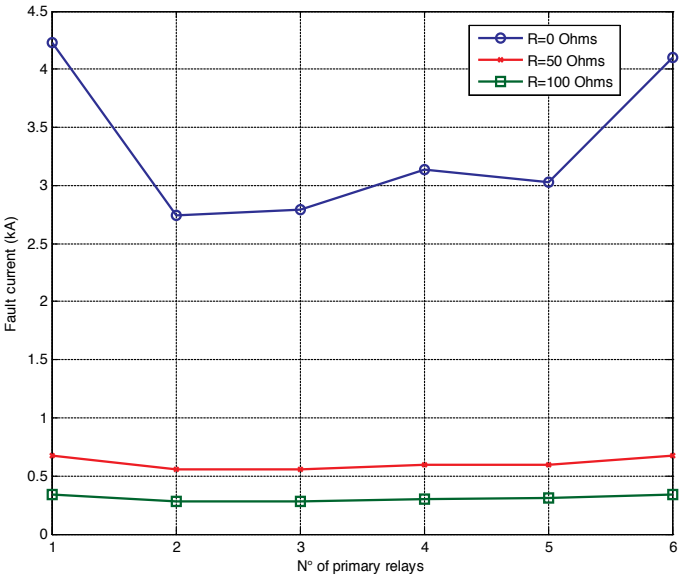

Figure 11. Impact of the resistance fault on the fault current seen by the primary relays.

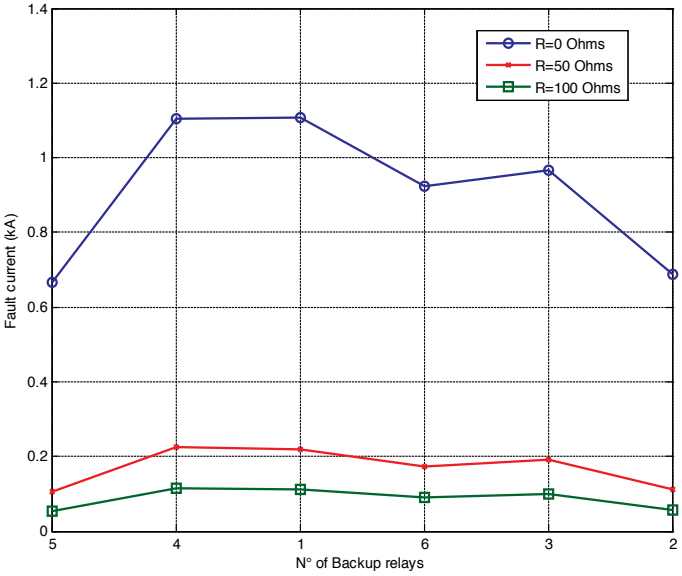

Figure 12. Impact of the resistance fault on the fault current seen by the backup relays.

http://dx.doi.org/10.5772/59713

Relay N°	Tipping time of primary relays		
	R=0 ohms	R=50 ohms	R=100 ohms
1	0.0846	0.5738	**1.2426**
2	0.0742	0.3882	0.8149
3	0.0974	0.5035	**1.0181**
4	0.1229	0.7057	**1.5317**
5	0.0666	0.3562	0.7446
6	0.0692	0.5676	**1.8724**
Number of violated constraints	0	0	4

Table 6. Tripping time of the primary relays.

P/B pair N°	Coordinated Time Interval		
	R=0 ohms	R=50 ohms	R=100 ohms
1	0.2342	2.4543	13.1957
2	0.2863	1.8581	5.5468
3	0.2396	1.6749	5.4234
4	0.2509	**-11.1708**	**-3.9663**
5	0.2186	1.2218	2.7125
6	0.2402	2.1459	9.0200
Number of violated constraints	0	**01**	**01**

Table 7. Coordinated time interval of P/B pair of relays

6.3.2. 8-bus test system

Table 8 presents the fault currents seen by the primary and backup relays in the 8-bus test system considering the fault resistance impact. Figures 13 and 14 depict respectively, the evolution of the fault currents seen by the primary and backup relays with respect to the resistance fault. From these figures, it is clear that the resistance fault has a great impact on the fault currents seen by the primary and backup relays, such a way, when the resistance value increases; the fault current decreases.

Table 9 presents the best overcurrent relays setting and coordination for the base case obtained by BBO. In this case the characteristic curves of the relays are fixed as IEC normal inverse (i.e. RT=2).

Table 10 presents the impact of the resistance fault value on the tripping time of the primary relays. From this table, we can observe that the tripping time of the primary relays satisfy the constraint presented in (6) for the base case only (i.e. R=0 ohms). For the case R=50 ohms the

tripping time of 13 primary relays exceeds the maximum limit, and for R=100 ohms, all relays violated the tripping time limit fixed as 1s. From this result, we can conclude that the resistance fault has a negative impact on the overcurrent relays performances and causes the miss of coordination between the relays.

Another parameter used for the assessment of the resistance fault impact on the overcurrent relays performances which is the CTI between the primary and the backup relays presented in table 11. From this table, we can remark that the resistance fault causes four miss of coordination cases for R=50 ohms and nine miss of coordination cases for R=100 ohms. The mines sign of the CTI means that the back relay trips before the primary relays. Thus, from the obtained results we can conclude that the resistance fault has a great impact on the relays performances and causes the miss of coordination between the primary and the backup relays.

P/B pair N°	PR No.	BR No.	Fault Current (kA)					
			R=0 ohms		R=50 ohms		R=100 ohms	
			PR	BR	PR	BR	PR	BR
1	1	6	3.2946	3.2946	0.8801	0.8801	0.4533	0.4533
2	2	1	6.1594	1.0094	1.4959	0.2451	0.7658	0.1255
3	2	7	6.1594	1.9164	1.4959	0.4654	0.7658	0.2383
4	3	2	3.7450	3.7450	1.0321	1.0321	0.5328	0.5328
5	4	3	3.9830	2.3214	1.0850	0.6324	0.5597	0.3262
6	5	4	2.5088	2.5088	0.6762	0.6762	0.3487	0.3487
7	6	5	6.2928	1.2325	1.5250	0.2987	0.7807	0.1529
8	6	14	6.2928	1.8182	1.5250	0.4406	0.7807	0.2256
9	7	5	5.2856	1.1843	1.2716	0.2849	0.6507	0.1458
10	7	13	5.2856	0.8525	1.2716	0.2051	0.6507	0.1050
11	8	7	6.2321	1.8105	1.5155	0.4402	0.7759	0.2254
12	8	9	6.2321	1.1894	1.5155	0.2892	0.7759	0.1481
13	9	10	2.5859	2.5859	0.7051	0.7051	0.3637	0.3637
14	10	11	4.0891	2.4289	1.1152	0.6624	0.5753	0.3417
15	11	12	3.9026	3.9026	1.0649	1.0649	0.5496	0.5496
16	12	13	6.1670	1.0084	1.4919	0.2440	0.7637	0.1249
17	12	14	6.1670	1.9145	1.4919	0.4631	0.7637	0.2371
18	13	8	3.0631	3.0631	0.8164	0.8164	0.4204	0.4204
19	14	1	5.2615	0.8621	1.2670	0.2076	0.6483	0.1062
20	14	9	5.2615	1.1499	1.2670	0.2769	0.6483	0.1417

Table 8. Short circuit current of P/B relays of 8-bus test system.

http://dx.doi.org/10.5772/59713

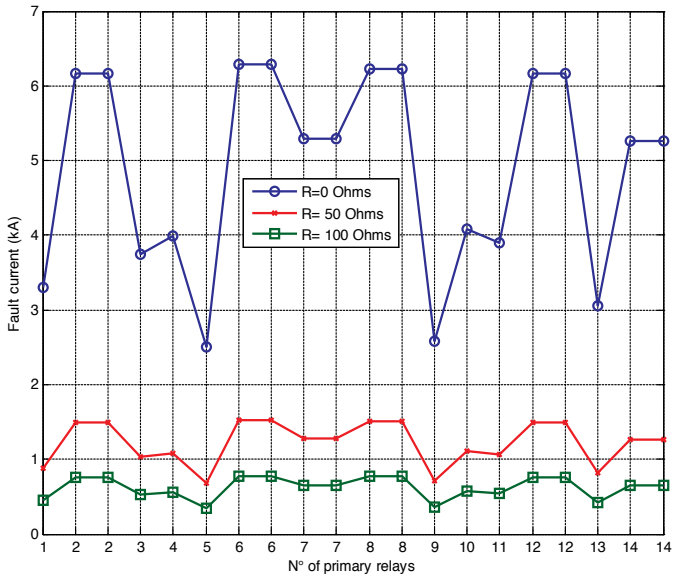

Figure 13. Impact of the resistance fault on the fault current seen by the primary relays.

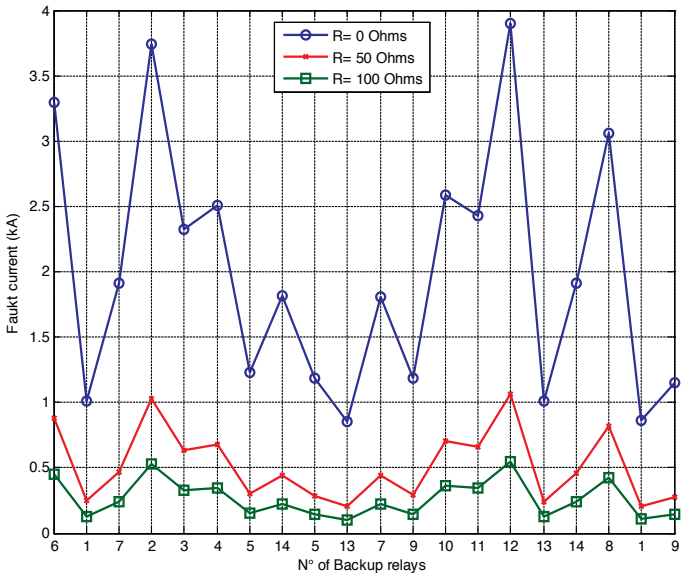

Figure 14. Impact of the resistance fault on the fault current seen by the backup relays.

Relay N°	TDS	Ip
1	0.4132	0.5000
2	0.6113	1.5295
3	0.6792	1.0000
4	0.3381	1.0000
5	0.1646	0.9359
6	0.6211	0.7714
7	0.3031	2.0000
8	0.4812	1.0000
9	0.1000	2.0000
10	0.3872	1.0000
11	0.7821	0.5000
12	0.5709	1.6259
13	0.1253	1.4088
14	0.5079	1.3422
F(s)	4.3061	

Table 9. Best relays coordination for original case.

Relay N°	Tipping time of primary relays		
	R=0 ohms	R=50 ohms	R=100 ohms
1	0.2109	0.8807	**2.0084**
2	0.5230	**2.6836**	**7.5977**
3	0.4092	**1.6822**	**3.9353**
4	0.2927	**1.2964**	**3.4265**
5	0.2185	**1.1053**	**4.0224**
6	0.2542	**1.1586**	**2.6065**
7	0.2637	**1.3760**	**3.9595**
8	0.2602	**1.2223**	**2.9093**
9	0.1907	**1.1218**	**9.8856**
10	0.3259	**1.4334**	**3.7415**
11	0.3350	**1.3409**	**2.9493**
12	0.5206	**2.7299**	**8.0524**
13	0.2099	**1.1958**	**6.9504**
14	0.2918	**1.3994**	**3.3963**
Number of violated constraints	0	**13**	**14**

Table 10. Tripping time of primary relays.

http://dx.doi.org/10.5772/59713

P/B pair N°	Coordinated Time Interval		
	R=0 ohms	R=50 ohms	R=100 ohms
1	0.2884	1.3530	3.7804
2	0.2296	2.6672	114.1085
3	0.2972	6.3218	**-23.6245**
4	0.4876	2.8730	14.3446
5	0.3861	1.8092	5.4007
6	0.2643	1.4061	6.0553
7	0.2411	5.5786	**-9.5662**
8	0.6642	5.3612	133.1309
9	0.2564	6.9035	**-10.2922**
10	0.8482	**-5.6759**	**-6.4129**
11	0.6183	9.6711	**-16.7506**
12	0.2367	**-15.2483**	**-5.4224**
13	0.3441	1.5755	0.2561
14	0.2228	0.9025	1.9734
15	0.5213	3.1167	15.9200
16	0.3327	**-8.8070**	**-10.7349**
17	0.3457	3.1992	57.8362
18	0.3424	1.5091	1.6920
19	0.6102	6.2420	**-51.9024**
20	0.2288	**-11.4226**	**-5.8192**
Number of violated constraints	0	**04**	**09**

Table 11. Coordinated time interval of P/B pair of relays

6.3.3. Impact of series compensation on overcurrent relay performances

In this section, the impact of series compensation on the overcurrent relays performances is presented. The relays performances are measured by checking the violation of the constraints represented by the primary relays tripping time and the CTI between the primary and backup relays. Three scenarios are considered in this study namely:

- Base case,
- SC=35%,
- SC=70%.

6.3.4. 3-bus test system

Table 12 presents the fault currents seen by the primary and backup relays in the 3-bus test system considering the series compensation of line 1-2. Figures 15 and 16 present the evolution of fault currents seen by the primary and backup relays respectively with respect to the series compensation ratio. From these figures, it is clear that the series compensation of line 1-2 has a great impact on the fault currents seen by the primary and backup relays, in such a way, when the compensation ratio increases; the impedance of the line decreases and therefore the fault current increases.

Table 13 presents the impact of the series compensation on the primary relays tripping time. From this table, we can observe that the tripping time of the primary relays for SC=35% and SC=70% satisfy the constraint presented in (6).

The CTI between the primary and the backup relays is presented in table 14. From this table, we can remark that the series compensation of line 1-2 causes a miss of coordination between the P/B relay pairs 3/1 and 6/2. Therefore, from the obtained results we can conclude that the series compensation of the power system has a great impact on the relays performances and causes a miss of coordination between the primary and the backup relays.

P/B pair N°	**PR**	**BR**	**Three phase fault current (kA)**					
	N°	**N°**	**R=0 ohms**		**SC=35%**		**SC=70%**	
			PR	**BR**	**PR**	**BR**	**PR**	**BR**
1	1	5	4.2336	0.6651	4.5655	0.6928	4.9407	0.7086
2	2	4	2.7391	1.1056	2.8561	1.1330	2.9656	1.1419
3	3	1	2.7929	1.1063	3.1028	1.4530	3.6611	2.0942
4	4	6	3.1340	0.9223	3.1161	0.9008	3.0896	0.8683
5	5	3	3.0325	0.9669	3.0500	0.9885	3.0760	1.0216
6	6	2	4.1044	0.6864	4.2338	0.8622	4.4401	1.1530

Table 12. Short circuit current of P/B relays of 3-bus test system.

Relay N°	Tipping time of primary relays		
	SC=0%	SC=35%	SC=70%
1	0.0846	0.0784	0.0723
2	0.0742	0.0711	0.0684
3	0.0974	0.0876	0.0742
4	0.1229	0.1237	0.1247
5	0.0666	0.0662	0.0656
6	0.0692	0.0669	0.0637
Number of violated constraints	0	0	0

Table 13. Tripping time of primary relays.

http://dx.doi.org/10.5772/59713

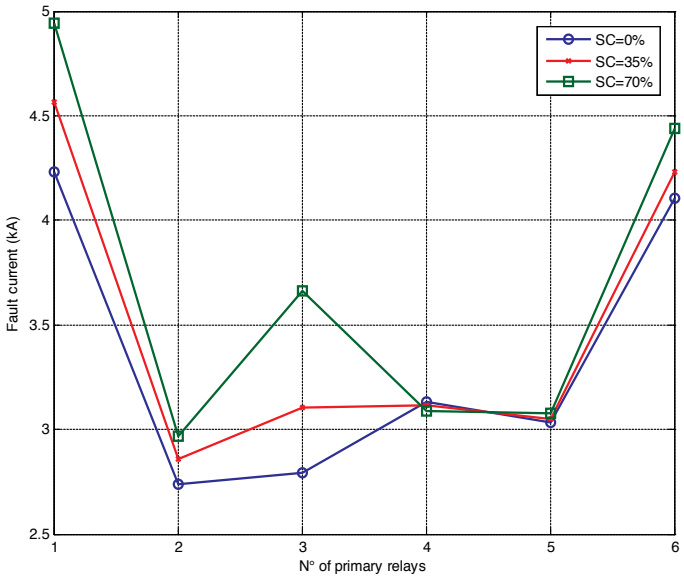

Figure 15. Impact of the series compensation on the fault current seen by the primary relays.

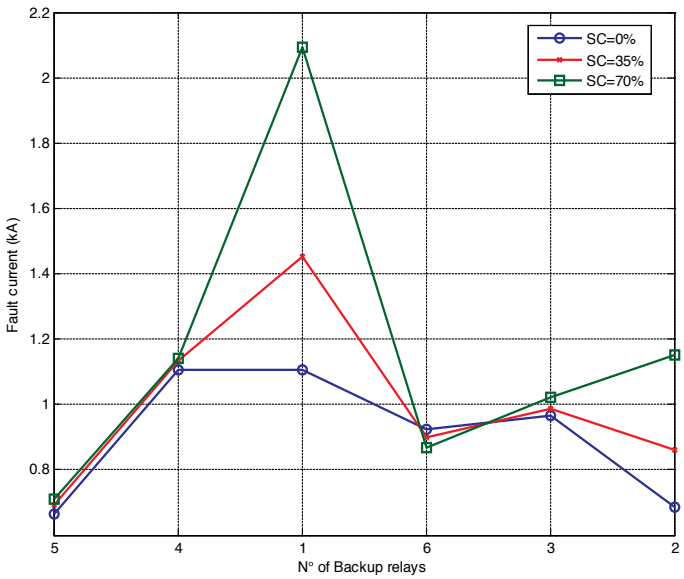

Figure 16. Impact of the series compensation on the fault current seen by the backup relays.

P/B pair N°	Coordinated Time Interval		
	SC=0%	SC=35%	SC=70%
1	0.2342	0.2269	0.2257
2	0.2863	0.2802	0.2800
3	0.2396	**0.1656**	**0.0993**
4	0.2509	0.2616	0.2793
5	0.2186	0.2126	0.2039
6	0.2402	**0.1763**	**0.1161**
Number of violated constraints	0	**02**	**02**

Table 14. Coordinated time interval of P/B pair of relays

6.3.5. 8-bus test system

Table 15 presents the fault currents seen by the primary and backup relays in the 8-bus test system considering the series compensation of line 1-6. Figures 17 and 18 present the evolution of fault currents seen by the primary and backup relays with respect to the series compensation percent, respectively. From these figures, it is clear that the series compensation of line 1-6 has a great impact on the fault currents seen by the primary and backup relays, in such a way, when the series compensation ratio increases; the impedance of the line decreases and therefore the fault current increases.

Table 16 presents the impact of the series compensation on the primary relays tripping time. From this table, we can observe that the tripping time of the primary relays for SC=35% and SC=70% satisfy the constraint presented in (6).

The CTI between the primary and backup relays is presented in table 17. From this table, we can observe that the series compensation of line 1-6 causes a miss of coordination between the P/B relays pairs 2/7 and 12/14. Thus, from the obtained results we can conclude that the power system series compensation has a great impact on the relays performances and causes a miss of coordination between the primary and the backup relays.

P/B pair N°	**PR No.**	**BR No.**	**Fault Current (kA)**					
			SC=0%		**SC=35%**		**SC=70%**	
			PR	**BR**	**PR**	**BR**	**PR**	**BR**
1	1	6	3.2946	3.2946	3.2825	3.2825	3.2646	3.2646
2	2	1	6.1594	1.0094	6.3396	0.7973	6.6124	0.4829
3	2	7	6.1594	1.9164	6.3396	2.3133	6.6124	2.9158
4	3	2	3.7450	3.7450	3.7951	3.7951	3.8692	3.8692
5	4	3	3.9830	2.3214	3.9762	2.3145	3.9662	2.3045
6	5	4	2.5088	2.5088	2.4577	2.4577	2.3821	2.3821

http://dx.doi.org/10.5772/59713

P/B pair N°	PR No.	BR No.	Fault Current (kA)					
			SC=0%		SC=35%		SC=70%	
			PR	BR	PR	BR	PR	BR
7	6	5	6.2928	1.2325	6.5653	1.1355	6.9768	0.9899
8	6	14	6.2928	1.8182	6.5653	2.1924	6.9768	2.7589
9	7	5	5.2856	1.1843	5.0740	1.1107	4.7174	0.9909
10	7	13	5.2856	0.8525	5.0740	0.6799	4.7174	0.4153
11	8	7	6.2321	1.8105	6.5026	2.1830	6.9111	2.7468
12	8	9	6.2321	1.1894	6.5026	1.0930	6.9111	0.9486
13	9	10	2.5859	2.5859	2.5384	2.5384	2.4681	2.4681
14	10	11	4.0891	2.4289	4.0860	2.4257	4.0812	2.4210
15	11	12	3.9026	3.9026	3.9592	3.9592	4.0429	4.0429
16	12	13	6.1670	1.0084	6.3472	0.7964	6.6200	0.4823
17	12	14	6.1670	1.9145	6.3472	2.3108	6.6200	2.9124
18	13	8	3.0631	3.0631	3.0340	3.0340	2.9912	2.9912
19	14	1	5.2615	0.8621	5.0469	0.6877	4.6861	0.4202
20	14	9	5.2615	1.1499	5.0469	1.0753	4.6861	0.9543

Table 15. Short circuit current of P/B relays of 8-bus test system.

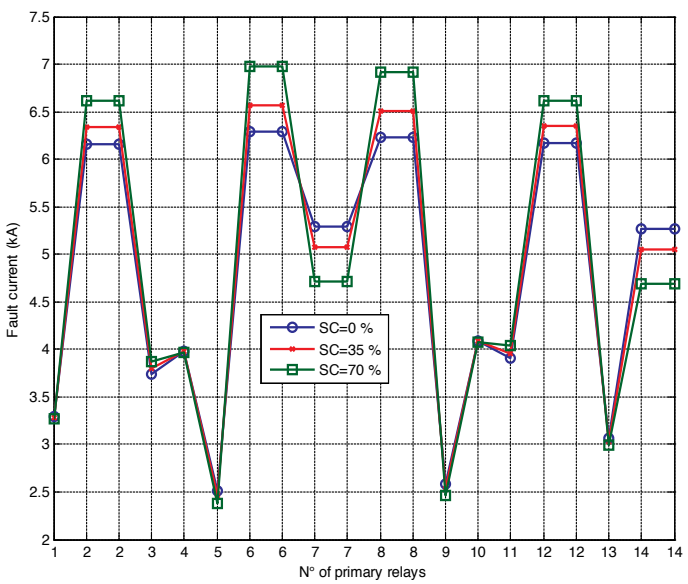

Figure 17. Impact of the series compensation on the fault current seen by the primary relays.

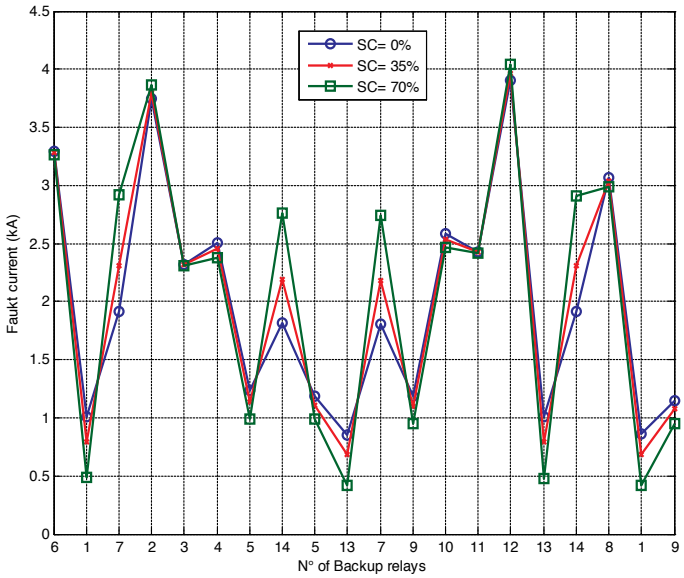

Figure 18. Impact of the series compensation on the fault current seen by the backup relays.

Relay N°	Tipping time of primary relays		
	SC=0%	SC=35%	SC=70%
1	0.2109	0.2117	0.2129
2	0.5230	0.5072	0.4851
3	0.4092	0.4036	0.3955
4	0.2927	0.2932	0.2940
5	0.2185	0.2235	0.2313
6	0.2542	0.2433	0.2286
7	0.2637	0.2754	0.2978
8	0.2602	0.2490	0.2337
9	0.1907	0.1947	0.2011
10	0.3259	0.3262	0.3266
11	0.3350	0.3300	0.3230
12	0.5206	0.5049	0.4828
13	0.2099	0.2122	0.2156
14	0.2918	0.3047	0.3293
Number of violated constraints	0	0	0

Table 16. Tripping time of primary relays.

http://dx.doi.org/10.5772/59713

P/B pair N°	Coordinated Time Interval		
	SC=0%	SC=35%	SC=70%
1	0.2884	0.2895	0.2912
2	0.2296	0.4811	1.3595
3	0.2972	**0.1497**	**0.0194**
4	0.4876	0.4801	0.4695
5	0.3861	0.3877	0.3901
6	0.2643	0.2704	0.2800
7	0.2411	0.3046	0.4236
8	0.6642	0.5013	0.3502
9	0.2564	0.2879	0.3536
10	0.8482	1.3979	7.1118
11	0.6183	0.4539	0.3058
12	0.2367	0.3099	0.4535
13	0.3441	0.3511	0.3619
14	0.2228	0.2233	0.2240
15	0.5213	0.5126	0.5004
16	0.3327	0.7431	3.4838
17	0.3457	**0.1976**	**0.0631**
18	0.3424	0.3459	0.3511
19	0.6102	0.8744	1.9005
20	0.2288	0.2672	0.3518
Number of violated constraints	**0**	02	02

Table 17. Coordinated time interval of P/B pair of relays

6.4. Intelligent coordination of overcurrent relays

In this section, we present the best relays setting and coordination obtained by the proposed BBO considering the impact of resistance fault and power system series compensation. The objective of this optimization is to minimize the relays tripping time and eliminate the miss of coordinated problem caused by the resistance fault and the power system series compensation. As mentioned above, the proposed BBO is able to manage both real (TDS, and Ip) and discrete decision variables (*RT*).

6.4.1. Considering resistance fault

6.4.1.1. 3-bus test system

Table 18 presents the best relays setting and coordination considering the impact of resistance fault. From this table, it is clear that the proposed BBO can find the optimal TDS, Ip, and characteristic type that minimize the relays tripping time and satisfy all the constraints presented in tables 19 and 20. Therefore, we can conclude that the proposed algorithm is able to eliminate the miss coordination problem caused by the resistance fault.

Relay N°	**R=50 ohms**			**R=100 ohms**		
	TDS	**Ip**	**RT**	**TDS**	**Ip**	**RT**
1	0.1523	0.9791	8	0.1000	1.2250	5
2	0.1118	1.5069	8	0.1193	0.7341	8
3	0.1876	1.0000	8	0.1148	0.7533	8
4	0.1495	0.8695	8	0.1000	1.1943	5
5	0.2327	0.8625	8	0.1683	0.6057	8
6	0.1665	0.7795	8	0.1000	0.7311	5
F(s)		0.315			0.38236	

Table 18. Best relays coordination for original case.

Relay N°	**Tipping time of primary relays**	
	R=50%	**R=100%**
1	0.0514	0.0788
2	0.0512	0.0506
3	0.0503	0.0505
4	0.0512	0.0843
5	0.0501	0.0501
6	0.0606	0.0681
Number of violated constraints	0	0

Table 19. Tripping time of primary relays.

http://dx.doi.org/10.5772/59713

P/B pair N°	Coordinated Time Interval	
	R=50%	R=100%
1	0.7577	1.1491
2	0.2088	0.2111
3	0.2970	0.2376
4	0.6592	0.2102
5	0.2151	0.3011
6	1.2068	1.1278
Number of violated constraints	0	0

Table 20. Coordinated time interval of P/B pair of relays

6.4.1.2. 8-bus test system

Table 21 presents the best relays setting and coordination considering the impact of resistance fault. Table 22 presents the primary relays tripping time, and table 22 presents the CTI of the P/B pairs of relays. From table 23, we can remark that the primary relays tripping time is within it limits. From table 23, we can observe that the P/B pairs of relays are fully coordinated in the case of R=50 ohms. However, we observe two miss of coordination of P/B relays pairs: 7/13 and 14/1.

Relay N°	R=50 ohms			R=100 ohms		
	TDS	Ip	RT	TDS	Ip	RT
1	0.1550	0.7097	5	0.1000	0.5000	5
2	0.2979	1.0000	8	0.2888	0.6186	7
3	0.1861	1.3632	7	0.5004	0.5578	5
4	0.3510	0.9479	5	0.2021	0.7796	5
5	0.1000	0.9103	5	0.1000	0.5000	5
6	0.3163	0.6700	8	0.1920	0.5000	7
7	0.1000	1.3611	8	0.1544	0.6021	7
8	0.1000	1.0000	8	0.2379	0.7194	5
9	0.1000	1.2983	5	0.1000	0.7310	5
10	0.1000	1.4484	6	0.1000	0.5239	7
11	0.1317	0.9083	8	0.1000	1.0000	5
12	0.2493	1.0000	8	0.1399	0.7696	7
13	0.1000	0.5000	8	0.1010	0.5118	5
14	0.2075	1.0000	8	0.1451	0.6137	8
F(s)		2.2552			2.51	

Table 21. Best relays coordination for original case.

Relay N°	Tipping time of primary relays	
	SC=35%	SC=70%
1	0.1141	0.0916
2	0.2582	0.3630
3	0.2620	0.3377
4	0.2722	0.2255
5	0.1082	0.1147
6	0.1388	0.1854
7	0.0974	0.1437
8	0.0847	0.1920
9	0.0998	0.1077
10	0.2297	0.1475
11	0.1785	0.1484
12	0.2171	0.2391
13	0.0744	0.1001
14	0.1201	0.1137
Number of violated constraints	0	0

Table 22. Tripping time of primary relays.

P/B pair N°	Coordinated Time Interval	
	SC=35%	SC=70%
1	0.2324	0.2864
2	0.2703	2.4238
3	0.5445	0.3043
4	0.2545	0.2808
5	0.3119	0.2447
6	0.2859	0.2861
7	0.2584	0.3280
8	0.7753	0.7886
9	0.3710	0.4957
10	1.3826	**-0.9511**
11	0.8413	0.5605
12	0.2906	0.3350
13	0.2731	0.2076
14	0.2374	0.2038
15	0.2281	0.2696
16	0.6947	7.3201
17	0.6013	0.6256

P/B pair N°	Coordinated Time Interval	
	SC=35%	SC=70%
18	0.2045	0.2281
19	0.8551	**-1.1394**
20	0.3123	0.5352
Number of violated constraints	0	02

Table 23. Coordinated time interval of P/B pair of relays

6.4.2. Considering series compensation

6.4.2.1. 3-bus test system

Table 24 presents the best relays setting and coordination considering the impact of the series compensation of line 1-2. Table 25 presents the primary relays tripping time. Table 26, presents the CTI of P/B relays. From these tables, we can observe that the proposed BBO find the best relays setting (TDS, Ip, characteristic curve) that minimize the relays tripping time and eliminate the miss of coordination caused by the impact of series compensation.

Relay N°	SC=35%			SC=70%		
	TDS	Ip	RT	TDS	Ip	RT
1	0.6487	1.0000	2	0.4918	1.4568	2
2	0.3760	1.0473	2	0.3649	1.4147	2
3	0.5507	1.0000	2	0.3821	1.3940	2
4	0.6244	1.6592	3	0.6449	1.6249	3
5	0.4558	0.9638	2	0.4119	1.0000	2
6	0.1000	1.8902	2	0.5901	1.8163	3
F(s)		0.46907			0.47048	

Table 24. Best relays coordination for original case.

Relay N°	Tipping time of primary relays	
	SC=35%	SC=70%
1	0.1166	0.1196
2	0.0756	0.0958
3	0.0971	0.0798
4	0.0510	0.0514
5	0.0788	0.0733
6	0.0500	0.0506
Number of violated constraints	0	0

Table 25. Tripping time of primary relays.

P/B pair N°	Coordinated Time Interval	
	SC=35%	SC=70%
1	0.2460	0.2131
2	0.3131	0.2830
3	0.2801	0.2094
4	0.2213	1.3087
5	0.2348	0.2245
6	0.2092	0.2036
Number of violated constraints	0	0

Table 26. Coordinated time interval of P/B pair of relays

6.4.2.2. 8-bus test system

Table 27 presents the best relays setting and coordination considering the impact of the series compensation of line 1-6. Table 28 presents the primary relays tripping time. Table 29, presents the CTI of P/B relays. From these tables, we can observe that the proposed BBO find the best relays setting (TDS, Ip, characteristic curve) that minimize the tripping time and eliminate the miss of coordination caused by the impact of series compensation.

Relay N°	SC=35%			SC=70%		
	TDS	Ip	RT	TDS	Ip	RT
1	0.2699	0.8473	8	0.2959	0.6785	8
2	0.6764	1.6191	3	0.4012	1.8342	3
3	0.3764	1.0000	2	0.3260	1.7588	3
4	0.3233	1.3192	3	0.3094	1.3517	3
5	0.2462	1.0000	8	0.2462	0.9938	8
6	0.4455	1.6548	3	0.3746	1.3334	3
7	0.6164	1.4758	3	0.5727	1.7551	3
8	0.5740	1.0000	3	0.3856	1.3088	3
9	0.2993	1.2410	3	0.2993	0.8069	3
10	0.4283	1.2532	3	0.2089	1.3065	3
11	0.4307	1.3304	3	0.3258	1.2470	3
12	0.4606	1.8140	3	0.4933	1.7360	3
13	0.2161	0.9550	8	0.2179	0.7803	8
14	0.5192	1.4616	3	0.7207	1.7408	3
F(s)		1.9368			1.6159	

Table 27. Best relays coordination for original case.

http://dx.doi.org/10.5772/59713

Relay N°	Tipping time of primary relays	
	SC=35%	SC=70%
1	0.0622	0.0568
2	0.2041	0.1429
3	0.2237	0.1387
4	0.1650	0.1667
5	0.0968	0.1003
6	0.1309	0.0632
7	0.1070	0.1629
8	0.0626	0.0639
9	0.1474	0.0657
10	0.1867	0.0992
11	0.2256	0.1436
12	0.1742	0.1569
13	0.0613	0.0507
14	0.0894	0.2044
Number of violated constraints	0	0

Table 28. Tripping time of primary relays.

P/B pair N°	SC=35%	SC=70%
1	0.4673	0.2339
2	0.3583	0.9637
3	0.3151	0.2861
4	0.3497	0.2822
5	0.2123	0.2281
6	0.3397	0.3675
7	0.2237	0.3947
8	0.3471	0.5305
9	0.2630	0.2940
10	0.7006	1.4320
11	0.5211	0.4201
12	0.7545	0.3880
13	0.3405	0.2085
14	0.4209	0.3052
15	0.2254	0.2800

P/B pair N°	SC=35%	SC=70%
16	0.4024	0.9605
17	0.2556	0.3753
18	0.2279	0.2933
19	0.6727	1.3062
20	0.7559	0.2420
Number of violated constraints	0	0

Table 29. Coordinated time interval of P/B pair of relays.

7. Conclusion

In this chapter, the overcurrent coordination problem in interconnected power systems has been formulated as non-linear constrained mixed integer optimization problem considering the impact of resistance fault and power system series compensation. The objective function is to minimize the total relays operating time with the optimal setting of real (TDS, and Ip) and integer (RT) decision variables. To solve this constrained mixed integer optimization problem, an improved Biogeography-based optimization (BBO) algorithm has been proposed. The BBO is validated on 3-bus, and 8-bus power test systems considering various scenarios related to the resistance fault and power system series compensation. The obtained results show that the resistance fault and the power system series compensation have a negative impact on the overcurrent relays performances in such a way increase the primary relays tripping time and cause the miss of coordination between the relays. Furthermore, it is concluded that the proposed BBO can solve, in almost the cases, the miss of coordination caused by the resistance fault the power system series compensation and therefore improve the energy efficiency of the power systems.

Appendix

Power systems test data

3-bus power system test data

Line	Vn (kV)	R (Ω)	X (Ω)	Y (S)	L (km)
1 - 2	69	5.5	22.85	0,0000	50
1 - 3	69	4.4	18.00	0,0000	40
3 - 4	69	7.6	27.00	0,0000	60

Table A.1. Line characteristics.

http://dx.doi.org/10.5772/59713

No.	Bus	Sn (MVA)	Vn (kV)	Xsc (%)
1	1	100	69	20
2	2	25	69	12
3	3	50	69	18

Table A.2. Generator data.

Relay N°	CT Ratio
1	300/5
2	200/5
3	200/5
4	300/5
5	200/5
6	400/5

Table A.3. Current Transformer Ratio.

8-bus power system test data

Line	Vn (kV)	R (Ω/km)	X (Ω/km)	Y (S/km)	L (km)
1 - 2	150	0,0040	0,0500	0,0000	100
1 - 3	150	0,0057	0,0714	0,0000	70
3 - 4	150	0,0050	0,0563	0,0000	80
4 - 5	150	0,0050	0,0450	0,0000	100
5 - 6	150	0,0045	0,0409	0,0000	110
2 - 6	150	0,0044	0,050	0,0000	90
1 - 6	150	0,0050	0,0500	0,0000	100

Table A.4. Line characteristics.

No.	Bus	Sn (MVA)	Vn (kV)	Xsc (%)
1	7	150	10	15
2	8	150	10	15

Table A.5. Generator data.

No.	Bus-Bus	Sn (MVA)	Vn.p (kV)	Vn.s (kV)	Xsc (%)
1	7 - 1	150	10	150	4
2	8 - 6	150	10	150	4

Table A.6. Transformer data.

Relay No.	In2 / In1	CT ration
1, 2, 4, 5, 6, 8, 10, 11, 12, 13	1200 / 5	240
3, 7, 9, 14	800 / 5	160

Table A.7. CT Ratio for 8-bus test system.

Author details

Rabah Benabid[1*] and Mohamed Boudour[2]

*Address all correspondence to: rabah_benabid@yahoo.fr

1 Electrical Engineering Department, CRNB, Ain oussera, Djelfa, Algeria

2 Laboratoire des Systèmes Electriques et Industriels (LSEI), Department of Electrical Engineering, USTHB, Algiers, Algeria

References

[1] A. Duchac, and M. Noel, "Disturbances in the European nuclear power plant safety related", Journal of Electrical Engineering, Vol. 62, pp. 173–180, 2011.

[2] Z. Moravej, M. Jazaeri, and M. Gholamzadeh, "Optimal coordination of distance and over-current relays in series compensated systems based on MAPSO", Energy Conversion and Management, Vol. 56, pp. 140–151, 2011.

[3] H. Zeienldin, E. F. El-Saadany, and M.A.A. Salama, "Novel problem formulation for directional overcurrent relay coordination", Large Engineering Systems Conference on Power Engineering, pp. 48–52, Canada, 28-30 July 2004.

[4] A.J. Urdaneta, H. Restrepo, S. Marquez, and J. Sanchez, "Coordination of directional overcurrent relay timing using linear programming", IEEE Transactions on Power Delivery, Vol. 11, pp.122–129, 1996.

[5] A.S. Noghabi, H.R. Mashhadi, and J. Sadeh, "Optimal coordination of directional overcurrent relays considering different network topologies using interval linear programming", IEEE Transactions on Power Delivery, Vol. 25, pp. 1348–1354, 2010.

[6] A.S. Braga, and J.T. Saraiva, "Coordination of directional overcurrent relays in meshed networks using the Simplex method", IEEE Mediterranean on Electrotechnical Conference (MELECON), pp. 1535–1538, 13-16 May 1996, Bari, Italy:

[7] P.P. Bedekar, S.R. Bhide, and V.S. Kale, "Optimum time coordination of overcurrent relays using two phase simplex method", Journal of World Academy of Science, Engineering and Technology, Vol. 28, pp. 1110–1114, 2009.

[8] D. Birla, R. Prakash, H. Om, K. Deep, and M. Thakur, "Application of random search technique in directional overcurrent relay coordination", International Journal of Emerging Electrical Power Systems, Vol. 7(1), pp. 1-14, 2006.

[9] R.M. Chabanloo, H.A. Abyaneh, S.S.H. Kamangar, and F. Razavi, "Optimal combined overcurrent and distance relays coordination incorporating intelligent overcurrent relays characteristic selection", IEEE Transactions on Power Delivery, Vol. 26(3), pp.1381-1391, 2011.

[10] P.P. Bedekar, and S.R. Bhide, "Optimum coordination of overcurrent relay timing using continuous genetic algorithm", Expert Systems with Applications, Vol. 38, pp. 11286-11292, 2011.

[11] A.S. Noghabi, J. Sadeh, and H.R. Mashhadi, "Considering different network topologies in optimal overcurrent relay coordination using a hybrid GA", IEEE Transactions on Power Delivery, Vol. 24(4), pp. 1857-1863, 2009.

[12] R. Thangaraj, T.R. Chelliah, and M. Pant, "Overcurrent relay coordination by differential evolution algorithm", IEEE International Conference on Power Electronics, Drives and Energy Systems (PEDES), Bengaluru-India, December16-19, 2012.

[13] R.Thangaraj, M. Pant, and K. Deep, "Optimal coordination of overcurrent relays using modified differential evolution algorithms", Engineering Applications of Artificial Intelligence, Vol. 23(5), pp. 820-829, 2010.

[14] T. Amraee, "Coordination of directional overcurrent relays using seeker algorithm", IEEE Transactions on Power Delivery, Vol. 27(3), pp. 1415-1422, 2012.

[15] M. Singh, B.K. Panigrahi, and A.R. Abhyankar, "Optimal coordination of directional overcurrent relays using teaching learning-based optimization (TLBO) algorithm", International Journal of Electrical Power and Energy Systems, Vol. 50, pp. 33-41, 2013.

[16] P.P. Bedekar and S.R. Bhide, "Optimum coordination of directional overcurrent relays using the hybrid GA-NLP approach", IEEE Transactions on Power Delivery, Vol. 26(1), pp. 109-119, 2011.

[17] J.A. Sueiro, E. Diaz-Dorado, E. Míguez, and J. Cidrás, "Ooordination of directional overcurrent relay using evolutionary algorithm and linear programming", International Journal of Electrical Power and Energy Systems, Vol. 42, pp. 299-305, 2012.

[18] R. Benabid, M. Boudour, and M. Abido, "Optimal location and setting of SVC and TCSC devices using non-dominated sorting particle swarm optimization", Electric Power Systems Research Journal, 79 (2009), pp. 1668-1677.

[19] R. Benabid, M. Boudour, and M. Abido, "Development of a new power injection model with embedded multi-control functions for static synchronous series compensator (SSSC)", IET Gener. Transm. Distrib., Vol. 6(7), pp. 680–692, 2012.

[20] Rabah Benabid, Mohamed Boudour, and Mohammad Ali Abido, "Optimization of UPFCs using hierarchical multi-objective optimization algorithms", Analog Integr Circ Sig Process, Vol. 69 pp. 91–102, 2011.

[21] R. Benabid, M. Zellagui, A. Chaghi, and M. Boudour, "Optimal coordination of IDMT directional overcurrent relays in the presence of series compensation using differential evolution algorithm", 3rd IEEE International Conference on Systems and Control, 29-31October 2013; Algiers, Algeria.

[22] R. Benabid, M. Zellagui, M. Boudour, and A. Chaghi, "Considering the Series Compensation in Optimal Coordination of Directional Overcurrent Protections using PSO Technique", IEEE Jordan Conference on Applied Electrical Engineering and Computing Technologies (AEECT), Amman-Jordan, 3-5 December 2013.

[23] D. Simon, "Biogeography-Based Optimization", IEEE Transactions on Evolutionary Computation, Vol. 12, No. 6, pp. 702-713, 2008.

Section 4

Energy Efficiency Improvements in Smart Grid Components - Recent Developments

Chapter 10

Recent Developments on Silicon Based Solar Cell Technologies and their Industrial Applications

Jiahe Chen

Additional information is available at the end of the chapter

http://dx.doi.org/10.5772/59171

1. Introduction

Solar energy is one of the most important alternative energy resources to the traditional fossil fuel energy. Since solar energy merely utilizes the solar radiation lights inducted from the sun, which are endless and available periodically to the earth planet, it is considered a renewable energy. It does not depend on the geographic location of the specific sources and is available everywhere in all countries in the planet. Since solar energy is completely natural, it is also considered a clean energy source. It does not disrupt the environment or create a threat to our eco-systems the way fossil fuel and some other energy sources might. It does not cause greenhouse gases, air or water pollution. With the development of solar technology in the past decades, solar energy becomes an economically affordable energy source and attracts more and more countries to include it in their national strategy for development.

There are several applications utilizing the solar energy, among which the photon thermal utilization and photovoltaic (PV) application are the most common applications. Photon thermal system generally converts the sunlight energy to thermal energy by collecting heats to the medium distributed within a structure or a district heating network. PV system is using the so called photovoltaic effect to convert sunlight energy into electricity. The energy conversion efficiency of a typical photon thermal system is around 28% while a typical PV system is around 18% in the current market. The utilization of photon thermal system normally requires complicate configuration in the system integration and is limited by the thermal consumption. PV system generating electricity can be used for direct residential and industrial utilization whose consumption is unlimited. Both photon thermal system and PV system require the conversion device to be positioned in the sunlight receiving surface, which is limited by the area of rooftop or land. Higher conversion efficiency of solar system is pursued in the market balancing the investment and the return.

In a PV system, the solar cells exercise the photovoltaic effect and determine the conversion efficiency of the whole system. Traditionally, semiconductor materials in the solar cell are doped to form P-N structure as an internal electric field. Among plenty of the semiconductor materials, silicon has a development history up to 50 years. The p-type (positive) silicon has the tendency to give up electrons and acquire holes while the n-type (negative) silicon accepts electrons. When sunlight hits the solar cell, the photons in light excite some of the electrons in silicon to become electron-hole (negative-positive) pairs. Under the internal electric field established in the P-N structure, these pairs are induced to separate. As a consequence, the electrons move to the negative electrode while the holes move to the positive electrode. If a conducting wire connects the negative electrode, the load and the positive electrode in series to form a circuit, an electric current is generated to supply the external load as a result. This is how the PV effect works in a solar cell.

Solar cells are assembled together to form solar modules, which can be arranged into arrays to form a so-called PV system that is large enough to function as a power station for industrial, commercial, and residential use. Through PV effect, the solar cells capture sunlight and turn it into direct current (DC) electricity. For off-grid PV system, the DC can be immediately used for the DC loads or the DC can be directed to an inverter, which converts DC into alternating current (AC) that is suitable for conventional electric appliances. In the off-grid system, the excess energy generated from the PV modules is usually stored in energy storage unit such as capacitors or batteries, controlled by charge controller, for use at night when there is no sunlight or when a larger energy consumption than generation is loaded. An optional backup power, such as diesel generator, can be installed if electricity from the energy storage unit runs out. For grid-tied system, DC electricity generated from the solar cells is converted into AC to be used on-site or stored for backup if the PV system includes energy storage unit. When there is more demand, power can be drawn from the tied grid. Excess supply of electricity from the PV modules can also be fed back into the grid after tuning the phases and frequency. This process of drawing and/or feeding electricity to the tied grid can be monitored by the solar production meter and the export/import meter.

Among all the components in a PV system, the solar cell that converts sunlight to electrical energy is considered to be the most critical device. Solar cell technology is thus deemed to be the most important sector in the solar industry for several decades. Increasing the conversion efficiency and reducing the cost of silicon based solar cells are the two mainstream trends in recent years. This paper attempts to briefly overview the developments in the fields of solar cell silicon materials, the emerging solar cell device architectures and the corresponding immerging silicon based solar cell manufacturing processes, especially from an industrial application point of view.

2. Traditional silicon material, cell structure and processes for silicon based solar cell

Silicon and some other semiconductor materials are the basic materials of solar energy. Today, about 90% of solar cells that installed globally are made from silicon. There are generally two

http://dx.doi.org/10.5772/59171

types of this semiconductor: monocrystalline (also called single crystal) silicon and multicrystalline silicon. Multicrystalline silicon is composed of a number of smaller silicon crystals.

Figure 1 shows a traditional manufacturing process from raw silicon (polycrystalline silicon) to final solar modules (also called solar panel) [1]. At first step, silica goes through carbothermic reduction process and forms the metallurgical grade silicon at a purity level of 2N-3N.The metallurgical grade silicon is then refined and subjected to the casting scratch process to become polysilicon raw materials at a purity level of around 6N. For growing the silicon crystals, polysilicon material is then introduced into two different production process for mono-crystalline silicon and multi-crystalline silicon production: monocrystalline silicon are generally produced with the Czochralski (CZ) method and multicrystalline silicon are commonly made with directional solidification methods (also called the brick casting method). The monocrystalline silicon ingot is then sliced into wafers. As for the multicrystalline silicon, the silicon brick is first diced into bars and then sliced into wafers [2]. The multiple crystals create boundaries for electrons resulting in less efficiency comparing to monocrystalline silicon. The difference in cell conversion efficiency between these two type silicon solar cell modules is typically 1.5-2% [2]. However, multicrystalline silicon can be produced at a lower cost than the mono-crystalline and it is used most in the solar industry. For traditional silicon based solar cells, the dopant in silicon is p-type (boron).

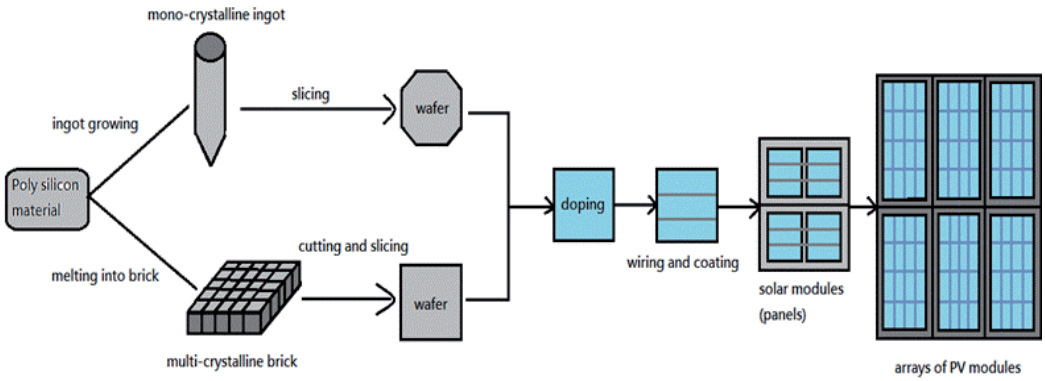

Figure 1. Traditional manufacturing process from raw polysilicon to the final solar module [2]

Compared to monocrystalline silicon, the surface of multicrystalline silicon wafer is more difficult to be passivated due to the existence of grain boundaries and the various grain crystallization orientations, which typically results in about 0.5% conversion efficiency loss. The crystallization defects in the bulk of multicrystalline silicon, such as grain boundaries and metal impurity contaminations, generate the carrier recombination centers and hence degrade the conversion efficiency further [3, 4]. However, ascribed to the low cost of crystallization, multicrystalline silicon wafers have gained more than 40% market share in the global solar market. The monocrystalline silicon wafer is popular especially in the rooftop applications due to its higher cell conversion efficiency per unit covering rooftop area.

Screen printing technology mainstreams the manufacturing processes for traditional silicon based solar cell. Figure 2 shows a structure and fabrication flow for a conventional screen printed solar cell [5]. Generally, the major processes in the common industrial screen printing technology include six core steps: texturing and surface cleaning, phosphorous doping diffusion to generate p-n junction, coating antireflection layer on the front side, printing aluminum paste on rear to form back side field (for metal impurity gettering, light reflection and rear passivation) and silver pastes on both sides, firing the printed pastes to form contacts to front emitter and rear base and isolating the emitter and base on cell edges. There are quite a few review papers covering the detailed description of the screen printing technology [6, 7].

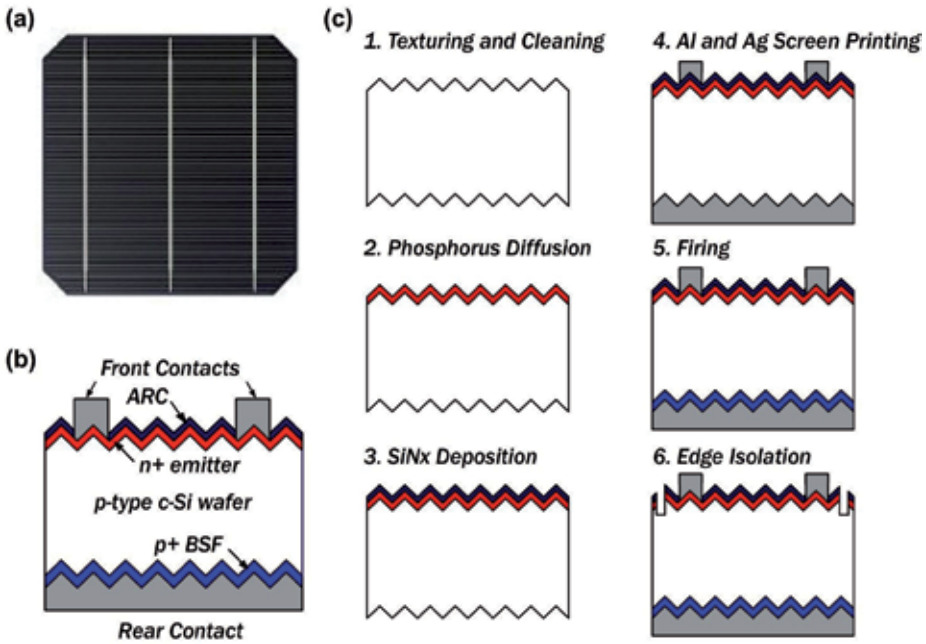

Figure 2. A structure and fabrication flow for a conventional screen printed solar cell. (a) A photo of a typical solar cell on a monocrystalline Si wafer. (b) Schematic diagram of the cross section of screen printed solar cell. (c) six core process flow steps which are used in manufacturing of basic screen printed cells. [5]

3. New developing silicon crystals and their challenges to the traditional silicon based solar cell processes

When the solar market demand shifts to the high efficiency side, to low down the preparation cost of material and improve the degradation resulted from the intrinsic and external defects are widely pursued in the silicon manufacturing industry. New silicon materials, such as cast-mono silicon, large-sized grain multicrystalline silicon and ultra-thin crystalline silicon are the representative silicon materials under development. Moreover, the n-type silicon material also

http://dx.doi.org/10.5772/59171

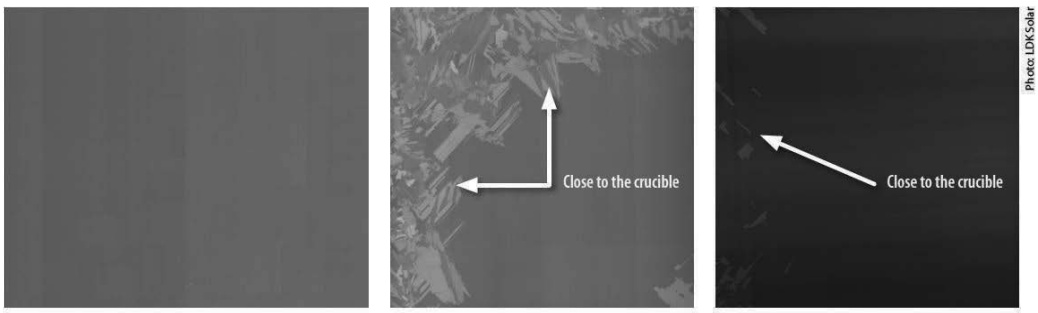

Figure 3. Image of silicon wafers with different categories of quasi-mono wafer sliced from the same ingot [8].

shows its growing tendency to be adopted as the solar cell substrate. Additionally, one shall note that recent market demands in the distributing PV system increases the market share of cells made from monocrystalline silicon steadily.

3.1. Quasi-monocrystalline silicon

The directional solidification method (also called casting method) was used to grow single crystals. The directional solidification system (DSS) furnace used for multicrystalline silicon production was originated from the heat exchange method (HEM) furnace for single crystals of sapphire. The growth of single crystal silicon with the directional solidification (or casting) method and the application of the resulting mono (or quasi-mono) silicon wafers for solar cells was also carried out by numerous researchers since 1987, implemented in large scale pilot application since 2006 and attracted the interests from industrial applications since 2011 [8]. Quasi-monocrystalline silicon is casted with the common crystal growth furnaces for multi-crystalline silicon. There are two casting approaches for obtaining the quasi-mono-crystalline silicon ingots, one is cast with the pre-grown seeds (cast-on-seed) and the other is to cast the ingot without seeding (seedless casting).

Casting ingot with seeds has been successfully commercialized. The major difference in the cast-on-seed process of growing the quasi-monocrystalline silicon ingots, compared to the growth process of multicrystalline silicon ingots, is that a layer of monocrystalline silicon seeds are employed on the surface of the bottom side of the crucible [9]. These seeds are usually sliced from the monocrystalline silicon ingot grown with the CZ method. Silicon feedstock and dopants are then loaded on top of the seed. In the process of melting, the silicon feedstock is controlled to start the melting from the top so that the seeds will not be completely melted. In the process of solidification, the silicon melt starts to nucleate on the remaining seeds and the grown crystal follows the orientation of the seeds and gradually form a large ingot consisting of crystals with some sections having multiple grains, especially in the areas close to the crucible and between the seeds. As a result, the ingot is with large single crystalline grains present in the center while plenty of small-sized grain exists in the edge regions of the same ingot. Figure 3 shows the image of silicon wafers with different categories of quasi-mono wafer sliced from the same ingot. [8]

Quasi-mono crystalline silicon can also be obtained without the pre-arranged CZ seeds. However, the challenges rely on a more precise control of the temperature distribution gradient in the silicon liquid as well as the solidification speed of the crystal ingot. In principle, a smoother temperature distribution gradient as well as a slower but steady solidification speed is beneficial for coarsening the grain sizes and in turn reduces the grain boundaries in the casted ingot, which can form the large grain multicrystalline crystal and eventually form quasi-mono crystal if the nucleation sites during solidification process are controlled ideally. Using such approaches to obtain quasi-mono crystal is still under early stage of development whereas using the principle to grow the large grain multicrystalline silicon has been adopted in practice. The electrical behavior of multicrystalline silicon is shown to be influenced by the properties of the grain boundaries, the study of the grain boundaries is very important for improving the efficiency of multicrystalline silicon solar cells over decades. Improving the thermal filed control through some simple retrofits on the traditional casting furnaces can form a multicrytalline silicon ingot with the large grains sizing up to 120-220mm. In such ingot, the amount of grain boundaries are greatly reduced compared to the common multicrystalline silicon ingot whose grain sizes are typically few millimeters [10].

Compared to the CZ monocrystalline, the small angle sub-grain boundaries originating from the gap of the seeds can be observed from the centered quasi-monocrystalline silicon, which increases the recombination of carriers. Nevertheless, the oxygen content of quasi-mono is less than that of mono-crystalline silicon, which reduces the effect of light induced degradation of quasi-mono solar cells. In such a way, the cell efficiency made from quasi-mono wafers with large percentage of quasi-mono grain is comparable to the mono wafers. However, for the quasi-mono wafer with low percentage of quasi-mono grains, the dislocation density, the concentration of oxygen and carbon, and the impurity made the efficiency obviously lower than that of a high percentage of large quasi-mono grains. The properties of the silicon wafers sliced from the edge regions of quasi-mono crystalline ingot are closed to the common multicrystalline silicon wafers. Typically, if the efficiency of a mono silicon cell is 18.5%, the efficiency of a quasi-mono silicon solar cell with a high large single grain percentage can reach about 17.5 to 18.2%. But for low single grain percentage quasi-mono silicon solar cells, the efficiency can be as low as about 16.6 to 17.0%. [8]

The major challenge that quasi-monocrytalline silicon materials brought to the common solar cell processing is mainly the texturing compatibility. In general, for different percentages of large grains of the quasi-mono wafer, different texturing processes should be selected, so as to minimize the textured surface reflectivity and in turn maximize the solar cell conversion efficiency. Typically, the alkali texturing process can be applied to the quasi-mono wafers with mono grain or large percentage of mono grain, so that the light reflection on the solar cell surface can be greatly reduced. For the large quasi-mono grain, alkali texturing can form an inverted pyramid texture surface, similar as the mono crystalline wafers, and improve the efficiency of the solar cell. But due to the anisotropic etching of alkaline, the pyramids that form on the other grains with an orientation different from that of the large quasi-mono grain will have a different structure and orientation. This area has a different reflectivity for the induced light and exhibits different colors from that of the large quasi-mono grain. For a quasi-

http://dx.doi.org/10.5772/59171

mono wafer with low percentage of large quasi-mono grains, acid texturing can be applied similar to that for multi silicon wafers [10]. Some compensated texturing processes comprising multiple-step alkaline and acid texturing as well as adopting specific additives in the wet-chemical solutions are also developed [11].

3.2. N type silicon

The very first solar cell, fabricated in 1954 in the Bell Labs, was made of a monocrystalline n-type Si wafer. However, the main industrial application of solar cell was for space applications like satellites until the 1980s. Because the p-type silicon was proved to be less sensitive to the degradation caused by exposure to cosmic rays, such as high-energy particles (protons and electrons), all industrial solar cell development was based on p-type silicon for decades. Since past decade, n-type (mainly phosphorus-doped) silicon material and related cell processes for the territorial application starts to attract a lot of attentions from the scientific researchers.

Compared to standard p-type (boron-doped) silicon solar cells, n-type silicon solar cells feature two important advantages. In one aspect, n-type silicon does not suffer from light induced degradation caused by the simultaneous presence of boron and oxygen (B-O pairs) in the wafers, a phenomenon that in standard p-type silicon solar cells leads to a reduction of the module power output by usually 2-3% within the first few weeks of installation. In another aspect, n-type silicon wafers are less sensitive to metal impurities that are usually present in the silicon feedstock and less effort has to be made to obtain n-type silicon wafers with a high electronic quality. In addition, the performance at low light intensities is predicted to be higher for n-type solar cells, as the lifetime increases in contrary to p-type cells [12], thus enabling an increased power output averaged over the year. As a consequence, n-type silicon wafers featuring high solar cell efficiency potential can be produced more cost effectively than the high quality p-type silicon wafers.

Although the n-type silicon has not yet been studied exhaustively, the industrial applications of n-type silicon have been pushed by the market. Very high quality monocrystalline n-type ingot can be pulled via CZ pulling method and the n-type wafers featuring a high diffusion length of the charge carriers can be manufactured in a routine industrial process used for p-type silicon. However, the challenge of n-type (phosphorus-doped) silicon material is, compared to the standard p-type (boron-doped) silicon, the poor homogeneity of the electrical properties throughout the height of the silicon ingot ascribed to the low segregation coefficient of phosphorus (0.35) compared to boron (0.8) dopant in the silicon liquid during solidification [13]. For instance, for boron doping, a range between 1-3 ohm.cm can be easily maintained throughout the height of whole ingot, while in the case of phosphorus doping, this range increases to 3-12 ohm.cm or more. As standard solar cell concepts require a narrow resistivity distribution to allow stable efficiencies for mass wafers from same ingot, the large variation of the resistivity of n-type silicon ingot decreases the yield for solar cell production thus increasing overall production costs. One solution is to develop new solar cell structures that are less sensitive to the base resistivity; however, a more feasible solution is the application of ingot growth techniques based on the continuous feeding of Si feedstock. Such continuous CZ-

pulling technologies can result in a better homogeneous and higher quality electrical properties distribution in the n-type silicon ingot and are currently under development.

The adoption of n-type silicon as the solar cell substrate also brings several challenges to the industrial processes established for traditional p-type solar cell. There are quite a lot of academic and industrial groups working on developing the n type cell technologies in various manufacturing processes, among which the aluminium rear emitter, passivation for p+surface and the metallization are three of the key fields. However, besides the improvements in solar cell technology, it is also necessary to advance the modules, in order not to lose the benefit of the enhanced performance of the cells. The most important topics besides material savings are the improvement or replacement of the absorbing EVA by silicones and the replacement of soldering by gluing techniques which will not be discussed herein.

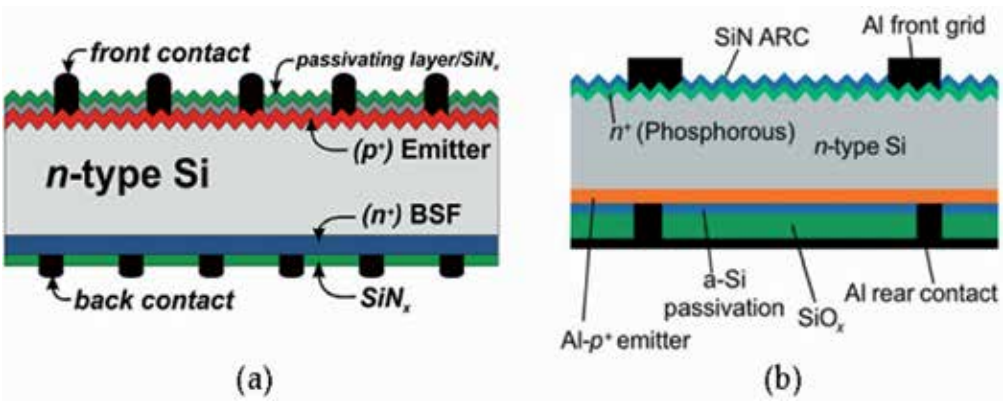

Figure 4. Two schematic cross-section of typical concept of n-type silicon based solar cells. (a) a fabricated n-type solar cells with front emitter [14]. (b) with screen printed rear Al-p+ emitter, full-area metalized a-Si passivated emitter and with local point contacts [15].

The most essential process for good processing of advanced n-type solar cells is the creation of a homogeneous and adapted p+ emitter. Figure 4 shows a typical n-type solar cell. [15] The rear p+ emitter is usually generated by the recrystallization process forming an Al-doped region [16]. In the more advanced solar cell structures, such as HIT concept, a boron-doped emitter is formed by the growth of an amorphous, boron-doped thin layer. Intrinsic and doped amorphous silicon layers are deposited at low temperatures on the front for the emitter (silane and diborane) and on the rear for back surface field creation (silane and phosphine) [17]. In such process, the cleanliness of the surface before amorphous silicon layer depositions is extremely important and several wet chemical processes are developed, for example, Piranha cleaning of H_2O_2/H_2SO_4 and HF/O_3 cleaning. Low temperature (<200°C) screen printing pastes also has to be used for such process since these layers are not stable against high temperatures above 300-400°C. Furthermore, boron-doped emitter for n-type silicon can be also realized by

the high temperature tube diffusion process using boron containing dopants as well as by ion implantation followed by thermal recrystallization anneal process [18].

However, the silicon nitride (SiN_x) layer formed by plasma enhanced chemical vapor deposition (PECVD) that widely used for passivating the n+surface of p-type silicon not only has no passivating effect but even deteriorates the surface passivation with respect to an unpassivated surface for boron-doped p+ emitter of a n-type cell. The efficient passivation material for n-type silicon includes, a stack consisted of a thin thermal SiO_2 (formed by anneal processing at a short process time and a low temperature), a PECVD SiNx layer and an aluminum oxide (Al_2O_3) layer deposited either by atomic layer deposition technology or PECVD. A stack of boron silicate glass (BSG) and PECVD SiN_x is also proposed [19]. Such stack has the advantage that no additional equipment is needed as the BSG is already formed during the formation of the boron emitter and the SiN_x requires only standard PECVD equipment as used in p-type cell production lines.

The classical screen printing process can be applied for n-type cell, however, the pastes have to be modified. As low temperature firing is preferred for the n-type cell and p+ surfaces have to be contacted, a simple Ag paste for p-type cell is not suitable. A silver aluminium (AgAl) paste is used and optimized. The aluminium (Al) in the paste allows a good contact resistance, reduces conductivity strongly and limits the open circuit voltage due to penetration into the space charge region, a substitute of Al in the paste is seeking. Additionally, other screen printed products such as diffusion pastes, diffusion barriers, etching and isolation pastes are gaining more and more importance for advanced cell concepts [18]. Furthermore, the tabbing of Al ribbons to interconnect neighbouring solar cells shall be more careful for n-type cell because the devices will be shunted completed if the AgAl emitter contacts contact the n-type base directly [16].

3.3. Kerfless ultra-thin crystalline silicon

In the 1980s, silicon based solar cells are made on crystalline silicon wafers with typically 400 micron thick, where the silicon material cost corresponds to a large fraction of the total cost of a final solar module. The wafers thickness has been significantly decreased from 400 micron to 200 micron while the cell's surface has increased from 100 cm^2 to 240 cm^2 between 1990 and 2006 [20]. Advanced solar cells were fabricated on wafers as thin as 140 um, resulting to efficiencies higher than 20% in 2006 [21]. Current silicon wafer thickness used for traditional silicon based solar cell is in the 150 micron range.

The development work on the ultra-thin silicon substrate was stimulated by the very high price of raw polysilicon materials. In 2008, the cost of silicon wafer accounted for more than 30% of a PV module cost with approximately 60% of the wafer cost coming from ingot growth and wafering. Additionally, the silicon wafer manufacturing consumed the major fraction of energies used to produce PV modules thus in turn increases the energy payback time. However, the price of polysilicon reduced from $400/kg in 2008 to a price as low as $30/kg in 2013 with the rapid expansion of manufacturing capacity primarily in China and Korea since 2010. Therefore, the advantages of kerfless approaches for reducing the silicon material cost were leveled to a big extent while most manufacturers have failed to scale their technologies

and compete with competitors who produce the substrates based on traditional ingot casting and wire sawing. Nevertheless, the use of thin substrate for reducing the consumption of silicon is till of interest for manufacturing high efficiency solar cells based on n-type CZ silicon presently because the n-type silicon material can be up to three times more expensive than the p-type material. However, the cost of n-type wafers may drop as the industry already shows a trend to shift towards n-type technology and some developing advanced ingot growing technologies, such as continuous CZ and magnetic CZ, will be available to a larger number of manufacturers in the near future.

Thinning the wafer can be beneficial for two reasons: reduce the consumption of expensive silicon and gain a higher open circuit voltage in the cell. Instead of wire sawing, lifting off thin wafers from a crystalline substrate could potentially reduce crystalline silicon material lost to kerf, which is usually 120-180 micron thick. Epitaxial growth the crystalline silicon could also potentially provide cost reduction since in this approach the substrates are obtained directly from silane bypassing the growth of polysilicon and pulling CZ silicon ingots. The challenge to produce ultra-thin crystalline silicon solar cells consists of three major tasks: the growth of a high quality large-grained crystalline silicon layer on inexpensive substrate, the incorporation of some light trapping scheme to compensate for the weak near-infrared absorption of crystalline silicon and effective passivation of grain boundaries and surfaces.

In the material preparation level, various approaches to manufacturing the kerfless ultra-thin silicon wafers are developed, among which the two main technologies are ion implantation followed by cleaving [22] and epitaxial growth followed by a lift off [23]. Several lifting off process are developed, including epitaxial growth of silicon film on dissolvable CaF_2 to fabricate the textured monocrystalline silicon film [24, 25], epitaxial growth of silicon on a preformed porous silicon layer as the lifting-off buffer layer [26] and the so-called perforated silicon process [27].

In the solar cell level, two critical requirements in achieving high efficiency on the ultra-thin silicon wafer are advance IR light trapping and very good surface passivation [28]. Light trapping in the ultra-thin monocrystalline silicon cells is important because the optical path length of the IR photons may reach the cell substrate several hundreds of microns. These photons may escape the device after multiple internal reflections through the front surface, thus reducing generation current. Very good surface passivation is also important since the contribution of surface recombination in overall recombination losses increases in the ultra-thin silicon cells and the moderately passivated surfaces may pull the efficiency down.

The basic idea of producing kerfless ultrathin crystalline silicon is to eliminate saws, furnaces, and cell finishing equipment as well as slurry and thick wafers. An ion implant machine is also proposed to replace the diffusion equipment in the commercial production chain. However, whether the new process fits seamlessly into the production flow with little impact on the wafer handling, interconnection, packaging and reliability have not been proven at a full production level. Therefore, developing a new wafer technology and integrating it into an existing process chain remains an enormous challenge [29].

http://dx.doi.org/10.5772/59171

4. Immerging architectures of high efficiency silicon based solar cells and their realization processes

Solar cell is an energy conversion device using the photovoltaic effect, which is basically a device separating the electron and hole in a semiconductor material and typically a p-n junction. However, the modern silicon based solar cell is not a device consisting of a single p-n junction as it was born any more. Thanks to the well-established semiconductor manufacturing technology, wet chemical processing, low cost thin film coating, chemical lithography as well as the laser patterning technologies keep attracting the attentions from of the solar industry globally. Surface structure optimization and better surface passivation both on the light induction front side and the rear side are developed in the past years. The deeper understanding of the device physics and specific material properties, solar cell architectures become more and more complicated. PERC/PERL, MWT/EWT, PHASHA, IBC and SHJ/HIT type solar cells structures are under development in the industry, which would increases the solar conversion efficiency gradually in the next few years.

4.1. Front emitter optimization: selective emitter

As it is shown in Figure 2(b), the most commonly used silicon based solar cell architecture is a planar diode structure, where a thin layer of heavily doped silicon (often called emitter, typically n+) is present at the front surface of a moderately doped wafer of the opposite type (often called base, typically p-type). The emitter area is the region that emits or injects most of the charge carriers under dark operation. In the current standard solar cell manufacturing process, the emitter is formed by in-diffusion at high temperature of an n-type dopant (typically phosphorous) into the surface region of a p-type wafer (typically doped with boron). Besides diffusion, the emitter can also be formed by exploiting ion implantation and/or epitaxy technologies.

A good emitter shall efficiently collect the photo-generated carriers in the emitter region, induce a low-loss lateral transport of the majority carriers from the location where they are collected to the nearby metal contacted region and maximize the output voltage with an optimum doping concentration [30]. In industrial practice, the best emitter is a very thin but heavy doped layer. In the very thin emitter, the photon-generated carriers can be collected from the depletion region as well as the moderately doped base underneath the emitter. The extremely high doping concentration at the surface reduces the contract resistance meanwhile act as a sink for metallic impurity gettering [31]. However, the further optimization of the homogeneous emitter approach requires the development of the printable pastes that can contact the emitters with higher sheet resistance which is a challenge to the front silver paste suppliers. A typical doping of 50 ohm/square on the front side of today's industrial type solar cells is therefore a compromise between the emitter performance and sufficiently low contact resistance.

Selective emitter is developed to overcome the above compromise. The selective emitter structure is normally formed by heavily doped the regions underneath the contact grid and by lightly doped in the light illuminated area at the same time. Figure 5 shows a selective

emitter that is a heavily doped region placed directly under the metal line [32]. Such selective doping regime leads to a reduced contact resistance and lower Auger-and SRH recombination and therefore results in an improved blue response and a higher open circuit voltage. Several selective emitter technologies have been developed in the past few years. Among which, the etch-back emitter, inline selective emitter, laser doping and doped silicon ink are successfully commercialized in industrial mass production.

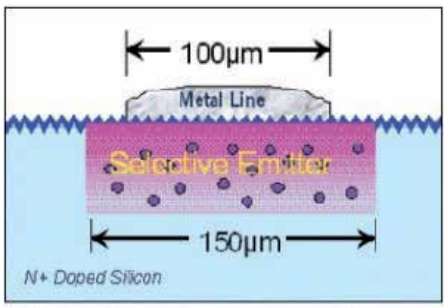

Figure 5. The selective emitter is a heavily-doped region placed directly under the metal line [32].

The etch-back process can be realized with highly homogeneous doping on large area wafers and followed by removing the porous silicon in a wet-chemical solution. The etch-back process in combination with a masking step is an industrially feasible scheme to form a selective emitter structure on p-type wafers. By changing the initial $POCl_3$ diffusion to 20 ohm/square and etching back to 95 ohm/square, a maximum efficiency of a selective emitter solar cell was measured to 19.0% [33].

An inline diffusion process can be realized by coating the wafer surfaces with a defined amount of phosphorus containing dopant with a doper before being laterally transported through a conveyor belt furnace in a controlled ambient at standard pressures. Applying inline selective emitter concept, an increase in open circuit voltage by 18.6 mV and an increase in short circuit current by 1.2 mA/cm^2 were obtained followed by an average efficiency gain of 1.4% and a fill factor improvement by 1.3% compared to homogeneous inline emitters [34].

A laser doping process can be realized by scanning the surface of lightly doped wafers so as to melt the wafer surface locally and enables the fast incorporation of phosphorus atoms from the PSG-layer to form a highly doped selective emitter by recrystallisation. Such process can generate an emitter as thin as 800nm within a few hundred nanoseconds and the emitter will not incorporate any grain boundaries and dislocations. An efficiency gain of 0.5% absolute is reported by adopting such laser doping process [35].

A silicon ink doping process to generate the selective emitter is also commercialised. Such process can be realized by printing the highly doped silicon nano-particles onto the silicon wafer surface prior to the common phosphorous diffusion. The ink is printed only in the areas where the screen-printed front contact is located afterwards. During the following doping diffusion step, a lightly doped emitter (for example 80-100 ohm/square) is realized in the

uncovered areas whereas a highly doped areas (for example 30-50 ohm/square) is formed and serves for electrode contacting [36].

4.2. Wafer surface passivation: dielectric materials

Coating a cost-effective antireflection layer is an important step during silicon-based solar cell fabrication. Ideally, the coating should not only reduce optical losses but simultaneously provide a reasonable degree of surface passivation and, for multicrystalline silicon material, a hydrogen passivation of bulk defects and /or grain boundaries. Thermal SiO_2 is one of the obvious candidates for the surface passivation of both n-and p-type silicon of arbitrary doping level and is used in the record-efficiency passivated emitter and the rear locally diffused (PERL) crystalline silicon solar cell [37]. However, the use of a high quality thermal oxide would lead to a high cost of ownership, and the high oxidation temperature may degrade the crystalline silicon bulk quality. Many alternatives based on low-temperature processes therefore receive currently strong research interest, including PECVD, rapid thermal oxidation and electro-chemical oxidation [38] Meanwhile, alternative novel dielectric materials, such as SiN_x, SiC_x, SiON and Al_2O_3 are being investigated [39].

SiN_x fabricated by PECVD is increasingly used in industry as it offers the possibility to fabricate a surface and bulk passivating antireflection coating at low temperature (≤450°C) and becomes the most promising candidate for p-type silicon wafers [40]. Recently, eexcellent surface passivation of silicon wafers has been achieved by about 30 nm thick Al_2O_3 layer prepared by plasma-assisted atomic layer deposition (ALD), yielding effective surface recombination velocities of 2 and 13 cm/s on low resistivity n-and p-type silicon, respectively. These results are comparable to the solar cells employing thermal oxide as used in record-efficiency solar cells [39]. Al_2O_3 layer also demonstrated a better UV stability than thermal SiO_2 with the surface passivation improving during UV irradiation [41].

Bi-layer antireflection coatings on the front side have significant advantages over single-layer antireflection coatings due to their broad-range coverage of the solar spectrum. For example, a solar cell with 60 nm / 20 nm SiN_X:H double stack coatings has 17.8% efficiency, while that with a 80 nm SiNX:H single coating has merely 17.2% efficiency. The improvement of the efficiency is due to the effect of better passivation and better antireflection of the stack of antireflection bilayer coating. The double stack antireflection coating is also stable against external stress, which is beneficial for the fabrication of solar module. [42] Bi-layer schemes with different dielectric materials, like SiO_2 capped with SiN_x, have also been explored [43].

Recently, the dielectric rear side passivation of crystalline silicon solar cells has expanded from small lab-scale cells to industrial production. One major advantage of using dielectric passivation instead of a full area Al back surface field is the substantial gain in short circuit current density. A major contribution of this gain stems from the enhanced reflectivity of the rear side of 90-95% at 1000 nm compared to 65% common for fully Al alloyed rear sides in the solar spectrum [44].

Figure 6 depicts the working principle of the solar cell with a rear passivation coating layer [45]. The introduction of backside passivation increases cell efficiency in two ways. Firstly, the

backside passivation layer reflects light that has travelled through the cell without generating electrons and reached the backside. The reflected light will pass through the cell a second time generating additional current. Secondly, the layer passivates the crystal matrix defects associated with the back surface of the silicon wafer better than a conventional cell. As a consequence, the electrons generated near the backside of the cell are less likely to be captured and lost. They will have a higher probability of reaching the interface between the base and emitter contributing to the current of the cell improving the cell output voltage. Since blue light will generate more electrons near the front of the cell whereas red light will generate electrons at the back of the cell or even pass the wafer without generating electrons, backside passivation increases the sensitivity of the cell to infrared light with a wavelength of between 1000 and 1180 nm. This additional sensitivity will result in an increased current and in the efficiency of the solar cell.

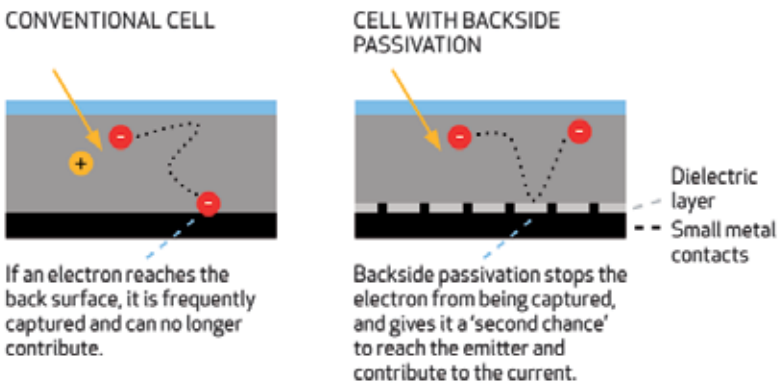

Figure 6. Backside passivation prevents electrons from being captured by the rear surface, resulting in an increased current and voltage of the cell. [45]

Most development efforts are geared towards an evolutionary approach, where the prevailing metallization by means of screen printing and co-firing of thick film paste is retained and the deposition and structuring of the dielectrics is merely added into an already established process [46]. In industrial practise, laser ablation of the dielectric layer for opening the contact channels has been employed on the rear side before printing AgAl paste for contacting the base while some innovative firing through pastes without opening the dielectric layer are also under development.

4.3. Cell structure innovation: Advanced architectures

High efficiency solar cell technologies that can replace screen printed cells in large volume manufacturing in the next 5-10 years are under development. The mainstream high efficiency technologies are passivated emitter and rear cell structure (PERC) or PERL solar cell, metal warp through (MWT) or emitter warp through (EWT) solar cell, bifacial cell with passivated

http://dx.doi.org/10.5772/59171

diffusion at the rear (PASHA cell), interdigitated back contact (IBC) solar cell and silicon hetero-junction (SHJ, also known as HIT cells which is a brand name by Panasonic) solar cell.

MWT/EWT technology has been regarded as industrially promising recently because of its high cost-effectiveness for increasing cell and module efficiency [47, 48]. In the MWT/EWT cells, the front metal grids or the front emitter will be wrapped through the laser opened via-holes to the rear side of the wafer inducing reduced shading losses, and reduced surface recombination, and as a result the cell efficiency will be improved [49]. Isolation between emitter and base region is required for MWT cells while the emitter formation on the via-holes is required for EWT cells. Figure 7 shows the cross-section structure of the MWT cells on the top and the EWT cells on the bottom, where the EWT cell is free of contact strips on the front surface [50]. On the MWT/EWT module level, the full back interconnection of the cells results in lower cell-to-module loss thanks to avoiding much of the resistive loss existing in the normal double-side interconnection of H-pattern solar cells with tabs [51]. MWT techniques can be used for commercial solar cells mainly focus on the p-type solar cells as well as n-type materials [52] and is successfully put into mass production.

The structures of the solar cells representing other four main high efficiency technologies are illustrated in Figure 8 [5]. In PERC cells (device a), the efficiency improvement is mainly due to the increase of open circuit voltage which is achieved by replacing a continuous Al BSF with the dielectric passivation layer having the local Al BSF [37]. Additionally, the front surface usually has a higher sheet resistance emitter, with or without higher doping underneath metal contacts (selective emitter), which is usually passivated by thermal SiO_2 and/or AlO_x layers.

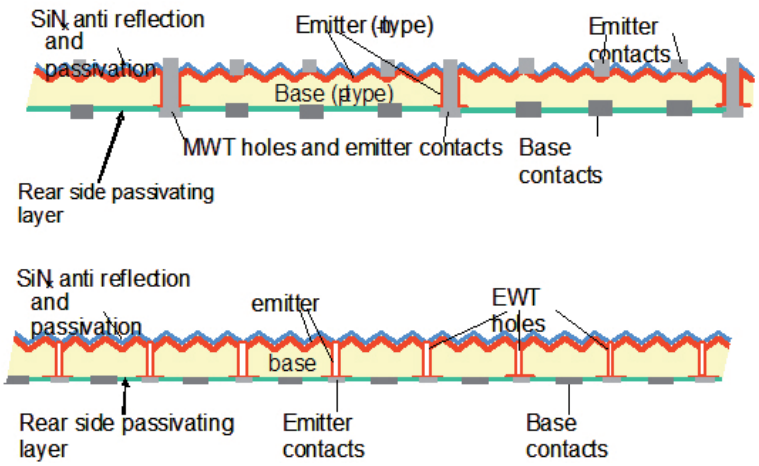

Figure 7. Cross-section structure of the MWT cells (top) and the EWT cells (bottom) [50]

One modification of PERC cell design is the PERL cell concept, where the rear local contacts are additionally passivated by p+ boron diffusion. Instead of annealing of the printed or evaporated Al on the rear side, the rear base contact can also be formed by laser firing. Alternatively, the entire rear surface may have additional boron doping formed either by

diffusion or implantation which may or may not be passivated by dielectric [5]. Such cell structure concepts are currently incorporated in the conventional p-type cells and have been developing in the campus of a large number of cell manufacturers.

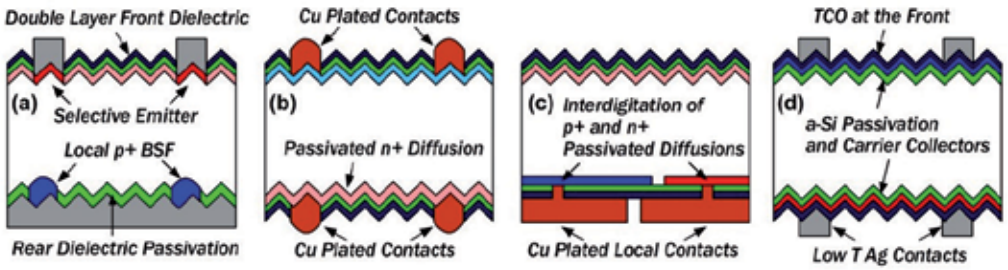

Figure 8. Structure of the solar cells representing four main high efficiency solar cell technologies: (a) PERC/PERL solar cell, (b) bifacial cell with passivated diffusion at the rear (PASHA cell), (c) interdigitated back contact (IBC) solar cell, and (d) silicon heterojunction (SHJ) solar cell. [5]

The other three advanced cell concepts are being developed mainly on the n-type CZ silicon wafers. Bifacial cells (device b) with the passivated diffused carrier collectors and either Al/Ag printed grid or Cu plated grid from both sides of the cell are being developed [53, 54]. The Cu plated metallization increases both short circuit current and filling factor by achieving very thin fingers down to 30 micron width with low resistance, showing the potential of adopting the plating technology in solar industry [55]. IBC cells (device c) utilize the concept that both carrier collectors are formed at the rear side of the cell [56]. This design avoids front metal shading losses and allows the use of thick plated Cu metallization which reduces resistance losses, a recorded efficiency with >21.5% is achieved by the module made from the advanced IBC cells [57]. However, the IBC technology induced a high number of additional manufacturing steps and the use of specialized equipment compared to the common solar cell production line. In SHJ cells, the carrier collectors are formed by depositing thin a-Si layers on both sides of the cell. A transparent conductive oxide (TCO) layer at the front surface (usually Indium Tin Oxide) serves as an antireflection coating, a contacting layer between a-Si and metal electrodes and a lateral conductivity layer. A TCO at the rear surface is usually used for making good ohmic contact and ensuring good internal reflectance of IR light. The efficiency record among large area crystalline silicon solar cells with 24.7% efficiency is reached [58]. The distinguishing feature of SHJ solar cells is due to the almost perfect surface passivation by intrinsic a-Si allowing very high open circuit voltage, which can be higher than 730 mV in commercial solar cell.

5. Conclusions

Upon reviewing of the recent technology developments on the silicon material, cell device architecture and manufacturing processing for the silicon based solar cell, this paper raises the prospective trends of solar industry driven by the global market demands.

Conclusively, pursuing the highest cost performance ratio of solar cell drives the development of the solar industry. The only measurement of a successful solar cell technology is whether the solar cell can be manufactured in a cost effective way. Restricted by the limitation of area available for installing PV system, the trend of pursing higher conversion energy efficiency does pursed steadily by the terminal users. Therefore, reducing the manufacturing process cost is the only way to survive in the solar industry.

Acknowledgements

Mrs. Shihua Guo is specially thanked for her contribution on global solar business market investigation, advanced technology evolution tracing and global patent retrieval.

Author details

Jiahe Chen[1,2*]

Address all correspondence to: jiahe_chen@hotmail.com

1 College of Materials Science and Engineering, Xiamen University of Technology, Xiamen, Fujian, P.R. China

2 Free consultant, South Haida, Haicang, Xiamen, Fujian, P.R. China

References

[1] http://pvinsights.com/Knowledge/WhySolar.php

[2] Weber, Eicke R. "Transition metals in silicon." Applied Physics A 30.1 (1983): 1-22.

[3] Chen Jiahe, EmanueleCornagliotti, Eddy Simoen, EllenHieckmann, Joerg Weber and JefPoortmans, "A deep level transient spectroscopy study on the interface states across grain boundaries in multicrystalline silicon." physica status solidi (RRL)-Rapid Research Letters 5, no. 8 (2011): 277-279.

[4] Chen Jiahe, EmanueleCornagliotti, Ellen Hieckmann, Simone Behrendt, Joerg Weber, Eddy Simoen, and JefPoortmans. "On the electrical characterization of grain boundaries in multicrystalline silicon." ECS Transactions 33, no. 17 (2011): 71-80.

[5] Herasimenka, StanislauYur'yevich. Large Area Ultrapassivated Silicon Solar Cells Using Heterojunction Carrier Collectors. Arizona State University, 2013.

[6] Armin, G. A., Matthew, B. B., Bram, H., & Thomas, M. (2012). Industrial Silicon Wafer Solar Cells–Status and Trends. Green, 2(4), 135-148.

[7] Neuhaus, D. H., &Münzer, A. (2008). Industrial silicon wafer solar cells.Advances in OptoElectronics, 2007.

[8] http://www.semi.org/sites/semi.org/files/docs/09046%20Standards%20Monolike%20Wafers_jg_PZ.pdf

[9] Chinese Patent: CN103320853A

[10] Chinese Patent: CN102185028B

[11] Chinese Patent: CN101864594A

[12] Gong Chun, NielsPosthuma, Frederic Dross, Emmanuel Van Kerschaver, Flamand Giovanni, Guy Beaucarne, JefPoortmans, and R. J. O. M. Hoofman. "Comparison of n-and p-type high efficiency silicon solar cell performance under low illumination conditions." In Photovoltaic Specialists Conference, 2008. PVSC'08. 33rd IEEE, pp. 1-4. IEEE, 2008.

[13] Fourmond, Erwann, Maxime Forster, Roland Einhaus, Hubert Lauvray, Jed Kraiem, and Mustapha Lemiti. "Electrical properties of boron, phosphorus and gallium co-doped silicon." Energy Procedia 8 (2011): 349-354.

[14] Mihailetchi, Valentin D., Johann Jourdan, Alexander Edler, Radovan Kopecek, Rudolf Harney, Daniel Stichtenoth, Jan Lossen, Tim S. Böscke, and Hans-Joachim Krokoszinski. "Screen printed n-type silicon solar cells for industrial application." In Proceedings of the 25th European Photovoltaic Solar Energy Conference and Exhibition, pp. 6-10. 2010.

[15] http://www.isfh.de/institut_solarforschung/alu-zellkonzept.php?_l=1

[16] Kopecek, R., A. Halm, L. Popescu, K. Peter, M. A. Vázquez, and Noaki Fukushima. "Aluminium rear emitter large area n-type Cz-Si solar cells for industrial application." In 25rd European Photovoltaic Solar Energy Conference and Exhibition Valencia, Spain. 2010.

[17] US patent: US5693957A

[18] Radovan Kopecek and JorisLibal, “Switch from p to n”, PV magazine, 06/2012, pp. 86-94

[19] Mihailetchi, Valentin D., Johann Jourdan, Alexander Edler, Radovan Kopecek, Rudolf Harney, Daniel Stichtenoth, Jan Lossen, Tim S. Böscke, and Hans-Joachim Krokoszinski. "Screen printed n-type silicon solar cells for industrial application." In Proceedings of the 25th European Photovoltaic Solar Energy Conference and Exhibition, pp. 6-10. 2010.

[20] Photovoltaic Technology Platform; (2007) "A Strategic Research Agenda for PV Energy Technology"; European Communities,2007

[21] Mason. N; Schultz. O; Russel.R; Glunz. S.W; Warta. W; (2006) "20.1% Efficient Large Area Cell on 140 micron thin silicon wafer", Proc. 21st EUPVSEC, Dresden 2006, pp. 521

[22] Henley, Francois, Sien Kang, Zuqin Liu, Lu Tian, Jusong Wang, and Yi-Lei Chow. "Beam-induced wafering technology for kerf-free thin PV manufacturing." In Photovoltaic Specialists Conference (PVSC), 2009 34th IEEE, pp. 001718-001723. IEEE, 2009.

[23] Moslehi, M. M. "SolexelInc.,"Thin-silicon, low-cost solar photovoltaic modules using kerfless epitaxial silicon lift-off technology,Standford Seminar on thin-silicon (2012).

[24] J. R. Groves, J. B. Li, B. M. Clemens, V. LaSalvia, F. Hasoon, H. M. Branz,C. W. Teplin, "BiaxiallyTextured Photovoltaic Film Crystal Silicon on Ion Beam Assisted Deposition CaF2 Seed Layers on Glass", Energy & Environmental Science. 01/2012; 5(5): 6905-6908.

[25] Weber, K. J., J. Babaei, P. N. K. Deenapanray, and A. W. Blakers. "Silicon as a Photovoltaic Material." In Materials Forum, vol. 27, pp. 9-14. 2004.

[26] PCTPatent Application:WO2012134866A1

[27] Brendel, R., H. Artmann, S. Oelting, W. Frey, J. H. Werner, and H. J.Queisser. "Monocrystalline Si waffles for thin solar cells fabricated by the novel perforated-silicon process." Applied Physics A: Materials Science & Processing 67, no. 2 (1998): 151-154.

[28] R. Brendel and A. Goetzberger, Thin-Film Crystalline Silicon Solar Cells: Physics and Technology. John Wiley & Sons, 2003.

[29] http://www.greentechmedia.com/articles/read/SiGen-Targets-Thin-Silicon-Wafers-with-Ion-Implant-Technology-for-Solar-PV

[30] J. Bultman, I. Cesar, B. Geerlings, Y. Komatsu and W. Sinke, "Methods of Emitter Formation for Crystalline Silicon Solar Cells," Photovoltaics International, Petten, 2010.

[31] Y. Komatsu, et al., "Innovative Diffusion Processes for Improved Efficiency on Industrial Solar Cells by Doping Profile Manipulation," Proceedings of the24th European Photovoltaic Solar Energy Conference and Exhibition, Hamburg, 21-25 September 2009, pp. 1063-1067.

[32] http://www.interpv.net/tech/tech_view.asp?idx=358&part_code=010010001&page=3

[33] H. Haverkamp, A. Shirazi, B. Raabe, F. Book and G. Hahn, "Minimizing the Electrical Losses on the Front Side: Development a Selective Emitter Process from a Single Diffusion," The33rd IEEE Photovoltaic Solar Energy Conference and Exhibition, San Diego, 11-16 May 2008, pp. 430-433.

[34] T. Lauermann, A. Dastgheib-Shirazi, F. Book, B. Raabe, G. Hahn, H. Haverkamp, D.Habermann, C. Demberger and C. Schmid, "Insect: An Inline Selective Emitter Concept with High Efficiencies at Competitive Process Costs Improved with Inkjet Masking Technology," The24th European Photovoltaic Solar Energy Conference and Exhibition, Hamburg, 21-25 September 2009, pp. 1767-1770

[35] J. Köhler, P. Grabitz, S. Eisele, T. Röder and J. Werner, "Laser Doped Selective Emitters Yield 0.5% Efficiency Gain," Proceedings of the24th European Photovoltaic Solar Energy Conference and Exhibition, Hamburg, 21-25 September 2009, pp. 1847-1850

[36] H. Antoniadis, F. Jiang, W. Shan and Y. Liu, "All Screen Printed Mass Produced Silicon Ink Selective Emitter Solar Cells," Proceedings of the35th IEEE Photovoltaic Solar Energy Conference and Exhibition, Honolulu, 20-25 June 2010

[37] ZhaoJianhua, Aihua Wang, Martin A. Green, and Francesca Ferrazza. "19.8% efficient "honeycomb" textured multicrystalline and 24.4% monocrystalline silicon solar cells." Applied Physics Letters 73, no. 14 (1998): 1991-1993.

[38] Chen Jiahe, EmanueleCornagliotti, XaviorLoozen, EllenSimoen, Jan Vanhellemont, Johan Lauwaert, HenkVrielinck, and JefPoortmans. "Impact of firing on surface passivation of p-Si by SiO2/Al and SiO2/SiNx/Al stacks" ,Journal of Applied Physics 110, no. 12 (2011): 126101.

[39] Hoex Bram, S. B. S. Heil, Erik Langereis, M. C. M. Van de Sanden, and W. M. M. Kessels. "Ultralow surface recombination of c-Si substrates passivated by plasma-assisted atomic layer deposited Al2O3." Applied Physics Letters 89, no. 4 (2006): 042112.

[40] Aberle, Armin G. "Overview on SiN surface passivation of crystalline silicon solar cells." Solar Energy materials and solar cells 65.1 (2001): 239-248.

[41] Dingemans, Gijs, et al. "Stability of Al 2 O 3 and Al 2 O 3/a-SiN x: H stacks for surface passivation of crystalline silicon." Journal of Applied Physics 106.11 (2009): 114907-114907.

[42] Lee, Youngseok, et al. "Stability of SiNX/SiNX double stack antireflection coating for single crystalline silicon solar cells." Nanoscale research letters 7.1 (2012): 1-6

[43] Simoen, Eddy, Chun Gong, N. E. Posthuma, Emmanuel Van Kerschaver, JozefPoortmans, and R. Mertens. "A DLTS study of SiO2 and SiO2/SiNx surface passivation of silicon." Journal of The Electrochemical Society 158, no. 6 (2011): H612-H617.

[44] T. Lauermann, T. Lüder, S. Scholz, G. Hahn, B. Terheiden, "Enabling dielectric rear side passivation for industrial mass production by developing lean printing-based solar cell processes", Proc. 35th IEEE PVSC, 2010, p. 28

[45] http://www.recgroup.com/Documents/REC_White_Paper_Backside_Passivation_20120713.pdf

[46] S. Gatz, H. Hannebauer, R. Hesse, F. Werner, A. Schmidt, T Dullweber, J. Schmidt, K. Bothe, R. Brendel, "19.4%-efficient large-area fully screen-printed silicon solar cells" Phys. Status Solidi RRL, vol. 5, No. 4, 2011, p. 147

[47] Clement, Florian, Michael Menkoe, Denis Erath, Tim Kubera, René Hoenig, Wolfram Kwapil, Winfried Wolke, Daniel Biro, and Ralf Preu. "High throughput via-metallization technique for multi-crystalline metal wrap through (MWT) silicon solar cells exceeding 16% efficiency." Solar Energy Materials and Solar Cells 94, no. 1 (2010): 51-56.

[48] Benjamin, Thaidigsmann, Linse Michael, Wolf Andreas, Clement Florian, Biro Daniel, and Preu Ralf. "The path to industrial production of highly efficient metal wrap through silicon solar cells." Green 2, no. 4 (2012): 171-176.

[49] E. Van Kerschaver, R. Einhaus, J. Szlufcik, J. Nijs, R. Mertens, "A Novel Silicon Solar Cell Structure with BothExternal Polarity Contacts on the Back Surface", Proceedings of the 2nd World Conference onPhotovoltaic Energy Conversion, Vienna, Austria, 1998, pp. 1479-1482

[50] https://www.ecn.nl/news/newsletter-en/2010/march-2010/plasma-for-solar-cells/

[51] N. Guillevin, B.J.B. Heurtault, I. Bennett, M.G. Guichoux, L.J. Geerligs, A.W. Weeber, J. Xiong, Z. Hu, G. Li,W. Zhao, Y. Chen, J. Wang, Z.. Wang, C. Chen. "Development towards 20% Efficient n-Type Si MWT Solar Cells for Low-Cost Industrial Production", 26th EUPVSEC, Hamburg, 2011, pp. 989-994

[52] WenchaoZhao, Jianming Wang, YanlongShen,Ziqian Wang,Yingle Chen,Zhiyan Hu,Gaofei Li,Jianhui Chen,JingfengXiong,Guillevin,, N,Heurtault B.J.B,Geerligs L.J.,Weeber, A.W., Bultman, J.H.,"0.35% Absolute efficiency gain of bifacial N-type Si Solar cells by industrial metal wrap through technology". In Photovoltaic Specialists Conference (PVSC), 2012 38th IEEE (pp. 002289-002291). IEEE.

[53] Romijn, I. G., BB van Aken, J. Anker, A. R. Burgers, A. Gutjahr, B. Heurtault, M. Koppes, E. Kossen, M. Lamers, D.S. Saynova, C.J.J. Tool, Lang Fang, XiongJingfeng, Li Gaofei, XuZhuo, Wang Hongfang, Hu Zhiyan, P.R. Venema and A.H.G. Vlooswijk. "Industrial implementation of efficiency improvements in n-type solar cells and modules." In Proceedings of 27th European Photovoltaic Solar Energy Conference, p. 533. 2012.

[54] Hoerteis, Matthias and Stefan W. Glunz. "Fine line printed silicon solar cells exceeding 20% efficiency." Progress in Photovoltaics: Research and Applications 16, no. 7 (2008): 555-560.

[55] Lennon, Alison, Yu Yao, and Stuart Wenham. "Evolution of metal plating for silicon solar cell metallisation." Progress in Photovoltaics: Research and Applications 21, no. 7 (2013): 1454-1468.

[56] M. D. Lammert and R. J. Schwartz, The interdigitated back contact solar cell: A silicon solar cell for use in concentrated sunlight, IEEE Transactions on Electron Devices, vol. 24, no. 4, pp. 337–342, 1977.

[57] D. D. Smith, P. J. Cousins, A. Masad, A. Waldhauer, S. Westerberg, M. Johnson, X. Tu, T. Dennis, G. Harley, G. Solomon, S. Rim, M. Shepherd, S. Harrington, M. Defensor, A. Leygo, P. Tomada, J. Wu, T. Pass, L. Ann, L. Smith, N. Bergstrom, C. Nicdao, P. Tipones, and D. Vicente, Generation III high efficiency lower cost technology: Transition to full scale manufacturing, in 2012 38th IEEE Photovoltaic Specialists Conference (PVSC), 2012, pp. 001594–001597.

[58] Taguchi, Mikio, Ayumu Yano, Satoshi Tohoda, Kenta Matsuyama, Yuya Nakamura, Takeshi Nishiwaki, Kazunori Fujita, and Eiji Maruyama. "24.7% record efficiency HIT solar cell on thin silicon wafer." (2013): 1-4.

Chapter 11

High Throughput Quantum Dot Based LEDs

P. Amini, M. Dolatyari, G. Rostami and A. Rostami

Additional information is available at the end of the chapter

http://dx.doi.org/10.5772/59092

1. Introduction

Today lighting and energy savings is an important part of life and traditional methods of lighting are inefficient, while the light emitting devices (LEDs) can be used in technologies applications for saving energy [1].LEDs produce light using a fundamentally different principle than those used by incandescent, neon, fluorescent, or high-intensity discharge (HID) lamps. Traditional light sources produce light by heating a filament to incandescence and this is inefficient but LEDs emit light from a small semiconducting chip when a current is applied. So controlling equipment and techniques is one of the most cost-effective and significant opportunities for reduce energy waste and improve output light quality. Researches have also provided new structures to improve the efficiency of LED devices. Conjugated polymers offer many advantages as materials for use in light-emitting diodes [2]. Because of the advantages of quantum dots and their application in optoelectronic devices such as LEDs, researches fabricated quantum dot light emitting diode with improvement efficiency; which was replaced with traditional light sources. Quantum dot light emitting diodes use in energy-efficient, high-color-quality thin-film display and solid-state lighting applications [3].

In 1907, H. J. Round found the effect of electroluminescence, so the notion of light emitting diode was introduced [4]. III-V materials were discovered in the 1950s, and by using of these materials the first p-n junctions GaAs LED, with epitaxial growth was made [5, 6]. In 1962 GaAsP LED with visible red light was realized by Holonyak [7]. In 1992, the first blue LED based on GaN with efficiency of 1 % was introduced by Akasaki et al [8], also green LEDs could be made using GaInN with improvement efficiencies up to 10% [9]. The possibility of color displays with blue, red, and green LEDs was successfully realized [10]. Different LEDs can have different characteristics, so they have different application in related technologies. According to the importance of LEDs in new technologies, in recent years there are so motivations by doing a lot of researches to improve the quality of LEDs, so recently they introduced quantum dot based light emitting diodes (QD-LEDs) [3, 11]. According to im-

provement of QD-LEDs the efficiency of this kind of LEDs has increased from 0.01% to 18%, in 1994 [3]. Nano crystals also known as quantum dots (QDs), are nano-sized semiconductor particles, by the synthetic method, the QDs can be classified into epitaxial and colloidal QDs. Colloidal QDs are chemically synthesized and consist of small inorganic semiconductor core (1–10 nm in diameter) and a wider-band gap inorganic semiconductor shell, and a coating of organic passivation ligands [3]. Original QDs contain a core; however, the optical properties of QDs can be improved by coating higher band gap materials or passivation of the surface of the core [12]. Colloidal QDs exhibit some advantages such as larger excitonic interaction between the electrons and holes, stronger carrier confinement, high quantum yield, narrow emission spectrum. Therefor colloidal QDs have the potential to change the way that electronic devices, including solar cells and LEDs, are manufactured [13, 14]. QDs exhibit quantum confinement effect, because of their radius which is smaller than the characteristic Bohr exciton radius, so the carriers in all three directions confined and the density of states will change. According to quantum confinement effect, the optical properties such as absorption and emission can be changed [12]. Band gap is tunable by controlling the size of the QDs during the synthesis process and cheap solution processability of them makes colloidal quantum-dot a promising candidate for optoelectronic devices [3, 15]. The color emitted from QDs and the wavelength of emission, depends on the size of the QDs. According to changing in the size of QDs, the emission wavelength can be changed, so the color of light emission can be changed, also QDs have the high photo-luminescence efficiency; therefore these advantages make colloidal QDs candidates for making quantum-dot light emitting diodes [3, 12]. Figure 1 shows the size changing of QDs and band gap of them.

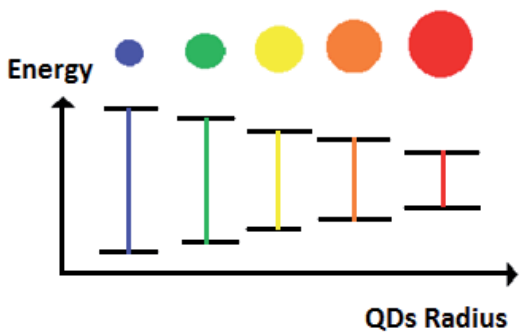

Figure 1. Increasing of energy gap by decreasing of the size of the QDs

QD-LEDs are multilayer structures, consist of hole transport layer (HTL), electron transport layer (ETL) and QD layer as an emissive layer. In this type of LEDs, Indium tin oxide (ITO) (as an anode) and Al (as a cathode) are used as usual electrodes [3, 16]. At first QD-LEDs presented in the form of hybrid organic/inorganic light emitting diodes by Colvin et al [16]. For the hybrid diodes, the QDs were fabricated from inorganic semiconductors and the transport layers from organic semiconductors. This kind of LEDs was later improved by Coe-Sullivan et al [16].

http://dx.doi.org/10.5772/59092

However organic transport layers have stability problems and these layers are sensitive to air, because of these problems the efficiency of hybrid organic/inorganic LEDs decreases [3, 16]. Therefore, inorganic semiconductor transport layers were developed and used in QD-LEDs. Using of inorganic charge transport layers lead to device stability in air [16]. Nevertheless the advantages of QD-LEDs and using them in optoelectronic devices like thin film displays, which cause the improvement in color saturation in this kind of displays, there are some problems limit the applicability of QD LEDs which can be listed as follows:

1. Efficient non-radiative Forster resonant energy transfer (FRET) of excitons within the inhomogeneous size distribution of QDs to non-luminescent sites, where they have non-radiative recombine, cause self-quenching phenomenon.
2. Quenching in photoluminescence (PL) of QDs by the surrounding conductive metal oxides because of carrier imbalance (due to a large hole or electron injection barrier between the p or n type metal oxides and the QDs) [3, 17].

Using of inorganic charge-transport materials is desirable because they can facilitate charge carrier injection and transport to the QD layer and also improve the charge confinement in the QD luminescent layer. As a result it is expected that HTL and ETL make the LEDs less susceptible to the problems [18]. Nowadays NiO and ZnO are common materials to use as charge transport layers, which NiO is a p-type material as a HTL and ZnO is a n-type material as an ETL [16, 18]. Engineering the defect energy levels in the structure of p and n type metal oxides can improve their charge transport properties. These defects levels can be engineered using synthesis methods and also by doping of different atoms in the structure of materials. These defect levels act as a radiative recombination center, therefore photon production probability will be increased [19]. The other way to increasing intensity of emitted light of LEDs is Forster resonance energy transfer (FRET). In this way inorganic materials act as core and organic molecules as capping materials. FRET is an energy transfer between these organic and inorganic materials, which one of them is as electron donor and the other one is as electron acceptor [20].

2. Physics and theory of LEDs and QD-LEDs

LEDs are pn-junction diodes which have many applications in displays and lighting. These LEDs made from III-V semiconductors. Figure 2 shows pn-junction and energy level of it, which indicate pn-junction under zero bias and forward bias. The junction between p-type and n-type is non-conductive, because of moving of electrons by diffusion from the n-type region into the p-type region and combine with the acceptors. So this causes to formation of depletion zone or space charge region. According to Figure2, E_V and E_C indicate valence band and conduction band of energy level diagram respectively, which shows under forward bias, the potential barrier between p-type and n-type reduces. Also E_F and W_D indicate Fermi level and depletion width respectively. By current injection and applying a voltage in the forward direction of the device, electrons and holes are pushed to the junction, so the electron-hole pairs appear and recombine together, this result in the formation of light. The electrolumines-

cence phenomenon causes the generation of light in LEDs. The wavelength of generated light depends on used materials as a p-type and n-type [21, 22].

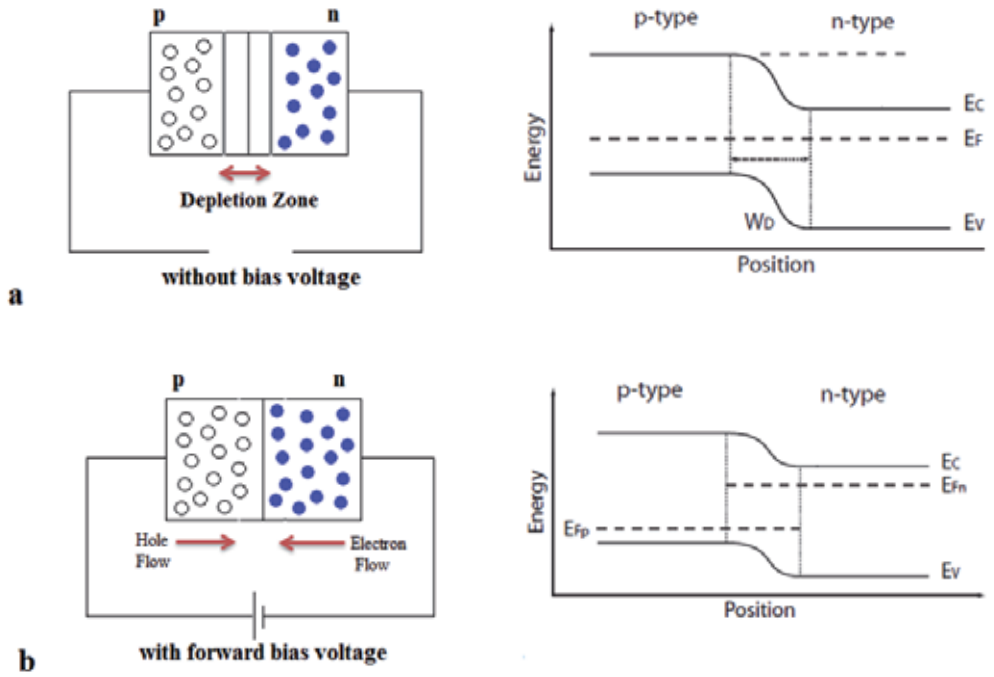

Figure 2. P-N junction and energy diagram, a) without bias b) under forward bias

In semiconductors electrons and holes recombine together radiative or non-radiative, which radiative recombination creates light (photon) and non-radiative recombination creates phonon. Figure 3 illustrates radiative and non-radiative recombination [21, 22].

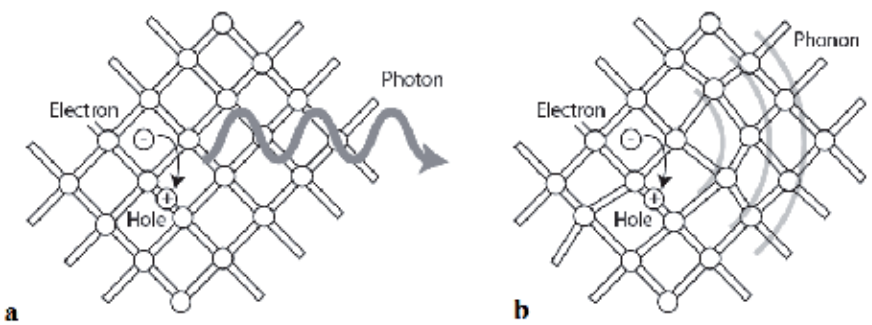

Figure 3. a) Radiative recombination b) non-radiative recombination

http://dx.doi.org/10.5772/59092

Because of the presence of electron and hole in recombination process, this process is called bimolecular recombination. The recombination rate, R is given by:

$$R = -\frac{dn}{dt} = -\frac{dp}{dt} = Bnp \tag{1}$$

where B is bimolecular recombination coefficient and R is proportional to the density of electron-hole pairs. In light emitting diodes non-radiative recombination is unwanted, because this process creates phonon, so the phonons causes to increase heat and heating of the material has harmful effects on emitted light and lifetime of device [21, 22]. QD-LEDs are another structure of LEDs that have multilayers and QD layer is an active layer. This LEDs consist of hole transport layer (HTL), electron transport layer (ETL) and QD layer as an emissive layer. In this type of LEDs, Indium tin oxide (ITO) (as an anode) and Al (as a cathode) use as usual electrodes. The HTL is contacted by ITO and ETL is contacted by Al, which acts as an injector [16]. In this device by applying forward bias and current injection, the holes and electrons are injected from anode and cathode respectively, and they are travel through of HTL and ETL to the QD layer, then they recombine together in QD layer [3, 16]. Figure 4 indicates QD-LEDs structure, energy level diagram, and physical performance of QD-LEDs. Forster resonant energy transfer (FRET) is excitation mechanism of QDs in close proximity to small organic molecules and inorganic layers. In FRET mechanism, in the charge transport layers formed electron-hole pairs transfer energy non-radiative to the QD layer by dipole-dipole coupling. Direct charge injection is the efficient method of injection carriers [3].

For explain the performance of QD-LEDs, these devices consist of five parts which listed as follow [16]:

a. Carrier injection from the electrodes

By assuming of position (0 and w), and ohmic contacts at anode and cathode, the carrier concentrations inside the transport layers are equal to the equilibrium carrier concentrations that are given in Eq. 2.

$$p(0)n(0) = n_i^2(0) \qquad p(W)n(W) = n_i^2(W) \tag{2}$$

At the electrodes, there is no space charge, so we have the following condition (Eq. 3).

$$\begin{aligned} N_d(0) - N_a(0) + p(0) - n(0) = 0 \\ N_d(W) - N_a(W) + p(W) - n(W) = 0 \end{aligned} \tag{3}$$

where n and p are electron and hole concentrations respectively, n_i is intrinsic carrier concentration, and N_d is the donor concentration and N_a is the acceptor concentration. At the electrodes, the electrostatic potential is given by the following equations (Eqs. 4 and 5).

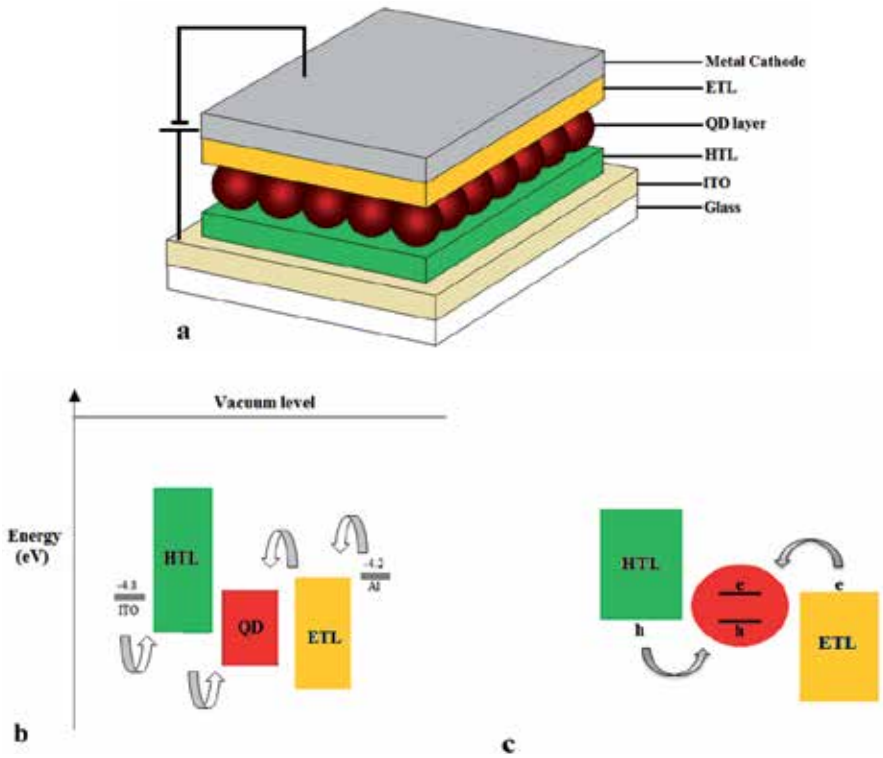

Figure 4. a) QD-LED structure, b) Energy level diagram, c) physical performance of QD-LED

$$\psi(0) = V - \frac{KT}{q} \ln\left[\frac{p(0)}{n_i(0)}\right] \tag{4}$$

$$\psi(W) = \frac{KT}{q} \ln\left[\frac{n(W)}{n_i(0)}\right] - \left(\frac{\Delta E_c + \Delta E_v}{2}\right) \tag{5}$$

According to Anderson's rule, the last term in equation, accounts for the discontinuities in the conduction band and valence band.

b. Transport in the ETL and HTL

The equations used to describe the transport in the HTL and ETL are similar to the bulk drift and diffusion equations, which is given as follows (Eqs. 6-10).

$$\frac{dp}{dt} = -\frac{1}{q}\frac{dJ_p}{dx} + G - U \tag{6}$$

http://dx.doi.org/10.5772/59092

$$\frac{dn}{dt} = \frac{1}{q}\frac{dJ_n}{dx} + G - U \tag{7}$$

$$\frac{d^2\psi}{dx^2} = -\frac{q}{\varepsilon}(N_d - N_a + p - n) \tag{8}$$

$$J_p = -qD_p\frac{dp}{dx} - qp\mu_p\frac{d\psi}{dx} \tag{9}$$

$$J_n = qD_n\frac{dn}{dx} - qn\mu_n\frac{d\psi}{dx} \tag{10}$$

G indicates generation parameter which is assumed to be negligible and U is recombination rate and given by Shockley-Read-Hall (SRH) recombination, which will be described in (e) section.

c. Carrier injection from transport layers into the QD layers

Assuming that the QD layer adjacent to the HTL, the nearest QDs are considered to be traps for holes. In equilibrium and using detailed balance, the rate of emission is equal to the rate of captured holes by these QDs, so, we have (Eq. 11):

$$e_0 p_0(0) = c_0 p_0(0^-)[N_T - p_0(0)] \tag{11}$$

p(0) and p(0^-) are hole density in the QD layer and HTL, which adjacent together, respectively. N_T is the density of trap states in the QD layer (each QD can only accommodate one hole). e and c are emission rate coefficient and the capture rate coefficient for the trap states, respectively. Also subscript (0) is used for equilibrium condition. The ratio of emission and capture coefficients is given by Eq. 12 as follows.

$$\frac{c_0}{e_0} = \frac{p_0(0)}{[N_T - p_0(0)]p_0(0^-)} \tag{12}$$

The difference of capture and emission can be describes the rate of change of carrier concentration under non-equilibrium conditions, thus, we have (Eq. 13):

$$\frac{dp}{dt} = cp(0^-)[N_T - p(0)] - ep(0) \tag{13}$$

The capture and emission coefficients can be taken to be the same as for equilibrium, if device is close to equilibrium. Also if the carrier concentration is non-degenerate, the following equation manage rate of carrier change (Eq. 14) as:

$$\frac{dp}{dt} = \frac{1}{\tau_{p1}}\left[\frac{p(0^-)}{p_0(0^-)}p_0(0) - p(0)\right] \tag{14}$$

where τ_{pl} is capture/emission time constant and equals to $\frac{1}{e}$, also τ_{pl} depends on the used material. At the interface of ETL and QD layer, which are adjacent together, equations for electrons are entirely similar to holes.

d. Transport among the quantum dot layers

The QDs can be assumed semiconductor particles with a surrounded insulating layer. The transport from one QD to another occurs by direct tunneling process. In this case the QDs act as potential wells and the insulating layer acts as tunnel barriers. Using a one-dimensional WKB approximation, the tunneling probability from QD layer 1→ 2, is given by Eq. 15:

$$T_{12} = e^{-2\kappa(2d_{ins})} \tag{15}$$

where κ is the inverse characteristic length for tunneling and d_{ins} is the thickness of the insulating layer around the QDs. The electron is "oscillating" in the well with "frequency" $\vartheta = \frac{\vartheta_{th}}{2d}$. ϑ_{th} is the thermal velocity of electron, d is the diameter of the QD, and it has probability of T_{12} to making a transition to the neighboring QD layer. The total density of electrons per second tunneling from 1 → 2 assuming an unoccupied layer 2 are:

$$N_{1\to2} = n_1 \vartheta T_{12} \tag{16}$$

where n_1 is the number of electrons in layer 1. Because of the same size of the particles and temperature in layer 1 and 2, so the total number of electrons per second tunneling from 2 → 1, assuming an unoccupied layer 1, is given by Eq. 17 as:

$$N_{2\to1} = n_2 \vartheta T_{21} \tag{17}$$

Therefore the flow of electrons from layer 1 to layer 2 is given by Eq. 18 as:

$$N_{1\to2} - N_{2\to1} = \vartheta(T_{12}n_1 - T_{21}n_2) \tag{18}$$

http://dx.doi.org/10.5772/59092

If n_{10} and n_{20} are equilibrium concentrations of electrons in layers 1 and 2 respectively, and $w_{12}=\vartheta T_{12}$, so the net exchange is given by Eq. 19 as:

$$N_{1\to 2} - N_{2\to 1} = W_{12}(n_1 - \frac{n_{10}}{n_{20}} n_2) \tag{19}$$

The equations of transporting of holes in QDs are similar to electrons equations.

e. Recombination in the QDs

In QD-LEDs like LEDs there are two types of recombination, radiative and non-radiative. If the recombination of electrons and holes are radiative, photons are emitted, and the wavelength of photon is independent to the charge transport layers and only depends on the QDs. According to doping of QDs, the radiative recombination can be either monomolecular or bimolecular. Monomolecular recombination occurs in doped quantum dots and the rate of recombination depends on minority carrier density. If the quantum dots are undoped, the recombination rate depends on both of the carriers, so this kind of recombination is bimolecular. Bimolecular recombination is given by Eq. 20 as:

$$U_r = \gamma(np - n_i^2) \tag{20}$$

where U_r is recombination rate, γ is recombination rate coefficient, n and p are electron and hole concentrations respectively, n_i is intrinsic carrier concentration. Also non-radiative recombination is given by Shockley-Read-Hall (SRH) recombination, as follow (Eq. 21).

$$U_{nr} = \frac{pn - n_i^2}{\tau_n(p + n_i) + \tau_p(n + n_i)} \tag{21}$$

where U_{nr} is non-radiative recombination rate, n and p are electron and hole concentrations respectively, n_i is intrinsic carrier concentration, also τ_n and τ_p are electron and hole recombination lifetimes.

3. Experimental

This section provides materials synthesis and fabrication methods of QD-LED devices that are realized by our research group. All of the fabricated devices consist of p-type and n-type materials as HTL and ETL, respectively. Synthesis of these materials will be explained in this section.

3.1. Synthesis of materials

3.1.1. P-type materials

3.1.1.1. Processing of NiO

NiO synthesized by electrochemical and sol-gel methods which is used in the structure of QD-LED, also ZnO:Cu is another material which is used as a HTL.

1. NiO film is fabricated using two electrode system at a deposition temperature of 50 °C. An indium tin oxide ITO/glass and a Pt wire were used as the cathode and anode, respectively. The electrolyte was an aqueous solution containing 5mmol nickel nitrate and 5mmol hexamethylenetetramine (HMT). The voltage during deposition was-2.2 V and the deposition time was 30 min [23].

2. The NiO sol–gel precursor was prepared by dissolving 0.01mol nickel nitrate in 20ml acetic acid and in a separate beaker 3ml tri-ethyleneamine dissolved in 30ml methanol and was added under stirring to the improve sol stability. The prepared gel were then placed immediately into a tube furnace and annealed under air at 600 °C for 2 hours, after that the gel changed to powder form. 0.01 g of obtained NiO dispersed in 2 ml methanol and the dispersed solution were deposited on the ITO substrate at 100°C.

3.1.1.2. Processing of ZnO:Cu

ZnO:Cu synthesized by sol-gel method by the following manner. For preparing of this material, 3.1g of zinc acetate and 0.18g of $CuSO_4$,were dissolved in 40ml distilled water, then 1.5g of citric acid and 1.5g of polyethylene glycol was added under stirring to the improve sol stability. The prepared gel were then placed immediately into a tube furnace and annealed under air at 600 °C for 15 hours, after that the gel changed to powder form.

3.1.2. N-type materials

1. The ZnO sol–gel precursor was prepared by dissolving 3.27g zinc acetate in 40ml distilled water, then 1.5g of citric acid and 1.5g of polyethylene glycol was added under stirring to the improve sol stability. The prepared gel were then placed immediately into a tube furnace and annealed under air at 500 °C for 15 hours, after that the gel changed to powder form.

2. ZnO:Ga was synthesized by solvothermal method using the following manner. In a typical experiment to synthesis $Zn_{0.95}Ga_{0.05}O$ nanoparticles, NaOH (1mmol), tri-octylphosphine-oxide (TOPO, 5mmol), $Zn(CH_3CO_2)_2(H_2O)_2$ (0.95 mmol), $Ga(NO_3)_3H_2O$ (0.05mmol), were mixed in 75ml 2-propanol and the mixture was transferred into autoclave. The autoclave was sealed and maintained at 180°Cfor 24 hour, then allowed to cool to room temperature naturally. The obtained powder material is centrifuged by distilled water, ethanol and 2-propanole for several times.

3. ZnO:Nd was synthesized by sol-gel method using the following manner. For preparing of $Zn_{0.95}Nd_{0.05}O$, 3.1g of zinc acetate and 0.26g of $NdCl_3(6H_2O)$, were dissolved in 40ml distilled water, then 1.5g of citric acid and 1.5g of polyethylene glycol was added under stirring to the improve sol stability. The prepared gel were then placed immediately into a tube furnace and annealed under air at 600 °C for 15 hours, after that the gel changed to powder form.

3.1.3. Quantum dots

1. We utilized CdSe\ZnS core\shell structures as quantum dots in the fabricated QD-LED. For synthesis of CdSe QDs, Cd $(NO_3)_2$(3.24 mmol) and Oleic acid (5ml) were mixed together under vacuum conditions at 100°C. Then Se (1.62mmol) dispersed in the 2-propanol (5ml) and 7mmol $NaBH_4$ added in it and the obtained colorless solution were injected to the mixture of $Cd(NO_3)_2$ and oleic acid and heated at 100°C for 30min. The obtained material was centrifuged with n-hexane, ethanol and acetone for several times. The obtained CdSe capped with oleic acid was dried at 70°C.Then 0.63g of CdSe and 0.37g of Zinc acetate solved in 10 ml n-hexane and 10ml 2-propanol at 100°C under vacuum conditions. 0.02g NaOH and 0.05g thioacetamide solved in 15ml 2-propanol and was added to the solution and the reaction was done for 30 min at 120°C. The obtained material was centrifuged with n-hexane, ethanol, acetone and distilled water for several times.
2. CdS is another quantum dot, which has been used in the fabrication of QD-LED. For synthesis of CdS QDs, CdO (1mmol) and TOPO (0.3g) and chloroform (30ml) were mixed together under vacuum conditions at 100°C. Then S (2mmol) dispersed in 2ml of Tri-tert-butylphosphine and this solution was injected to the mixture of CdO (1mmol) and TOPO (0.3g) and chloroform (30ml) at 100°C for 30min. The obtained material was centrifuged with n-hexane, ethanol and acetone for several times.

Surface of the synthesized CdS QDs for applying in QD-LEDs should be improved. For this purpose we got help from FRET mechanism and capping molecules for using as surface modification, selected based on enhancement of illumination of CdS using FRET mechanism. So we carried out surface modification of QDs by organic molecules, which listed as follow:

3. One of the materials for modification of QD surface is Thioacetamide (TAA). For preparing of CdS with TAA ligands, CdS (0.01g) capped with TOPO (synthesized QD) and TAA (0.01) and 2-propanol (5ml) were mixed together under stirring for 24 hours, after that the obtained material was centrifuged with 2-propanol, n-hexane, ethanol and distilled water for several times.
4. Ammonium hexafluorophosphate (F_6H_4NP) is another material which used as surface modification of QD. For preparing of CdS with this molecule, CdS (0.01g) and F_6H_4NP (0.01g) and 2-propanol (5ml) were mixed together under stirring for 24 hours, after that the obtained material was centrifuged with 2-propanol, n-hexane, ethanol and distilled water for several times.
5. Mercaptoacetic acid (MAA) is used as surface modification of CdS too. For preparing of CdS with Mercaptoacetic acid, NaOH (1mmol) and Mercaptoacetic acid (0.01 g) and 2-

propanol (5ml) were mixed together. Then the obtained solution was added on 0.01 g of the CdS and 5ml 2-propanol and the mixture stirred at room temperature for 24 hours; then the obtained material was centrifuged with 2-propanol, n-hexane, ethanol and distilled water for several times.

3.2. Device fabrication

This section provides seven kinds of QD-LEDs by using p-type, n-type and quantum dots materials which the synthesis of them were explained above. For fabrication of first, second and third QD-LEDs, ITO coated glasses with a sheet resistance of 20ohm/sq was purchased from Aldrich. Also For fabrication of fourth, fifth, sixth and seventh, flexible ITO which was coated on PET was utilized. For fabrication of all of the devices, traditional physical method and solution processed method were utilized.

For fabrication of first QD-LED, NiO synthesized by sol-gel method as HTL layer was used. In this case CdSe/ZnS QD layer used as emissive layer and ZnO:Ga as ETL. All of applied materials dispersed in 2-propanole and coated by spin coating method.

For fabrication of second QD-LED, electrochemically synthesized NiO was deposited on ITO and CdSe/ZnS QD layer and ZnO:Ga as ETL layer were deposited on it by spin coating method respectively.

For fabrication of third QD-LED, ZnO:Cu as HTL layer was deposited on ITO and CdSe/ZnS QD layer was fabricated by spin coating method and ZnO:Nd as ETL layer was deposited on it by spin coating method respectively.

For fabrication of fourth, fifth, sixth and seventh QD-LED, sol-gel NiO as HTL, QD layer, ZnO:Nd ETL were all deposited by spin coating method. The QD layer in fourth QD-LED is CdS capped with TAA molecule and in fifth QD-LED the QD layer consist of CdS capped with F_6H_4NP molecule, also the QD layer in sixth QD-LED is CdS capped with MAA, in seventh QD-LED the QD layer consists of CdS-TOPO.

In all seven devices, the Al cathode was deposited by the electron beam evaporation technique.

3.2.1. Spectroscopic studies and structural characterization

In this chapter all the measurements and characterizes carried out by the following devices:

Photoluminescence (PL) measurements were carried out by a Perkin-Elmer LS45 luminescence spectrophotometer. UV-Vis absorption spectra were recorded using a PG instrument T70 UV/V is spectrophotometer. Surface morphology and distribution of the particles were studied via a TESCAN model MIR3 scanning electron microscope (SEM), and by a Dual-scope C26 scanning probe and microscope DME atomic force microscope (AFM) operating in tapping mode. The crystal structure of nanoparticles were characterized by X-ray diffraction (XRD) on a Siemens D500 using Cu-kα radiation (λ=1.541 A°). X-Ray photoelectron spectroscopy (XPS) was carried out by Surface Science Instruments (SSX-101 M-Probe ESCA).

http://dx.doi.org/10.5772/59092

4. Results

4.1. Increasing efficiency

Because of the importance of light quality and lifetime of QD-LEDs, nowadays increasing efficiency of QD-LEDs is very considerable; therefore our group (OIC) by introducing new structures of QD-LEDs and using solution process method for fabrication of QD-LEDs has several works for improving of efficiency of this type of LEDs. In this way, crystal engineering and effects of FRET in QD-LED were investigated, which both of them improve quality of QD-LEDs [24].

4.1.1. Crystal engineering

This section is based on trap level engineering in inorganic materials to achieve improved QD based LEDs. For this purpose, we investigate three types of QD-LEDs which in two types of them NiO applied as transparent, conductive hole transport layer (HTL) and CdSe/ZnS QDs as luminescent layer and ZnO:Ga as electron transport layer (ETL). The arrangement of the layers that form the QD-LED is illustrated in Figure 5. As Figure 5a shows, there is an energy barrier for hole injection from ITO to the p-NiO layer and from p-NiO layer to the QD layer. Such a barrier is not present for electron injection and transportation. This causes a carrier density imbalance in QDs that prevents efficient recombination of electron-hole pairs. This phenomenon causes self-quenching in QD-LEDs. One way to solve this problem is synthesis of NiO nanoparticles with a wider band gap to decreasing energy barrier between p-NiO and QDs. To improve hole injection from ITO to the p-NiO layer, trap levels in the band gap of NiO are created that results in a much lower barrier for hole injection. As mentioned previously, engineering these trap energy levels is possible with considering different methods for nano structure synthesis. For this purpose, we investigate two types of NiO synthesized via sol–gel and electrochemical methods.

The purity and crystallinity of the NiO nanoparticles synthesized by sol-gel and electrochemical methods were examined using powder X-ray diffraction (XRD). XRD pattern of nanoparticles synthesized by sol-gel method is shown in Figure 6 which is similar to the pattern for material synthesized by electrochemical method. This figure shows narrow diffraction peaks which indicate high crystallinity of the synthesized materials and the peaks appeared at 2θ=37.39°, 43.38°, 62.94° are related to (111), (200), (220) crystal planes of the synthesized NiO which crystallizes in cubic system. Metal-Oxides like NiO usually contain a large number of defects and these defects convert the NiO to conductive material. In equilibrium defect chemistry, NiO usually has an oxygen excess accommodated by nickel vacancies [25, 26]. To preserve the overall electrical neutrality in the crystal, some Ni^{2+} ions must be converted to Ni^{3+} ions, which are responsible for conduction in NiO. Lattice defects are not well-defined in NiO films synthesized by different methods. On the other hand, the vacancy model is little discussed with regard to NiO films prepared by different methods. Due to its uncertain mechanism most papers use nickel vacancy and/or interstitial oxygen to explain the electrical properties of the NiO films [26].

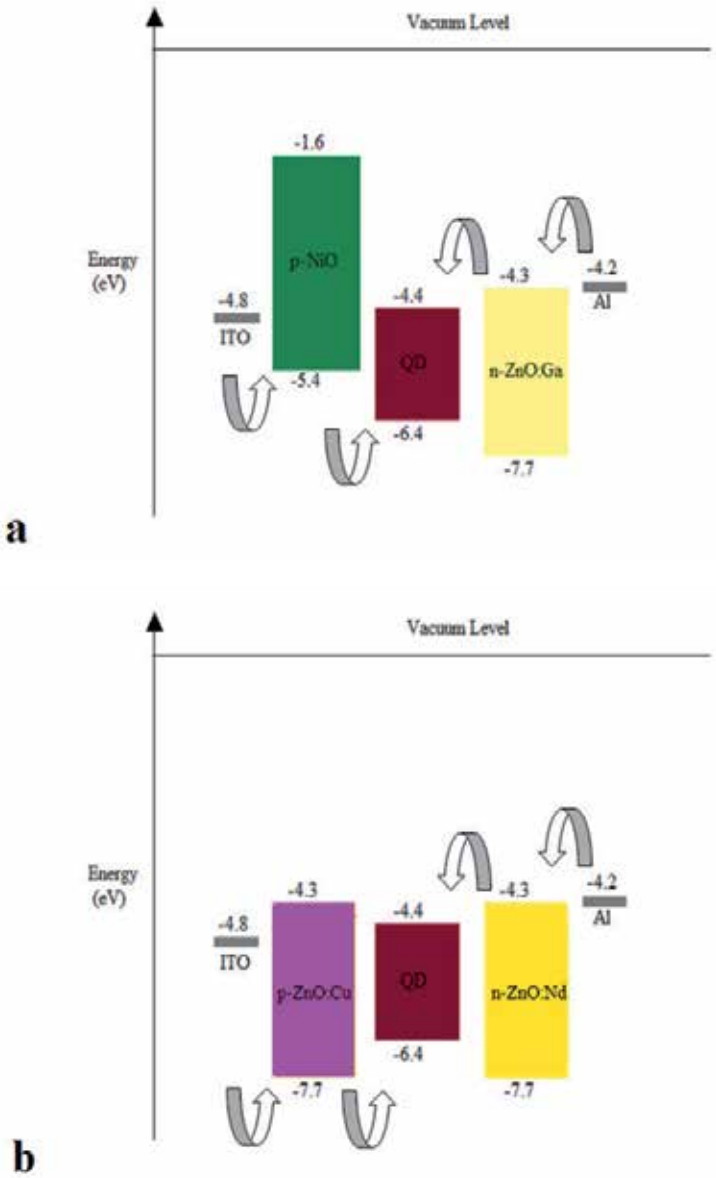

Figure 5. Energy level diagram of fabricated Quantum-dot light emitting diode

The PL spectra of the synthesized materials are studied for characterization of trap levels, formed in the structures. Figure 7 shows strong narrow bands appeared in UV and visible ranges for both spectra. A strong UV emission at 350 nm for electrochemically synthesized NiO and 335nm for NiO synthesized by sol-gel method are generally originated from the direct recombination of the free excitons through an exciton-exciton collision process which is called near band edge emission. It is believed that the visible emission is due to

http://dx.doi.org/10.5772/59092

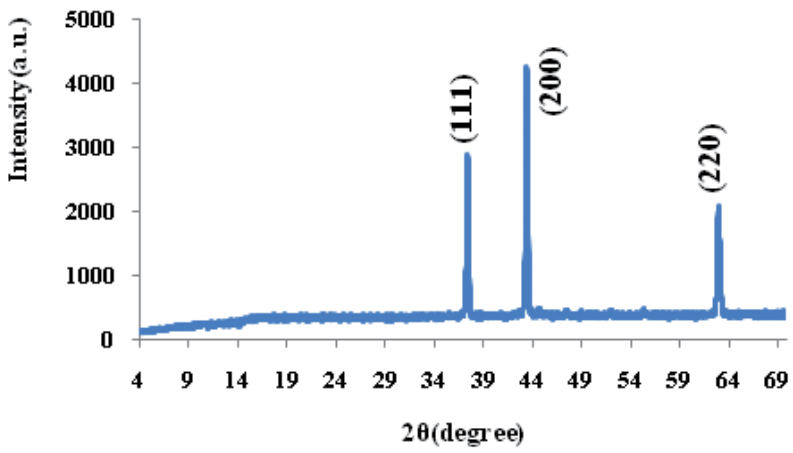

Figure 6. XRD pattern of NiO nanoparticles

the crystalline defects in the NiO structures and is related to intrinsic defects and Ni^{2+} vacancies play a key role for it.

As figures show, intensity of the emission bands appeared in visible range for the material synthesized by sol-gel method is higher than electrochemical method that indicates density of trap levels in the material synthesized by so-gel method is high. Absorption spectra for synthesized materials show broad bands in the range of 190-350 nm for the material synthesized by electrochemical method which is narrower in the material synthesized by sol-gel method. This result indicates high uniformity of the particles synthesized by sol-gel method. On the other hand appearing the band at 335 nm for the material synthesized by sol-gel method shows a blue shift rather than electrochemically synthesized material which this peak appears at 350 nm. This result shows creation of wide band gap material with sol-gel method.

Figure 9 shows the scanning electron microscope (SEM) images of the synthesized NiO using sol-gel and electrochemical methods which indicates uniform and smaller size of particles for NiO synthesized by sol-gel method. AFM images (Figure 10) confirm smooth surface and uniform size of NiO synthesized by sol-gel method.

Intrinsic defects are created during crystallization process of ZnO and by this way n-type ZnO can obtain [27-30]. In previously reported devices ZnO with intrinsic n-type defects has been used. We tried to fabricate such devices with extrinsic defects that are created by Ga or Nd doping in the structure of ZnO. The reason for choosing these atoms as dopant atoms will describe in DFT calculation section. Since ZnO is crystalizes as n-type semiconductor, the number of p-type ZnO is limited and synthesis of this type of ZnO is not usual. Here we describe the devices based on Cu doped ZnO as the HTL beside devices based on p-type NiO which is applied as HTL layer in these structures.

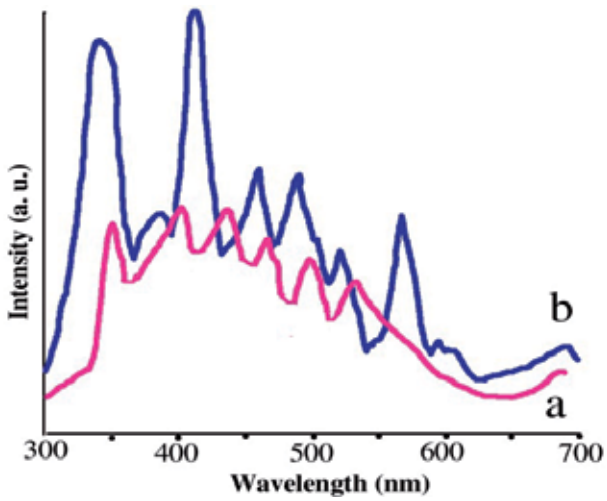

Figure 7. PL spectra of the synthesized NiO by: a) electrochemical and b) sol-gel methods

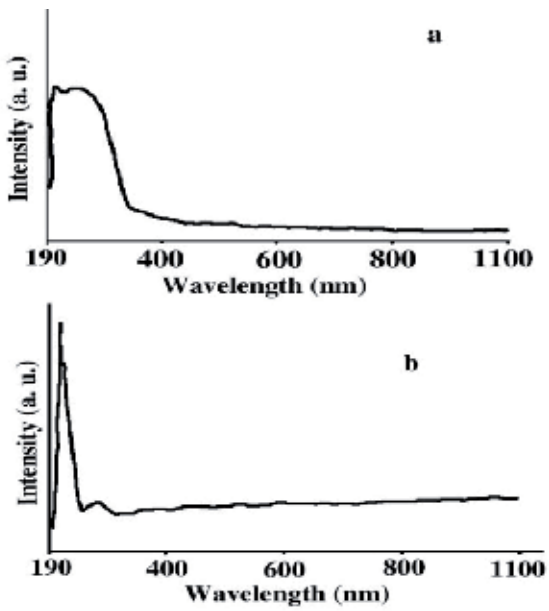

Figure 8. UV-Vis spectra of NiO synthesized by a) electrochemical and b) sol-gel methods.

Figure 5a shows, electron injection between Al (as electrode)-ZnO and ZnO-QD depends on electronic structure of ZnO. Although there is a small energy barrier in this case, increasing electronic levels in conduction band of ZnO can improve electron transport between layers. As calculations show, with doping of Ga^{3+} in the structure of ZnO electronic levels are created in the band structure of ZnO which these new levels appears inside the conduction band (Figure 11).

http://dx.doi.org/10.5772/59092

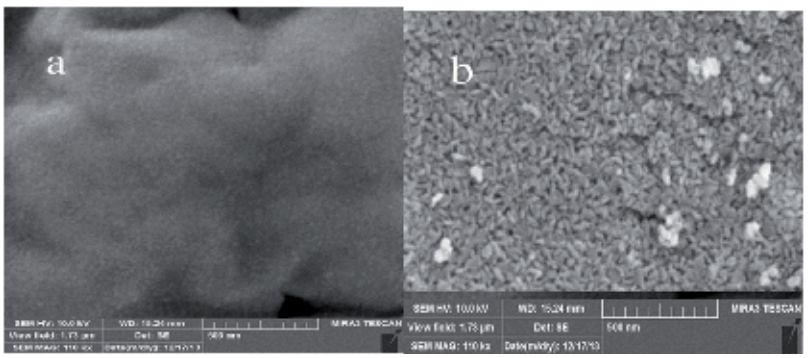

Figure 9. SEM images of NiO synthesized by a) sol-gel b) electrochemical methods.

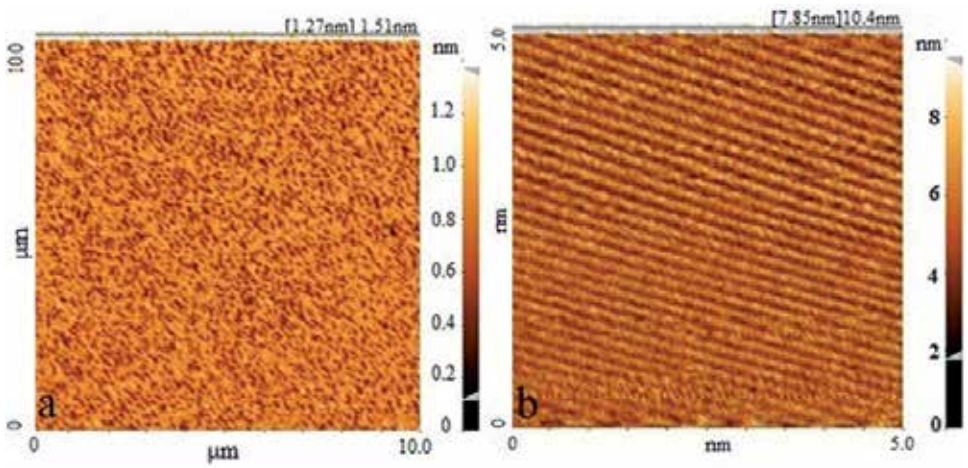

Figure 10. AFM images of NiO synthesized by a) sol-gel and b) electrochemical methods.

However, from view point of crystal structure, Ga^{3+} is expected to cause only a small lattice distortion because of their similar tetrahedral radii. The X-ray diffraction (XRD) patterns of ZnO: Ga nanoparticles are shown in Figure 12 which peak positions correspond to crystalline ZnO with the hexagonal wurtzite structure. The morphology of the ZnO: Ga analyzed by SEM and AFM images (Figure 13). These images confirm the small size of ZnO:Ga nanoparticles which are about 50nm.The surface composition of films was determined using XPS technique. The XPS spectra of the ZnO: Ga films (Figure 14) show that the binding energy (BE) of each constituent element was positioned at 1117.72 eV (Ga $2p_{3/2}$), 1022.23 eV (Zn $2p_{3/2}$) and 530.9 eV (O_{1s}) as calibrated to 285.43 eV (C_{1s}). The Ga-doped ZnO sample prepared using the 5 wt. % Ga $(NO_3)_3$ reveals 4.75% Ga on the surface of the films. The broadening of oxygen spectrum (Figure 13) is believed to be composed of two components located around 531 eV and 532 eV respectively. The low BE component is ascribed to covalently bonded oxygen in ZnO structure (lattice oxygen) while the high BE is attributed to the adsorbed oxygen. The higher binding

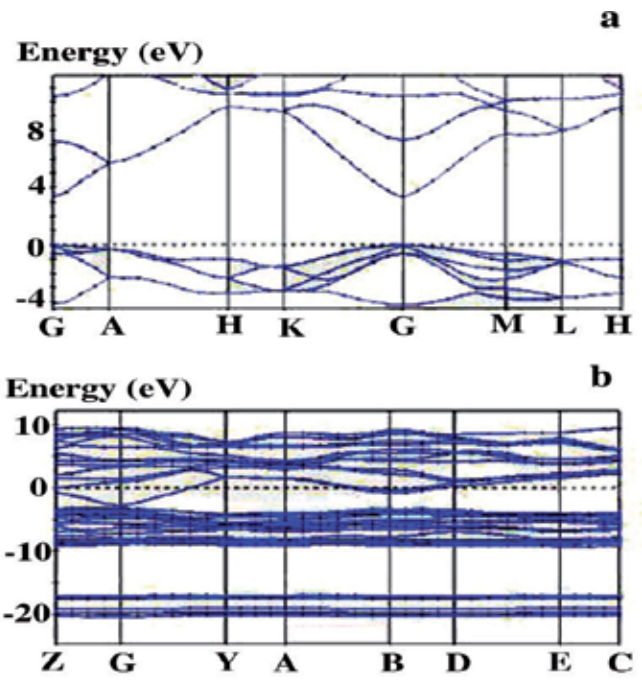

Figure 11. a) Band structure a) bare and b) Ga doped ZnO

energy at 532 eV is usually attributed to chemisorbed or dissociated oxygen or OH species on the surface of the ZnO thin film, such as adsorbed H_2O or adsorbed O_2[31].

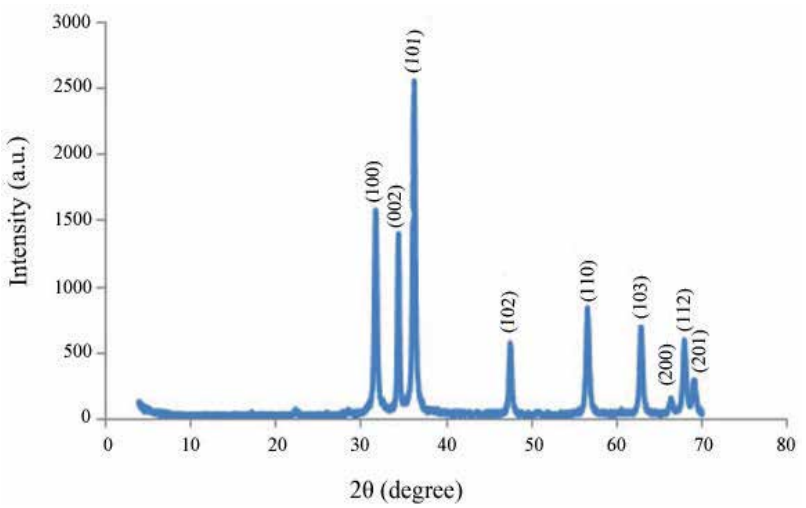

Figure 12. XRD pattern of ZnO:Ga nanoparticles

http://dx.doi.org/10.5772/59092

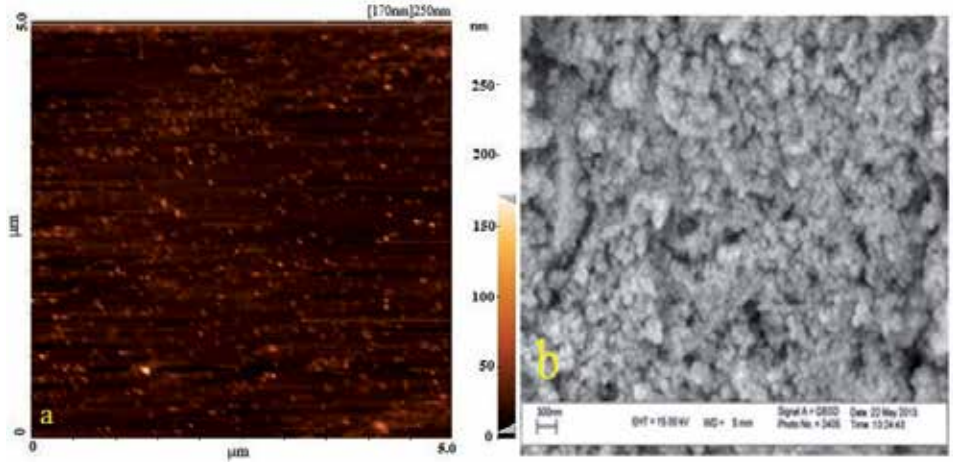

Figure 13. a) AFM b) SEM images of synthesized ZnO:Ga nanoparticles

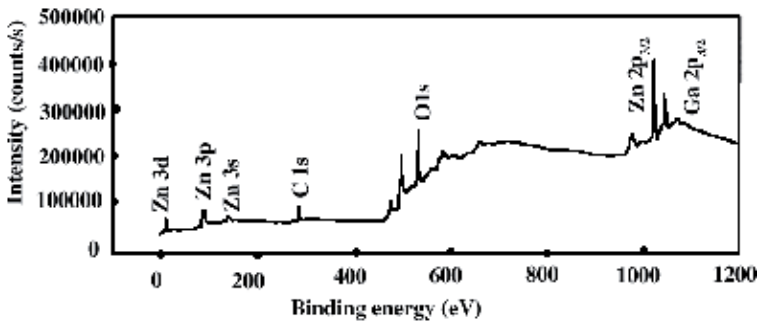

Figure 14. XPS spectra of the ZnO: Ga films

PL study of this thin ZnO film indicates high degree of surface and structural trap levels characterized by visible-region fluorescence (Figure 15).

Nd doped ZnO has been synthesized previously by Zheng and coworkers [32]. DFT calculations show, doping of Nd in the structure of ZnO increases electronic levels in conduction band of ZnO (Figure 16) and these levels are more than levels in Ga doped ZnO structure which is expected that this structure will improve the efficiency of LED more than previous structure.

Figure 17 shows the X-ray diffraction (XRD) patterns of ZnO: Nd nanoparticles. Peak positions correspond to crystalline ZnO with the hexagonal wurtzite structure. For $Zn_{0.95}Nd_{0.05}O$, diffraction peaks become broader and weaker compared to undoped ZnO which shows decreasing of crystallinity of the structure by increasing in doping concentration. The morphology of the ZnO: Nd analyzed by AFM images (Figure 18). The grain sizes of the nanoparticles were 50-70nm.

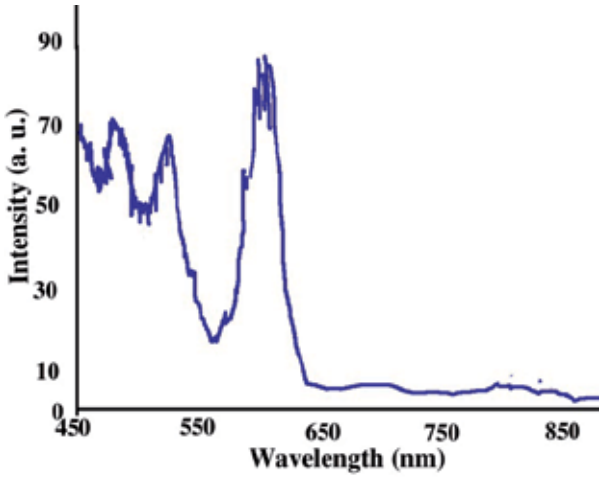

Figure 15. PL spectra of the synthesized ZnO:Ga nanoparticles

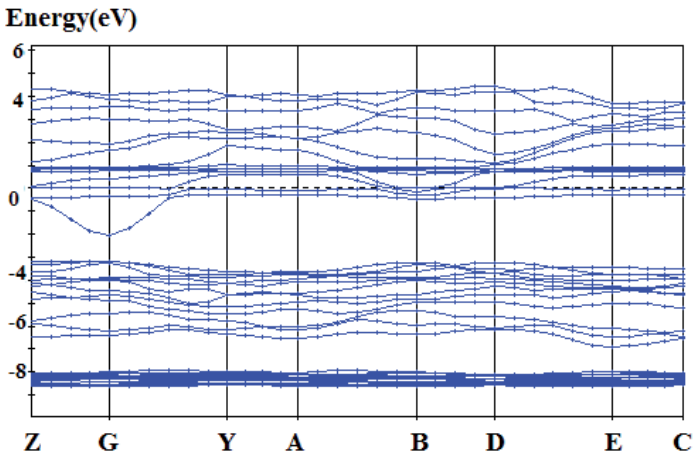

Figure 16. Band structure of Nd doped ZnO

For making improvement in HTL layer, a structure based on Cu doped ZnO (instead of p-type NiO) is fabricated. Doping of Cu^{2+} has effect on photoluminescence (PL) and structure of ZnO [33]. Calculation results indicate that with doping of Cu^{2+} in the structure of ZnO electronic levels are created in the band structure of ZnO which these new levels appears inside the valence band. Since electronic configuration in Cu^{2+} is d^9, so, there is a level in created levels that is half full and can act as hole transfer. Figure 19 indicates the band structure of ZnO: Cu.

To get the information about the morphology and size of the ZnO:Cu nanoparticles, AFM studies had been carried out. It is observed from the AFM images, shape of the nanoparticles

http://dx.doi.org/10.5772/59092

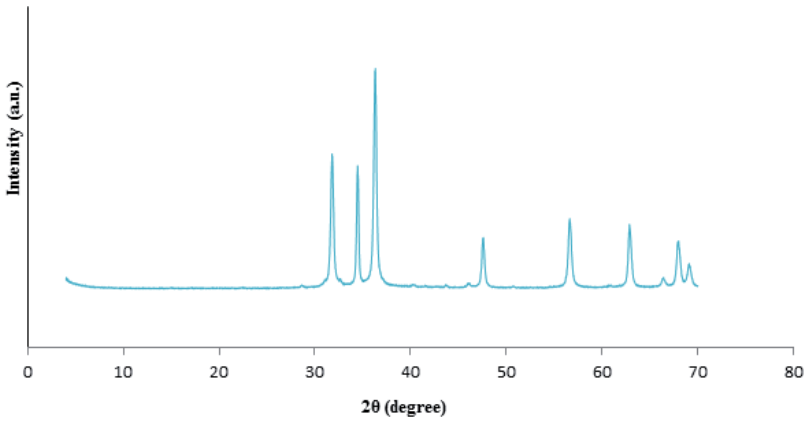

Figure 17. XRD pattern of ZnO: Nd nanoparticles

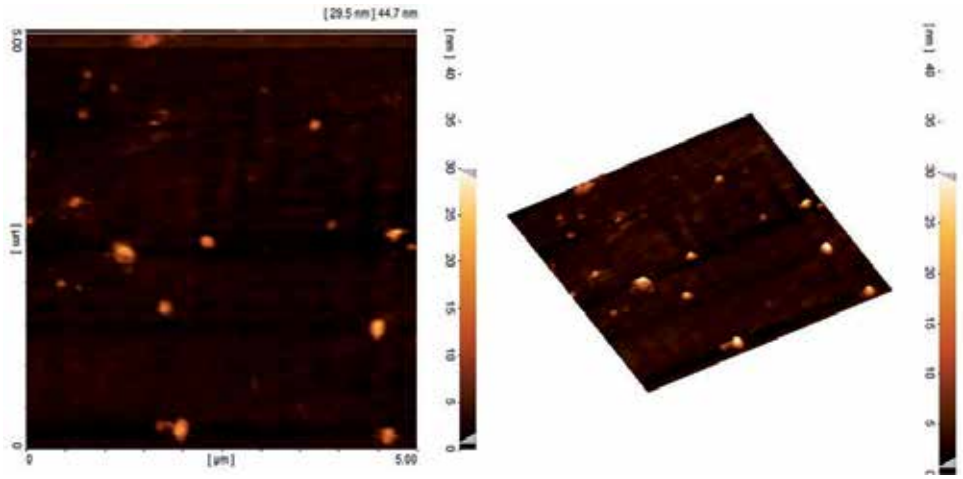

Figure 18. AFM images of ZnO:Nd

are spherical type. Figure 20 shows AFM image of ZnO: Cu. Nanoparticles size are about 10-40nm.

Figure 21 shows photoluminescence spectra of ZnO: Cu and ZnO: Nd which confirm the defects created in the structure of doped materials (visible region emission). According to Figure 21 in both of the doped (Cu and Nd) ZnO there is a peak in the UV region which shows band edge of ZnO.

The colloidal QDs employed in our synthesized structures contain a core/ shell; CdSe/ZnS. Figure 22 shows PL spectra of CdSe/ZnS nanoparticles that demonstrate high emission peak at 600 nm. The absence of other peaks in the spectrum and relatively narrow emission band at 600 nm show uniformity of particles and good passivation of the surface of CdSe using ZnS

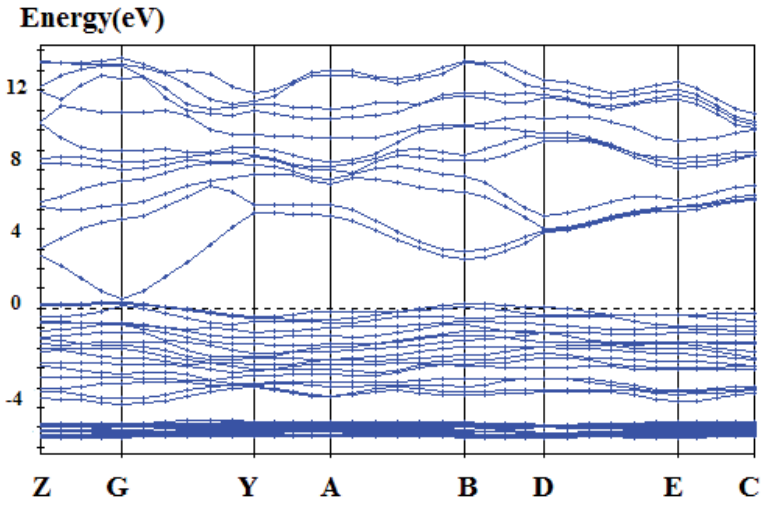

Figure 19. Band structure of Cu doped ZnO

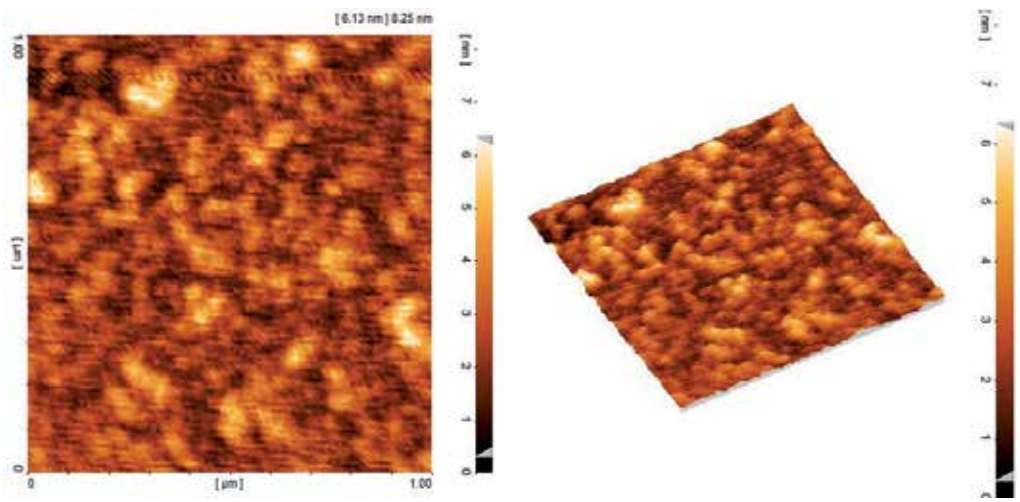

Figure 20. AFM images of ZnO:Cu

shell. The SEM image of synthesized CdSe/ZnS core/shell material is illustrated in Figure 23 in which the diameter of particles is about 30nm.

The PL spectra of QD-LEDs are shown in Figure 24 and indicate that electron–hole recombination is occurring predominantly in the QD layer, as required for optimal device operation. I-V behavior of the devices is illustrated in Figure 25 which confirms PL and EL emission results. Turn-on voltage for the devices based on NiO nano-materials is about 1V which is higher than the device based on ZnO: Cu. This turn-on voltage demonstrates that an ETL such

http://dx.doi.org/10.5772/59092

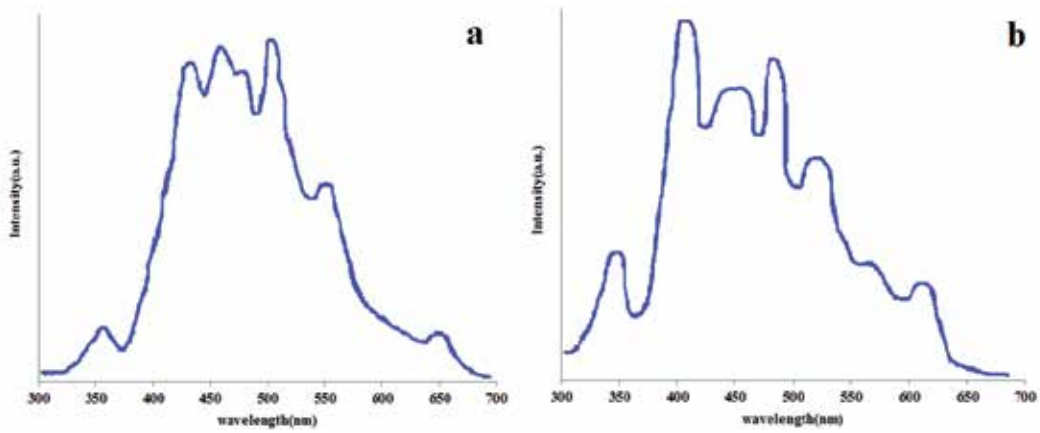

Figure 21. a) PL of ZnO:Cu b) PL of ZnO:Nd

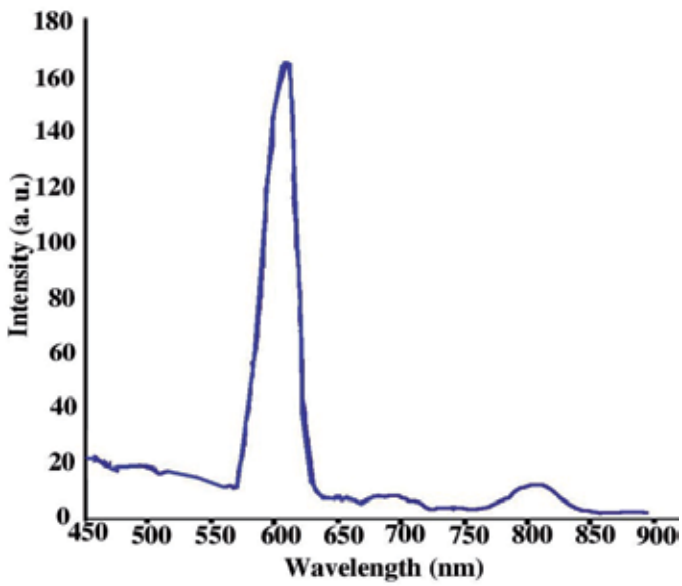

Figure 22. PL spectrum of the synthesized CdSe/ZnS

as ZnO: Ga and ZnO: Nd and NiO HTL or ZnO: Cu facilitate effective electron and hole injection into the QD conduction and valence bands. According to Figure 25a and 25b measurements of the EL emission intensity yield a peak brightness of 500 cdm^{-2} and 340 cdm^{-2} at an applied operating bias of 5 V for fabricated LEDs based on materials synthesized by sol-gel and electrochemical methods respectively, which is considerable compared with other recently reported QD-LEDs. This brightness is 700cdm^{-2} for the device based on ZnO: Nd (as ETL layer) and ZnO: Cu (as HTL layer) which the result confirms by I-V curve. As we can see in Figure 25 the current for it is higher than others. Also the current for the device based on NiO

synthesized by sol-gel method is higher than NiO synthesized by electrochemical method. This shows that by engineering in the structure of QDLEDs their performance can be improved.

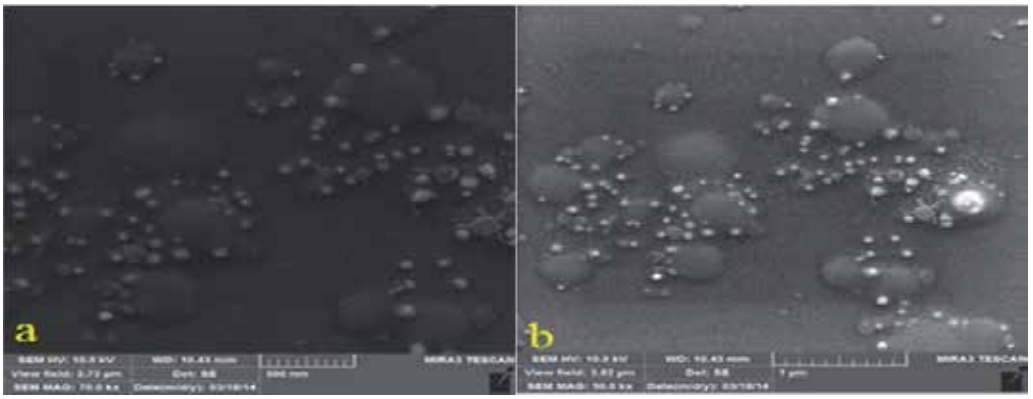

Figure 23. SEM images of synthesized CdSe/ZnS QDs

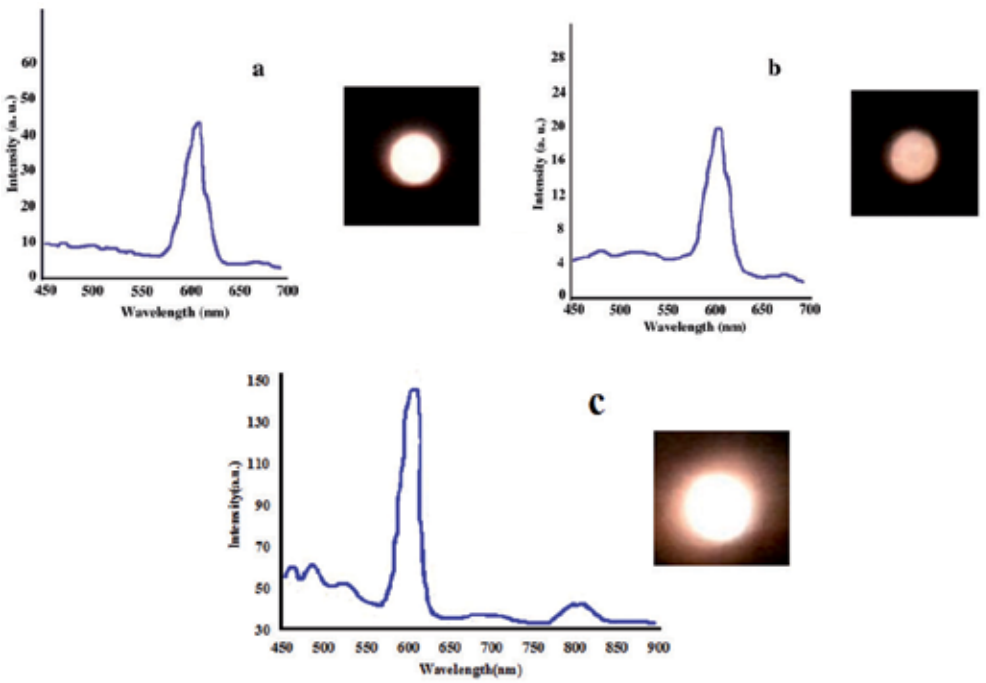

Figure 24. PL spectra and observed light for fabricated QD-LEDs a) with NiO synthesized by sol-gel b) with NiO synthesized by electrochemical methods c) with ZnO:Cu HTL and ZnO:Nd ETL

http://dx.doi.org/10.5772/59092

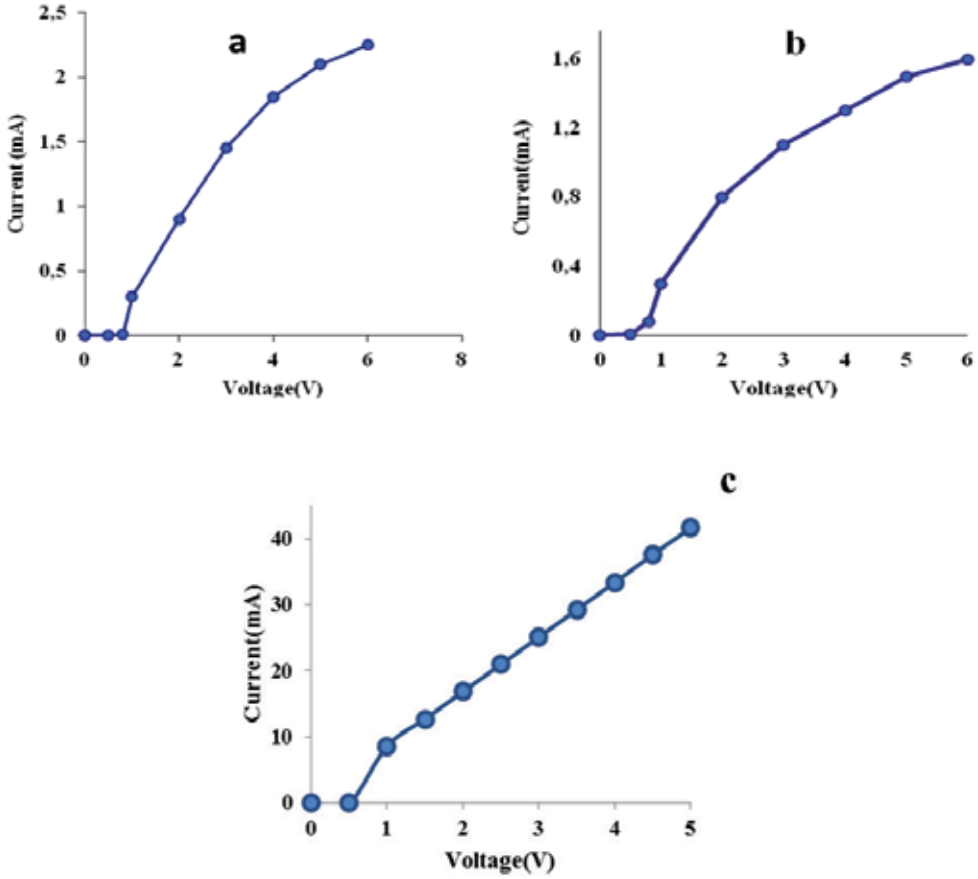

Figure 25. I-V characteristics of QD-LEDs a) based on NiO synthesized by sol-gel b) based on NiO synthesized by electrochemical methods as HTL c) based on ZnO:Cu HTL and ZnO:Nd ETL

4.1.2. Effects of FRET in QD-LEDs

4.1.2.1. Effects of organic molecules as shell around QDs

The emitted light and efficiency of QD-LEDs can be increased by Forster resonance energy transfer (FRET); in this way organic materials act as capping molecules for inorganic QDs. FRET is an energy transfer between two molecules, which one of them is a donor and the other is an acceptor. In the FRET process, first a donor material absorbs the energy and then transfer absorbed energy to a nearby acceptor and this process occurs through long-range dipole-dipole interactions [20, 34]. So, FRET mechanism leads to enhancement in the emission of fabricated QD-LEDs when QDs use as acceptor. Also in FRET process there are some important factors for transfer energy between acceptor and donor, such as the distance between the donor and acceptor molecules and the extent of spectral overlap [34]. Figure 26 shows FRET mechanism.

$$D + h\vartheta \rightarrow D^*$$

$$D^* + A \rightarrow D + A^* \text{ (D is Donor and A is Acceptor)}$$

$$A^* \rightarrow A + h\,A'$$

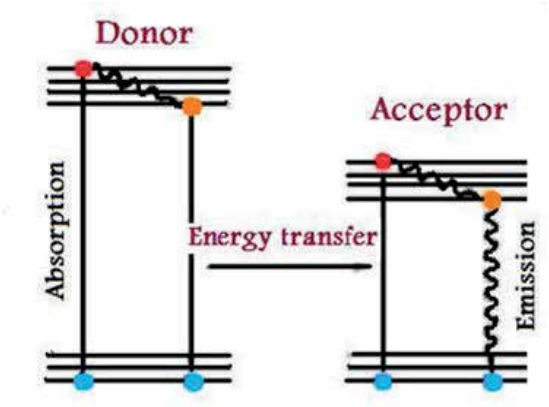

Figure 26. Energy diagram illustrating the FRET process

In the devices with luminescent species like inorganic semiconductors and organics molecules which in close proximity to the QDs, FRET is a mechanism that is unique to these devices. So, at first in the luminescent species, an exciton formed, and then the excitons energy is transferred to a QD non-radiative by dipole–dipole coupling [3]. QDs exhibit tune able emission by controlling their size and structure, therefor the spectral tune ability of QDs with quantum confinement effect allows to control FRET energy flow [35]. In our research group we utilized different capping organic molecules synthesized for surface passivation of synthesized QDs and these materials used as an active layer in the fabrication of QD-LEDs. The PL spectra of these materials indicate enhancement of emitted light via FRET mechanism. Figure 27 shows PL spectra of CdS QD and modified CdS QDs.

Figure 27 shows Intensity of emitted light for the CdS passivated by Ammonium hexafluorophosphate is higher than TAA and the PL intensity of CdS passivated by TAA is higher than CdS passivated by MAA. In this structure organic molecules are as donors and QDs are as acceptors. In FRET process the suitable distance for transmission of energy is about 1 to 10 nm, so for generating of an energy gradient structure and occurring of FRET mechanism the donor organic molecules should be close to the acceptors (QDs). The trapped exciton can be transferred to the nearby QD and a fraction of the migrated excitons from trapped states can contribute to the acceptor luminescence by radiative recombination. So, this leads to enhancement in the emission. Figure 28 illustrates I-V behavior of the devices, fabricated by capped QDs; turn on voltage of three devices is about 1V, however, for the device based on CdS: TAA the turn on voltage is 1.5 volt, which is more than the other devices. This is while; the PL result of QD capped by TAA is higher than others.

http://dx.doi.org/10.5772/59092

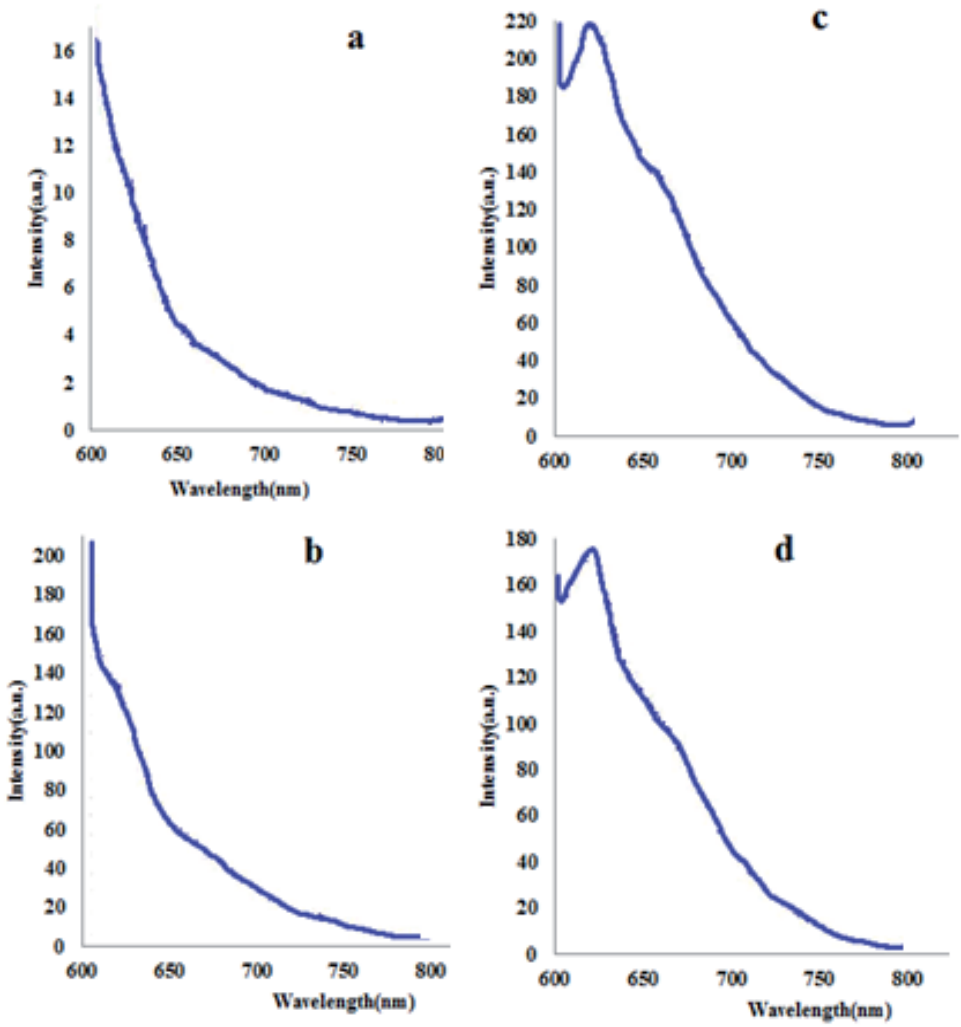

Figure 27. PL spectra of a)CdS b)CdS passivated by Ammonium hexafluorophosphate c) CdS passivated by TAA d) CdS passivated by MAA

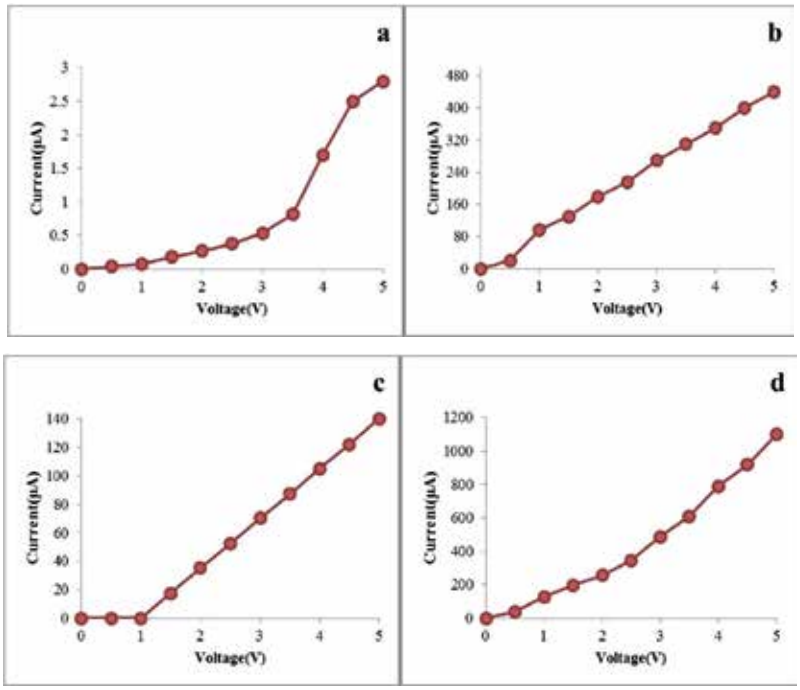

Figure 28. I-V behavior of a) CdS b) CdS passivated by Ammonium hexafluorophosphate c) CdS passivated by TAA d) CdS passivated by Mercaptoacetic acid

The PL and EL results of fabricated QD-LEDs based on FRET mechanism indicate high intensity of emitted light. It is necessary to be mentioned that in the structure of FRET based QDLEDs, ZnO:Nd acts as ETL and NiO synthesized by sol-gel method is used as HTL layers.

5. Conclusions and perspectives

In this section design and fabrication of QD-LEDs and solution of their problems including self-quenching and carrier injection have been described. All of described devices are fabricated by solution-processed methods. The base is finding the materials with suitable defect levels for achieving improved QD based LEDs. For this purpose, we investigated three types of QD-LEDs, which in both of them NiO applied as the transparent, conductive hole transport layer (HTL), and in the other one ZnO:Cu is the HTL. However, in one device, the synthesis route of NiO was sol-gel, whereas in the other, the electrochemical synthesis route is used. Characterization of NiO synthesized by sol-gel and electrochemical methods showed that different trap levels are created in the crystalline structures of NiO. Also DFT calculations indicate doping of Gallium and Neodymium atoms in the structure of ZnO increases electronic levels in the conduction band of ZnO. These calculations confirm experimental results. The obtained structure facilitates electron injections, and doping of Copper atoms in ZnO causes

this material acts as a p-type, so facilitates hole injections, when that used as HTL. Fabrication of FRET based QD-LEDs could introduce suitable organic capping molecules for fabrication of high performance LEDs. In this way Ammonium hexafluorophosphate as capping molecule acts the best performance from view point of PL and EL results. Increasing in drive voltage and created heating in the light emitting diodes cause that the intensity of output light decrease and this is inefficient. In this work by introducing novel structures and improvement in the optical properties of materials used in devices, drive voltage and so, creating of heating in the fabricated devices is decreased so the light efficiency increases.

Acronym list

Light emitting devices; LEDs

high-intensity discharge; HID

Quantum dots; QDs

Hole transport layer; HTL

Electron transport layer; ETL

Indium tin oxide; ITO

Forster resonant energy transfer; FRET

Shockley-Read-Hall; SRH

Photoluminescence; PL

Scanning electron microscope; SEM

Atomic force microscope; AFM

X-ray diffraction; XRD

X-Ray photoelectron spectroscopy; XPS

Binding energy; BE

Polyethylene terephthalate; PET

Author details

P. Amini, M. Dolatyari*, G. Rostami and A. Rostami

*Address all correspondence to: m.dolatyari@tabrizu.ac.ir

OIC Research Group, School of Engineering-Emerging Technologies, University of Tabriz, Tabriz, Iran

References

[1] Mills E., "The $230-billion global lighting energy bill". In Proceedings of the 5th International Conference on Energy-Efficient Lighting, Nice., France., May 2002.

[2] Yang Y., Pei Q., and Heeger A.J., "Efficient blue light-emitting diodes from a soluble poly (para-phenylene): internal field emission measurement of the energy gap in semiconducting polymers". Synthetic Metals. 1996; 78: 263-267.

[3] Shirasaki Y., Supran G. J., Bawendi M. G., and Bulović V., "Emergence of colloidal quantum-dot light-emitting technologies". Nat. Photonics. 2013; 7: 13-23.

[4] Round H. J., "A note on carborundum". Electr. World. 1907; 47: 309.

[5] Hall R. N., Fenner G.E., Kingsley J., Soltys T. J., and Carlson R. O., "Coherent light emission from GaAs junctions". Phys. Rev. Lett., 1962; 9: 366.

[6] Nathan M., Dumke W., Burns G., Jr F. D., and Lasher G., "Stimulated Emission of Radiation from GaAs pn Junctions". Appl. Phys. Lett., 1962; 1: 62-64.

[7] Jr N. H., and Bevacqua S., "Coherent (visible) light emission from Ga (AsP) junctions". Appl. Phys. Lett., 1962; 1: 82.

[8] Akasaki I., Amano H., Itoh K., Koide N., and Manabe K., "GaN based UV/blue light-emitting devices, GaAs and Related Compounds conference". Inst. Phys. Conf. Ser., 1992; 127: 851.

[9] Nakamura S., Senoh M., Iwasa N., and Nagahama S., "High-brightness In-GaN blue, green and yellow light-emitting diodes with quantum well structures". Jpn. J. Appl. Phys., Part 2, 1995; 34:797.

[10] Muthu S., Schuurmans F. J. P., and Pashley M. D., "Red, Green, and Blue LEDs for White Light Illumination". IEEE J. Quantum Electron., 2002; 8: 333-338.

[11] Qasim Kh., Lei W., and Li Q., "Quantum Dots for Light Emitting Diodes". J. Nanosci. Nanotechnol., 2013; 13: 3173-3185.

[12] Kim S., Im S. H., and Kim S.W., "Performance of light-emitting-diode based on quantum dots". Nanoscale, 2013; 5: 5205–5214.

[13] Sionnest P. G., "Electrical transport in colloidal quantum dot films". J. Phys. Chem. Lett., 2012; 3:1169-1175.

[14] Sun K., Vasudev M., Jung H.S., Yang J., Kar A., Li Y., Reinhardt P., Snee K., Stroscio M. A., and Dutta M., "Applications of colloidal quantum dots". Microelectron. J., 2009; 40: 644-649.

[15] Bae W. K., Park Y.S., Lim J., Lee D., Padilha L. A., McDaniel H., Robel I., Lee Ch., Pietryga J. M., and Klimov V. I., "Controlling the influence of Auger recombination

on the performance of quantum-dot light-emitting diodes". Nat. Commun., 2013; 4: 1-8.

[16] Kumar B., Campbell S. A., and Ruden P. P., "Modeling charge transport in quantum dot light emitting devices with NiO and ZnO transport layers and Si quantum dots". J. Appl. Phys., 2013; 114: 044507.

[17] Kim J., Park Y. J., Kim Y., Kim Y.H., Han Ch. J., Han J. I., and Oh M. S., "Effects of Oxide Electron Transport Layer on Quantum Dots Light Emitting Diode with an Organic/Inorganic Hybrid Structure". Electron. Mater. Lett., 2013; 9: 779-782.

[18] Mashford B. S., Nguyen T. L., Wilsonb G. J., and Mulvaney P., "All-inorganic quantum-dot light-emitting devices formed via low-cost, wet-chemical processing". J. Mater. Chem., 2010; 20: 167-172.

[19] Amini E., Dolatyari M., Rostami A., Shekari H., Baghban H., Rasooli H., and Miri S., "Solution-Processed Photoconductive UV Detectors Based on ZnO Nanosheets". IEEE Photonics Technol. Lett., 2012; 24: 1995-1997.

[20] Willard D. M., Carillo L. L., Jung J., and Orden A. V., "CdSe–ZnS Quantum Dots as Resonance Energy Transfer Donors in a Model Protein–Protein Binding Assay". Nano Lett., 2001; 1: 469-474.

[21] Schubert E. F., "Light-Emitting Diodes". Cambridge University Press, Second edition 2006.

[22] Thorseth A., "Characterization, Modeling, and Optimization of Light-Emitting Diode Systems". Ph.D. Thesis, DTU Fotonic, 2011.

[23] Xi Y. Y., Hsu Y. F., Djurišić A. B., Ng A. M. C., Chan W. K., Tam H. L., and Cheah K. W., "NiO/ZnO light emitting diodes by solution-based growth". Appl. Phys. Lett., 2008; 92: 113505.

[24] Amini P., Rostami A., Dolatyari M., Rostami G., Torabi P., Mathur S., Singh T., "High performance Solution Processed Inorganic Quantum Dot LEDs" IEEE, J. Nanotech., 2014; submitted.

[25] Irwin M. D., Servaites J. D., Buchholz D. B., Leever B. J., Liu J., Emery J. D., Zhang M., Song J.H., Durstock M. F., Freeman A. J., Bedzyk M. J., Hersam M. C., Chang R. P. H., Ratner M. A., and Marks T. J., "Structural and Electrical Functionality of NiO Interfacial Films in Bulk Heterojunction Organic Solar Cells". Chem. Mater., 2011; 23: 2218-2226.

[26] L. Jang W., Lu Y. M., Hwang W.S., Hsiung T. L., and Wang H. P., "Point defects in sputtered NiO films". Appl. Phys. Lett., 2009; 94: 062103.

[27] Oh M. S., Hwang D.K., Seong D. J., Hwang H.S., Park S.J., and Kim E.D., "Improvement of Characteristics of Ga-Doped ZnO Grown by Pulsed Laser Deposition Using Plasma-Enhanced Oxygen Radicals". J. Electrochem. Soc., 2008; 155: D599-D603.

[28] Gonc A. S. ¸ alves, Davolos M. R., Masaki N., Yanagida S., Morandeira A., Durrant J. R., Freitasd J. N., and Nogueira A. F., "Synthesis and characterization of ZnO and ZnO:Ga films and their application in dye-sensitized solar cells". Dalton Trans., 2008; 1487–1491.

[29] Aneesh P. M., Vanaja K. A., and Jayaraj M. K., "Synthesis of ZnO nanoparticles by hydrothermal method". Nanophotonics Mater., 2007; 6639: 66390J1-9.

[30] Khan Z. R., Khan M. Sh., Zulfequar M., and Khan M. Sh., "Optical and Structural Properties of ZnO Thin Films Fabricated by Sol-Gel Method". Mater. Sci. Appl., 2011; 2: 340-345.

[31] Rao T.P., and Kumar M. C. S., "Resistivity Stability of Ga Doped ZnO Thin Films with Heat Treatment in Air and Oxygen Atmospheres". J. Cryst. Process Technol., 2012; 2: 72-79.

[32] Zheng J. H., Song J. L., Zhao Z., Jiang Q., and Lian J. S., "Optical and magnetic properties of Nd-doped ZnO nanoparticles". Cryst. Res. Technol., 2012; 1-6.

[33] Sahare P. D., and Kumar V., "Optical and Magnetic Properties of Cu-Doped ZnO Nanoparticles". International Journal of Innovative Technology and Exploring Engineering, 2013; 3: 16-21.

[34] Sapsford K. E., Berti L., and Medintz I. L., "Materials for Fluorescence Resonance Energy Transfer Analysis: Beyond Traditional Donor–Acceptor Combinations". Angew. Chem., Int. Ed., 2006; 45: 4562-4588.

[35] Nizamoglu S., Sari E., Baek J. H., Lee I. H., Sun X. W. and Demir H. V., "FRET-LEDs involving colloidal quantum dot nanophosphors". Journal of Light Emitting Diodes., 2010; 2: 1-5.

Chapter 12

Experimental Research on Development Energy Efficiency of Non-Thermal Plasma Technology

Tao Zhu

Additional information is available at the end of the chapter

http://dx.doi.org/10.5772/58881

1. Introduction

NTP has been recently used to distinguish the one-atmosphere, near room temperature plasma discharges from other plasmas, operating at hundreds or thousands of degrees above ambient. Industrially applied plasma technologies, is that they are 1) non-thermal and 2) operate at or near atmospheric pressure. NTP is a new technology for environmental protection, especially in the field of air pollution control, and has been studied by many researchers for 20 years [1]. Due to NTP generated at normal temperature and atmospheric pressure, easy operation and higher treatment efficiency, compare to the other technologies [2]. So far, NTP technology has been used in many fields and decomposed many kinds of air pollutants. There are many researches focusing on volatile organic compounds (VOCs) decomposition [3], and SO_2 and NOx degradations [4,5], and CFCs and odors and mercury treatments [6-8], etc. But during of NTP technology development and application, there is a key problem restricting NTP technology for commercial application [9], that is, how to solve energy consumption [10,11].

In order to resolve this problem, a series of researches were carried out in the world. Platinum based catalyst with NTP generated by a high voltage bipolar pulsed excitation was adopted by some researchers [12]. They found the energy efficiency is 0.14 mol/kWh for 2-Heptanone decomposition when the energy density is 200 J/L, and the energy efficiency decreased to 0.029 mol/kWh using an uncoated monolith when the energy density is 500 J/L. Ogata *et al.* [13] used NTP reactor packed with $BaTiO_3$ pellets to decompose the aromatics benzene, toluene and *o*-xylene. The results show $BaTiO_3$ pellets have a function for enhancing electric field strength and improving VOCs decomposition.

In our research, we developed a new ferroelectric packed bed NTP reactor and prepared a sample of $Ba_{0.8}Sr_{0.2}Zr_{0.1}Ti_{0.9}O_3$. Doped some ions (Sr & Zr) into the powder particles and crystal boundary in the experiment, the metal ions such as strontium, zinc and zirconium entered into

crystal lattices of $BaTiO_3$ equably and the Curie temperature (Tc) fell [14]. Because of higher permittivity and lower dielectric loss of $Ba_{0.8}Sr_{0.2}Zr_{0.1}Ti_{0.9}O_3$ than those of $BaTiO_3$, $Ba_{0.8}Sr_{0.2}Zr_{0.1}Ti_{0.9}O_3$ shows a better ferroelectric physical property to increase the energy efficiency for VOCs removal.

2. Material and methods

2.1. NTP System

The NTP system consisted of a tube-wire packed-bed reactor system, an AC power supply, a continuous flow gas supplying system and an electric and gaseous analytical system [14]. Dry air (78% N_2, 21% O_2) was used as a balance gas for toluene decomposition. The whole NTP system refer to reference [14]. The NTP packed-bed reactor was shown in Fig.1. And the schematic diagram of NTP system is shown in Fig.2. As the packed materials in NTP reactors, we selected four packed materials, respectively, including no packed materials, ceramic rings, $BaTiO_3$ rings and $Ba_{0.8}Sr_{0.2}Zr_{0.1}Ti_{0.9}O_3$ rings [14].

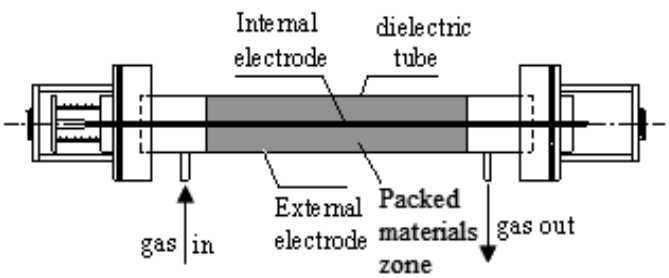

Figure 1. NTP reactor

Reactor: organic-glass tube (i.d.32mm, packed infilling length of packed materials of 200mm); Internal electrode: tungsten filament (i.d.0.5mm); External electrode: dense steel mesh; Packed materials packed in the dark zone, respectively selected ceramic rings, $BaTiO_3$ rings and $Ba_{0.8}Sr_{0.2}Zr_{0.1}Ti_{0.9}O_3$ rings. (after T.Zhu [14])

2.2. Materials and methods

In the experiment, three kinds of packed materials, including ceramic rings, $BaTiO_3$ rings and $Ba_{0.8}Sr_{0.2}Zr_{0.1}Ti_{0.9}O_3$ rings (hollow cylinder shape, 5 mm i.d., 1 mm wall thick, and 10 mm length), were used to pack into the NTP reactor.

We use the method of water-thermal composite action to prepare a kind of modified ferro-electric of nano-size $Ba_{0.8}Sr_{0.2}Zr_{0.1}Ti_{0.9}O_3$ powder at atmospheric pressure. The prepared detail of nano-$Ba_{0.8}Sr_{0.2}Zr_{0.1}Ti_{0.9}O_3$ refers to our former research [15].

http://dx.doi.org/10.5772/58881

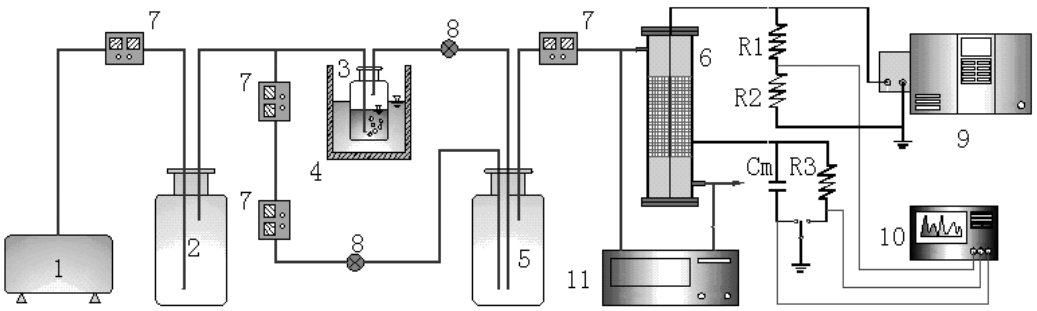

Figure 2. Schematic diagram of NTP system for toluene removal 1.air compressor 2.buffer 3.toluene liquid bottle 4.attemperator 5.blender 6.NTP reactor 7.mass flow meter 8.needle valve 9.high voltage 10. oscilloscopes 11.gas chromatograph

We detected the crystal structures and the surface conditions of the $Ba_{0.8}Sr_{0.2}Zr_{0.1}Ti_{0.9}O_3$ samples by XRD (manufactured by Germany Bruker Co., D8 ADVANCE) and SEM (manufactured by Japan, JEOL-JSM-6500F). We used Micromeritics (manufactured by American Quantachrome Co., NOVA 1000) to determine BET surface area. Using an LCR automatism test instrument (manufactured by China, 4210), we measured the relative permittivity of $Ba_{0.8}Sr_{0.2}Zr_{0.1}Ti_{0.9}O_3$ samples. Toluene analysis was carried out by gas chromatography (manufactured by Aglient Co., HP6890N) with a flame ionization detector (FID). The byproducts were detected by GC-MS (manufactured by American Thermo Finnegan Co.) using EI mode, 70 eV and full scan. Ozone concentration produced in the NTP reactor was measured by an iodine-titration method. The plasma reactor employed an AC power supply of 150 Hz scanning from 0 kV to 100 kV was applied to the reactor in the radial direction. The voltage and current waveforms were measured by oscillograph (manufactured by American Tektronix Co., TDS2014). To investigate the electric characteristics of dielectric barrier discharge (DBD), the voltage applied to the reactor was sampled by a voltage divider with a ratio of 12500:1. Also, the current was determined from the voltage drop across a shunt resistor (R3 =10kΩ) connected in series with the grounded electrode. In order to obtained the total charge and discharge power simultaneously, a capacitor (Cm =2μF) was inserted between the reactor and the ground. The electrical power provided to the discharge was measured using the Q–V Lissajous diagram. Typical Lissajous diagram represents to be a parallelogram, and we could calculate power though calculated the area of parallelogram. The whole methods can be seen in the reference [14].

The removal efficiency, reactor energy density, and energy efficiency of toluene were calculated in the process of NTP as follows [14]:

Toluene removal efficiency (η):

$$\eta(\%) = \frac{[toluene]_{inlet} - [toluene]_{outlet}}{[toluene]_{inlet}} \times 100\% \quad (1)$$

Reactor Input energy density (RED):

$$RED(kJ/L) = \frac{input \cdot power(W)}{gas \cdot flow \cdot rate(L/\min)} \times 60 \times 10^{-3} \quad (2)$$

Energy efficiency (ζ):

$$\zeta(g/kWh) = \frac{[toluene]_{inlet} \times \eta}{RED} \times 3.6 \times 10^{-3} \quad (3)$$

3. Results and discussion

3.1. Detection of modified ferroelectric

The crystal structure of $Ba_{0.8}Sr_{0.2}Zr_{0.1}Ti_{0.9}O_3$ is detected by XRD as shown in Fig.3. From Fig.3, we can think the crystal structure of $Ba_{0.8}Sr_{0.2}Zr_{0.1}Ti_{0.9}O_3$ is a kind of ferroelectric, and very close to $BaTiO_3$ and 59 nm diameter. That means crystal structure of nano-$Ba_{0.8}Sr_{0.2}Zr_{0.1}Ti_{0.9}O_3$ should be a kind of cube crystal structure of calcium-titanium oxide. The BET surface area of $Ba_{0.8}Sr_{0.2}Zr_{0.1}Ti_{0.9}O_3$ are 8.8 m^2/g, and Longmuir surface area is 12.3 m^2/g or so. The relative permittivity of $Ba_{0.8}Sr_{0.2}$ $Zr_{0.1}Ti_{0.9}O_3$ is 12000.

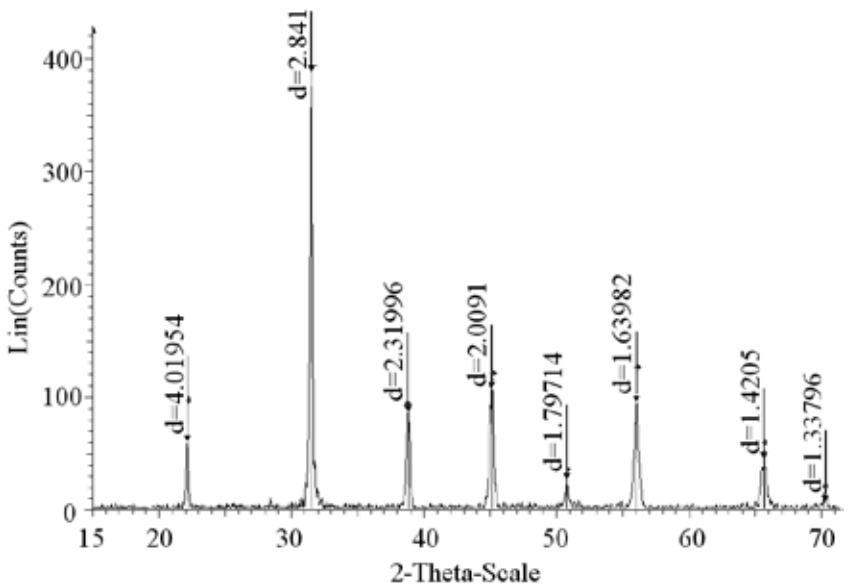

Figure 3. XRD testing results of $Ba_{0.8}Sr_{0.2}Zr_{0.1}Ti_{0.9}O_3$

3.2. Effect of nano-$Ba_{0.8}Sr_{0.2}Zr_{0.1}Ti_{0.9}O_3$ on toluene decomposition

Fig.4 shows the effect of nano-$Ba_{0.8}Sr_{0.2}Zr_{0.1}Ti_{0.9}O_3$ on toluene removal efficiency (toluene: 600 mg/m^3; flow velocity: 1 mL/min; dry air) [14]. At the same RED, the removal efficien-

http://dx.doi.org/10.5772/58881

cy of toluene had an order of no packed materials < ceramic rings < $BaTiO_3$ rings < nano-$Ba_{0.8}Sr_{0.2}Zr_{0.1}Ti_{0.9}O_3$ rings. Packed materials in NTP reactor could effectively enhance the energy intensity of input reactor and accelerated toluene decomposition. NTP operating at the RED of 0.76 kJ/L, toluene removal efficiency arrived at 97% and the energy efficiency attained 6.48 g/kWh when the packed materials of $Ba_{0.8}Sr_{0.2}Zr_{0.1}Ti_{0.9}O_3$ are used in NTP reactor [14].

In the electrode gap, if we add the presence of solid material, NTP will be enhance, and homogeneous plasma would be formed rather than a filamentous one. Eliasson et al. [16] found that it is important to pack the packed materials into NTP reactor, and the more high energy electrons properly generated by dielectric barrier discharge (DBD). Due to high energy electrons could destroy the molecular structure of toluene, the removal efficiency is increasing with the numbers of high energy electrons increase.

During the preparation of $Ba_{0.8}Sr_{0.2}Zr_{0.1}Ti_{0.9}O_3$ samples, strontium (Sr) and zirconium (Zr) metal ions can enter crystal lattices of $BaTiO_3$ equably and lower the Curie temperature (Tc) [17]. As a result, the permittivity of $Ba_{0.8}Sr_{0.2}Zr_{0.1}Ti_{0.9}O_3$ is 12000, 8 times higher than that of pure phase of $BaTiO_3$ (1500) in room temperature [15]. According to Yamamoto et al.[18], the permittivity had a significant influence on the discharge energy of NTP reactor.

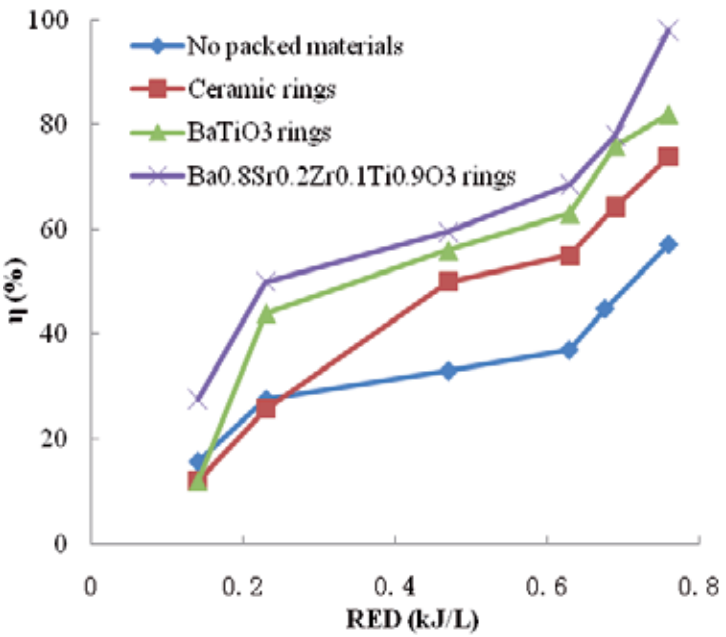

Figure 4. Relationship between RED and removal efficiency in four NTP reactors

Fig.5 shows the ozone (O_3) concentration with and without the packed materials [14]. O_3 concentration is the highest with $Ba_{0.8}Sr_{0.2}Zr_{0.1}Ti_{0.9}O_3$ and is in the order of no packed materials < ceramic rings <$BaTiO_3$ rings < $Ba_{0.8}Sr_{0.2}Zr_{0.1}Ti_{0.9}O_3$ rings at the identical RED.

As a kind of main long-living radicals, O_3 was generated and transported to the packed materials to take part in oxidation reaction on the surface of packed materials [14, 19].

$$e + O_2 \rightarrow 2O + e \tag{4}$$

$$O + O_2 + M \rightarrow O_3 + M \tag{5}$$

$$O + O_3 \rightarrow 2O_2 \tag{6}$$

$$e + O_3 \rightarrow O + O_2 + e \tag{7}$$

In fig.6, we can find O_3 concentration increases when REDs change from 0 to 0.7 kJ/L, and the maximum ozone concentration appears at the RED of 7 kJ/L. Yamamoto et al. also found the same change of the pattern of ozone production [20]. $Ba_{0.8}Sr_{0.2}Zr_{0.1}Ti_{0.9}O_3$ has higher relative permittivity than $BaTiO_3$ so that $Ba_{0.8}Sr_{0.2}Zr_{0.1}Ti_{0.9}O_3$ can be electric polarized at normal temperature. Therefore, electric field strength and RED are enhanced significantly [14]. As a result, O_3 concentration increases according to Eq.(6) (RED ≤ 0.7 kJ/L). While RED ≥ 0.7 kJ/L, the superfluous high-energy electrons accelerate O_3 to transform into O_2 according to Eq.(7) and Eq.(8).

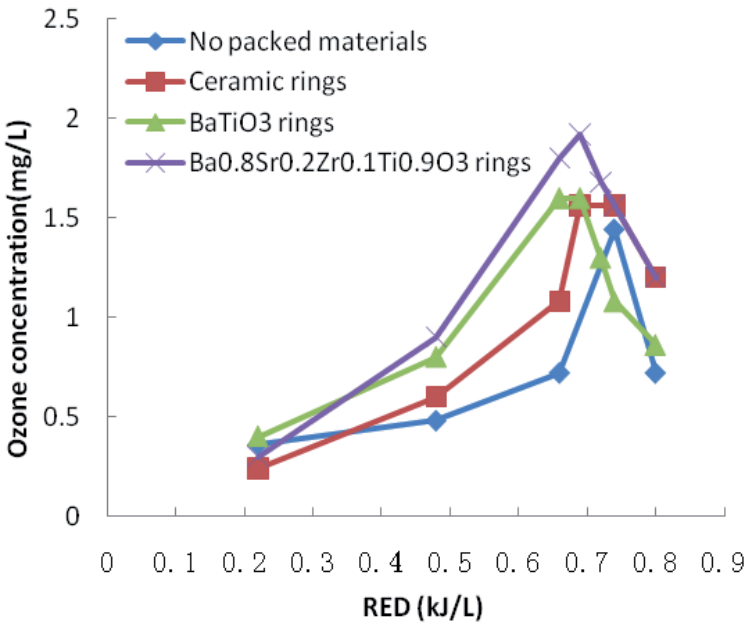

Figure 5. Relationship between RED and ozone concentration in four NTP reactors

http://dx.doi.org/10.5772/58881

Chang et al.[21] found that there are two main mechanisms for VOC decomposition. 1) Directly, electrons attack VOC molecules. 2) indirectly reactions happen between VOC molecules and radicals. And these radicals involve oxygen plasma, free radical groups, ozone, etc. Chang's results indicate higher O_3 concentration is positive to higher removal efficiency. So as packed materials, $Ba_{0.8}Sr_{0.2}Zr_{0.1}Ti_{0.9}O_3$ seems to be better than $BaTiO_3$.

Fig.6 shows the change of energy efficiency (ζ) for toluene removal under the different conditions [14]. The energy efficiency has an order as show as follows at the same RED: no packed materials <ceramic rings <$BaTiO_3$ rings < $Ba_{0.8}Sr_{0.2}Zr_{0.1}Ti_{0.9}O_3$ rings. The energy efficiency is 15 g/kWh with $Ba_{0.8}Sr_{0.2}Zr_{0.1}Ti_{0.9}O_3$ and 11 g/kWh with $BaTiO_3$ at RED of 0.23 kJ/L in the NTP reactor. The results show that $Ba_{0.8}Sr_{0.2}Zr_{0.1}Ti_{0.9}O_3$ has a better ferroelectric property to improve energy efficiency and reduce energy consumption in the NTP process for VOCs control, compared with $BaTiO_3$.

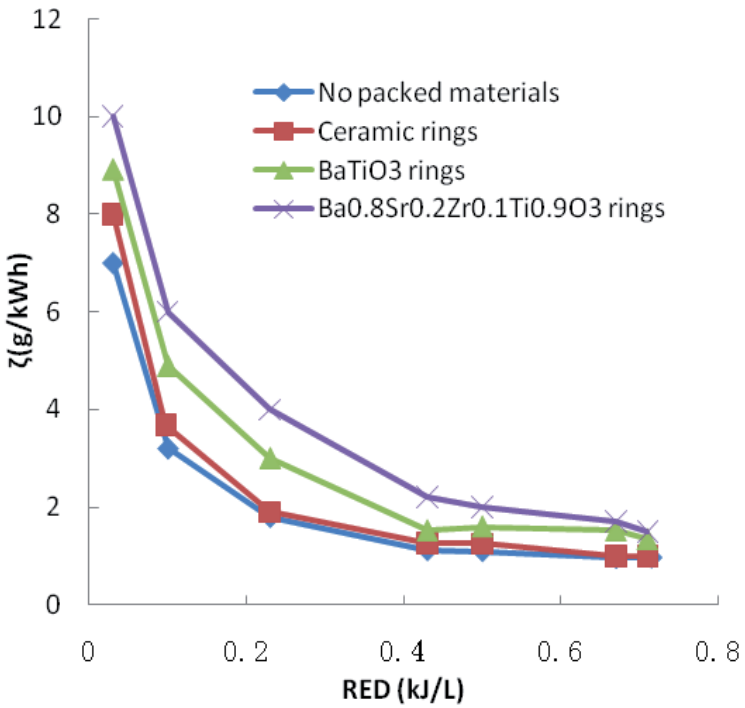

Figure 6. Relationship between RED and energy efficiency in four NTP reactors

3.3. Byproducts analysis

In the process of toluene abatement, the emission in the outlet was detected by GC-MS at electric field strength of 8 kV/cm in Fig.7 (a). By NIST2000 mass spectrum, the polymerization products formation can be observed, including aldehyde, alcohols, amide, and benzene derivative [22].

In fig.7 (b), the byproducts are very few at electric field strength of 14 kV/cm. We can assume that toluene molecules would be completely oxidized to CO_2, CO and H_2O in the enough high electric field strength of the enough high input power. In fact, there are a large number of high-energy electrons, ions and free radicals in NTP process. Firstly, eq.(5~8) indicate high-energy electrons take part in reaction with oxygen in air [22]. And at the same time, high-energy electron reacted with H_2O and N_2 in contaminated air:

$$e + O_2 \rightarrow 2O^{\bullet} \tag{8}$$

$$e + H_2O \rightarrow 2H^{\bullet} + O^{\bullet} \tag{9}$$

$$e + H_2O \rightarrow OH^{\bullet} + H^{\bullet} + e \tag{10}$$

$$e + 2H_2O \rightarrow HO_2^{\bullet} + 3H^{\bullet} + e \tag{11}$$

$$e + N_2 \rightarrow 2N^{\bullet} + e \tag{12}$$

Toluene bond energy between carbon of benzene ring and carbon of substituent radical is 3.6 eV, which is the lowest than that of carbon-carbon bond or hydrocarbon bond. Hydrogen of benzene ring is replaced by methyl, which lead to the stability of benzene ring is broken [14]. So molecule structure of toluene is not stable. In the theoretical point of view, this bond is the most vulnerable and broken. Of course, the other bonds are also likely to be destroyed by high energy electrons. Eq.13 is the possible reaction equations of the process of toluene decomposition [23].

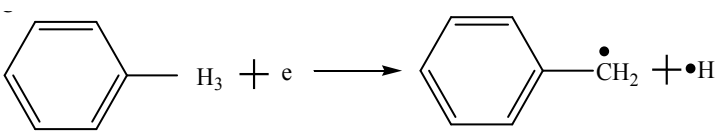

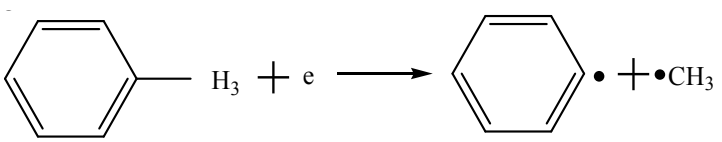

http://dx.doi.org/10.5772/58881

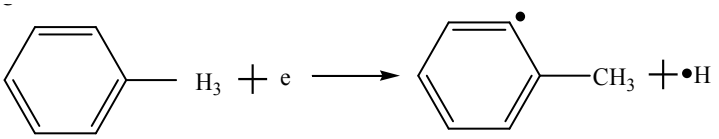

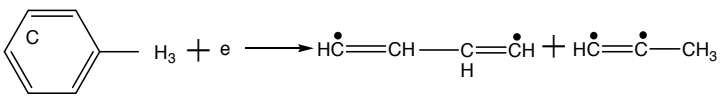

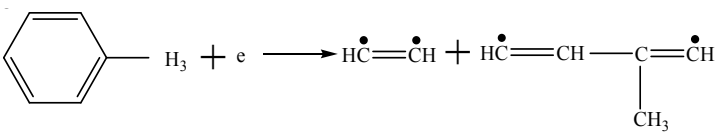

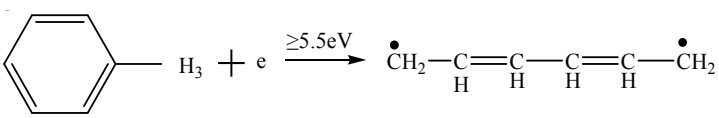

Aldehyde, alcohols, amide, and benzene derivative were form in NTP process during above all of free radical groups reacted with the other reaction fragments. When energy efficiency continuing to increase, the byproducts ought to degraded into CO_2, CO and H_2O.

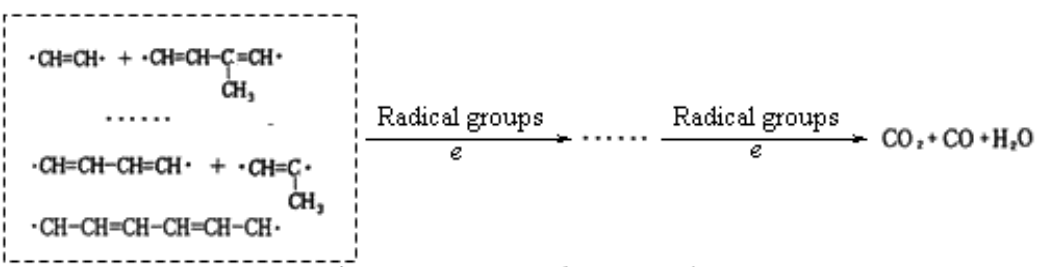

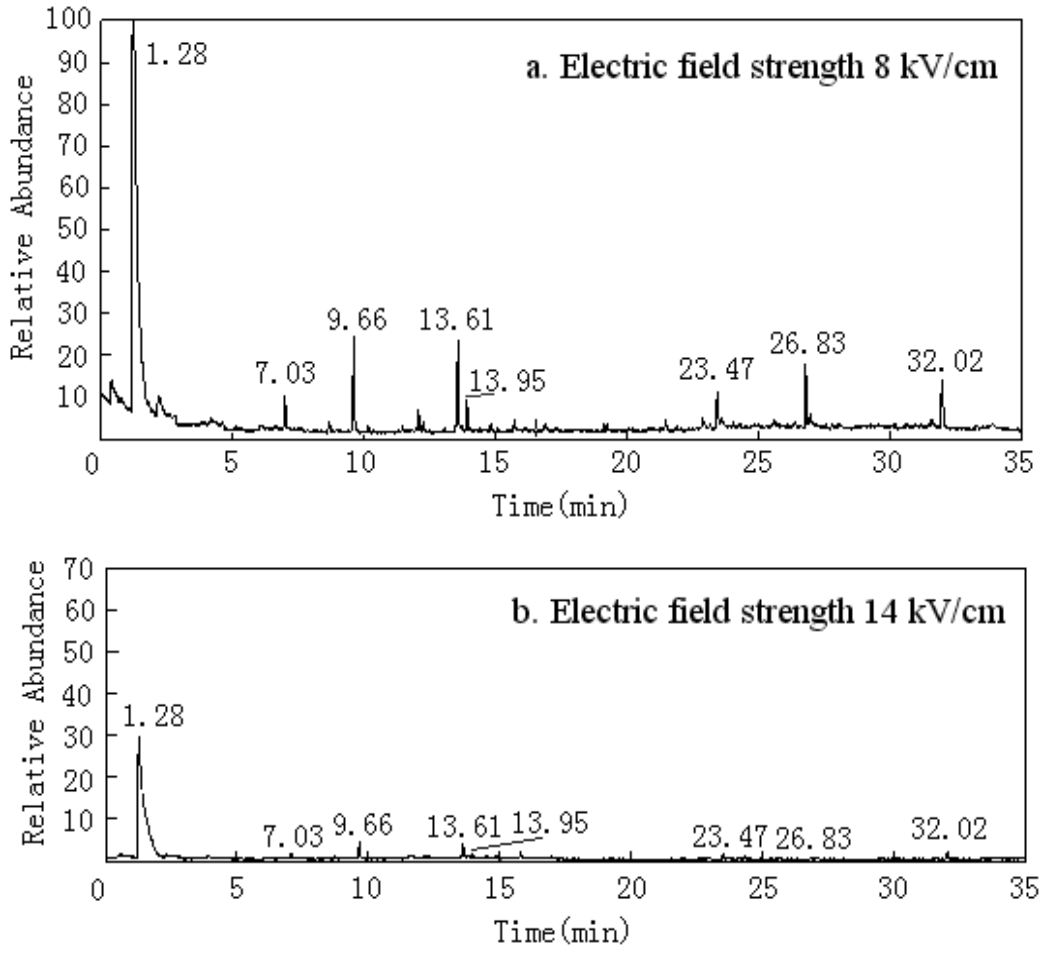

Figure 7. Mass spectrum of byproducts of toluene decomposition

4. Conclusion

In this paper, NTP was generated by DBD at 20℃ and 1 atm. We selected four kinds of packed materials, including no padding, ceramic rings, $BaTiO_3$ rings and $Ba_{0.8}Sr_{0.2}Zr_{0.1}Ti_{0.9}O_3$ rings, which to pack into NTP reactor. Nano-$Ba_{0.8}Sr_{0.2}Zr_{0.1}Ti_{0.9}O_3$ was prepared by the method of water-thermal composite action in our laboratory. By detected, $Ba_{0.8}Sr_{0.2}Zr_{0.1}Ti_{0.9}O_3$ shows better ferroelectric characteristic than $BaTiO_3$. Then this kind of new modified ferroelectric of $Ba_{0.8}Sr_{0.2}Zr_{0.1}Ti_{0.9}O_3$ as the packed materials is used in the packed bed NTP reactor for the first time. During the whole experiments, we attained the best removal efficiency of toluene and the best energy efficiency with $Ba_{0.8}Sr_{0.2}Zr_{0.1}Ti_{0.9}O_3$ rings as packed materials in NTP reactor. For example, toluene removal efficiency arrived at 97% and the energy efficiency stopped at

6.48 g/kWh when RED was 0.76 kJ/L or so, and ozone concentration reached the maximum value when RED was 0.7 kJ/L or so. Ozone concentration is positive to higher removal efficiency. There are aldehyde, alcohols, amide, and benzene derivative, which generated as the byproducts in NTP process and detected by GC-MS. Of course, these byproducts could be decomposed into CO_2, CO and H_2O entirely at last if we further increased input energy intensity. So nano-$Ba_{0.8}Sr_{0.2}Zr_{0.1}Ti_{0.9}O_3$ as the packed materials in the packed bed NTP reactor would effectively improve energy efficiency for VOCs removal than the other packed materials in NTP reactor.

Acknowledgements

This work was supported by the National Natural Science Foundation of China (No.51108453), and Program for New Century Excellent Talents in University, and Beijing outstanding talent training project, and the Fundamental Research Funds for the Central Universities (No. 2009QH03).

Author details

Tao Zhu*

Address all correspondence to: bamboozt@cumtb.edu.cn

School Chemical & Environmental Engineering, China University of Mining & Technology-Beijing, Beijing, China

References

[1] S. Masuda, S. Hosokawa, and X. L Tu. The performance of an integrated air purifier for control of aerosol, microbial, and odor. *IEEE Trans. Ind. Appl*. 29, 774-780, 1993.

[2] B. Eliasson, and U. Kogelschatz. Nonequilibrium volume plasma chemical processing. *IEEE Trans. Plasma Sci*. 1991, 19, 1063-1068.

[3] T. Zhu, J. Li, Y. Q. Jin, and G. D. Ma. Gaseous phase benzene decomposition by non-thermal plasma coupled with nano-titania catalyst. *Int. J. Environ. Sci. Tech.* 2008, 6 (1), 141-148.

[4] M. B. Chang, J. H. Balbach, M. J. Rood, and M. J. Kushner. Removal of SO_2 from gas streams using a dielectric barrier discharge and combined plasma photolysis. *J. Appl. Phys*. 1991, 69, 4409-4418.

[5] Y.S. Mok, M. Dors, J. Mizeraczyk. Effect of reaction temperature on NOx removal and formation of ammonium nitrate in nonthermal plasma process combined with selective catalytic reduction. *IEEE Trans. Plasma Sci.* 2004, 32, 799-807.

[6] C. L. Ricketts, A. E. Wallis, and J. C. Whitehead. A mechanism for the destruction of CFC-12 in a nonthermal, atmospheric pressure plasma. *J. Phys. Chem. A*. 2004, 108, 8341-8345.

[7] M. B. Chang, and T. D. Tseng. Gas-phase removal of H_2S and NH_3 with dielectric barrier discharges. *J. Environ. Eng.* 1996, 122, 41-46.

[8] S. Masuda, Pulse corona induced plasma chemical process: a horizon of new plasma chemical technologies. *Pure Appl. Chem*. 1988, 60, 727-731.

[9] T.Zhu, J.Li, Y.Q.Jin, et al. Research Progresses in Treatment of Waste Gas Containing Volatile Organic Compounds by Combined Plasma Technology. *Environ. Protec. Chem. Ind.* 2008, 28 (2), 121-125.

[10] J. Van Durme, J. Dewulf, C. Leys, H. Langenhove: Combining non-thermal plasma with heterogeneous catalysis in waste gas treatment: A review, *Appl. Cata. B: Environ*. 2008, 78, 324-333.

[11] T. Zhu, J. Li, W. J. Liang, Y. Q. Jin. Synergistic effect of catalyst for oxidation removal of toluene. J. Hazard. Mater. 2009, 165,1258-1260.

[12] C. Ayrault, J. Barrault, N. Blin-Simiand, F. Jorand, S. Pasquiers, A. Rousseau, J. M. Tatibouet. Oxidation of 2-heptanone in air by a DBD type plasma generated within a honeycomb monolith supported Pt-based catalyst, Cata. Today. 2003, 89, 75-83.

[13] A.Ogata, H.Einaga, H.Kabashima, et al. Effective combination of nonthermal plasma and catalysts for decomposition of benzene in air. *Appl. Catal. B: Environ.* 2003, 46(1), 87-95.

[14] Tao Zhu, Yandong Wan, Hairong Li, Che Sha, Yan Fang. VOCs decomposition via modified ferroelectric packed bed dielectric barrier discharge plasma, *IEEE Trans. Plasma Sci*., 2011, 39(8), 1695-1700.

[15] Tao Zhu. Chemistry, emission control, radioactive pollution and indoor air quality, Chapter 4. InTech Publisher, 2011.

[16] B. Eliasson, U. Kogelschatz. Nonequilibrium volume plasma chemical processing, *IEEE Trans. Plasma Sci*. 1991, 19, 1063-1068.

[17] S. W. Ding, J. Wang, J. L. Qin. The structure and performance of complex of nanometer $BaTiO_3$, *Sci. China, Ser. B*. 2001, 31, 525-529.

[18] T. Yamamoto, K. Ramanatiran, P. A. Lawless, D. S. Ensor, J. R. Nwesome, N. Plaks, G. H. Ramsey. Control of Volatile organic compound by ac energized ferroelectric pellet reactor and a pulsed corona reactor, IEEE Trans. Ind. Appl. 1992, 28, 528-532.

http://dx.doi.org/10.5772/58881

[19] S. Delagrange, L. Pinard, J. M. Tatiboue°t. Combination of a non-thermal plasma and a catalyst for toluene removal from air: Manganese based oxide catalysts, Appl. Catal. B: Environ. 2007, 68, 92-98.

[20] T. Yamamoto. Methods and apparatus for controlling toxic compounds using catalysis-assisted non-thermal plasma, Environ. Int. 1997, 23, 3-10.

[21] M. B. Chang, C. C. Lee. Destruction of formaldehyde with dielectric barrier discharge plasmas, Environ. Sci. Tech. 1995, 29, 181-186.

[22] Tao Zhu. Toluene removal using non-thermal plasma technology coupled with nano-$Ba_{0.8}Sr_{0.2}Zr_{0.1}Ti_{0.9}O_3$. 2010 4th International Conference on Bioinformatics and Biomedical Engineering, 06/2010.

[23] Atkinson R., Pitts J.N., Jr. Kinetics and mechanism of the gas phase reaction of hydroxyl radicals with aromatic hydrocarbons over the temperature range 296-473 K. J. Phys. Chem. 1977, 81(4), 296–304.

Edited by Moustafa M. Eissa

This book is intended for academics and engineers who are working in universities, research institutes, utility and industry sectors wishing to enhance their idea and get new information about the energy efficiency developments in smart grid. The readers will gain special experience with deep information and new idea about the energy efficiency topics. This book includes lots of problems and solutions that can easily be understood and integrated into larger projects and researches. The book enables some studies about monitoring, management and measures related to smart grid components, Energy Efficiency Improvements in smart grid components and new intelligent Control strategies for Distributed energy resources, boosting PV systems, electrical vehicles, etc. It included optimization concepts for power system, promoting value propositions; protection in power system, etc. The book also has some recent developments in solar cell technologies, LEDs and non thermal plasma technology. As I enjoyed preparing this book I am sure that it will be very valuable for large sector of readers.

ISBN 978-953-51-4225-6

Photo by WangAnQi / iStock

IntechOpen